TESIS DOCTORAL

"Diseño de sistemas metálicos soportados para reacciones de hidrogenación de interés industrial"

"Design of several supported metal systems for diverse industrially-relevant hydrogenation processes"

Vicente Montes Jiménez

Departamento de Química Orgánica

Facultad de Ciencias

Universidad de Córdoba

2015

TITULO: *DISEÑO DE SISTEMAS METÁLICOS SOPORTADOS PARA REACCIONES DE HIDROGENACIÓN DE INTERÉS INDUSTRIAL*

AUTOR: *Vicente Montes Jiménez*

Campus de Rabanales
Ctra. Nacional IV, Km. 396 A
14071 Córdoba

www.uco.es/publicaciones
publicaciones@uco.es

TÍTULO DE LA TESIS: DISEÑO DE SISTEMAS METÁLICOS SOPORTADOS PARA REACCIONES DE HIDROGENACIÓN DE INTERÉS INDUSTRIAL

DOCTORANDO/A: Vicente Montes Jiménez

INFORME RAZONADO DEL/DE LOS DIRECTOR/ES DE LA TESIS

(se hará mención a la evolución y desarrollo de la tesis, así como a trabajos y publicaciones derivados de la misma).

Como Directores de esta Tesis Doctoral consideramos que durante el desarrollo de la misma, el doctorando ha adquirido las habilidades y competencias necesarias para obtener el título de Doctor, y que el trabajo desarrollado constituye una aportación relevante en el campo del diseño y aplicación de catalizadores heterogéneos a procesos de hidrogenación de interés industrial. Estas afirmaciones se apoyan en los siguientes puntos:

1. El doctorando ha superado con buen aprovechamiento los créditos correspondientes a la formación teórico-práctica de la parte formativa del Programa de Doctorado en Química Fina (Máster en Química Fina Avanzada).

2. El doctorando ha adquirido una sólida formación en la gran variedad de técnicas instrumentales y metodologías que han sido utilizadas durante el desarrollo de la extensa labor experimental asociada a esta Tesis.

3. Los resultados obtenidos han puesto de manifiesto la necesidad de diseñar un catalizador a medida para cada tipo de proceso de interés. Asimismo, el doctorando ha establecido interesantes relaciones estructura-actividad que han arrojado más luz acerca de los procesos estudiados. Así, por ejemplo, mediante la síntesis de nanopartículas metálicas mediante el método de microemulsión, ha logrado un mejor control del tamaño de partícula. Sus resultados en el proceso de hidrogenolisis del glicerol han mostrado aspectos relevantes como la influencia del metal tanto en el proceso de deshidratación del glicerol a acetol como en la posterior hidrogenación de éste a 1,2-PDO. Además, pudo obtener una anormalmente alta selectividad a acetol debido a la presencia residual de surfactante, que podría de algún modo inhibir o desactivar la capacidad hidrogenante del metal. En el proceso de *Fischer-Tropsch,* pudo relacionar la actividad catalítica con aspectos como la presencia de especies reducidas de cobalto (Co^0) y de interacciones Co-TiO_2, este último empleado como soporte. Finalmente, en el caso de la hidrogenación enantioselectiva de piruvato a lactato de etilo sobre sistemas de platino soportado, describió un aditivo, la 4-hidroxi-D-(-)-fenilglicina que puede aumentar el exceso enantiomérico a bajo contenido de alcaloide tipo cinchona, evidenciando mediante UV-Vis la existencia de interacciones sustrato-modificador-aditivo en disolución.

4. Como resultado de la labor desarrollada directamente relacionada con la presente Tesis, se han presentado 7 comunicaciones a congresos nacionales y 8 a internacionales y publicado tres artículos científicos en la prestigiosa revista

Catalysis Today, fruto de la colaboración con los equipos de la Doctoras Magali Boutonnet (KTH, Estocolmo, Suecia) y Catherine Pinel (IRCELYON, Francia), en el marco de la Acción COST CM0903:

- V. Montes, M. Checa, A. Marinas, M. Boutonnet , J.M. Marinas, F. J. Urbano, S. Järas, C. Pinel, *Synthesis of different ZnO-supported metal systems through microemulsion technique and application to catalytic transformation of glycerol to acetol and 1,2-propanediol*, Catalysis Today, 223 (2014) 129-137.

- V. Montes, M. Boutonnet, S. Järas, A. Marinas, J.M. Marinas, F. J. Urbano, *Selective transformation of glycerol into 1,2-propanediol on several Pt/ZnO solids: further insight into the role and origin of catalyst acidity*, Catalysis Today, en prensa, DOI: http://dx.doi.org/10.1016/j.cattod.2014.11.014

- V. Montes, M. Boutonnet, S. Järas, M. Lualdi, A. Marinas, J.M. Marinas, F. J. Urbano, M. Mora, *Preparation and characterization of Pt-modified Co-based catalysts through the microemulsion technique. Preliminary results on the Fischer-Tropsch synthesis*, Catalysis Today, 223 (2014) 66-75

Esto ha permitido la presentación de la presente Memoria como compendio de artículos.

5. El doctorando ha participado activamente en el proyecto COST CM0903 sobre "*Utilisation of biomass for sustainable fuels and chemicals*", en el que han participado científicos de 26 países diferentes. Gracias a dicha Acción europea, pudo realizar dos estancias de 3 meses cada una en el KTH de Estocolmo (Suecia) bajo la supervisión de la Dra. Magali Boutonnet. Fruto de dicha estancia, se ha familiarizado con la síntesis de materiales mediante el proceso de microemulsión y con el proceso de *Fischer-Tropsch*. Se trata de dos campos en los que nuestro grupo investigador no tenía experiencia previa, lo que ha contribuido a ampliar el

abanico de procesos de catálisis heterogénea en la que trabajamos. Además, esto le ha permitido presentar la presente Memoria como Doctorado Internacional.
Por todo ello, se autoriza la presentación de la Tesis Doctoral.

Córdoba, 12 de Enero de 2015

Firma de los directores

Fdo.: Alberto Marinas Aramendía Fdo.: Francisco José Urbano Navarro

D. Antonio Ángel Romero Reyes, Director del Departamento de Química Orgánica de la Universidad de Córdoba

CERTIFICA:

Que el presente Trabajo de Investigación Titulado "**DISEÑO DE SISTEMAS METÁLICOS SOPORTADOS PARA REACCIONES DE HIDROGENACIÓN DE INTERÉS INDUSTRIAL**" que constituye la Memoria presentada por Vicente Montes Jiménez para optar al Grado de Doctor en Ciencias, ha sido realizado en los laboratorios del Departamento de Química Orgánica, bajo la dirección de D. Alberto Marinas Aramendía y D.Francisco Urbano Navarro.

Y para que conste, firmo el presente certificado en Córdoba a 14 de Enero de 2015.

Fdo: Antonio Ángel Romero Reyes

Las investigaciones realizadas en la presente Memoria de tesis forman parte de un Plan de Investigación desarrollado por el grupo de investigación FQM-162 del PAIDI, subvencionado con cargo a los Proyectos de excelencia P07-FQM-02695, P08-FQM-03931 y P09-FQM-04781 de la Consejería de Innovación, Ciencia y Empresa de la Junta de Andalucia, cofinanciados con fondos FEDER. Asimismo, la Acción Cost CM0903 ha concedido dos becas para la realización de dos estancias cortas en el "*Departament of Chemical Technology*" del KTH, Estocolmo, Suecia permitiendo, de esta forma, cumplir con los requisitos para optar a la mención internacional.

Agradecimientos

En medio de un sinfín de prisas y nervios que conlleva la finalización de una Tesis Doctoral, uno encuentra un momento para sosegarse y echar la vista atrás; es entonces cuando se sorprende de la cantidad de personas que, de una forma u otra, han puesto su granito de arena para que dicha Tesis haya llegado a buen término.

En primer lugar y de forma especial, quiero expresar un enorme agradecimiento a mis directores, los profesores Dr. D. Alberto Marinas Aramendía y Dr. D. Francisco J. Urbano Navarro. Quiero agradecerles el apoyo y la enorme paciencia en la difícil tarea de iniciarme en el mundo de la investigación. Gracias por enseñarme a aprender.

A D. Jose María Marinas Rubio, quiero agradecerle especialmente la confianza que depositó en mí desde el principio, y el apoyo que ha sido hasta el final. Además junto a Dña. María Angeles Aramendía, su mano derecha, consiguieron inculcarme uno de los pilares fundamentales de la ciencia: la perseverancia. Mil gracias.

A Magali Boutonnet por darme la oportunidad de realizar dos estancias cortas en el Departamento de Tecnología Química del KTH, Estocolmo. Allí me enseñó muchas cosas sobre microemulsión y Fischer-Tropsh, pero sobre todo me enseñó a abrirme al mundo a través de colaboraciones científicas. Muchísimas gracias.

A todos los miembros del Departamento de Química Orgánica de la Universidad de Córdoba, Antonio Angel, Campelo, Victor, Angel, Feli, Rafa Luque, Diego Luna, César, Rafa Arrebola, Paco Romero, Pablo y Rafael Barbudo

agradecerles su amabilidad y profesionalidad en los muchísimos momentos compartidos tanto dentro como fuera del laboratorio.

Al personal del S.C.A.I. agradecerles las enseñanzas, consejos y correcciones.

Sin lugar a duda, uno de los grandes éxitos de este periodo ha sido que comencé a dar mis primeros modestos pasos en el laboratorio con muchos compañeros becarios, y he terminado con muy buenos experimentos gracias a maravillosos amigos. Fran, Checa, Lucrecia, Kaquisco y Elena, con los que he compartido mucho más que una línea de investigación. Susana, que me daba la guerrilla, que animaba los días y me impulsaba a ser mejor. Fátima, que es un ejemplo de esfuerzo y autosuperación; Marisa, que nunca ha escatimado su ayuda.

A las últimas incorporaciones, Rafa, Alfonso, Juan, Carlos y Dani. A muchos que ya no están entre las filas del Departamento, como Pineda, Yimo, Ojeda, Silvia, Manolo Mora, Rafa Navarro, Dolo, M José, Cristóbal. A muchos visitantes que han dejado huella: Selvin, Diego, "Polacos", "Americanas"…. Todos y cada uno de ellos, cada cual a su modo, me han ayudado y enseñado su particular forma de ver y hacer ciencia.

De igual forma yo fui "el extranjero" en el KTH, Suecia, en dos ocasiones, gracias a las cuales conseguí una visión distinta y complementaria tanto de la ciencia como de la vida. Allí encontré a grandísimas personas como Jorge, Fátima, Francesco, Matteo, Rodri, Barri, Robert, Sara, Moa y Angelica. Gracias por hacer de mis estancias unas experiencias increíbles e inolvidables.

Debo agradecer a toda mi familia y amigos su apoyo incondicional y su empeño en que yo tenía que llegar a ser Doctor, dándome empujones de moral, especialmente a mi hermana, por su enorme paciencia conmigo. A todos, muchas gracias por haber sido un gran apoyo en momentos buenos, y aún mucho mejor en los malos.

A Darío, Celia, Jaime, Carmen y José Angel por no entender el significado “de no puedo, que tengo que trabajar” y a los que espero poder mostrarles algún día lo bonita que puede ser la ciencia.

Me resulta imposible expresar la gratitud y todo lo que debo a Lorena, mi vida, que gracias a mi y a mi carrera, ha sufrido enfados que no tenían nada que ver con ella y los respondía con una sonrisa y un relájate; ha sufrido falta de atención y me devolvía el doble de lo que yo le debía, y aún así está dispuesta a seguir a mi lado lejos de su tierra. Gracias a ella me veo aquí, ya que me ha apoyado en las incontables ocasiones que yo miraba lo que me perdía con otras opciones y me cuestionaba mi carrera. Para empezar, infinitas gracias.

A mis padres, que con su cariño y apoyo incondicional son los verdaderos responsables de que haya conseguido llegar hasta aquí; sin ellos no hubiera logrado un ápice ni de lo que tengo, ni de lo que soy.

Indice General

Introducción

Capítulo 1

1-Introducción

1.1-Preámbulo

1.2-Química verde

1.3-Catálisis

1.4-Hidrogenación

-A) Hidrogenolisis del glicerol (Capítulo 2, artículos 1 y 2)

-B) Proceso Fischer Trospsch (Capítulo 3, artículo 3)

-C) Hidrogenación enantioselectiva del piruvato al lactato de etilo (capítulo 4)

-D) Hidrogenación quimioselectiva del crotonaldehido a alcohol crotílico (capítulo 5)

1.5- Referencias

1.1-Preámbulo

Las cuestiones medioambientales están cobrando mucha importancia en nuestra vida cotidiana. Cada día, los medios informativos narran noticias relacionadas con temas como las energías renovables, el agujero en la capa de ozono, el cambio climático, la contaminación de las aguas, desastres medioambientales, el reciclado… Esto incrementa la concienciación de la sociedad de los graves problemas medioambientales existentes hoy día en nuestro planeta y favorece un cambio en la actitud de las personas hacia el medio ambiente. Aunque difícilmente la sociedad está dispuesta a renunciar al estilo de vida que actualmente mantiene, exigiendo niveles de calidad iguales o superiores a los actualmente disponibles. Ligado a esta tendencia, desde los principales órganos administrativos, se está promoviendo el desarrollo de soluciones mediante financiación de proyectos científicos relacionados con estas temáticas, como es el proyecto de excelencia de la Junta de Andalucía en el cual se enmarca el presente trabajo de Tesis Doctoral, P09-FQM-4781 titulado "*catalizadores sólidos para procesos de síntesis orgánica en el contexto de la Química Verde (Química Sostenible)".*

La concienciación social y política sobre un futuro más sostenible, conjuntamente con el aumento de la demanda energética, han creado una importante necesidad de buscar tecnologías y materias primas alternativas más benévolas con el medio ambiente que las actualmente existentes.

Traducido a nivel científico, son muy numerosos los avances que se están llevando a cabo en diversas áreas del conocimiento, desde la ingeniería industrial hasta las ciencias puras. El campo de la Química ha sido uno de los que ha experimentado un mayor progreso, permitiendo desarrollar nuevos materiales y procedimientos que protegen el medio ambiente, además de conservar la calidad y propiedades de los productos, permitiendo así al ciudadano preservar el estilo de vida que desea. Esto es gracias a que en las últimas décadas, durante el desarrollo tecnológico, no sólo se han premiado los resultados de las investigaciones sino que

al mismo tiempo se ha exigido la adecuación de los procesos al medio ambiente. A finales de los años 1990 se acuñó el concepto de Química Verde, la cual vela por la protección del medio ambiente postulando doce principios a seguir por los químicos. Posteriormente, considerando el aspecto económico, se introdujo el término genérico de Química Sostenible, que considera la triple vertiente social, medioambiental y económica que debe considerarse al diseñar un proceso químico. No obstante, en adelante, emplearemos cualquiera de los términos indistintamente.

Por otro lado, el problema del tratamiento de los residuos que se generan en los distintos sectores industriales junto con la deficiencia de materias primas ha hecho que se estudie la posibilidad de valorizar dichos residuos. En este sentido, la biomasa, con una producción anual estimada de 10^{11} toneladas, de las cuales sólo el 3% se cultiva, cosecha y emplea, presenta, indudablemente, un tremendo potencial.

Además, la biomasa se presenta como la única fuente sostenible de productos químicos alternativa a los combustibles fósiles. Otra ventaja de la utilización de la biomasa como materia prima, está relacionada con la presencia de un alto contenido en heteroátomos (O, N,…) en los compuestos presentes en la misma, lo que posibilita un sinfín de transformaciones a compuestos oxigenados y/o nitrogenados sin la necesidad de cambios significativos de entalpía en los sistemas, permitiendo, por tanto, un importante ahorro energético.

Así mismo, a menudo, al hablar de la biomasa y en contraposición al petróleo u otros combustibles fósiles, se indica que no contribuye de modo significativo al aumento del CO_2. Con esto se quiere indicar que, por ejemplo, si bien en el proceso de combustión de la misma se genera CO_2, ese gas fue previamente fijado por la planta en su ciclo fotosintético. La producción de compuestos químicos y materiales a partir de la biomasa (en concreto la de "segunda generación", que no compite con la alimentación) es otro de los desafíos de la química para el siglo XXI, con el objeto de valorizar un recurso a nuestro alcance.

En la presente Memoria, la valorización de la biomasa ha estado enmarcada dentro de una iniciativa europea, la **Acción COST CM0903, "Utilisation of Biomass for Sustainable Fuels and Chemicals (UBIOCHEM)".** Esta tenía como principal objetivo la utilización de la biomasa para la generación de combustibles y productos químicos sostenibles (o sustentables). Han colaborado equipos de investigación de 26 países, los cuales se subdividían en cuatro grupos para atender los distintos objetivos pretendidos con dicha acción.

WG1: Conversión primaria de la lignocelulosa

WG2: Conversión de la biomasa en energía

WG3: Conversión de la biomasa en materiales

WG4: Valorización de "moléculas plataforma"

El plan general de trabajo queda resumido en la Figura 1.1 Esta muestra cómo a partir de lignocelulosa se puede alcanzar una gran variedad de productos químicos o combustibles.

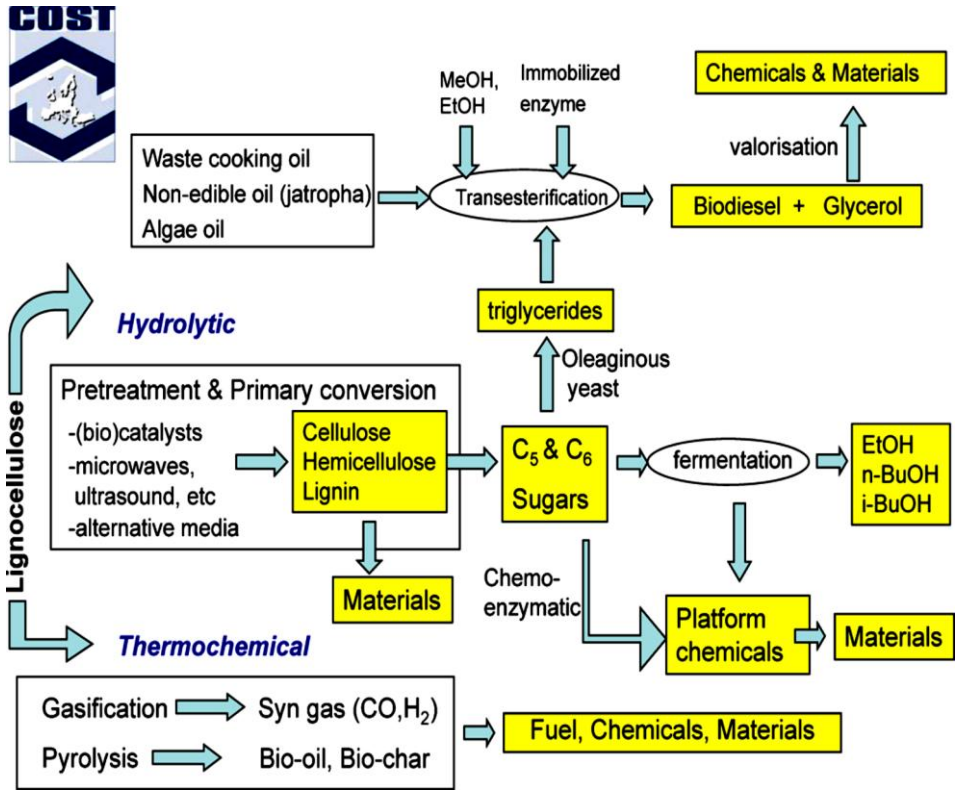

Figura 1.1 *Representación esquemática de los principales procesos involucrados en la Acción COST CM0903.*

Durante la presente tesis doctoral se han realizado dos estancias en el centro tecnológico del KTH de Estocolmo gracias a dicha Acción COST, en las cuales se ha trabajado en la valorización del glicerol mediante hidrogenolisis (WG4), y en el proceso *Fischer-Tropsch* (WG2). Las investigaciones realizadas forman parte de los capítulos 2 y 3, respectivamente.

1.2-Química verde

La química verde se define como el desarrollo, diseño y aplicación de productos químicos y procesos para reducir o eliminar el uso y la generación de sustancias peligrosas. La química verde no se diferencia de la química tradicional en tanto y cuanto requiere la misma creatividad e innovación que siempre ha sido esencial en la química y en el desarrollo tecnológico en general. No obstante, históricamente, los químicos sintéticos no han tenido los temas medioambientales como una de sus mayores prioridades; tal es así que tradicionalmente la palabra química denotaba algo malo en el lenguaje común.

Anastas *y* Warner [1] se consideran los padres de la química verde y en 1998 enunciaron los "doce principios de la química verde". Dichos principios sirven como guía para la práctica y desarrollo de una química sostenible y, además, ayudan en la evaluación de cuán verde es una tecnología, proceso, síntesis o compuesto químico. Los doce principios se refieren a:

- Prevención de residuos/subproductos.
- Incorporación máxima de reactivos en el producto final (*Factor E* lo más bajo posible).
- Prevención o minimización de productos peligrosos.
- Diseño de compuestos químicos más seguros.
- Minimización del requerimiento energético.
- Selección del disolvente más apropiado.
- Selección de los productos de partida más idóneos.
- Supresión del uso de grupos protectores.
- Empleo de catalizadores.
- Obtención de productos biodegradables.
- Diseño de plantas industriales que eliminen las posibilidades de accidentes durante las operaciones.

- Mayor empleo de técnicas analíticas para controlar la formación de compuestos peligrosos.

Claramente el mensaje de estas reglas es que hay que primar la prevención de la contaminación frente a la subsanación una vez ya está hecha.

Un clarísimo ejemplo de evaluación de la contaminación a raíz de estos principios, es el *factor E* (kg de subproductos generados por kg de producto deseado), el cual fue introducido por Roger Sheldon, Profesor emérito de la Universidad Tecnológica de Delft [2]. Teniendo en cuenta únicamente este factor, la industria "más limpia" sería la del Petróleo, con un *factor E* menor de 0,1. En el extremo opuesto se situaría la Industria Farmacéutica con unos valores de *factor E* que pueden ir de 25 a más de 100. Obviamente no se puede medir el nivel de contaminación de un proceso o producto únicamente con este factor, ya que intervienen otros aspectos como la toxicidad de los subproductos, en qué se transforman una vez usados, el nivel de producción… No obstante, el *factor E* sí que da una idea del nivel de rendimiento obtenido de la materia prima.

Otro de los objetivos que se ha de tener en cuenta es la viabilidad económica del proceso o compuesto químico desarrollado, ya que de esto dependerá la aplicabilidad industrial. Con la introducción del término económico se pasa a hablar de "química sustentable" [3]. Así, la química sustentable necesita tener en cuenta numerosos aspectos como la posibilidad de la implantación industrial, evaluación de la toxicidad de los subproductos, estudio de la viabilidad económica, uso de materias primas existentes en cantidad suficiente para el proceso a desarrollar, impactos ambientales… En consecuencia, esto implica la integración de multitud de disciplinas: ingeniería, química, biología, ciencias económicas… La importancia creciente de la química verde/sostenible queda reflejada en la evolución de las publicaciones relacionadas con el tema, tal y como puede verse reflejado en la Figura 1.2.

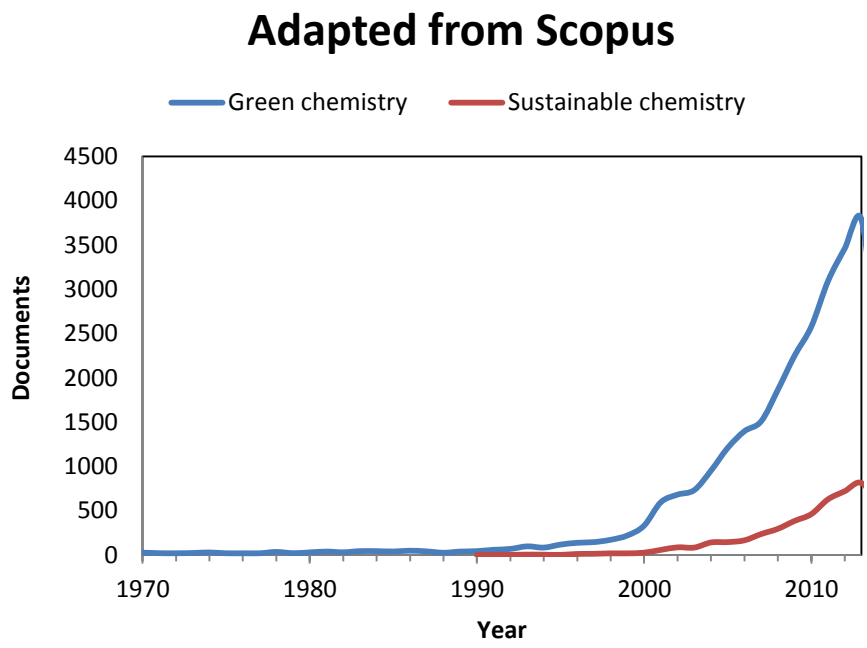

Figura 1.2 *Número de documentos publicados por año con la palabra clave "Green Chemistry" o " Sustainable Chemistry". Fuente SCOPUS (período 1970-2013).*

De hecho, existen revistas especializadas sobre la temática con un alto índice de impacto, como Green Chemistry o ChemSusChem.

El grado de implicación de las distintas nacionalidades con la química verde queda reflejado en la Figura 1.3 Es posible ver cómo España está dentro de los puestos de cabeza, dejando claro el gran esfuerzo y dedicación de nuestro país en este campo. Tal es así que en 2003 se fundó la Red Española de Química Sostenible (REDQS). La Red Española de Química Sostenible surge como una iniciativa de profesores e investigadores jóvenes y entusiastas. La mayoría de los socios de la REDQS son científicos que desarrollan su actividad en universidades, institutos de investigación, e industrias químicas. Así, el objetivo de la tesis encaja

dentro de la estrategia de España, siendo, además, un paso más en la intensa investigación del grupo de investigación en la Química Verde/Sostenible.

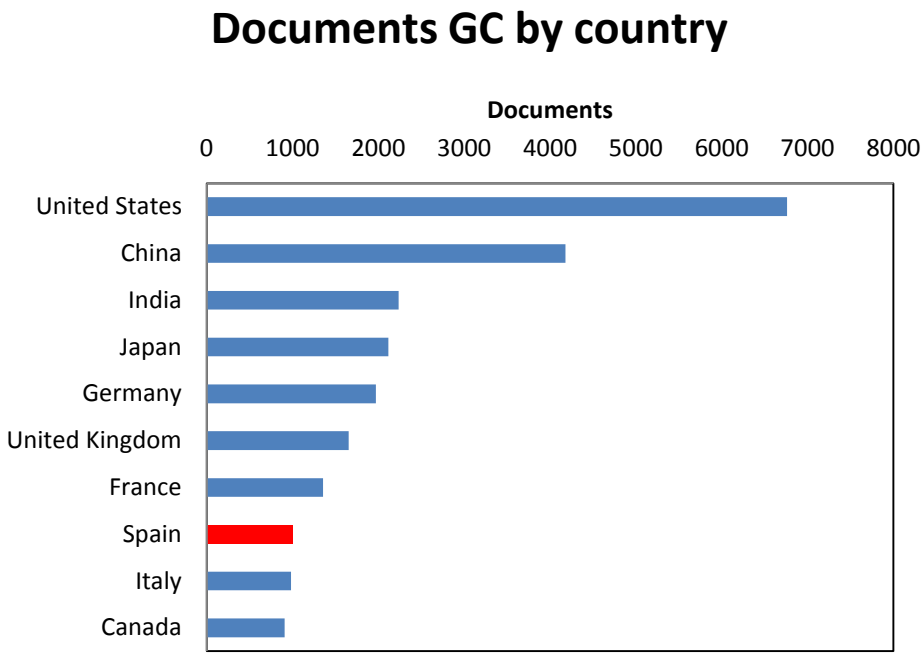

Figura 1.3 *Número de documentos publicados sobre Química Verde por los diferentes países entre 1970 y 2013, basado en una búsqueda en SCOPUS.*

Los desafíos para el futuro a los que se enfrenta la química verde son tan numerosos que es inviable discutir en detalle todos y cada uno de ellos. Epicoco y col. [4] apuntan a que se deben abordar varios tipos de cambios, desde el punto de vista científico, político y social.

Entre los desafíos desde el punto de vista científico, se encuentra la necesidad de diseñar procesos y materiales aún más selectivos y que no supongan

un riesgo para el medioambiente ni para la salud humana. El descubrimiento de dicha tecnología medioambientalmente benigna no garantiza su aplicación a escala industrial. Existe un gran número de barreras que dicha tecnología tiene que pasar para ser aplicable a escala industrial. Una de las más condicionantes es que ha de ser económicamente viable, con lo que este punto debería ser tenido en cuenta en el curso de la investigación y desarrollo.

Desde el punto de vista medioambiental, el crecimiento de la química verde necesita ser acelerado y fomentado a escala industrial. Para ello es imprescindible que los doce principios de la química verde sean incorporados al día a día en las investigaciones y procesos [5].

Finalmente, el desarrollo y todos los esfuerzos por parte de los científicos necesitan llevar aparejados una mayor concienciación, implicación y participación por parte de la sociedad. En este sentido, resultan claves el consumo responsable, el reciclado o la denuncia de los delitos medioambientales.

1.3-Catálisis

La importancia de la catálisis dentro la química queda demostrada por los innumerables procesos químicos, tanto a escala de laboratorio como a nivel industrial, en los que es utilizada. Una gran variedad de productos tales como medicamentos, polímeros, fibras, combustibles, pinturas, lubricantes y otros productos químicos de alto valor añadido no serían posibles sin el empleo de catalizadores. Se estima que el 90% de todos los procesos industriales usa algún tipo de catalizador en alguno de los distintos pasos del proceso [6]. Si bien el 9º principio se refiere de manera expresa al uso de catalizadores, de una u otra forma, la catálisis está implicada en la mayor parte de los 12 principios, hasta el punto de que Anastas y col. se refieren a esta disciplina como el pilar fundamental de la Química Verde [7]. Con todo esto en las últimas décadas el diseño de catalizadores altamente activos y selectivos ha experimentado un gran auge.

Los catalizadores homogéneos presentan una gran variedad de aplicaciones, con selectividades muy altas a los productos deseados y con gran reproducibilidad. Sin embargo, la dificultad de separar un catalizador homogéneo de los productos de reacción ha hecho que químicos e ingenieros hayan investigado una gran variedad de estrategias para poder solucionar dicho problema. Entre las distintas soluciones, el uso de catalizadores heterogéneos aparece como una de las opciones más lógica. Los catalizadores heterogéneos ofrecen la oportunidad de diseñar un catalizador de acuerdo a los requerimientos de una reacción. Permiten el uso de una gran variedad de grupos activos, como ácidos o bases tipo Brönsted o Lewis [8], centros redox [9], metálicos, etc. Además ofrecen la posibilidad de discriminación por tamaño de poro, facilitando el acceso de moléculas concretas a los sitios activos [10]. Presentan numerosas ventajas para la industria química entre las que cabe destacar:

1. Fácil separación del catalizador de los reactivos y/o productos.
2. Fácil reciclado del propio catalizador.

3. Menor contaminación del producto por el catalizador.
4. Fácil adaptabilidad a un proceso en flujo continuo.

Por todo ello, existe un gran interés en la industria química en reemplazar los catalizadores homogéneos por catalizadores heterogéneos. En las últimas décadas, dentro de la catálisis heterogénea se ha desarrollado la nanociencia o nanotecnología. Un nanomaterial puede definirse como un material que posee una estructura en la que al menos una de sus fases tiene una o más de sus dimensiones en el rango de los nanómetros (1-100 nm). El empleo de estos nanomateriales en catálisis ha surgido como una alternativa interesante a los materiales convencionales ya que, debido a su pequeño tamaño, se incrementa el área superficial expuesta de la fase activa como muestra la Figura1.4, aumentando así el contacto entre los reactivos y el catalizador, imitando el comportamiento de un catalizador homogéneo [11].

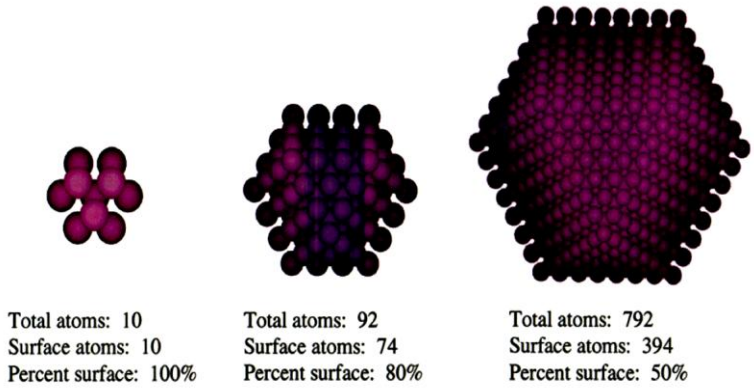

Figura 1.4 *Superficie expuesta del metal en función del tamaño de partícula [11].*

Sin embargo, este pequeño tamaño y alta superficie les confiere una gran inestabilidad debido a sus elevadas energías superficiales, de tal forma que tienden a agregarse con objeto de estabilizarse. Así, su principal ventaja se convierte a su vez en una de las principales razones por la que este tipo de catalizadores pierde gradualmente actividad catalítica o alcanza su completa desactivación.

La continua y creciente creación de empresas relacionadas con la nanotecnología y lo catalizadores deja patente la importancia del tema. El mercado de nano-partículas ha crecido rápidamente, desde 147 billones de dólares en 2007 a 3.1 trillones previstos para 2015. Tal ha sido el crecimiento que la Unión Europea ha dedicado un total de 14 millones de € a un proyecto llamado Sun (http://www.sun-fp7.eu/) para estudiar los posibles riesgos del uso de las nanopartículas [12].

1.4-Hidrogenación

En 1897 Paul Sabatier observó que la presencia de Ni en el medio de reacción facilitaba la adición de hidrógeno a moléculas orgánicas. En 1912 obtuvo el Premio Nobel en por "su método de hidrogenación de compuestos orgánicos en presencia de metales finamente divididos". Desde entonces, el conocimiento en el campo de las hidrogenaciones ha crecido continuamente.

Se investigó cuál era el papel del metal a nanoescala y pronto se descubrió que es generar hidrogeno atómico. A diferencia de la, en comparación, relativamente "inerte" molécula de hidrogeno, H_2, el hidrógeno atómico adsorbido sobre la superficie del metal es altamente reactivo y puede fácilmente ser adicionado a varios enlaces insaturados: C=C, C=O, C=N, etc. Así, el uso de catalizadores metálicos en forma de nanopartículas soportadas se ha convertido en habitual para este tipo de procesos.

El uso del hidrógeno, H_2, está ampliamente extendido entre los diversos sectores industriales. Esto encuentra su razón de ser en que la hidrogenación es un proceso ampliamente utilizado por la Industria Química Pesada y Petroquímica, así como en la Industria Alimentaria, Farmacéutica y las basadas en Química Fina. Los usos tecnológicos del H_2 a mayor escala son la hidrogenación y la hidrogenolisis.

Algunos ejemplos son:

-Hidrogenolisis e hidrogenaciones en la industria petroquímica.

-Hidrogenaciones de compuestos orgánicos insaturados, como alquenos, aldehídos, cetonas y nitrilos especialmente de interés en química fina.

-Hidrogenaciones de aceites vegetales y de pescado.

-La hidrogenación de nitrógeno para dar amoníaco, que se realiza a gran escala por el proceso de Haber-Bosch.

Teniendo en cuenta la gran experiencia del grupo FQM-162, en el cual se ha desarrollado el trabajo de investigación de la tesis, en reacciones de hidrogenación y uniéndolo a los temas candentes de la química verde, catálisis y nano-materiales, se plantea el objetivo de la tesis que es la síntesis y mejora de catalizadores en reacciones mediadas por hidrógeno de interés industrial. Dentro de todos los procesos mencionados, en el presente trabajo de tesis se aborda:

Hidrogenolisis del glicerol (capítulo 2): El glicerol es el principal subproducto de la bio-refinería, con lo que se produce en enormes cantidades lo que nos lleva a la necesidad de buscar nuevas aplicaciones.

Proceso *Fischer-Tropsch* (capítulo 3): Uno de los procesos de la industria petroquímica que usa el H_2 es el conocido como síntesis tipo *Fischer-Tropsch*. Es una tecnología implantada a nivel industrial para la obtención de cadenas

hidrocarbonadas a partir de gas de síntesis (CO y H_2). Existen compañías muy fuertes en el sector e industrias que producen millones de toneladas anuales usando este tipo de tecnología. Hoy día, además, se está postulando como una de las posibles vías para el aprovechamiento de la biomasa.

Hidrogenaciones de grupos carbonílicos quimio y enantioselectiva (capítulos 5 y 4, respectivamente): En lo relacionado con la industria de química fina y farmacéutica, la hidrogenación selectiva de un doble enlace en presencia de otros grupos también susceptibles de ser hidrogenados es un tema de especial interés. También lo es la obtención de un enantiómero frente a otro. Este tipo de procesos tiene un *factor E* muy alto lo que eleva el costo del producto tanto a nivel económico como medioambiental.

1.4. A-Hidrogenolisis del glicerol

Durante los últimos años, los investigadores han dirigido sus esfuerzos hacia la protección del medio ambiente y al desarrollo de procesos sostenibles con el entorno. Esta tendencia ha conducido a avances importantes en temas como los biocombustibles (biogás, biodiésel,…). El biodiesel puede obtenerse por transesterificación de aceites vegetales con metanol, dando lugar a los ésteres metílicos de los ácidos grasos (biodiesel) y glicerol (o glicerina) como subproducto.

El glicerol obtenido viene acompañado de diversas moléculas disueltas e impurezas y, tras su purificación, se ha venido utilizando directamente en alimentación, farmacia, cosmética y productos de higiene personal. No obstante, su elevada producción a partir de las biorefinerías (10 Kg de glicerol por cada 100Kg de biodiesel) ha impulsado la búsqueda de nuevas aplicaciones.

El glicerol es una molécula presente en la biomasa y altamente funcionalizada. Aunque es una molécula muy estable, posee tres grupos OH y puede ser empleada para sintetizar una amplia gama de productos químicos. Tanto es así que es incluida en diversas listas como "molécula plataforma" (Tabla 1.1), esto es, molécula que puede ser obtenida con relativa facilidad a partir de la biomasa y, por tanto, cuya valorización resulta especialmente interesante [13, 14].

Building Blocks
1,4 succinic, fumaric and malic acids
2,5 furan dicarboxylic acid
3 hydroxy propionic acid
aspartic acid
glucaric acid
glutamic acid
itaconic acid
levulinic acid
3-hydroxybutyrolactone
glycerol
sorbitol
xylitol/arabinitol

Tabla 1.1 *Algunas moléculas plataforma obtenidas a partir de biomasa (fundamentalmente de carbohidratos) [13]***.**

Los diferentes procesos químicos que se han empleado en la valorización del glicerol pasan por su reformado en fase acuosa, polimerización, fermentación, deshidratación, eterificación, esterificación, oxidación selectiva e hidrogenolisis [15]. El número de publicaciones relacionadas con la transformación del glicerol ha crecido, especialmente en la última década. Muy desde el comienzo, la mayoría de los trabajos se han centrado en el estudio de los procesos de oxidación del glicerol, ya que al tener grupos OH y ser el H un buen grupo saliente era una opción lógica. Aunque últimamente se observa un claro aumento en el número de publicaciones relacionadas con la hidrogenolisis.

Los principales productos de interés obtenidos en el proceso de hidrogenolisis son el acetol, el 1,3-propanodiol (1,3-PDO) y el 1,2- propanodiol o propilenglicol (1,2-PDO ó PG).

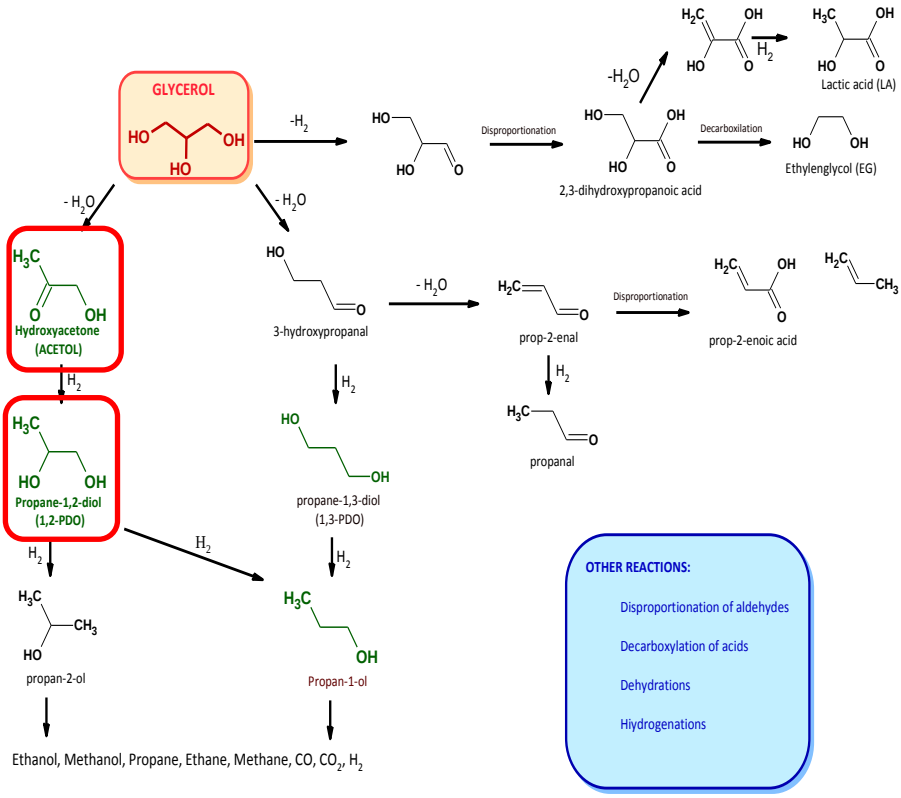

Figura 1.5 *Algunas posibles transformaciones catalizadas del glicerol bajo atmósfera inerte o de H_2 [16]. Los compuestos señalados son los principales productos obtenidos en los artículos 1 y 2.*

El acetol es una molécula muy usada como intermedio en la síntesis de otros compuestos orgánicos, en la industria alimentaria para dar aroma, en textil y en cosmética (productos de bronceado). Los usos típicos del 1,2-PDO se centran en la síntesis de resinas de poliéster insaturadas, fluidos funcionales, productos farmacéuticos y cosméticos, pinturas, etc. Por otro lado, el 1,3-PDO se emplea fundamentalmente en la producción de poliésteres mediante co-polimerización con ácido tereftálico. Ambos compuestos se han producido tradicionalmente a partir de derivados del petróleo como el óxido de propileno (1,2-PDO) o la acroleína (1,3-PDO), mediante transformaciones químicas catalizadas. En el caso del 1,3-PDO, la

colaboración entre DuPont y Genencor ha conducido al desarrollo de un método enzimático para su obtención [17]. Para el 1,2-PDO no hay, sin embargo, una ruta enzimática hasta el momento.

Marinas y col. comparan la ruta tradicional desde los recursos fósiles para la obtención del 1,2-PDO con la obtención via hidrogenolisis desde el glicerol, concluyendo que esta última ruta puede resultar competitiva con respecto a la primera [18].

A pesar de los esfuerzos realizados por la comunidad científica, la aplicación de esta reacción potencialmente importante a escala industrial presenta una serie de desventajas. Una de estas limitaciones es la utilización de elevadas presiones y temperaturas que, finalmente, se traducen en un equipamiento con un elevado coste. Las presiones de hidrógeno típicas para estos experimentos se sitúan entre 1 y 10 MPa (aunque se puede llegar hasta 35 MPa) y las temperaturas en el intervalo 120-250ºC (o incluso superiores) [16, 19-29]. Una desventaja adicional es la necesidad de utilizar disoluciones diluidas de glicerol, del orden del 1-30% en peso, lo que aumenta el consumo energético del proceso disminuyendo la rentabilidad del mismo. Finalmente, otro problema del proceso es la baja selectividad hacia los productos de interés, debido a un elevado rendimiento a otros productos como etilenglicol, CO_2, e infinidad de compuestos poliméricos. Los esfuerzos investigadores se centran, por tanto, en desarrollar tecnologías que permitan llevar a cabo el proceso a menores temperaturas y presiones, empleando glicerol concentrado y con selectividades mejoradas a los compuestos de interés (acetol, 1,2-PDO…).

En trabajos previos de nuestro grupo de investigación en colaboración con el de la Dra. Catherine Pinel (Lyon, France) se sintetizaron varios catalizadores de metales nobles, Pt, Pd, Au y Rh sobre óxido de zinc consiguiendo resultados prometedores [16]. Uno de los principales problemas fue la gran variabilidad del tamaño de partícula entre los distintos metales estudiados. Así se planteó la

necesidad de usar un método sintético que permitiera un mejor control del tamaño de partícula.

En el **artículo 1** se discute en detalle y se usa la microemulsión como método de síntesis de catalizadores.

Posteriormente, a la vista de los resultados obtenidos, en el **artículo 2** nos centramos en el Pt y se aborda la modificación del soporte (ZnO) mediante diferentes agentes dopantes.

1.4 B-Proceso *Fischer-Tropsch*

En el uso de la biomasa como fuente de materia prima se pueden distinguir dos grandes tipos de tendencias. Una es el aprovechamiento de la estructura natural de la biomasa. Así, con procesos que no alteren demasiado la materia, se hace la separación y extracción de los compuestos deseados. En muchos casos no es posible la aplicación de esta filosofía por la dificultad de la separación de los compuestos... Así, la otra alternativa es la completa destrucción en moléculas sencillas y pequeñas (ej. CO o CO_2) para posteriormente usarlas en la síntesis selectiva de la molécula deseada. Esta vía proporciona ventajas con respecto a la primera y es que se pueden obtener una infinidad de productos químicos y sin importar el tipo de biomasa de partida. Una de las rutas más prometedora en este tipo de filosofía es la obtención de los combustibles que hoy día conocemos a partir de la biomasa. El proceso se esquematiza en la figura1.6.

Actualmente esta vía es usada a nivel industrial en países que poseen grandes reservas de gas natural (pero no petróleo) del cual obtener carburantes, con lo que hoy día ya es un proceso industrial a gran escala. Grandes empresas internacionales como Shell o SASOL actualmente cuentan con plantas en funcionamiento en distintos lugares del mundo.

El problema que presenta el uso de la biomasa en este proceso es que la cantidad de materia prima cercana a una gran industria no sería suficiente para abastecerla. Esto hace necesario aumentar el rendimiento de los catalizadores para hacer económicamente viable una industria de dimensiones más reducidas. Por la cantidad que se necesitaría se postula que la biomasa no puede ser un sustituto completo de las fuentes fósiles como materia prima para la obtención de combustibles. Sin embargo, sí que es una vía susceptible para poder ser aplicada para el aprovechamiento de este recurso natural y contribuir con un porcentaje al total consumido.

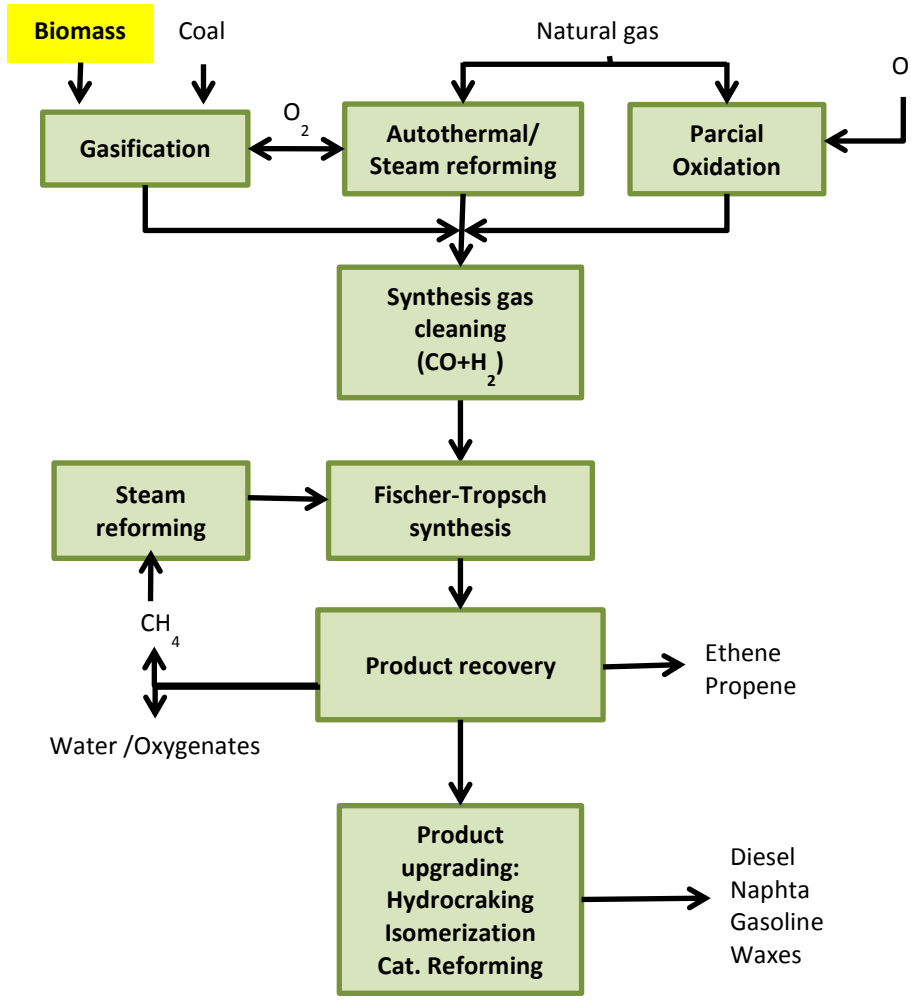

Figura 1.6 *Representación esquemática de una planta para la transformación de la biomasa a energía y carburantes*.

Tanto es así que un informe publicado en KEY WORLD ENERGY STATISTICS 2013 elaborado por la Agencia Internacional de la Energía (IEA) muestra (Figura 1.7) cómo la contribución de la biomasa en la producción de combustibles ha aumentado desde 1973 hasta alcanzar un 5.2% en 2012. Además, pronostica que tanto la producción como el consumo de biocombustibles ha de aumentar con el paso de los años.

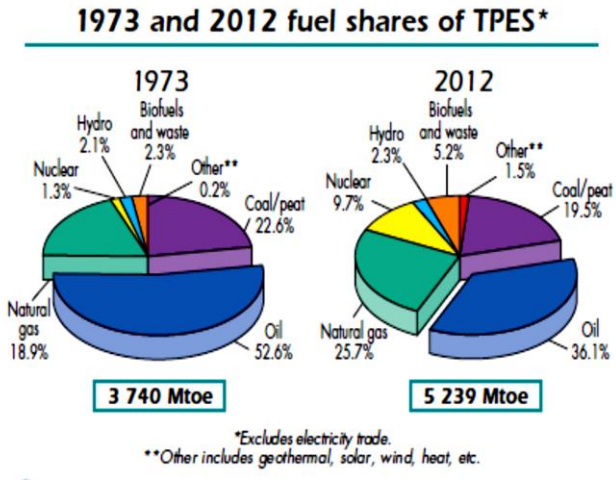

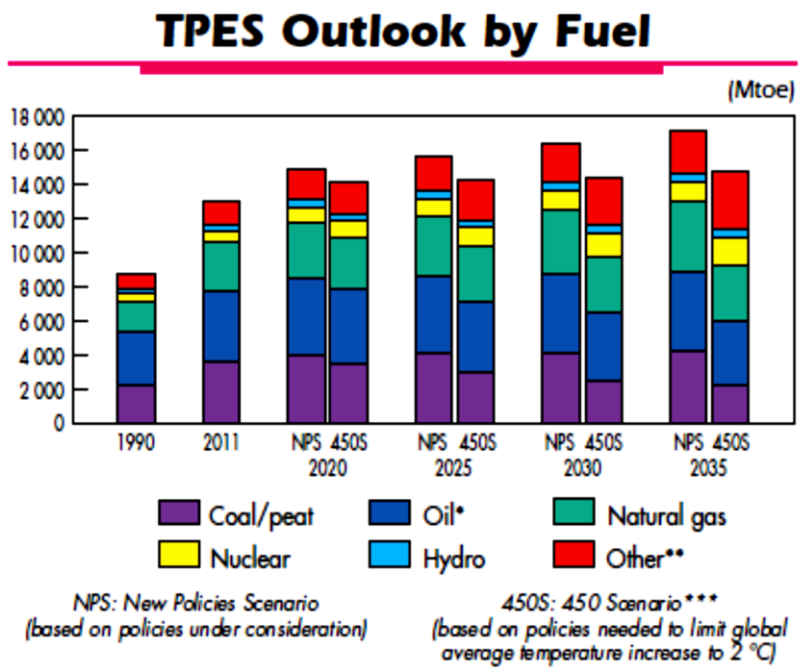

Figura 1.7 *Datos de consumo y procedencia de energía publicados en KEY WORLD ENERGY STATISTICS 2013 elaborado por la Agencia Internacional de la Energía (IEA).*

Además del aprovechamiento de la biomasa como recurso, como se ha comentado con anterioridad, este tipo de tecnología ayudaría a bajar las emisiones de CO_2 a la atmósfera. En este sentido, las previsiones publicadas por este informe para 2035, 37037 Mt de CO_2 están muy lejos de las propuestas por el Scenario 450 (necesidad para no aumentar la temperatura global en 2ºC) que son de 22055Mt de CO_2. Esto deja patente la necesidad de buscar una fuente de combustible renovable y sin emisiones de gases de efecto invernadero.

Entre los procesos de transformación de la biomasa en combustibles, en esta Memoria nos centramos en el proceso *Fischer-Tropsch*. Este usa catalizadores heterogéneos, compuestos por una fase activa de Fe, Co o Ru depositada sobre un soporte [30-34]. Desde el punto de vista práctico, sólo las dos primeras tienen aplicación industrial debido al elevado precio del Ru. Echando un vistazo a la bibliografía, es comúnmente aceptado que existe un tamaño de partícula óptimo, de 8-12nm, para obtener una buena conversión y selectividad a hidrocarburos de cadena larga [35-38]. Además, los catalizadores suelen tener trazas de otros metales para mejorar alguna de sus propiedades. Uno de los casos más estudiado es la adición de metales nobles para mejorar la reducibilidad del catalizador final, aunque hoy día aún el papel del metal noble es un tema de debate [31, 32, 39, 40].

En colaboración con el grupo de Tecnología Química del KTH, el trabajo realizado se basó en una patente desarrollada por dicho grupo de investigación [41] y posteriormente adquirida por SASOL. En ésta se describe la síntesis de catalizadores de Co sobre TiO_2 mediante el método de microemulsión. Este tipo de síntesis permite un buen control del tamaño de partícula, obteniéndose catalizadores muy homogéneos. El **artículo 3 (capítulo 3)** aborda la adición de trazas de Pt durante la síntesis de dichos catalizadores a través de microemulsión.

1.4 C-Hidrogenación enantioselectiva del piruvato al lactato de etilo

La síntesis de compuestos quirales ópticamente puros resulta de interés desde el punto de vista de la Química Verde, al conducir a procesos con un menor *factor E*. Así, resulta deseable la consecución de un proceso con la mayor enantioselectividad posible. Pero es que, además, las propiedades de las moléculas susceptibles de ser empleadas en la Industria Farmacéutica o Agroquímica dependen de su configuración. En la Figura 1.8 se muestran algunos ejemplos, como el de la (R)-asparagina que tiene un sabor dulce mientras que la (S)-asparagina confiere un sabor amargo. De nefasto recuerdo resulta el caso de la talidomida, recetado por primera vez en la década de 1950 en Europa para tratar la ansiedad, el insomnio y, en las mujeres embarazadas, las náuseas y vómitos matutinos. Se retiró a comienzo de la década de 1960 porque se descubrió que producía terribles malformaciones fetales. El isómero R es el responsable de la actividad antiinflamatoria o sedante, mientras que el S lo es de la actividad teratogénica. Cabría pensar en la posibilidad de evitar esos efectos suministrando el isómero R puro. Sin embargo, lamentablemente, el hígado contiene una enzima que lo convierte en S. Hoy en día, la talidomida es empleada para el tratamiento de una complicación de la lepra (el eritema nodoso de la lepra).

Este caso sirvió para dar un toque de atención sobre la importancia del empleo de compuestos enantioméricamente puros. No hemos de olvidar que, en último término, el deseo de obtener una alta enantioselectividad no es sino una tendencia a imitar a la naturaleza. Más del 98% de los productos naturales empleados en droguería son ópticamente puros.

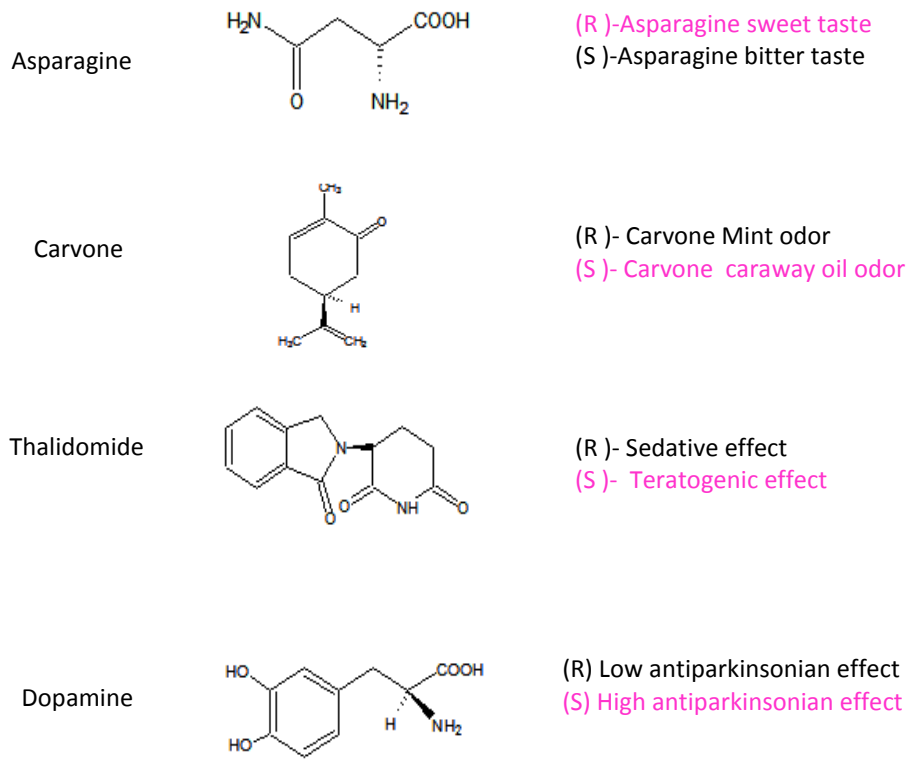

Figura 1.8 *Algunos ejemplos de enantiómeros con diferentes propiedades. Los compuestos marcados en rosa se corresponden con los representados en la fórmula.*

Existen diferentes maneras de llevar a cabo hidrogenaciones quirales en fase heterogénea:

a) Mediante inmovilización de catalizadores homogéneos quirales. A su vez, la inmovilización puede efectuarse mediante enlace covalente, adsorción, formación de pares iónicos o encapsulamiento (“ship-in-a-bottle”).

b) Empleo de polímeros quirales como soportes o catalizadores. Tal es el caso del sistema de paladio soportado sobre fibroína de la seda, empleado por Akabori y col., en 1956, para la obtención de aminas y aminoácidos óptimamente activos.

c) Modificación de catalizadores de hidrogenación clásicos. Esta aproximación consiste en tomar un catalizador que se sabe funciona en esa reacción y modificarlo mediante la adsorción de un compuesto quiral que le inducirá esa quiralidad. Existen descritos fundamentalmente tres sistemas de este tipo:

   c.1. Sistemas de níquel modificado con ácido tartárico, para la hidrogenación quiral de β-cetoesteres y otras cetonas β-funcionalizadas.

   c.2. Sistemas de Pd modificado con alcaloides de la familia de la cinchona (o cincona), para hidrogenar enlaces C=C activados.

   c.3. Sistemas de Pt modificado con alcaloides de la familia de la cincona, para hidrogenar enantioselectivamente cetonas α-funcionalizadas.

En el presente trabajo, adoptaremos la tercera aproximación y más concretamente, nos centraremos en la modificación de sistemas platino, buscando alternativas a los llamados sistemas de Orito.

Esta aproximación consiste en llevar a cabo la reacción con un catalizador y en un disolvente aquirales e inducir la quiralidad con una molécula quiral añadida al medio de reacción sin que ésta se incorpore a los productos. Se trata de un fenómeno bastante complejo pues, además de requerir la adsorción del sustrato proquiral en el catalizador (común a los procesos de catálisis heterogénea), debe co-adsorberse, en las inmediaciones del sustrato el compuesto quiral, que habrá de interaccionar de un modo específico para transferirle esa quiralidad. De ahí la escasez de sistemas descritos hasta la fecha que conduzcan a excesos enantioméricos apreciables, reduciéndose en la práctica, en procesos de reducción, a los tres casos descritos anteriormente.

El catalizador más apropiado es el platino, seguido de iridio y rodio, mientras que el rutenio y el níquel no son efectivos en el proceso. Además es necesario que los tamaños de partícula de dichos catalizadores se sitúen entre 3-6 nm para un óptimo resultado en la reacción [42-44]. Como soporte, se suelen emplear alúmina, sílice y carbón [45-48]. También hay ejemplos de aplicación de zeolitas y materiales mesoporosos de alta superficie específica. No obstante, los sistemas zeolíticos pueden presentar problemas de difusión en el caso de emplear sustratos voluminosos [49, 50]. Los dos sistemas comerciales más empleados, utilizados como referencia, consisten en Pt/Al_2O_3 al 5% en peso (Engelhard 4759) y el JMC 94 de Johnson Matthey. Además, sólo unas pocas moléculas que se pueden encontrar en la naturaleza funcionan como modificadores. En el caso del platino, los mejores resultados corresponden al empleo de alcaloides de la familia de las cinconas. Se ha investigado bastante sobre otros posibles modificadores sintéticos sin mejoras significativas en los resultados [51-54]. Asimismo, en los últimos años se está estudiando el efecto del uso de aditivos con el fin de esclarecer los posibles mecanismos de reacción, los cuales hoy día siguen siendo tema de debate [55-57]. En el **capítulo 4** se aborda el empleo de materiales porosos ordenados (zeolita USY y material mesoporoso MCM-41) como soporte de platino y su posterior modificación con cinconidina o cinconina para su empleo en la reducción enantioselectiva de piruvato a lactato de etilo. Asimismo se aborda el empleo de otros compuestos quirales como co-modificadores o la optimización de las variables de reacción mediante diseño factorial.

1.4. D-Hidrogenación quimioselectiva del crotonaldehido a alcohol crotílico

La hidrogenación selectiva de un grupo carbonilo en presencia de un doble enlace C=C en una misma molécula conduce a alcoholes insaturados. No obstante, la hidrogenación del doble enlace C=C es más favorable termodinámicamente que la hidrogenación del doble enlace C=O. Si hablamos en términos de energía de enlace, el grupo carbonílico tiene 35 kJ/mol más que el enlace olefínico.

Los alcoholes insaturados tienen gran interés en industrias farmacéuticas y de fragancias. Estas son las que presentan un *factor E* más alto en sus procesos, principalmente debido a la baja selectividad de las reacciones hacia el producto deseado. Este bajo *factor E* no sólo es perjudicial desde el punto de vista medioambiental, sino que en la industria implica un gran esfuerzo económico por la pérdida de materia prima y por la necesaria separación del producto deseado del resto, incrementando considerablemente el precio final del producto. Por eso existe un interés creciente en los últimos años en la hidrogenación selectiva de compuestos insaturados, como ponen de manifiesto el número de referencias bibliográficas existentes que estudian la hidrogenación del C=C y/o C=O para una serie de moléculas más o menos complicadas (cinamaldehido, crotonaldehido, óxido de mesitilo, aldehídos aromáticos [58] ….)

Existen dos estrategias principales para la hidrogenación quimioselectiva del doble enlace en compuestos carbonílicos α,β-insaturados:

1.- Mediante procesos de reducción por transferencia de hidrógeno, empleando como catalizador un óxido metálico y como dador de hidrógeno un alcohol (generalmente secundario) a través del proceso denominado reducción de Meerwein-Ponndorf-Verley (MPV)[8, 59, 60].

2.- Utilizando como agente reductor hidrógeno gaseoso y como catalizador un metal noble depositado sobre un soporte inorgánico [61, 62]. Una de las principales ventajas de este tipo de catalizadores es la estabilidad que

tienen bajo las condiciones de reacción. Esta característica es una de las más buscadas en la industria ya que permite mantener una producción continuada en el tiempo.

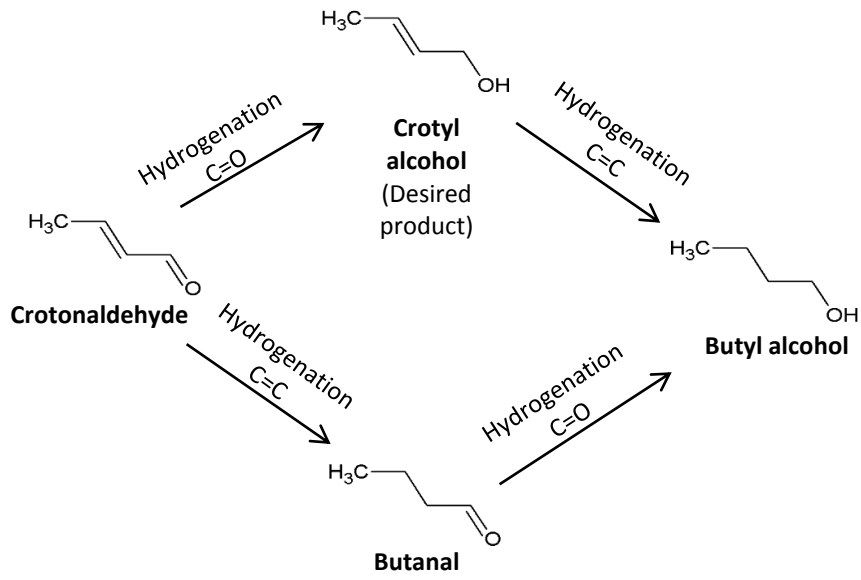

Figura 1.9 *Diferentes productos originados mediante hidrogenación del crotonaldehido.*

Los catalizadores monometálicos convencionales más utilizados en hidrogenaciones, están basados en metales del grupo 10, como por ejemplo Ni, Pd y Pt, además del Rh del grupo 9 y Ru del grupo 8 [61, 63, 64].

Cada metal tiene unas propiedades electrónicas y geométricas características, que influirán en la conversión y selectividad de la reacción, como se ha dicho anteriormente. Las propiedades electrónicas del metal pueden verse modificadas por varios factores como son el tamaño de la partícula metálica, el

soporte, la presencia de un segundo metal u otro aditivo [65-69]. Asimismo, el precursor metálico utilizado, método de síntesis y las distintas variables que se seleccionen en ella serán importantes en las características finales del catalizador. Además, el pre-tratamiento del catalizador va a ser determinante para las características geométricas y electrónicas del metal soportado [70-73].

En la presente Memoria, en el **capítulo 5**, nos centraremos en el segundo tipo de estrategia, esto es, en el uso de catalizadores metálicos soportados, y modificados mediante varias estrategias para mejorar su selectividad hacia la obtención del alcohol insaturado. El sustrato modelo empleado será el crotonaldehido (figura 1.9).

1.5-Referencias

[1] A. Paul, W. John, Green chemistry theory and practice, New York: Oxford University Press, 1998.

[2] R.A. Sheldon, Comptes Rendus de l'Académie des Sciences - Series IIC - Chemistry 3 (2000) 541-551.

[3] G. Centi, S. Perathoner, Catalysis Today 77 (2003) 287-297.

[4] M. Epicoco, V. Oltra, M. Saint Jean, Technological Forecasting and Social Change 81 (2014) 388-402.

[5] P.T. Anastas, M.M. Kirchhoff, Accounts of Chemical Research 35 (2002) 686-694.

[6] M.S. Simmons, in: P.T. Anastas, T.C. Williamson (Eds), Green Chemistry; Designig Chemistry for the Enviroment, American Chemical Society, Washinton, DC, 1996, Ch.10, p. 116.

[7] P.T. Anastas, M.M. Kirchhoff, T.C. Williamson, Applied Catalysis A: General 221 (2001) 3-13.

[8] J.F. Miñambres, A. Marinas, J.M. Marinas, F.J. Urbano, Applied Catalysis B: Environmental 140–141 (2013) 386-395.

[9] P. Gupta, S. Paul, Catalysis Today 236 (2014) 153-170.

[10] T. Kugita, S.K. Jana, T. Owada, N. Hashimoto, M. Onaka, S. Namba, Applied Catalysis A: General 245 (2003) 353-362.

[11] A.I. Frenkel, C.W. Hills, R.G. Nuzzo, The Journal of Physical Chemistry B 105 (2001) 12689-12703.

[12] V. Subramanian, E. Semenzin, D. Hristozov, A. Marcomini, I. Linkov, Nano Today 9 (2014) 6-9.

[13] T. Werpy, G. Petersen, A. Aden, J. Bozell, J. Holladay, J. White, A. Manheim, D. Eliot, L. Lasure, S. Jones, Top value added chemicals from biomass. Volume 1-Results of screening for potential candidates from sugars and synthesis gas, DTIC Document, 2004.

[14] J.J. Bozell, G.R. Petersen, Green Chemistry 12 (2010) 539-554.

[15] C.-H. Zhou, J.N. Beltramini, Y.-X. Fan, G.Q. Lu, Chemical Society Reviews 37 (2008) 527-549.

[16] M. Checa, F. Auneau, J. Hidalgo-Carrillo, A. Marinas, J.M. Marinas, C. Pinel, F.J. Urbano, Catalysis Today 196 (2012) 91-100.

[17] R.A. Sheldon, Green Chemistry 16 (2014) 950-963.

[18] A. Marinas, P. Bruijnincx, J. Ftouni, F.J. Urbano, C. Pinel, Catalysis Today 239 (2015) 31-37.

[19] F. Auneau, C. Michel, F. Delbecq, C. Pinel, P. Sautet, Chemistry - A European Journal 17 (2011) 14288-14299.

[20] F. Auneau, S. Noël, G. Aubert, M. Besson, L. Djakovitch, C. Pinel, Catalysis Communications 16 (2011) 144-149.

[21] A. Bienholz, H. Hofmann, P. Claus, Applied Catalysis A: General 391 (2011) 153-157.

[22] J. Chaminand, L.a. Djakovitch, P. Gallezot, P. Marion, C. Pinel, C. Rosier, Green Chemistry 6 (2004) 359-361.

[23] I. Gandarias, P.L. Arias, J. Requies, M. El Doukkali, M.B. Güemez, Journal of Catalysis 282 (2011) 237-247.

[24] N. Hamzah, N.M. Nordin, A.H.A. Nadzri, Y.A. Nik, M.B. Kassim, M.A. Yarmo, Applied Catalysis A: General 419–420 (2012) 133-141.

[25] A. Iriondo, J.F. Cambra, V.L. Barrio, M.B. Guemez, P.L. Arias, M.C. Sanchez-Sanchez, R.M. Navarro, J.L.G. Fierro, Applied Catalysis B: Environmental 106 (2011) 83-93.

[26] Y. Nakagawa, K. Tomishige, Catalysis Science & Technology 1 (2011) 179-190.

[27] M.R. Nimlos, S.J. Blanksby, X. Qian, M.E. Himmel, D.K. Johnson, The Journal of Physical Chemistry A 110 (2006) 6145-6156.

[28] W. Suprun, M. Lutecki, R. Gläser, H. Papp, Journal of Molecular Catalysis A: Chemical 342–343 (2011) 91-100.

[29] W. Suprun, M. Lutecki, T. Haber, H. Papp, Journal of Molecular Catalysis A: Chemical 309 (2009) 71-78.

[30] E. Iglesia, S.C. Reyes, R.J. Madon, S.L. Soled, in: H.P. D.D. Eley, B.W. Paul (Eds.), Advances in Catalysis, Academic Press, 1993, pp. 221-302.

[31] D. Schanke, S. Vada, E.A. Blekkan, A.M. Hilmen, A. Hoff, A. Holmen, Journal of Catalysis 156 (1995) 85-95.

[32] A. Kogelbauer, J.J.G. Goodwin, R. Oukaci, Journal of Catalysis 160 (1996) 125-133.

[33] M. Reinikainen, M.K. Niemelä, N. Kakuta, S. Suhonen, Applied Catalysis A: General 174 (1998) 61-75.

[34] J. Li, N.J. Coville, Applied Catalysis A: General 181 (1999) 201-208.

[35] R.C. Reuel, C.H. Bartholomew, Journal of Catalysis 85 (1984) 78-88.

[36] G. Prieto, A. Martínez, P. Concepción, R. Moreno-Tost, Journal of Catalysis 266 (2009) 129-144.

[37] S. Lögdberg, M. Lualdi, S. Järås, J.C. Walmsley, E.A. Blekkan, E. Rytter, A. Holmen, Journal of Catalysis 274 (2010) 84-98.

[38] Z.-j. Wang, S. Skiles, F. Yang, Z. Yan, D.W. Goodman, Catalysis Today 181 (2012) 75-81.

[39] Z. Zsoldos, F. Garin, L. Hilaire, L. Guczi, Journal of Molecular Catalysis A: Chemical 111 (1996) 113-122.

[40] K.M. Cook, S. Poudyal, J.T. Miller, C.H. Bartholomew, W.C. Hecker, Applied Catalysis A: General 449 (2012) 69-80.

[41] S.L. Sven Järas, Magali Boutonnet, European Patent Application

(2007) Number EP07106863.07106869

[42] J.T. Wehrli, A. Baiker, D.M. Monti, H.U. Blaser, Journal of Molecular Catalysis 49 (1989) 195-203.

[43] H.-U. Blaser, Tetrahedron: Asymmetry 2 (1991) 843-866.

[44] H.U. Blaser, H.P. Jalett, D.M. Monti, A. Baiker, J.T. Wehrli, in: R.K. Grasselli, A.W. Sleight (Eds.), Studies in Surface Science and Catalysis, Elsevier, 1991, pp. 147-155.

[45] U. Böhmer, F. Franke, K. Morgenschweis, T. Bieber, W. Reschetilowski, Catalysis today 60 (2000) 167-173.

[46] M.U. Azmat, Y. Guo, Y. Guo, Y. Wang, G. Lu, Journal of Molecular Catalysis A: Chemical 336 (2011) 42-50.

[47] C.H. Campos, C.C. Torres, A.B. Dongil, D. Ruiz, J.L.G. Fierro, P. Reyes, Catalysis Today 235 (2014) 226-236.

[48] C.C. Torres, C.H. Campos, J.L.G. Fierro, P. Reyes, D. Ruiz, Journal of Molecular Catalysis A: Chemical 392 (2014) 321-328.

[49] A. Baiker, Journal of Molecular Catalysis A: Chemical 115 (1997) 473-493.

[50] M. Studer, H.U. Blaser, C. Exner, Advanced Synthesis & Catalysis 345 (2003) 45-65.

[51] M. Schürch, T. Heinz, R. Aeschimann, T. Mallat, A. Pfaltz, A. Baiker, Journal of Catalysis 173 (1998) 187-195.

[52] T. Mallat, A. Baiker, Applied Catalysis A: General 200 (2000) 3-22.

[53] A. Marinas, T. Mallat, A. Baiker, Journal of Catalysis 221 (2004) 666-669.

[54] A.B. Merlo, J.F. Ruggera, G.F. Santori, A. Moglioni, G.Y.M. Iglesias, M.L. Casella, O.A. Ferretti, Catalysis Today 133 (2008) 654-660.

[55] J.L. Margitfalvi, E. Tálas, Catalysis Communications 46 (2014) 142-145.

[56] E. Tálas, J.L. Margitfalvi, Catalysis Communications 9 (2008) 984-989.

[57] E. Tálas, F. Zsila, P. Szabó, J.L. Margitfalvi, Journal of Molecular Catalysis A: Chemical 357 (2012) 87-94.

[58] P.G.N. Mertens, H. Poelman, X. Ye, I.F.J. Vankelecom, P.A. Jacobs, D.E. De Vos, Catalysis Today 122 (2007) 352-360.

[59] S. Axpuac, M.A. Aramendía, J. Hidalgo-Carrillo, A. Marinas, J.M. Marinas, V. Montes-Jiménez, F.J. Urbano, V. Borau, Catalysis Today 187 (2012) 183-190.

[60] M.a.A. Aramendía, V. Borau, C. Jiménez, J.M. Marinas, J.R. Ruiz, F. Urbano, Applied Catalysis A: General 249 (2003) 1-9.

[61] A. Giroir-Fendler, D. Richard, P. Gallezot, in: J.B.C.B.D.D.C.M. M. Guisnet, G. Pérot (Eds.), Studies in Surface Science and Catalysis, Elsevier, 1988, pp. 171-178.

[62] M. Consonni, D. Jokic, D. Yu Murzin, R. Touroude, Journal of Catalysis 188 (1999) 165-175.

[63] J. Kašpar, M. Graziani, G.P. Escobar, A. Trovarelli, Journal of Molecular Catalysis 72 (1992) 243-251.

[64] O.S. Alekseev, T. Beutel, E.A. Paukshtis, Y.A. Ryndin, V.A. Likholobov, H. Knözinger, Journal of Molecular Catalysis 92 (1994) 217-223.

[65] M. Abid, G. Ehret, R. Touroude, Applied Catalysis A: General 217 (2001) 219-229.

[66] F. Ammari, J. Lamotte, R. Touroude, Journal of Catalysis 221 (2004) 32-42.

[67] P. Mäki-Arvela, J. Hájek, T. Salmi, D.Y. Murzin, Applied Catalysis A: General 292 (2005) 1-49.

[68] D. Wang, F. Ammari, R. Touroude, D.S. Su, R. Schlögl, Catalysis Today 147 (2009) 224-230.

[69] X.-X. Wang, H.-Y. Zheng, X.-J. Liu, G.-Q. Xie, J.-Q. Lu, L.-Y. Jin, M.-F. Luo, Applied Catalysis A: General 388 (2010) 134-140.

[70] J. Ruiz-Martínez, F. Coloma, A. Sepúlveda-Escribano, J.A. Anderson, F. Rodríguez-Reinoso, Catalysis Today 133–135 (2008) 35-41.
[71] J. Hidalgo-Carrillo, J. Sebti, A. Marinas, J.M. Marinas, S. Sebti, F.J. Urbano, Journal of Colloid and Interface Science 382 (2012) 67-73.
[72] V. Gutiérrez, F. Nador, G. Radivoy, M.A. Volpe, Applied Catalysis A: General 464–465 (2013) 109-115.
[73] Q. Yu, X. Zhang, B. Li, J. Lu, G. Hu, A. Jia, C. Luo, Q. Hong, Y. Song, M. Luo, Journal of Molecular Catalysis A: Chemical 392 (2014) 89-96.

Hipótesis y objetivos

De forma general, en la presente Tesis Doctoral se pretende sintetizar y caracterizar diversos sólidos mediante distintos procedimientos así como estudiar su actividad catalítica en procesos de interés industrial mediados por H_2, tales como hidrogenolisis del glicerol, síntesis de *Fischer-Tropsch*, reducción enantioselectiva del grupo carbonilo (tomando como compuesto modelo el piruvato de etilo) y reducción quimioselectiva del grupo C=O frente al C=C (crotonaldehido como sustrato modelo). Esto supondrá un eslabón más en la cadena de investigaciones llevada a cabo desde hace más de 35 años por el grupo de investigación FQM-162 en el campo de la catálisis heterogénea.

Las hipótesis y objetivos a alcanzar en este proyecto de tesis pueden ser resumidas en los siguientes puntos.

Hipótesis 1

Uno de los temas candentes en el campo de la Química Sostenible es el aprovechamiento de la biomasa. En este sentido, conviene tener en cuenta que si bien existen diversas alternativas a los llamados combustibles fósiles para obtener energía (energía eólica, solar, biomasa…), sólo la biomasa es, además, fuente de productos químicos. Por este motivo, resulta especialmente interesante la obtención de productos químicos a partir de la biomasa. Entre las diferentes moléculas de la biomasa a valorizar, el glicerol (o glicerina), obtenido como subproducto en la producción de biodiesel, presenta un especial interés. Dentro de las diferentes alternativas a la valorización del glicerol se encuentra la hidrogenolisis, empleando catalizadores metálicos soportados. Existen diversos metales descritos como fase activa (ej. Pt, Rh, Pd, Au) encontrando la dificultad de comparar los resultados debido al diferente tamaño de partícula metálica. Otro de los aspectos a tener en cuenta en el comportamiento catalítico es el soporte empleado, cuyo papel puede no limitarse a la mera dispersión de la fase activa metálica, sino que por sus característica ácido-base y/o redox puede influir en la reacción. De particular

interés son los soportes parcialmente reducibles (como TiO_2, SnO_2, CeO_2 y ZnO) que pueden inducir la llamada interacción fuerte metal-soporte (SMSI). En particular, nuestro grupo de investigación tiene experiencia previa en el empleo del ZnO como soporte de Pt, describiendo la aparición de esta interacción a temperaturas de reducción de 200-400ºC y su influencia en algunos procesos catalizados como los de reducción quimioselectiva del C=O frente al C=C.

Objetivo 1

En un primer objetivo planteamos la síntesis de nanopartículas metálicas de varios metales nobles, como Pt, Pd, Rh y Au, soportadas sobre ZnO por dos métodos de síntesis: microemulsión y deposición-precipitación. Se busca un mejor conocimiento de los factores determinantes en la actividad catalítica, para lo que se hace especial hincapié en el método sintético, en especial en el control del tamaño de partícula metálica. Tras la obtención de los sólidos se determinarán sus propiedades como catalizadores en el proceso de hidrogenolisis del glicerol (**artículo 1**).

En un segundo paso hacia la optimización de la transformación selectiva del glicerol en diversos productos de interés (ej. 1,2-PDO o acetol), se trata de mejorar las propiedades del ZnO como soporte del metal. Para ello se procede a la síntesis de ZnO, tanto puro como dopado con distintos metales como Al, Ce, y Zr y a su posterior utilización como soporte del metal noble. Tras la obtención del catalizador, éste se caracteriza mediante distintas técnicas y se ensaya en la reacción anteriormente mencionada (**artículo 2**).

Hipótesis 2

El aumento de la demanda energética unido a la escasez de los recursos petrolíferos ha contribuido a que la utilización de la biomasa para su transformación en energía y combustibles esté siendo uno de los temas de actualidad.

Entre las distintas posibilidades para conseguir dicho objetivo, se encuentra la de descomponer los polímeros que constituyen la biomasa en moléculas más pequeñas y sencillas y la posterior utilización de éstas en la síntesis de otras más complejas. Dentro de las alternativas se encuentra el proceso de gasificación, que permite la obtención de gas de síntesis (CO e H_2) a partir del cual, mediante el proceso *Fischer-Tropsch* se puede obtener, por ejemplo, diésel. Aunque la síntesis de *Fischer Tropsch* ha sido ampliamente estudiada, aún hoy día aún quedan temas susceptibles de debate como son el tamaño de partícula metálica (generalmente cobalto o hierro) óptimo o la influencia de la adición de pequeñas cantidades de metal noble. Asimismo, la aparición de nuevos métodos de síntesis, como la microemulsión, ha permitido un mejor control del tamaño de partícula metálica y con ello un aumento de la actividad del catalizador.

Objetivo 2

La patente Europea EP07106863.9 (S. Jaras, S. Logdberg, M. Boutonnet, 2007) desarrollada en el grupo de investigación del Departamento de Tecnología Química del KTH de Estocolmo, Suecia, describe la síntesis de catalizadores de cobalto soportados en TiO_2 a través del método de microemulsión. La síntesis conduce a la obtención de un catalizador final con un 12% en peso de la fase activa, en este caso Co, sobre el soporte, realizándose en seis deposiciones consecutivas de un 2% cada una, hasta alcanzar el 12% deseado. Se hace necesario este proceso ya que la síntesis en una sola deposición conduce a una fase activa con

un tamaño de partícula mayor y una estructura amorfa del cobalto, provocando una notable pérdida de actividad catalítica.

El objetivo se centra en mejorar la cristalinidad y tamaño de partícula del Co en la síntesis con una sola deposición del 12%. En el **artículo 3** se detalla la síntesis de catalizadores de Co soportados sobre soportes parcialmente reducibles como TiO_2 y ZnO. Mediante el uso de la técnica de microemulsión se trata de controlar el tamaño de partícula de la fase activa y además se evaluará la influencia de la adición de pequeñas cantidades de Pt mediante dos métodos distintos. La incorporación de pequeñas cantidades de Pt puede mejorar la reducibilidad del cobalto.

Hipótesis 3

Una de las reglas de la Química Verde es la mejora de la selectividad en los procesos catalíticos, conduciendo a un descenso en el *factor E*. La hidrogenación quimioselectiva del grupo C=O en presencia de C=C es difícil, ya que está termodinámicamente desfavorecida. Igualmente, la hidrogenación enantioselectiva de moléculas pro-quirales, un proceso muy interesante para la industria farmacéutica, presentando *factores E* muy altos. En ambos procesos el Pt ha demostrado ser uno de los más activos cuando el tamaño de partícula se encuentra dentro de un rango determinado, aunque requiere de cierta modificación.

Para la hidrogenación quimioselectiva, es posible encontrar en bibliografía mejoras en las selectividades como consecuencia de interacciones metal-soporte o de la presencia de especies cloradas provenientes del precursor. Así, bajo un tamaño de partícula metálica controlado, se hace necesario estudiar la influencia del precursor metálico, el método de síntesis y la naturaleza del soporte.

En el caso de la hidrogenación enantioselectiva, la modificación del catalizador a través de la adsorción de moléculas que inducen la quiralidad

(modificadores quirales) ha sido muy estudiada desde su descubrimiento por Orito. Hasta hace poco existía la creencia de que el modificador del platino debía de tener unas partes fundamentales para poder actuar como tal, entre ellas la presencia de un grupo amino, pero se han descrito casos como el naftil-etanodiol que no presentan dicho grupo. Asimismo se pensaba que, en el catalizador, el tamaño óptimo de partícula del Pt debía de oscilar entre 4-6 nm, pero se ha descrito un catalizador con un tamaño de partícula de 0,4-1,4nm que conduce a un 97% de exceso enantiomérico a R-Lactato. Además, recientemente, el efecto de la presencia de aditivos en el medio de reacción está cuestionando los mecanismos de reacción comúnmente aceptados.

Todo esto demuestra que aún existen aspectos que resolver, como por ejemplo la influencia del tamaño de partícula, la necesidad de un grupo amino en el modificador quiral, el uso de aditivos o el soporte.

Objetivo 3

Como objetivo principal se plantea la mejora de la selectividad de ambas reacciones a los productos de interés. Para evaluar la influencia del soporte se procede a la síntesis de nanopartículas metálicas sobre soportes de distinta naturaleza; parcialmente reducibles como el ZnO o alumino-silicatos estructurados como zeolitas tipo USY y MCM41. Asimismo se estudiará la influencia del precursor metálico y de la técnica de síntesis usada.

En la hidrogenación enantioselectiva se empleará piruvato de etilo como molécula modelo y el catalizador comercial 5%wt Pt/Al_2O_3 Engelhard 4759 como referencia. Se indagará en una de las piezas clave en este tipo de sistemas, el modificador quiral. Se evaluará una serie de compuestos quirales comercialmente disponibles como posibles modificadores o aditivos de la reacción y se optimizarán las variables de la reacción a través del diseño factorial (**Capítulo 4).**

Para estudiar la hidrogenación quimioselectiva se usará el crotonaldehido como molécula modelo. Se abordará el empleo de diversos sistemas de platino soportado sobre ZnO, zeolitas tipo USY o materiales mesoporosos MCM-41. Se estudiará el efecto sobre el comportamiento catalítico de aspectos como el precursor metálico empleado, la interacción fuerte metal-soporte (caso del ZnO) o la existencia de problemas difusionales (empleo de USY vs MCM-41) **(Capítulo 5).**

Chapter 2

Glycerol hydrogenolysis on different ZnO-supported metal systems

Paper I

Synthesis of different ZnO-supported metal systems through microemulsion technique and application to catalytic transformation of glycerol to acetol and 1,2-propanediol

V. Montes[1], M. Checa[1], A. Marinas*[1], M. Boutonnet[2] , J.M. Marinas[1], F. J. Urbano[1], S. Järas[2], C. Pinel[3]

[1]Faculty of Sciences, University of Córdoba, Campus de Rabanales, Marie Curie Building, E-14014-Córdoba (Spain)

[2]KTH (Royal lnstitute of Technology), Chemical Technology, Teknikringen 42, SE-100 44 Stockholm, Sweden

[3]IRCELYON, UMR 5256 CNRSAJCBL, 2 avenue Albert Einstein, 69626 Villeurbanne Cedex, France

Keywords: glycerol hydrogenolysis; platinum; rhodium; palladium; gold; 1,2-propanediol (1,2-PDO); hydroxyacetone (acetol)

*Corresponding author. Tel.: +34 957218622; fax: +34 957212066. E-mail address: alberto.marinas@uco.es

Abstract

Different systems consisting in diverse metals (Au, Pt, Pd, Rh) supported on ZnO (5% by weight) were synthesized through the microemulsion technique (ME) and tested for glycerol hydrogenolysis, the main product being hydroxyacetone (acetol) and 1,2-propanediol (1,2-PDO). The solids synthesized using sodium borohydride as the reducing agent (B series) had smaller particle sizes as compared to the use of hydrazine (H series) which, in turn, resulted in a better catalytic performance. This synthetic method allowed us to obtain similar metal particle sizes (2-4 nm) for Pt, Pd and Rh solids in B series, whereas average gold metal particle was higher (>8 nm) which probably accounts for Au-containing systems being inactive under our experimental conditions. Reactivity order followed the sequence Rh>Pt>Pd. A comparison of the systems synthesized in the present paper through ME technique with those obtained in a previous work through the deposition-precipitation process revealed a higher activity and selectivity to acetol for the former solids which could be related to the presence of surfactant. Moreover, results suggested that metal sites could participate not only in hydrogenation of acetol to 1,2-propanediol but also in the previous dehydration step of glycerol to acetol.

Graphical Abstract

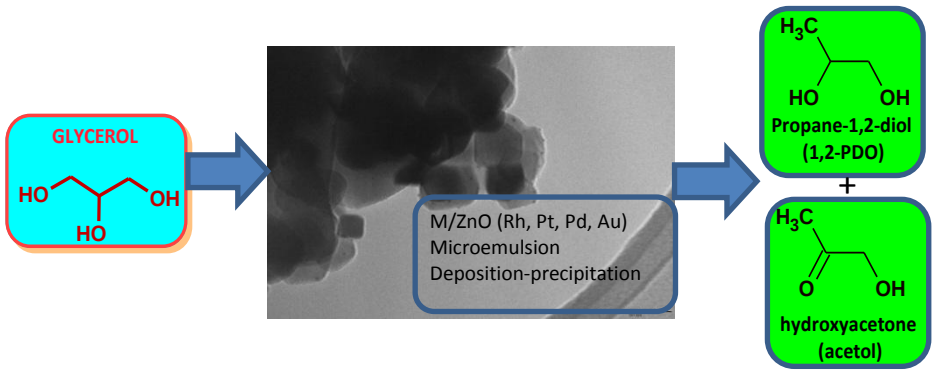

1. Introduction

Glycerol is a byproduct obtained during production of biodiesel through transesterification of vegetable oils. Approximately 10% weight of the converted feedstock is released as glycerol which makes its possible valorisation an interesting issue. One possibility is its catalytic transformation on different metals under hydrogen or inert atmosphere. One of the chemicals produced from glycerol in neutral medium is 1,2-propanediol (PDO) resulting from a dehydration process (leading to hydroxyacetone or acetol) followed by a hydrogenation step. 1,2-PDO can be used as antifreeze, in food industry or as feedstock in the preparation of polyester resins for film and fiber manufacture [1]. As for acetol, it is used as an interesting organic intermediate to produce polyols and acrolein, in food industry to give aroma to food, in textiles or in cosmetic industry as skin tanning agent [2]. Some of the metals used in the transformation of glycerol into 1,2-PDO include Cu [3-5], and noble metals such as Ir [6], Ru [7-9], Rh [10, 11], Pd [10, 12] or Pt [13, 14].

In a previous study [14], different reducible oxides (TiO_2, ZnO, SnO_2 and ZrO_2) were screened as support for platinum and tested for glycerol hydrogenolysis, ZnO being the solid with the highest selectivity to 1,2-PDO. This prompted us to select ZnO as the support for diverse metals (Pt, Rh, Pd and Au) which were incorporated through the deposition-precipitation technique in a nominal content of 5% by weight. All the solids exhibited the best catalytic performance on reduction treatment at 200ºC whereas higher temperatures led to the formation of a metal-Zn alloy which under our experimental conditions was detrimental to activity. Catalytic activity followed the sequence Pt>Rh>Pd>>Au. However, XRD and TEM studies revealed quite different metal particle sizes, for Pt and Rh as compared to Pd and Au (3.1, 3.7, 15 and 12 nm, respectively). Therefore, it was not clear to what extent catalytic results had been influenced by the different metal particle size. In order to cast further light on that, in the present

study a new synthesis under similar conditions (same metal precursor, support and metal content) is carried out by the microemulsion technique.

A microemulsion (ME) is a thermodynamically stable colloidal dispersion in which two immiscible liquids (polar and non-polar) form nanosized droplets dispersed in a continuous phase and stabilized by a third component: the surfactant. These nanodroplets can be used as nanoreactors to synthesize metal particles in a very narrow particle size range. There are several reviews on the preparation of nanoparticles of noble metals through this technique and their application as catalyst to several processes [15-18]. Basically, some of the crucial parameters to be considered are the type of surfactant (anionic, cationic or non-ionic, the latter normally being less sensitive to temperature), the oil phase (oil-surfactant interaction influences the shape and size of microemulsion) or the concentration of metal solution (normally high concentrations lead to larger final metal particle sizes). The internal structure of the ME is determined by the relative fractions of these three constituents: surfactant, oil and water solution. The ME is only formed for certain ratios of the constituents, outside which a two-phase system is formed. The ratios for which the ME exists depend on the system, nature and polarity of the components, and changing these ratios the size of droplets are controlled and hence the final particle size. Another important point to be considered is the reducing agent which will lead to the formation of metallic particles, the most commonly used being hydrazine (N_2H_4) and sodium borohydride ($NaBH_4$). Typically a stoichiometric excess is used in order to ensure the full reduction of precursor salt. Furthermore, such an excess results in smaller metal particle sizes because the nucleation is favored over particle growth [19]. Others parameters influencing the process are temperature, speed of stirring or atmosphere, just to cite some of them.

2. Experimental

2.1. Materials

Synperonic 13/6.5 was a gift from Croda. All the other chemicals (2,2,4-Trimethylpentane (99.9%, TMP), hydrazine monohydrate 98%, sodium borohydride 96%, 8wt% H_2PtCl_6 aqueous solution, $HAuCl_4$, $Pd(NO_3)_2$, $RhCl_3$, ZnO nanopowder, acetone (technical grade), tetrahydrofuran (99.9%, THF), glycerol 99%, 1,2-propanediol 99.5%, 1,3-propanediol 98%, hydroxyacetone (acetol, 95%), ethylene glycol 99.5%, n-propanol 99.5%, acrolein (≥95%) and lactic acid ≥85%) were purchased from Sigma-Aldrich. MilliQ water was used for preparation of the aqueous solutions of metal salts.

2.2. Synthesis of ZnO-supported systems

Figure 1A summarizes the main steps for the preparation of the catalysts from a water in oil microemulsion (reverse micelle). The total amounts of reagents were calculated in order to obtain a nominal content of 5wt% metal in 2 grams of catalyst.

Under optimized conditions, the composition of microemulsions (ME) was Surfactant: Synperonic 13/6.5 (28.6wt%), Oil: Trimethylpentane (TMP) (66.8wt%), Water: 2wt% metal precursor salt (4.6wt%).

As depicted in Figure 1A, the synthesis began mixing the corresponding amounts of Synperonic 13/6.5 and TMP in a flask. The mixture was kept under vigorous stirring (1000 rpm) and then the water solution of precursor was added dropwise resulting in a transparent solution of microemulsion encapsulating the dissolved metallic precursor. ME was then deoxygenated bubbling N_2 for a couple of minutes and for the rest of the process an inert atmosphere was created with N_2. Afterwards, the reducing agent ($NaBH_4$ or N_2H_2), in a 1:5 molar ratio (metal:reducing agent) was added as a fresh water solution 10M (maximum 1

minute old). The color of solution changed from yellow (Pt, Pd and Au), red (Rh) to black just with the first drop of reducing agent solution. At that point, the metallic particle had already been formed and stabilized by surfactant. In order to ensure a full reduction of precursor the mixture was kept under stirring for one hour. The inert atmosphere was then removed and the system was kept stirred one additional hour. The next step was the addition of the support (1.8 g ZnO) directly followed by acetone (50% weight of total ME) as destabilizing agent all at once. The suspension was kept stirring for two hours for a full destabilization of the ME.

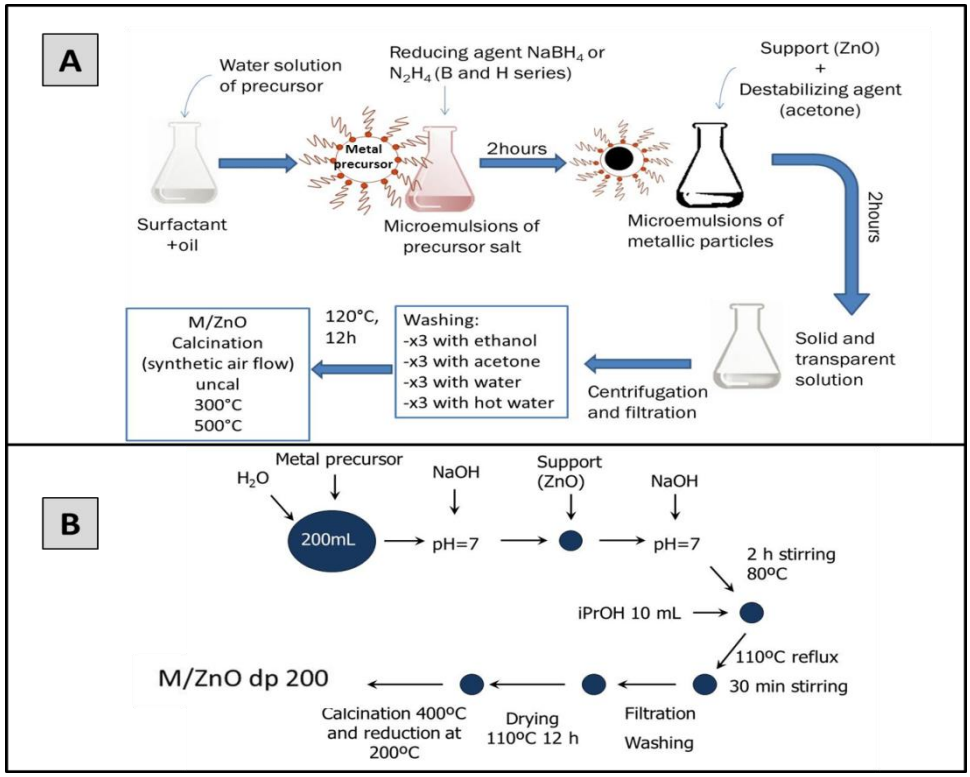

Figure 1. *Schematic representation of the synthetic procedure followed to obtain the different ZnO-supported metal systems through microemulsion technique (A) and deposition-precipitation method (B).*

The suspension was then centrifuged (3000 rpm) for 15 min. A good indicative of a successful reduction and destabilization was that after separation of the solid, the liquid was transparent and colorless.

Then the solids were carefully washed with ethanol, acetone, cold water (at room temperature) and hot water (boiling water), three times each with half the weight of acetone employed for destabilization. Finally, the systems were dried for 12 h at 120˚C and when applicable calcined at 300˚C or 500˚C for 16 h (ramp of 1˚C/min) with a flow of synthetic air of 2L/h.

Catalyst nomenclature includes the metal, the support (ZnO), the reducing agent (B or H for sodium borohydride or hydrazine, respectively) and the thermal treatment. Therefore, for instance, 'Pt/ZnO-H unred' denotes the platinum system synthesized through reduction with hydrazine and tested as synthesized (unreduced) whereas ´Pd/ZnO-B calc500 red 200´ refers to the palladium solid obtained through reduction with $NaBH_4$ and submitted to calcination at 500ºC first followed by reduction at 200ºC.

For comparative purposes, the corresponding systems synthesized through the deposition-precipitation method using the same precursor salt, support and nominal metal content (5% by weight) were also tested in this study. Figure 1B summarizes the main synthetic steps whereas full details on the synthesis and characterization of the catalysts can be found elsewhere [14]. The nomenclature of these systems is M/ZnO dp 200 where M refers to the metal, dp to the synthetic method (deposition-precipitation) and 200 to the reduction temperature (200ºC).

2.3. Characterization

Elemental analysis of metal-containing samples was performed by the staff at the Central Service for Research Support (SCAI) of the University of Córdoba. It was performed using inductively coupled plasma mass spectrometry (ICP-MS). Measurements were made on a Perkin-Elmer ELAN DRC-e instrument following dissolution of the sample in a 1:3 HNO_3/HCl mixture with a soft heating. Calibration was done by using PE Pure Plus atomic spectroscopy standards, also from Perkin-Elmer.

Surface areas of the solids were determined from nitrogen adsorption–desorption isotherms obtained at liquid nitrogen temperature on a Micromeritics ASAP-2010 instrument, using the Brunnauer–Emmett–Teller (BET) method. All samples were degassed to 0.1 Pa at 120ºC prior to measurement.

Transmission electron microscopy (TEM) images were obtained using a Philips CM-10 microscope. All samples were mounted on 3 mm holey carbon copper grids.

EDX measurements were performed on a JEOL JSM-6300 scanning electron microscope (SEM) equipped with an energy-dispersive X-ray (EDX) detector. It was operated at an acceleration voltage of 20keV with a resolution of 65eV.

X-ray patterns of all M/ZnO-B and M/ZnO-H samples (Figure 3) were obtained on a Siemens D5005 X-ray diffractometer utilizing Cu Kα radiation. A secondary monochromator was used. The metallic particle sizes were estimated by using the Scherrer formula assuming spherical crystallites. X-ray diffractograms of Pd/ZnO-B calcined/reduced at different temperatures (Figure 8) were recorded on a Siemens D-5000 diffractometer equipped with a DACO-MP automatic control and data acquisition system. The instrument was equipped with a graphite monochromator and used Co Kα radiation.

X-ray photoelectron spectroscopy (XPS) data were recorded on 4 mm × 4 mm pellets 0.5 mm thick that were obtained by gently pressing the powdered

materials following outgassing to a pressure below about 2×10^{-8} Torr at 150ºC in the instrument pre-chamber to remove chemisorbed volatile species. The main chamber of the Leibold–Heraeus LHS10 spectrometer used, capable of operating down to less than 2×10^{-9} Torr, was equipped with an EA-200MCD hemispherical electron analyser with a dual X-ray source using MgKα (hv = 1253.6 eV) at 120 W, at 30 mA, with C(1s) as energy reference (284.6 eV).

Surface acidity was determined by thermal programmed desorption (TPD) of pyridine previously adsorbed on the solids monitored by TCD. An amount of 50 mg of sample was placed under a He stream flowing at 10 mL/min in a reactor 10 mm in diameter that was placed inside an oven. The He stream was used to clean the solids by heating to 350ºC at a rate of 10°C/min and then cooling by thermal inertia to room temperature. At that point, the surface of the solid was saturated with the probe molecule for 30 min. Pyridine was supplied by bubbling the He stream through liquid pyridine at room temperature. After saturation, excess physisorbed probe substance was removed by passing a He stream at 10 mL/min for 1 hour. Then, desorption was started by raising the temperature to 400°C at 10°C/min and holding the final level for 30 min.

2.4. Catalytic tests

Hydrogenolysis of glycerol was conducted in a Berghof HR-100 stainless steel high-pressure autoclave equipped with a 75 mL PTFE vessel and a magnetic stirrer. Under standard conditions, 20 mL of a 1.36 M solution of glycerol in water and 50 mg of catalyst were introduced in the vessel. Reactor was then purged with hydrogen and temperature (180ºC) and hydrogen pressure (6 bar) adjusted. The stirring rate was 1200 rpm. After 15 hours of reaction, stirring was stopped and the vessel cooled in an ice bath. The catalyst was spin-dried and the liquid passed through a filter of PTFE 0.45μm. Then it was analyzed by GC-FID (Agilent

Technologies 7890, with a Supelco 25357 NukolTM capillary column). Quantification was carried out through the corresponding calibration curves.

3. Results and discussion

As indicated in the experimental section, the optimized composition of ME system was Surfactant: Synperonic13/6.5 (28.6%), Oil: Trimethylpentane (66.8%), Water: 2% wt of precursor salt (4.6%). In order to find such a composition, different experiments were performed. It is important to point out that the relative fraction of the constituents of ME is a key feature to control the size of micelles and thus the final metal particle size. With a view to optimize the process, different mixtures of surfactant and oil at room temperature were prepared. Then an aqueous solution of 1% and 2% weight (wt) of precursor was added dropwise in order to know the solubility limit. Determination of this limit is easy because the microemulsions are isotropic and transparent, and when they destabilize the transparent solution turns into a cloudy system. These experiments determined the region of relative fractions of constituents to form stable reverse micelles. Finally in order to simplify the process, the same system of microemulsion was applied to synthesize all catalysts once ensured that ME was stable for all metal precursors. Also in order to minimize the environmental impact, the system of choice was that in which less amount of surfactant and oil was required.

Figure 2 shows the TEM micrographs of microemulsions of metallic particles (precursor reduced using $NaBH_4$). As can be seen, at this point the synthetic method ensured metal particles in the 2-4 nm range. Support (ZnO) was then added and microemulsions were destabilized using acetone. The solid was centrifuged and washed to obtain the different M/ZnO systems (M=Pt, Pd, Rh and Au). Some features concerning characterization of the systems are depicted in Table 1. Surface areas of all the systems are in the 15-17m^2/g range, quite similar to that of the support, ZnO (15m^2/g). Moreover, a comparison of metal nominal

contents (5% by weight) with the values determined by ICP-MS evidences that the synthesis of metal particles through ME technique led to a low incorporation of rhodium (0.3%), a higher incorporation of platinum (1.2 and 2.9% for Pt/ZnO-B and Pt/ZnO-H, respectively) and the almost quantitative incorporation of palladium (4.4 and 4.5% for Pd/ZnO-B and Pd/ZnO-H, respectively). It is possible that the washing process of the solids resulted in the partial dissolution of the metals. In fact, ICP-MS monitoring of the washing process of Pt/ZnO-B solid confirmed that there was a progressive loss of platinum, especially during washing with cold water (that step accounts for ca. 53% Pt loss). However, subsequent treatment with hot water did not lead to any further loss thus confirming that the noble metal remained stabilized thereafter on the catalyst surface. Consequently, no significant metal leaching was observed during catalytic studies.

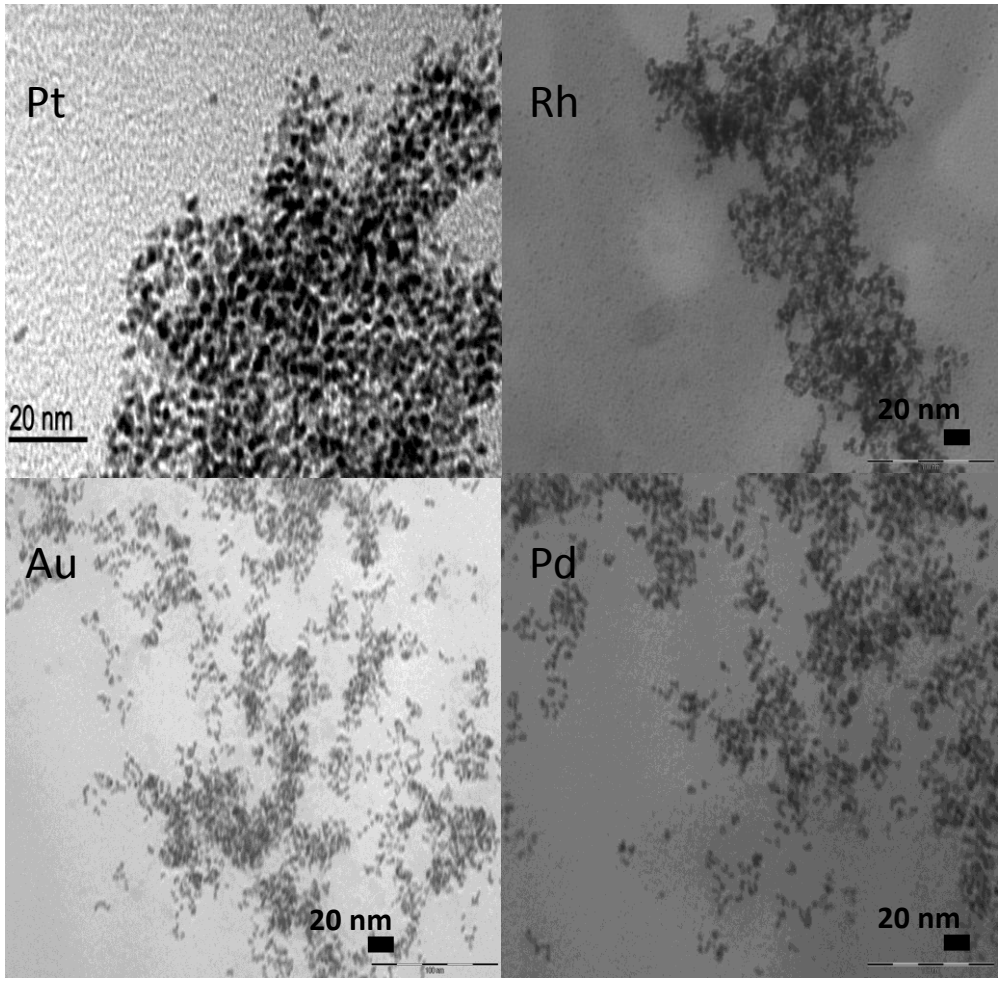

Figure 2*. TEM micrographs of the different microemulsions after the addition of sodium borohydride.*

Table 1. *Some features concerning characterization of the different ZnO-supported metal systems*.

Catalyst[1]	Metal/ZnO weight %				BET surface[2]	Mean particle size (nm)	
	Nominal	ICP-MS	EDAX	XPS	(m^2/g)	TEM	XRD[3]
Pt/ZnO-H			3.4	1.2	15	5.3	5.5
Pt/ZnO-H calc300	5	2.9	2.9	1.3	15	-	-
Pt/ZnOH calc500			-	1.3	15	-	-
Pt/ZnO-B			0.8	0.8	16	2.2	NS
Pt/ZnO-B calc300	5	1.2	0.6	0.6	16	-	-
Pt/ZnO-B calc500			-	0.7	16	-	-
Pt/ZnO dp 200	5	5.2	-	5.3	19	3.1	NS
Pd/ZnO-H			4.1	4.6	15	9.0	6.8
Pd/ZnO-H calc 300	5	4.5	2.8	-	15	-	12.2
Pd/ZnO-H calc 500			3.5	-	15	-	17.7
Pd/ZnO-B			5.3	3.6	16	3.0	NS
Pd/ZnO-B calc 300	5	4.4	4.8	3.4	16	-	7.4
Pd/ZnO-B calc 500			5.7	3.4	16	-	14.2
Pd/ZnO dp 200	5	4.1	-	0.9	17	-	15.0
Rh/ZnO-B		0.3	0.6	0.4	16	2.1	NS
Rh/ZnO-B calc 300	5		0.4	0.4	16	-	-
Rh/ZnO-B calc 500			-	0.3	16	-	-
Rh/ZnO dp 200	5	2.4	-	3.2	25	3.7	-

[1]Rh/ZnO-H does not exist since hydrazine was not able to reduce Rh.

[2]The support (ZnO) has a surface area of 15 $m^2 \cdot g^{-1}$.

[3]The measurement of particle sizes of calcined Pd samples corresponded to the peak of PdO at 2theta 39.9°. NS denotes that no signal of the metal was observed by XRD. Au/ZnO-B, Au/ZnO-H and Au/ZnO dp 200 exhibited average particle sizes of 19, 22 and 12 nm, respectively and were inactive for glycerol conversion under our experimental conditions. Therefore, no further characterization was performed.

X-Ray diffractograms of the systems are depicted in Figure 3 and mean particle sizes, as determined from Scherrer equation are indicated in Table 1. From Figure 3 and Table 1 it is clearly evident that the use of sodium borohydride as the reducing agent (B series) led to smaller metal particles as compared to the utilization of hydrazine (H series). Furthermore, hydrazine was not able to reduce rhodium which was clearly evident during the synthetic method, since unlike the other cases no change in the color of the microemulsion of $RhCl_3$ was observed when hydrazine was added. Finally, in all cases, and particularly for H series, destabilization of ME with acetone resulted in an increase in metal particle size which was especially dramatic in the case of gold. This testifies to the importance of the different steps (and in particular of ME destabilization) in the synthesis of metal nanoparticles through microemulsion.

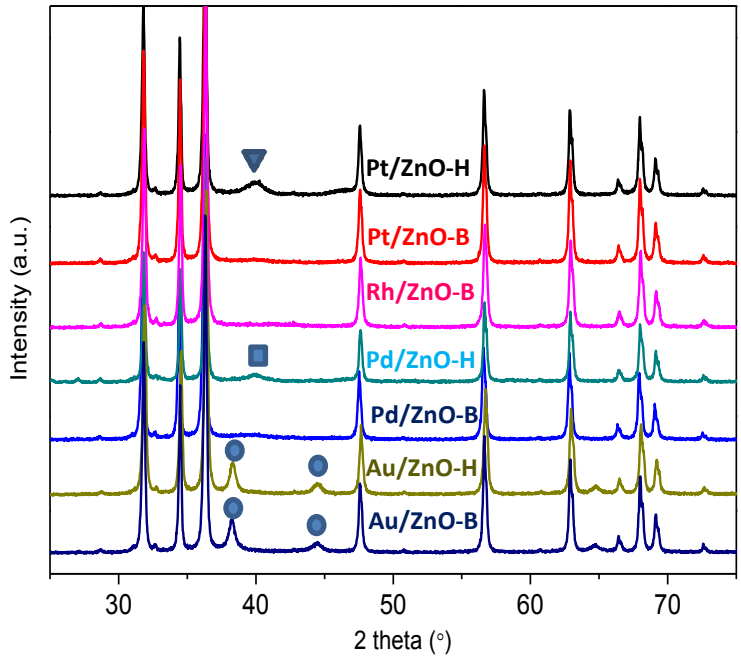

Figure 3. *X-ray diffractograms of the different systems. Symbols indicate the signal corresponding to the metal: Au (circle), Pd (square) and Pt (triangle).*

In order to try to obtain smaller gold metal particle sizes, different modifications were applied to the destabilization step, including the substitution of acetone by THF as the destabilization agent and the modification of the order of addition of such an agent and ME. All in all, the smaller particle sizes (8nm) were obtained when ME was added dropwise into a suspension of the support of acetone under vigorous stirring.

TEM micrographs of the different solids after destabilization, filtration and calcination confirmed XRD results. Therefore, B series (Figure 4 and Table 1) presented metal particle sizes in the 2-4 nm range, the exception being gold in which case bigger particles were obtained. It is also interesting to note the relatively low particle size interval obtained by ME synthetic method (see inset of Figure 4 for Pt/ZnO-B).

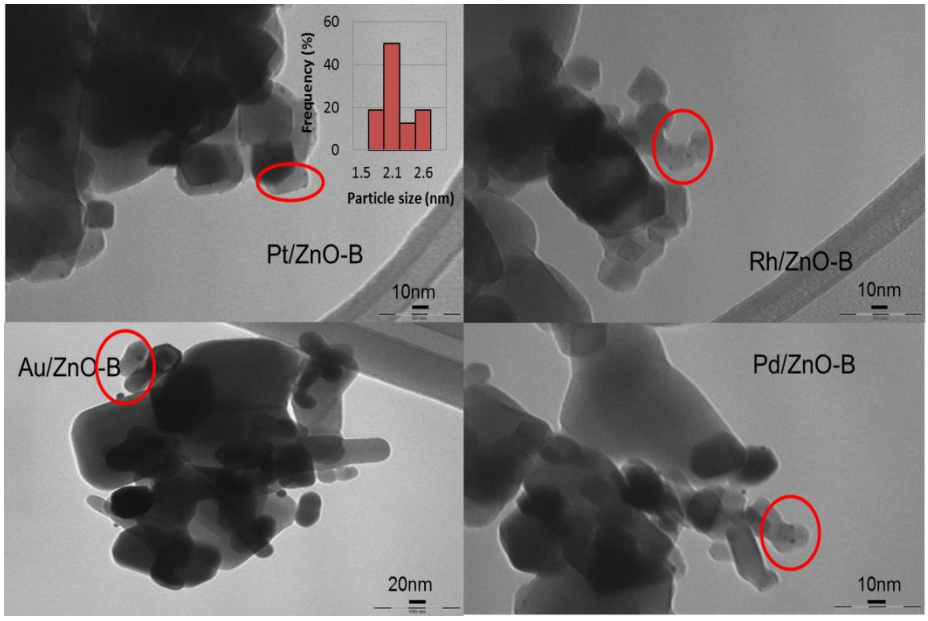

Figure 4*. TEM micrographs of the different M/ZnO-B solids.*

The systems were then tested for glycerol hydrogenolysis. Results expressed as mol of glycerol converted per mol of metal and selectivity to 1,2-PDO after 15h are summarized in Figures 5 and 6. For comparative purposes, catalytic performance of the corresponding system synthesized through the deposition-precipitation method and reduced at 200ºC (M/ZnO dp 200) is also included. As can be seen, data for Rh/ZnO-H and Au/ZnO-B and Au/ZnO-H are absent. In the first case, as explained above, hydrazine was unable to reduce rhodium particles whereas gold systems were inactive for the reaction, probably as a result of their big particle size (above 8nm).

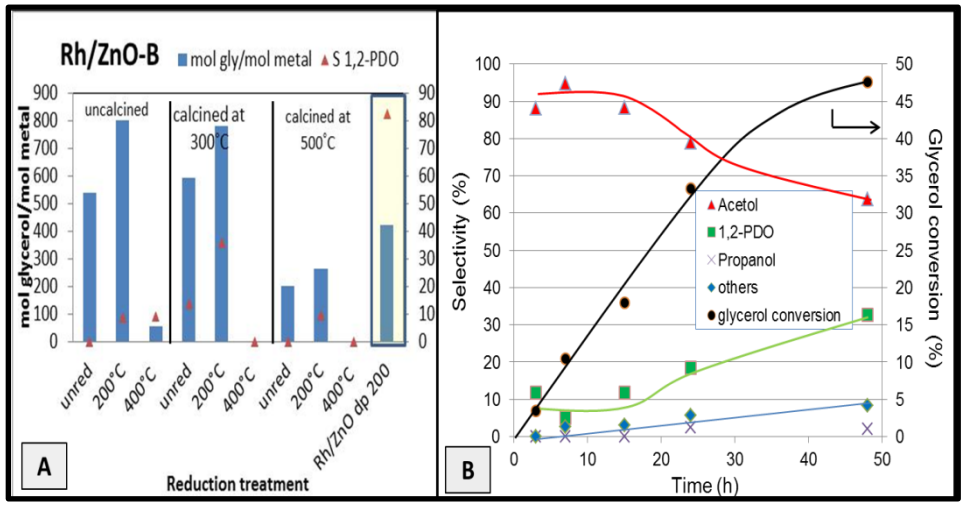

Figure 5. *A) Catalytic transformation of glycerol on Rh/ZnO-B solid A) results for t=15h. B) Kinetic profile for Rh/ZnO-B uncalc 200. Reaction conditions: 50 mg catalysts, 5mL 1.36 M water solution of glycerol. 180ºC and 6 bar of initial hydrogen pressure.*

Conversion of glycerol into 1,2 or 1,3-propanediol on bifunctional catalysts has been described to occur via dehydration followed by hydrogenation. Depending on the hydroxyl group in glycerol involved in the dehydrogenation (either terminal or central), 1,2-PDO or 1,3-PDO are obtained, respectively (Scheme 1). Moreover, some other liquid (e.g. ethylene glycol, 1-propanol) and gaseous (e.g. methane, ethane and propane) by-products could be obtained [14].

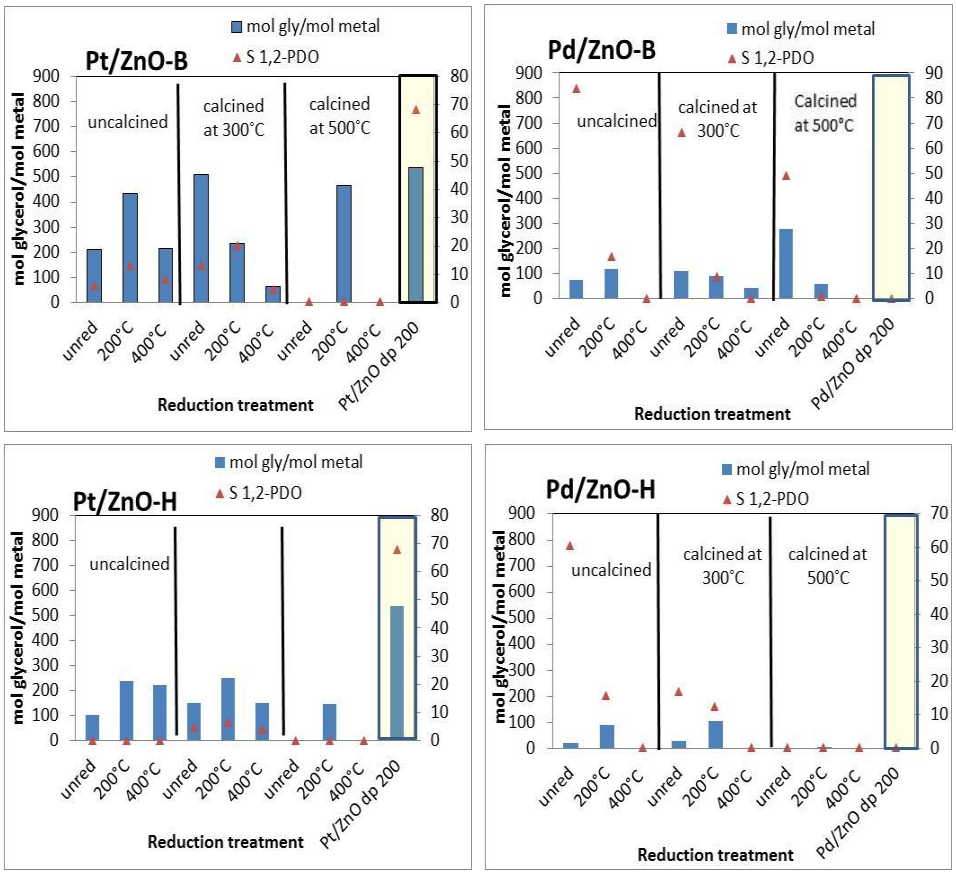

***Figure 6**. Catalytic transformation of glycerol on several Pt and Pd solids. Reaction conditions: 50 mg catalysts, 20mL 1.36 M water solution of glycerol. 180ºC and 6 bar of initial hydrogen pressure*

In our case, under standard conditions (15h of reaction, 180°C, 6 bar H_2) all catalysts yielded acetol or 1,2-PDO mainly, accounting for ca. 100% selectivity (Figures 5 and 6) which confirms the dehydration through terminal OH. For longer reaction times (i.e. conversions over ca. 20%), some other by-products were obtained though still 1,2-PDO and acetol accounted for over 90% selectivity (Figure 5B).

The formation of dehydration products in water environment has already been described not only for glycerol transformation into acrolein or acetol [20] but also for some other processes (e.g. dehydration of fructose to 5-hydroxymethylfurfural (HMF) [21]. There is some controversy in the literature concerning the nature of the active sites responsible for acetol formation. On the one hand, most of the papers report that dehydration of glycerol to acetol occurs on acid sites [10] although some other works describe the acetol formation on basic sites by a dehydrogenation process followed by dehydration and enolization [22]. In addition, redox properties of metal oxide catalysts could also influence the performance of those solids in the gas-phase dehydration of glycerol [23, 24]. Subsequent hydrogenation of acetol on the metal catalysts gives 1,2-propanediol. Kim et al [25] studying the gas-phase dehydration of glycerol over silica-alumina catalysts concluded that acrolein was formed on Brønsted acid sites whereas acetol yield was proportional to the concentration of Lewis acid sites. However, in batch processes and in an aqueous environment, Brønsted acid sites will be responsible for both acrolein and acetol production [26]. Moreover, a study of glycerol dehydration based on quantum mechanical calculations reported that neutral glycerol showed a high barrier to dehydration whereas protonated glycerol exhibited a much lower barrier for dehydration to acetol [27]. Density functional calculations indicate that glycerol dehydrates to either acetol or acrolein through alkoxide species formed by competitive adsorption of the primary or secondary glycerol OH groups, respectively (Scheme 1). The stronger adsorption mode of

glycerol through the secondary OH group was responsible for the higher selectivity to acrolein at moderated temperatures [26]. On the other hand, some other authors conclude that the metal could be involved in the dehydration of glycerol to acetol. Sato et [28] found that dehydration of glycerol in gas phase occurred via Cu-alkoxide species formed by the release of an OH radical from the primary OH group. Similarly, Bienholz et al [29] prepared a set of different silica supported copper catalysts and found a linear relationship between the specific copper surface and the catalytic activity not only in the hydrogenation of acetol to 1,2-PDO but also in the dehydration of glycerol to acetol thus suggesting that both processes occurred at the copper surface. The influence of the metal in the dehydration step has been suggested for some other metals (e.g. Pt [30]). Nevertheless, Wang et al. [31] working with Cu-ZnO catalysts in the batch conversion of glycerol to 1,2-PDO found that the dehydration step to acetol was carried out on the ZnO acidic surface and the subsequent hydrogenation of acetol to 1,2-PDO takes place in the Cu domains. Furthermore, the activation energy for acetol hydrogenation is about 30 kJ lower than that of glycerol dehydration [32] and therefore dehydration step determines the overall glycerol conversion while hydrogenation by Cu is responsible for the final selectivity to 1,2-PDO [31, 32].

In our study, different preliminary experiments were conducted in order to ensure that M/ZnO solids catalyzed the formation of both acetol and 1,2-PDO. First of all, a blank experiment (1.36 M glycerol, no catalyst) showed that glycerol was stable under reaction conditions. Pure ZnO was then tested as the catalyst and again glycerol was not transformed evidencing that, even though transformation of glycerol into acetol is a simple dehydration process, ZnO cannot catalyze the process under our experimental conditions. Finally, a 1.36 M solution of acetol in water was submitted to the reaction conditions and acetol did not rehydrate. These results seems to support the hypothesis of metal sites participating in both dehydration to acetol and subsequent hydrogenation to 1,2-PDO or, at least, that

incorporation of the metal to the ZnO creates a new population of acid sites able to dehydrate the glycerol to acetol.

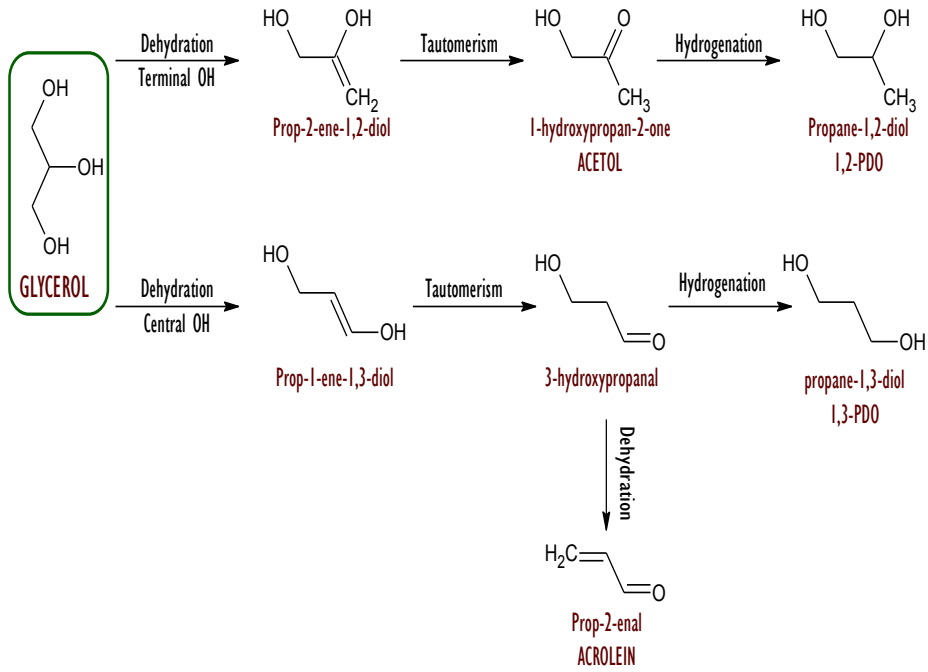

***Scheme 1**. Transformation routes of glycerol into 1,2-PDO or 1,3-PDO through an initial dehydration step.*

In order to cast further light on the nature of active sites responsible for formation of acetol, acidity of several systems was determined by thermal programmed desorption (TPD) of pre-adsorbed pyridine (Figure 7). As can be seen, the support (ZnO) did not exhibit any peak which could account for its inactivity in the process. On the contrary, Pt/ZnO systems synthesized through deposition-precipitation technique, exhibited well-defined pyridine desorption

peaks which evidences the existence of acid sites which in turn could result in their observed activity. Those acid sites could originate from the platinum precursor (chloroplatinic acid) [33]. In fact, a comparison of Pt/ZnO dp unred and Pt/ZnO dp 200 systems shows the loss of the peak appearing at higher temperature (ca. 300ºC) in the latter which could be due to the release of chloride during reduction pretreatment as HCl.

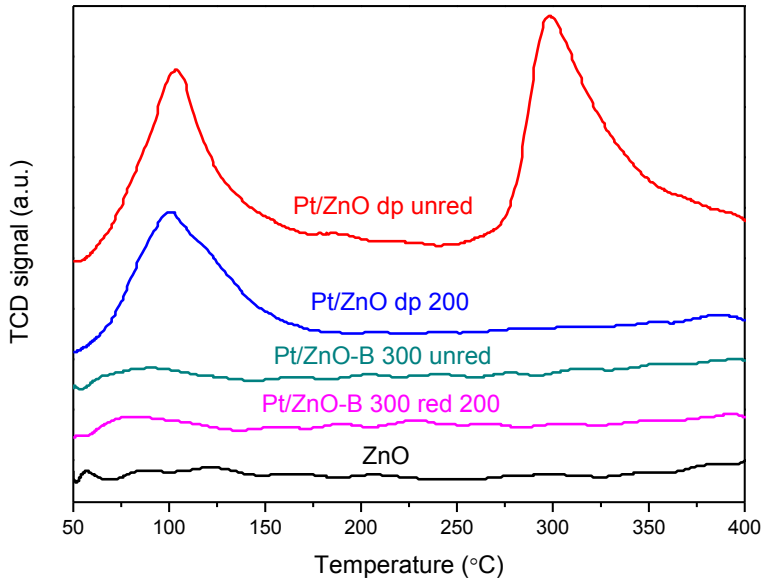

Figure 7*. TPD profile of pre-adsorbed pyridine for some of the Pt-based solids.*

Interestingly, despite the fact that Pt/ZnO solids obtained through microemulsion technique did not exhibit any pyridine peak, they were active in glycerol conversion. This could be supportive of the above-mentioned role of metal sites in dehydration of glycerol to acetol. Nevertheless, the possibility of some

influence of remaining surfactant or even the existence of low-acidity active sites (not titrated with pyridine) cannot be ruled out.

Results achieved for platinum (Pt/ZnO-B and Pt/ZnO-H), palladium (Pd/ZnO-B and Pd/ZnO-H) and rhodium (Rh/ZnO-B) solids are summarized in Figures 5 and 6. In all cases B series led to better catalytic results as compared to H series. The lower metal particle sizes (as evidenced by XRD and TEM, see Table 1) in the former case can account for that. Focusing on B series, reactivity order follows the sequence Rh>Pt>Pd. In our previous study on systems synthesized through the deposition-precipitation method [14], palladium was also found to be the least active system though its greater particle size as compared to that of Rh and Pt (22nm and 3-4 nm, respectively) could explain such catalytic results. In the present work ME technique allowed us to better control metal particle sizes (2-4nm for all Pt, Pd and Rh in M/ZnO-B series) which confirms that under our experimental conditions Pd is less active.

Focusing on B-series, the best catalytic results for each metal corresponds to Pt/ZnO-B calc300 unred (510 mol glycerol/mol of metal, 87% selectivity to acetol), Pd/ZnO-B calc500 unred (279 mol glycerol/mol of metal, 51% selectivity acetol) and Rh/ZnO-B uncalc red 200 (800 mol glycerol/mol of metal, 91% selectivity to acetol). In the first case, catalytic activity is quite close to that of the corresponding DP counterpart (Pt/ZnO dp 200, 538 mol glycerol/mol Rh) whereas in the other two cases, synthesis through the ME method led to a significant improvement in activity (see Figures 5A and 6). Furthermore, ME systems are comparatively more selective to acetol than their DP counterparts. If we assume a separate function of catalyst components (acidic and metallic) this would mean that in ME systems the metallic function is lower than in DP catalysts in which acetol is readily hydrogenated to 1,2-PDO. Some remaining surfactant in the surrounding of metallic particles could be the reason for the low hydrogenating activity of the ME systems. Moreover, interestingly, despite the fact that as-synthesized M/ZnO-B

systems consist of metal particles in the zero oxidation state, their optimum catalytic performance is achieved upon thermal pretreatment (calcination and/or reduction) normally at ca. 200-300°C. In order to cast further light on the reason for that, different characterization studies were carried out.

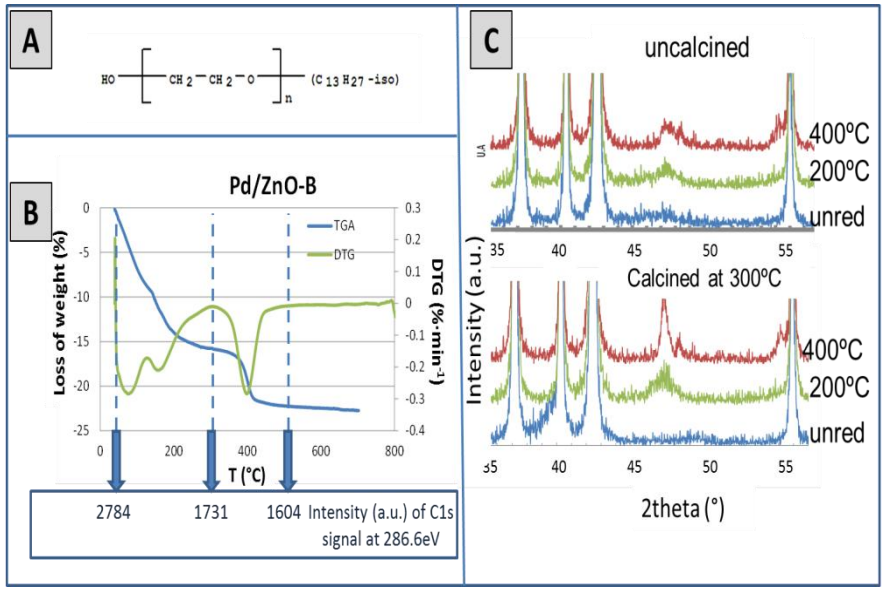

Figure 8. *A) Chemical structure of the surfactant (Synperonic 13/6.5). B) TG analysis of Pd/ZnO-B and relative percentage of carbon associated to C-O species (from C1s signal by XPS). C) X-ray diffractograms of Pd/ZnO-B under different thermal treatments.*

Figure 8 shows the results for Pd/ZnO-B system. First, a thermogravimetric study (TG) of the system revealed that the solid exhibited a weight loss of ca. 22% upon calcination at temperatures up to 400°C. This is probably due to decomposition of remaining surfactant. In fact, an XPS study of Pd/ZnO-B as synthesized and calcined at 300°C and 500°C in the C1s region (not shown) revealed the progressive decrease in the signal at 286.6 eV assigned to C-O species

in alcohol and ether groups [34]. More interestingly, an XRD study of the system showed that smaller metal particles were obtained upon reduction for uncalcined systems as compared to previously calcined ones suggesting that the remaining surfactant prevents to a certain extent sintering of metal particles. Therefore, thermal treatment has two opposite effects on catalytic performance of M/ZnO-B solids. On the one hand, as temperature rises less surfactant remains which should be positive since metal particles are more accessible. On the other, thermal treatment results in an increase in particle size and appearance of strong metal-support interaction (SMSI) effect (at ca. 400°C) which is detrimental to activity. It seems that there is an optimum temperature (ca. 200-300°C) for which a compromise is reached.

4. Conclusions

ME technique is an adequate method to control metal particle size though it requires optimization of several parameters. The method allowed us to synthesize Pt, Pd and Rh systems with similar metal particle sizes (2-4nm, B-series). $NaBH_4$ used as reducing agent gave smaller particle sizes than hydrazine thus accounting for the better catalytic performance in glycerol transformation to acetol and 1,2-PDO of B-series. Systems obtained through ME technique contained particles in the metal state though thermal treatment to temperatures in the 200-300ºC range led to an improvement of catalytic performance. As temperature rises there are two opposite effects. On the one hand, surfactant is removed which is positive to activity. On the other, progressive loss of surfactant favors sintering of metal particles and at 400ºC a metal-Zn alloy is formed both being detrimental to activity. In this sense, a compromise between both trends seems to be reached at temperatures of 200ºC-300ºC. Reactivity order followed the sequence Rh>Pt>Pd and ME systems were found to be comparatively more selective to acetol than DP solids. This could be due to some remaining surfactant in the surroundings of

metallic particles thus limiting their hydrogenation activity. Moreover, metal seems to participate both in hydration of glycerol to acetol and the subsequent reduction to 1,2-PDO.

Acknowledgements

The authors are thankful to Junta de Andalucia and FEDER funds (P07-FQM-02695, P08-FQM-3931 and P09-FQM-4781 projects) for financial support. SCAI at the University of Cordoba is also acknowledged for ICP-MS measurements and the use of TEM and XPS. Finally, the authors are grateful to COST Action CM0903 for financial support, including a short-term scientific mission (STSM) of V. Montes.

References

1. Z. Yuan, P. Wu, J. Gao, X. Lu, Z. Hou, X. Xheng, Catal. Lett. 130 (2009) 261–265.
2. M. H. Mohamad, R. Awang, W. M .Z. W. Yunus, Am. J. Appl.Sci. 8 (2011) 1135-1139.
3. F. Vila, M. López Granados, M. Ojeda, J.L.G. Fierro, R. Mariscal, Catal. Today 187 (2012) 122– 128,
4. Z. Huang, F. Cui, J. Xue, J. Zuo, J.Chen, C. Xia, Catal.Today 183 (2012) 42– 51.
5. I. Gandarias, P. L. Arias, J. Requies, M. El Doukkali, M. B. Güemez, J. Catal. 282 (2011) 237–247.
6. F. Auneau, S. Noël, G. Aubert, M. Besson, L. Djakovitch, C. Pinel, Catal. Commun. 16 (2011) 144–149.
7. N. Hamzah, N. M. Nordin, A.H. A. Nadzri,Y. A. Nik, M. B. Kassim, M. A.Yarmo Appl.Catal. A 419– 420 (2012) 133– 141.
8. C. Montassier, J.C. Ménézo, L.C. Hoang, C. Renaud, J. Barbier, J. Mol. Catal. 70 (1991) 99–110.

9. K. Tomishige, Catal. Sci. Technol. 1 (2011) 179–190.

10. T. Miyazawa, Y. Kusunoki, K. Kunimori, K. Tomishige, J. Catal. 240 (2006) 213–221.

11. F. Auneau, C. Michel, F. Delbecq, C.Pinel, P. Sautet, Chem. Eur. J. 17 (2011) 14288-14299.

12. J. Chaminand, L. Djakovitch, P. Gallezot, P. Marion, C. Pinel, C. Rosier, Green Chem. 6 (2004) 359–361.

13. R. Rodrigues, N.Isoda, M.Gonçalves, F.C.A.Figueiredo, D.Mandelli, W.A.Carvalho, Chem. Eng. J. 198–199 (2012) 457–467

14. M. Checa, F. Auneau, J. Hidalgo-Carrillo, A. Marinas, J. M. Marinas, C. Pinel, F. J. Urbano, Catal. Today 196 (2012) 91-100.

15. M. Boutonnet, Curr. Op. Coll. Interf. Sci. 13 (2008) 270–286.

16. M. Boutonnet, J. Kizling, P. Stenius, Coll. Surf. 5 (1982) 209-225.

17. C. Destrée, J. B.Nagy, Adv. Coll. Interf. Sci. 123–126 (2006) 353–367.

18. I. Capek, Adv. Coll. Interf. Sci. 110 (2004) 49–74.

19. J. B.Nagy, A. Gourgue, E.G. Derouane Stud. Surf. Sci. Catal. 16 (1983) 193-202.

20. W. Suprun, M. Lutecki, T. Haber, H. Papp, J. Mol. Catal. A 309 (2009) 71-78.

21. P. Carniti, A. Gervasini, M. Marzo, Catal. Commun. 12 (2011) 1122-1126.

22. A.K. Kinage, P.P. Upare, P. Kasinathan, Y.K. Hwang, J.S. Chang, Catal. Commun. 11 (2010) 620-623.

23. W. Suprun, M. Lutecki, R. Gläser, H. Papp, J. Mol. Catal. A 342-343 (2011) 91-100.

24. W. Suprun, M. Lutecki, and H. Papp, Chem. Eng. Technol. 34 (2011) 134-139.

25. Y. T. Kim, K.-D. Jung, E.D. Park, Appl. Catal. B 107 (2011) 177-187.

26. K. Kongpatpanich, T. Nanok, B. Boekfa, M. Probst, J. Limtrakul, Phys. Chem. Chem. Phys. 13 (2011) 6462-6470.

27. M.R. Nimlos, S.J. Blanksby, X. Qian, M.E. Himmel, and D.K. Johnson, J. Phys. Chem. A 110 (2006) 6145-6156.

28. S. Sato, M. Akiyama, R. Takahashi, T. Hara, K. Inui, M. Yokota, Appl. Catal. A 347 (2008) 186-191.

29. A. Bienholz, H. Hofmann, P. Claus, Appl. Catal. A 391 (2011) 153-157.

30. I. Gandarias, P.L. Arias, J. Requies, M.B. Güemez, J.L.G. Fierro, Appl. Catal. B 87 (2010) 248-256.

31. S. Wang and H. Liu, Catal. Lett. 117 (2007) 62-67.

32. Z. Zhou, X. Li, T. Zeng, W. Hong, Z. Cheng, W. Yuan, Chinese J. Chem.Eng. 18 (2010) 384-390.

33. J. Hidalgo-Carrillo , M. A. Aramendía, A. Marinas, J. M. Marinas, F. J. Urbano, Appl. Catal. A 385 (2010) 190–200.

34. K.S. Kim, C.M. Ryu, C.S. Park, G. S. Sur, C. E. Park, Polymer 44 (2003) 6287-6295.

Paper II

Selective transformation of glycerol into 1,2-propanediol on several Pt/ZnO solids: further insight into the role and origin of catalyst acidity

V. Montes[1], M. Boutonnet[2] S. Järas[2], A, Marinas[*1], J.M. Marinas[1], F. J. Urbano[1]

[1]Organic Chemistry Department, University of Córdoba, Campus de Rabanales, Marie Curie Building, E-14014 Córdoba, Spain.

[2]KTH (Royal Institute of Technology), Chemical Technology, Teknikringen 42, SE-100 44 Stockholm, Sweden.

Keywords: glycerol transformation; microemulsion technique; Pt/ZnO; 1,2-propanediol; role of acid sites; effect of chlorine

*Corresponding author. Tel.: +34 957218622; fax: +34 957212066. E-mail address: alberto.marinas@uco.es

Abstract

Microemulsion technique allowed us to synthesize different ZnO solids with similar particle sizes and textural properties. Platinum was subsequently incorporated by deposition-precipitation and impregnation methods and solids tested for glycerol selective transformation into 1,2-PDO. Incorporation of platinum led to the creation of new (mainly Lewis) acid sites. A good correlation between conversion and acidity of Pt/ZnO solids was obtained. Interestingly, despite exhibiting some acidity, supports alone were inactive in the process which evidenced the role of the metal in dehydration of glycerol into acetol. Furthermore, as the reaction proceeded some chlorine coming from the precursor (H_2PtCl_6) was leached which led to the disappearance of the strongest acid sites, associated to side reactions (catalytic cracking) thus resulting in an increase in selectivity to 1,2-PDO. Eventual formation of Pt-Zn alloy upon reduction of the systems at ca. 400ºC was beneficial to 1,2-PDO selectivity.

Graphical abstract

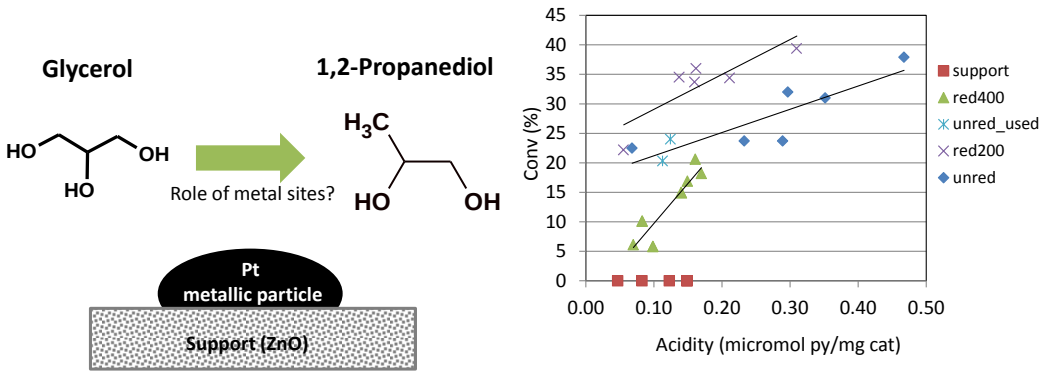

1. Introduction

Glycerol is a by-product from biodiesel production (ca. 100kg of glycerol per tonne of biodiesel produced). Therefore, its valorization through transformation into other valuable chemicals is of great interest. One of those valuable products is 1,2-propanediol (1,2-PDO), which is used in food industry, as a less toxic alternative to 1,2-ethanediol in antifreeze and as a deicer or as a feedstock in the preparation of polyester resins, just to cite some examples of applications [1]. This chemical is traditionally obtained through the petrochemical route via hydration of propylene oxide. Alternatively, 1,2-PDO could be produced through a biomass route from glycerol via dehydration of primary hydroxyl group (thus forming acetol) followed by hydrogenation of acetol into 1,2-PDO [2].

There are different features affecting activity and selectivity of glycerol transformation on metals, such as the metal of choice (e.g. Pt [3, 4], Rh [5, 6], Pd [5, 7], Ir [8], Cu [9-11]) the addition of a second metal [12,13], of acid or basic additives [14, 5], the metal particle size [15, 16] or the support [17, 18], just to cite some of them.

As for the mechanistic studies, there are some discrepancies in the literature concerning the nature of active sites responsible for selective transformation of glycerol into 1,2-PDO, in particular for initial dehydration of glycerol into acetol. Selective dehydroxylation of polyols can proceed through 3 different mechanisms. i) E1 (acid-catalyzed), involving protonation of a hydroxyl group which is then expelled as water, the resulting carbocation being neutralized by the elimination of a neighboring proton; ii) E2 (base-catalyzed) involving simultaneous H^+ removal, loss of the OH and formation of C=C bond and iii) homolytic cleavage of a C-O bond on a metallic surface (hydrogenolysis). Therefore, on acidic systems E1 mechanism is followed. In principle, dehydration of glycerol could take place through the primary or the secondary hydroxyl group, the former being thermodynamically favored [19].

According to Zhu et al. [20] Brønsted acid sites catalyze 1,3-propanediol formation whereas Lewis acid sites lead to 1,2-propanediol. On the contrary, Peng et al. [21] speculate on Brønsted acid sites being responsible for glycerol dehydration processes in aqueous medium given the fact that Lewis acid sites would be converted into Brønsted centers. As for the strength needed for the process, in a study on gas phase hydrogenolysis of glycerol catalyzed by Cu/ZnO/MOx (MOx =Al_2O_3, TiO_2, and ZrO_2) solids, Feng et al. [22] concluded that strong acid sites were responsible for 1,2-PDO formation whereas weak acid sites led to 1,3-PDO. In the liquid phase, Vasiliadou et al. [18] found that moderate acid sites are sufficient to activate glycerol dehydration. Finally, some studies give support to the role of the metal not only in hydrogenation of acetol but also in glycerol activation [18, 23, 24].

In a previous paper, a screening of different partially reducible oxides to be used as supports for platinum was described, ZnO being selected for subsequent studies [4]. Moreover, systems reduced at 200ºC exhibited better catalytic performance than those reduced at 400ºC, a temperature at which Pt-Zn alloy was formed which was detrimental to activity. In a follow-up study [24], different solids consisting in a noble metal supported on ZnO were synthesized through the microemulsion method. This allowed us to obtain quite similar metal (Pt, Rh, Pd) particle sizes. Under our experimental conditions, reactivity followed the order Rh > Pt > Pd. Furthermore, the presence of some remaining surfactant seemed to somehow hinder hydrogenation activity of the metal, thus leading to an unusually high selectivity to acetol.

In the present paper, the good control of particle size ensured through microemulsion (ME) technique is used to synthesize diverse ZnO solids (either alone or modified with Al, Ce or Zr) with a view to tune acidity of the support. Platinum is subsequently incorporated onto the systems through deposition-precipitation technique or impregnation from H_2PtCl_6 aqueous solutions. For

comparative studies, a system starting from a different precursor (platinum nitrate) was also synthesized. The final goal is to cast further light on the nature and origin of active sites responsible for the initial dehydration step of glycerol into acetol.

2. Experimental

2.1. Materials

Synperonic 13/6.5 was a gift from Croda. Zn(II)-2-ethylhexanoate (89%) dissolved in mineral spirit, Al(III)-2-ethylhexanoate, Zr(IV)-2-ethylhexanoate, Ce(IV)-2-ethylhexanoate, and 15%w/w Pt(IV) nitrate solution were purchased from Alfa Aesar. 8% weight H_2PtCl_6 aqueous solution, ZnO nanopowder, acetone (technical grade), glycerol 99%, 1,2-propanediol 99.5%, 1,3-propanediol 98%, (hydroxyacetone) acetol 95%, ethylenglycol 99.5%, n-propanol 99.5%, n-hexane >99%, HCl 33% in water, and NaOH >99% were purchased from Sigma-Aldrich. MilliQ water was used for preparation of water solutions.

2.2. Synthesis of the solids

2.2.1. Synthesis of ZnO solids through ME technique

The solids, ZnO (either alone or doped with 5% by weight of Al, Zr or Ce) were synthesized using the commonly known method of oil in water (O/W) microemulsion (ME) [25]. The internal structure of the ME is determined by the relative fractions of three constituents: surfactant, oil and water. The ME is only formed for certain ratios of the constituents, outside which a two-phase system is formed. The first step was to determine the relative fractions of components where the ME was stable. So, different composition mixtures of surfactant and water were prepared at different temperatures. Then a solution of organometallic precursor was added dropwise in order to know the maximum soluble amount. Determination of this amount is easy because the microemulsions are isotropic and transparent, and

when they destabilize the transparent dissolution turns into a cloudy system. These experiments allowed us to determine the region of relative fractions of constituents to form microemulsion. Under optimized conditions, the composition of microemulsions (ME) was surfactant: synperonic 13/6.5 (18.8 wt%), oil: organic precursor of metal (10 wt % of Zn) dissolved in n-hexane (24.5%), water: 56.7 wt%. In the case of doping of ZnO with Al, Ce or Zr, the oil is formed by 10% wt Zn+(Al, Ce or Zr). Moreover, Al, Ce or Zr content was calculated to have 5wt% of these metals in the resulting ZnO solid.

Once the microemulsion had been obtained in the presence of the Zn(II) ethylhexanoate aqueous solution, pH was increased up to 11 with NH_4OH in order to precipitate ZnO [26]. Resulting solids were aged under stirring for 7h, centrifuged and carefully washed with 3 portions of 100mL n-hexane. The solids were dried at 70ºC for 12 hours and calcined at 400ºC for 2 hours at a rate of 10 ºC/minute with a synthetic air flow of 2L/h.

For comparative purposes, a commercial ZnO solid was also used as the support in the present study.

2.2.2. Incorporation of Platinum

a) Deposition precipitation method

The synthetic procedure was as follows: a volume of 6.57 mL of chloroplatinic acid solution (or 1.67 mL of $Pt(NO_3)_4$ solution) was diluted to 200 mL with Milli-Q water and adjusted to pH 7 by adding 0.1 M NaOH. Then, an amount of 4.75 g of support was added and the mixture readjusted to pH 7 with 0.1 M HCl. The solution containing the support was refluxed at 70ºC under vigorous stirring for 2 h. Then, a volume of 10 mL of isopropanol was added, the temperature raised to 110ºC and refluxing continued for 30 min, after which the mixture was vacuum filtered and the filtrate washed with three portions of 25 mL

of water each. The resulting solid was dried in a muffle furnace at 110ºC for 12 h, ground and calcined at 400ºC for 4 h with a rate of 1ºC/min. After calcination, the solid was ground again, sieved through a mesh of 0.149 mm pore size and stored in a flask.

b) Impregnation method

200 mL of water containing the metal precursor (chloroplatinic acid) was adjusted to pH 7 with NaOH. Then, the corresponding amount of ZnO solid (in order to obtain 5wt% Pt/ZnO in final systems) was suspended and pH re-adjusted to 7 with HCl. Suspensions were stirred for 5h at room temperature and then the solvent was rota-evaporated and calcined at 400ºC. After calcination, the solid was ground, sieved through a mesh of 0.149 mm pore size and stored in a flask.

The nomenclature of the solids includes an N or Cl prefix indicating the platinum precursor (platinum nitrate or chloroplatinic acid, respectively), followed by the method of incorporation (dp or im for deposition-precipitation or impregnation, respectively) and the origin of the ZnO used (com or ME for commercial or synthesized through microemulsion, respectively). In the latter case, when applicable, Al, Ce or Zr refers to the metal doping ZnO. Finally, the name is followed by the reduction treatment. Therefore, for instance, a catalyst synthesized by deposition-precipitation method from chloroplatinic acid on an Al-doped ZnO solid synthesized through microemulsion and pre-reduced at 200ºC is denoted as Cl-dp-ME-Al-200 whereas N-dp-com-unred would indicate that platinum nitrate was incorporated on a commercial ZnO through deposition-precipitation method and tested in the reaction without any reduction pre-treatment.

2.3 Characterization

Elemental analysis of metal-containing samples was performed by the staff at the Central Service for Research Support (SCAI) of the University of Córdoba. It was performed using inductively coupled plasma mass spectrometry (ICP-MS). Measurements were made on a Perkin-Elmer ELAN DRC-e instrument following dissolution of the sample in a 1:3 HNO_3/HCl mixture with a soft heating. Calibration was done by using PE Pure Plus atomic spectroscopy standards, also from Perkin-Elmer.

Thermogravimetric analyses (TGA–DTA) were performed on a Setaram SetSys 12 instrument. An amount of 20 mg of sample was placed in an alumina crucible and heated at temperatures from 30 to 1000ºC at a rate of 10ºC/min under a stream of synthetic air at 40 mL/min in order to measure weight loss, heat flow and derivative weight loss.

EDX measurements were performed on a JEOL JSM-6300 scanning electron microscope (SEM) equipped with an energy-dispersive X-ray (EDX) detector. It was operated at an acceleration voltage of 20keV with a resolution of 65eV.

Surface areas of the solids were determined from nitrogen adsorption–desorption isotherms obtained at liquid nitrogen temperature on a Micromeritics ASAP-2010 instrument, using the Brunnauer–Emmett–Teller (BET) method. All samples were degassed to 0.1 Pa at 120ºC prior to measurement.

Transmission electron microscopy (TEM) images were obtained using a JEOL JEM 1400 microscope. All samples were mounted on 3 mm holey carbon copper grids. Particle sizes were obtained by counting 100 particles.

X-ray patterns of the samples were obtained on a Siemens D-5000 diffractometer equipped with a DACO-MP automatic control and data acquisition system. The instrument was equipped with a graphite monochromator and used Cu Kα radiation. Metal particle sizes were calculated using Scherrer equation.

X-ray photoelectron spectroscopy (XPS) data were recorded on 4 mm × 4 mm pellets 0.5 mm thick that were obtained by gently pressing the powdered materials following outgassing to a pressure below about 2×10^{-8} Torr at 150ºC in the instrument pre-chamber to remove chemisorbed volatile species. The main chamber of the Leibold–Heraeus LHS10 spectrometer used, capable of operating down to less than 2×10^{-9} Torr, was equipped with an EA-200MCD hemispherical electron analyser with a dual X-ray source using AlKα (hv = 1486.6 eV) at 120 W, at 30 mA, with C(1s) as energy reference (284.6 eV).

Temperature-programmed reduction (TPR) measurements were made with a Micromeritics TPD-TPR 2920 analyser. An amount of 100 mg of catalyst was placed in the sample holder and reduced in a 10:90 H_2/Ar stream flowing at 20 mL min^{-1}. The temperature was ramped from 50 to 350ºC.

Surface acidity in the catalysts were determined by thermal programmed desorption (TPD) of a pre-adsorbed probe molecule, pyridine (Py) monitored by TCD. An amount of 50 mg of sample was placed under a He stream flowing at 75 mL/min in a reactor 10 mm in diameter that was placed inside an oven. The He stream was used to clean the solids by heating to 350ºC at a rate of 10ºC/min and then cooling to 50ºC. At that point, the surface of the solid was saturated with the Py for 30 min. Pyridine was supplied by bubbling the He stream through liquid pyridine at room temperature over the samples. After saturation, excess physisorbed Py was removed increasing the-temperature up to 50ºC and passing a He stream at 75 mL/min for 60 minutes. Then temperature was increased up to 400ºC at 10ºC/min, holding the final level for 30 min. Desorbed pyridine was quantified against a calibration graph previously constructed from variable injected volumes of pyridine.

The above-described overall acidity study by TPD-Py was supplemented with one by diffuse reflectance infrared (DRIFT) spectroscopy of the pyridine-saturated solids intended to identify the specific types of acid sites present.

Measurements were made with an ABB Bomen MB Series IR spectrophotometer equipped with a SpectraTech P/N 0030-100 environmental chamber including a diffuse reflectance device capable of performing 258 scans at 8 cm^{-1} resolution at an adjustable temperature. Prior to analysis, each catalyst was thermally cleaned at 400ºC for 30 min. The last few minutes of the thermal treatment were used to record reference spectra.

2.4 Catalytic tests

Hydrogenolysis of glycerol was conducted in a Berghof HR-100 stainless steel high-pressure autoclave equipped with a 75 mL PTFE vessel and a magnetic stirrer. Under standard conditions, 10 mL of a 1.36 M solution of glycerol in water and 100 mg catalysts were introduced in the vessel. Reactor was then purged with the selected atmosphere (H_2 or N_2), and temperature (180ºC) and pressure (2 or 6 bar) adjusted. The stirring rate was 1200 rpm. After 15 hours of reaction, stirring was stopped and the vessel cooled with an ice bath. The reaction mixture was centrifuged to separate the catalyst and the liquid passed through a filter of PTFE 0.45μm. Then it was analyzed by GC-FID (Agilent Technologies 7890, with a Supelco 25357 NukolTM capillary column). Quantification was carried out through the corresponding calibration curves.

3. Results and discussion

3.1. Characterization of support

TG-DTA profiles of all uncalcined solids obtained through ME method are quite similar. Figure 1 shows that of ME system. There are two main weight losses centered at ca. 140ºC and 330ºC, respectively. The first one could be due to water whereas the second one could be attributed to the decomposition of remaining organic compounds (e.g. surfactant, organic precursor) [27, 28]. In fact, the loss weight % (41.6%) is much higher than the theoretical one corresponding to the

conversion of $Zn(OH)_2$ into ZnO (ca. 18.1%) thus evidencing the presence of remaining organics. Interestingly, there is no significant weight loss at temperatures above calcination temperature (400ºC). In fact, TG-DTA profile of the solid calcined at 400ºC (Fig. 1) did not exhibit any weight loss thus ensuring thermal stability of the obtained solid.

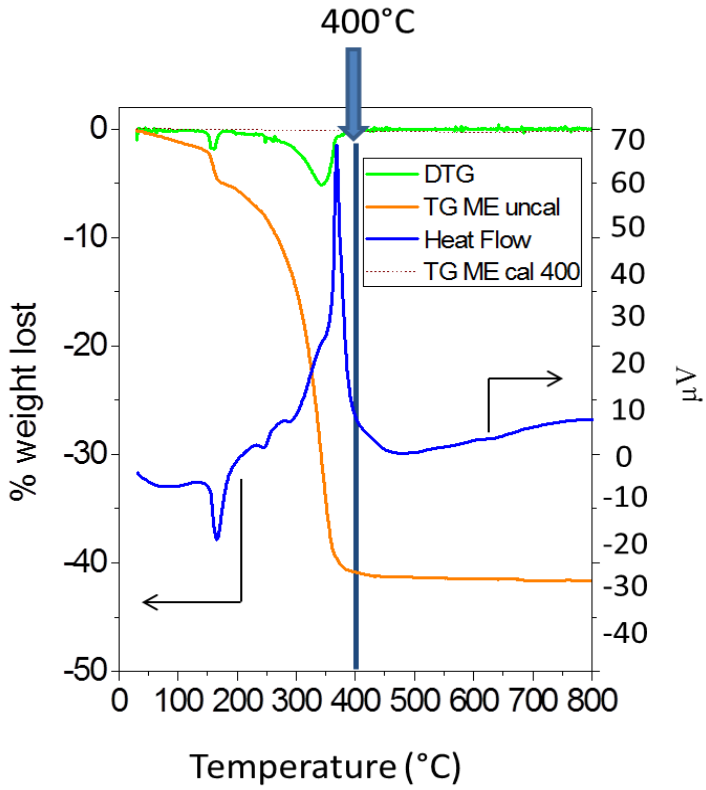

Figure 1. *TG-DTA profile obtained in synthetic air for the ME uncalcined system. Dotted line corresponds to weight loss of ME calcined at 400ºC.*

The main features concerning characterization of the supports are given in Table 1. As can be seen, and as expected, ME method ensured quite similar particle sizes (22-26 nm) for all ZnO-based solids, BET surface areas being in the 27-36 m^2/g range. For comparative purposes, commercial ZnO solid has also being included in Table 1, its surface area being significantly lower (15 m^2/g). In all cases, ZnO-systems are mesoporous solids, with mean pore diameters ranging 7-11 nm. As regards elemental analyses of samples, bulk analyses (ICP-MS and EDX) reveal that the metals (Al, Ce or Zr) have been incorporated below the nominal value (5% wt).

One possible reason could be the partial re-dissolution of precipitated hydroxides at the high pH (11) used in the synthesis [29, 30]. X-Ray diffractograms of ZnO supports (not shown) revealed that in all cases ZnO have a zincite (wurzite) structure with the typical peaks at 2θ values of 31.7, 34.4, 36.2º corresponding to (100), (002) and (101) reflections, respectively [31]. No signals corresponding to ceria, zirconia or alumina were observed which is hardly surprising considering the above-mentioned low incorporation. Acidity of the solids was determined by TPD of pre-adsorbed pyridine (Table 1). Interestingly, despite the relatively low metal-doping content, incorporation of Al, Ce or Zr led to a significant increase in acidity, in the 50-88% range. Moreover, acidity of commercial ZnO solid is lower than that of the pure ZnO system obtained through microemulsion technique. No change in acidity of the supports was observed after treatment under H_2 flow for 2h at 200ºC or 400ºC.

Table 1. *Some features concerning characterization of ZnO supports.*

Support	N_2 isotherms		Particle size diameter (XRD)	Metal content (%)			Acidity (μmol py per mg catalyst)
	BET area (m^2/g)	Mean pore diameter (nm)		ICP-MS	EDX	XPS	
Com	15	11	50	--	--	--	0.05
ME	29	8	26	--	--	--	0.08
ME-Al	27	9	23	0.36	0.46	1.65	0.15
ME-Ce	31	7	22	0.53	3.67	3.44	0.15
ME-Zr	36	8	24	0.19	1.26	1.61	0.12

3.2.Characterization of platinum-containing solids

Some features concerning characterization of Pt-containing systems are summarized in Table 2. ICP-MS results confirm a good incorporation of platinum, quite close to the nominal content (5% wt).

XRD profiles of the samples (Figure 2) reveal that in general, reduction at 200ºC results in the appearance of a band at ca. 39.8º attributed to (1 1 1) crystal plane of the Pt^0 face-centered-cubic phase [32] whereas subsequent reduction at 400ºC leads to the shift of the band to higher 2θ values (ca. 40.9º) which is indicative of the formation of PtZn alloy [4, 33]. The exceptions are Cl-dp-ME-Ce and Cl-im-com systems. In the former case, unred system already exhibits a signal at ca. 39.8º which could be indicative of some kind of Pt-support interaction (Pt-Zn or Pt-Ce [34]). In the latter case, Pt-Zn alloy seems to be already present in the solid reduced at 200ºC (see signal at ca. 45.9º). In any case, the influence of other factors on the appearance of Pt bands (e.g. metal particle size, oxidation state) should be studied by other techniques (e.g. TEM, XPS).

Table 2*. Some features concerning characterization of the different Pt/ZnO solids.*

Catalyst	Pt weight %		Average Pt particle size (TEM, nm)		Total acidity (μmol py/mg catalyst)			
	ICP-MS	EDX	200	400	unred	200	400	used
Cl-dp-com	4.2	2.7	1.9	3.6	0.23	0.14	0.14	0.11
Cl-dp-ME	4.7	3.0	1.8	3.0	0.29	0.20	0.14	0.15
Cl-dp-ME-Al	4.5	3.9	1.7	3.3	0.35	0.21	0.17	0.13
Cl-dp-ME-Ce	6.1	4.0	1.3	2.2	0.30	0.16	0.15	0.11
Cl-dp_ME-Zr	4.8	5.5	1.5	3.2	0.47	0.31	0.16	0.12
Cl-im-com	4.5	2.9	2.0	3.3	0.20	0.11	0.08	0.0
N-dp-com	4.3	6.0	2.8	4.2	0.07	0.06	0.07	0.0

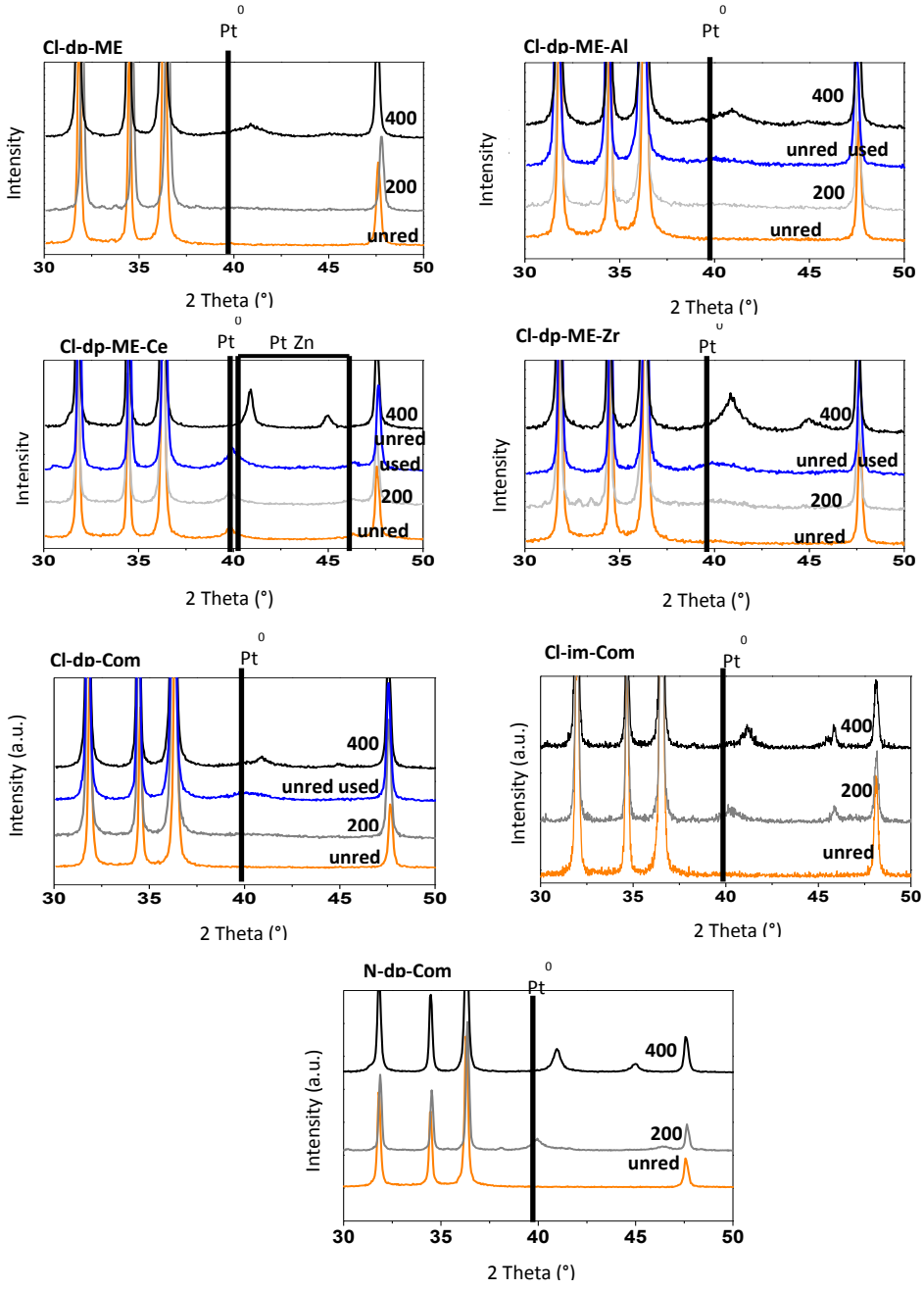

Figure 2. *X-Ray diffractograms of the different Pt/ZnO systems unreduced or reduced at 200ºC and 400ºC. In some cases the profiles of unreduced systems after 15h of reaction have also been included.*

H_2 TPR profiles are shown in Figure 3. There are different factors affecting reducibility of metal particles such as size, the metal environment (e.g. presence of chloride species coming from the precursor) or when using partially reducible oxides as the support, as it is the case of the present study, existence of strong-metal support interactions [35-37]. Therefore, smaller metal particles are more difficult to be reduced than larger ones thus resulting in a shift to higher temperatures in the TPR profile. Moreover, the presence of chloride ions at the metal-support interface has been described to hinder electron exchange between the metal and the oxide support thus leading to higher reduction temperatures. Finally, reduction peaks appearing at the highest reduction temperatures are typically associated to those platinum particles strongly interacting with the support.

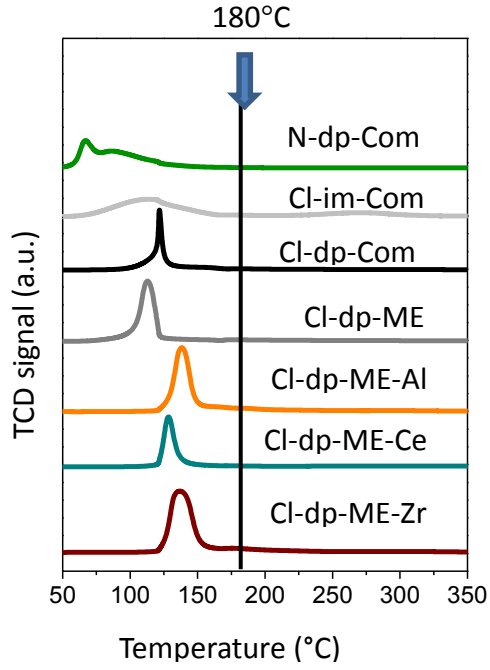

Figure 3. *TPR profiles of the different Pt/ZnO systems. The vertical line indicates reaction temperature in catalytic experiments of glycerol transformation (180ºC).*

Figure 3 confirms that at the temperature selected for catalytic experiments (180ºC) all systems are reduced. Furthermore, TPR signals of all the systems obtained through ME exhibit a single relatively narrow peak which suggests a homogeneous platinum particle size distribution. As regards the solids based on commercial ZnO, results suggest the influence of both the synthetic method and the metal precursor on metal dispersion. Therefore, a more homogeneous distribution of platinum particle sizes would be expected for Cl-dp-com than for Cl-im-com judging by the narrower TPR peak in the former case. Comparing the effect of the employed Pt precursors (Cl-dp-com vs N-dp-com), larger and more heterogeneous in size platinum particles seem to have been obtained from platinum nitrate, as suggested by the wider TPR profile appearing at lower reduction temperatures. The influence of chlorine residues shifting TPR peaks to higher temperatures in the case of Cl-dp-com, cannot be ruled out. TEM micrographs (Figures 4-6) cast further light on these issues. The first conclusion that can be drawn from this study is that the average particle sizes for the samples reduced at 200ºC are quite similar for all types of solids (in the 1.3-2.0 nm range, Table 2), the exception being N-dp-com for which larger metal particles (2.8 nm, Figure 6) were obtained. This could be ascribed to the different metal precursor used and is in line with TPR profiles which evidenced an easier reduction of platinum particles in that solid. If TEM figures of Cl-im-com-200 and Cl-dp-com-200 are compared (Figure 5), quite similar particle size distributions are obtained. This suggests that above-commented observed differences in TPR and XRD profiles could be ascribed to different metal-support interactions. Finally, in all cases, increase in reduction temperature from 200ºC up to 400ºC resulted in metal sintering.

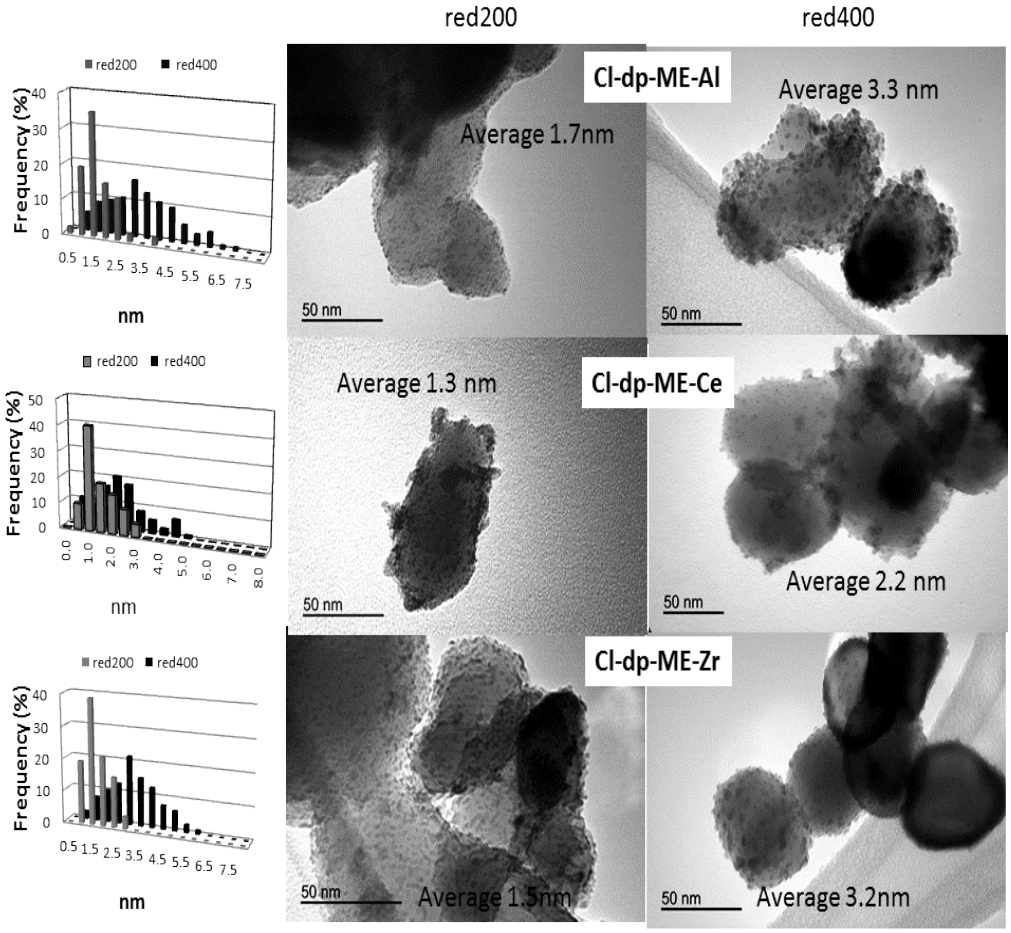

Figure 4*. TEM micrographs of Cl-dp-ME-Al, Cl-dp-ME-Ce and Cl-dp-ME-Zr reduced at 200 and 400ºC.*

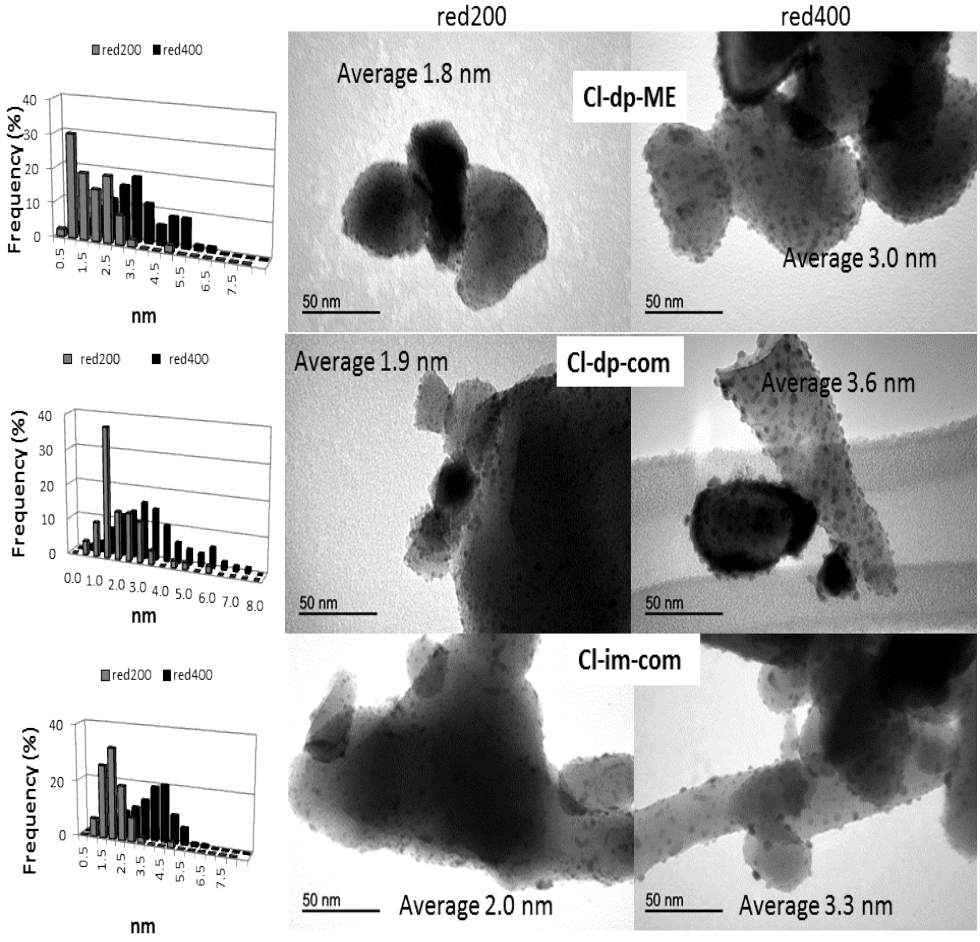

***Figure 5**. TEM micrographs of Cl-dp-ME, Cl-dp -com and Cl-im-com reduced at 200 and 400ºC*

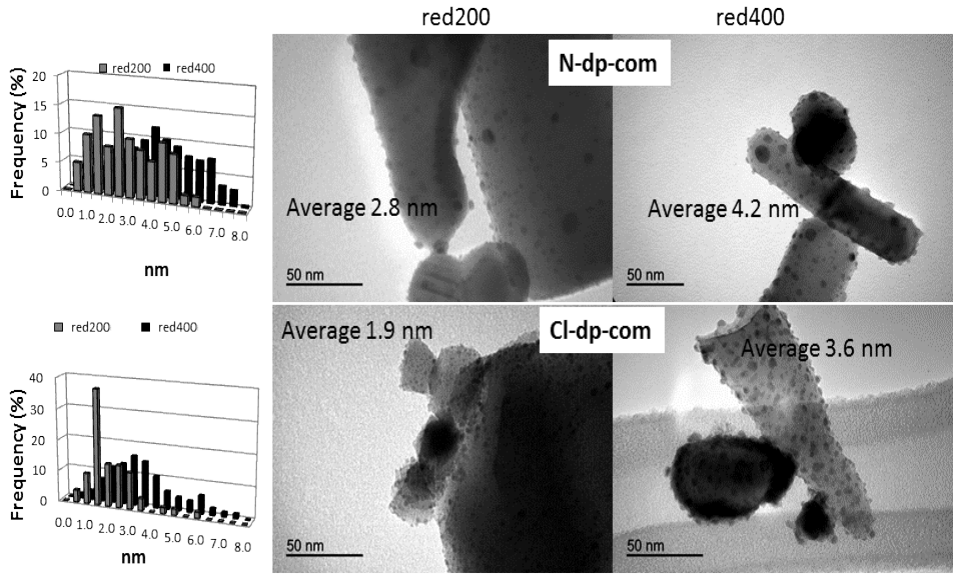

Figure 6*. TEM micrographs of N-dp-com and Cl-dp-com reduced at 200 and 400ºC.*

XPS spectra of unreduced samples in the Zn $2p_{3/2}$ region showed a peak centered at ca. 1022 eV which can be ascribed to ZnO. In the case of solids obtained from H_2PtCl_6, reduction at 200ºC resulted in the appearance of a second peak at ca. 1023 eV whose relative intensity decreased upon subsequent reduction at 400ºC (see Figure 7). This second peak can be associated to oxychlorinated Zn^{2+} species [38]. As regards Pt $4f_{5/2}$, unreduced systems are formed by Pt^{2+} (72.4-72.8 eV) and Pt^{4+} (73.7-74.9 eV) whereas no signals corresponding to Pt^0 at ca. 70.6-71.0 eV were observed. Interestingly, the highest Pt^{2+} percentage (ca. 44%) corresponded to Cl-dp-ME-Ce solid which could be ascribed to Ce interacting with Pt (remember XRD profiles, Fig. 2). Reduction of the solids at 200ºC resulted in the formation of Pt^0 which is concordant with XRD and TPR profiles. As regards XPS spectra of metal-doping species (Figure 8), Al2s signals of Cl-dp-ME-Al unreduced and reduced at 200 and 400ºC remained at 118.5eV which suggests an Al_2O_3 environment [39]. Similarly, $Zr3d_{5/2}$ signal of Cl-dp-ME-Zr-unred, 200 and 400ºC solids appeared at 182eV which suggests the presence of ZrO_2 [40]. In contrast, $Ce3d_{5/2}$ signal of Cl-dp-ME-Ce-unred solid differed from those of the solid reduced at 200ºC and 400ºC thus suggesting different Ce(III)/Ce(IV) ratios in those samples depending on the reduction treatment [34].

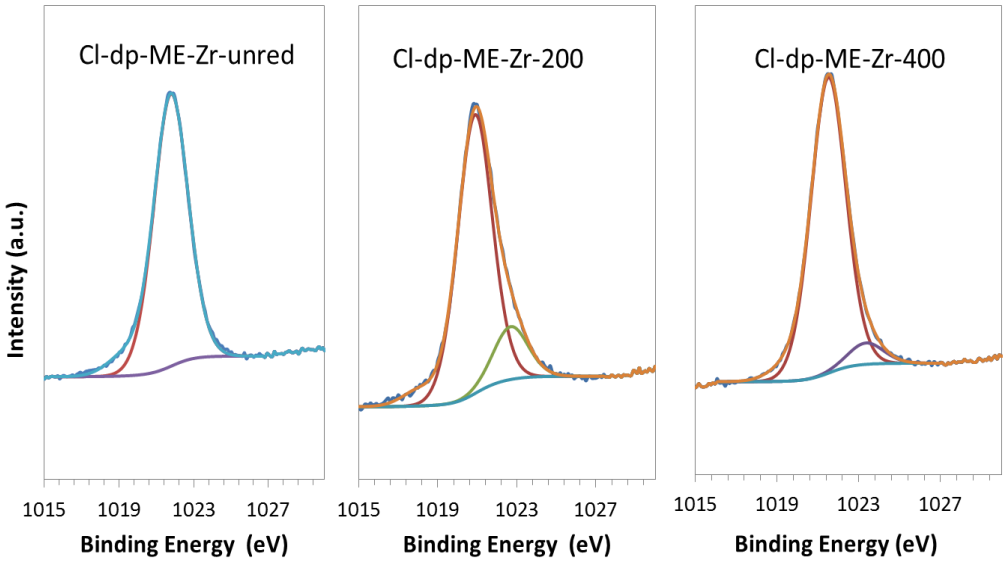

***Figure 7**. XPS profiles in the Zn(2p3/2) region of Cl-dp-ME-Zr system unreduced and reduced at 200ºC or 400ºC*

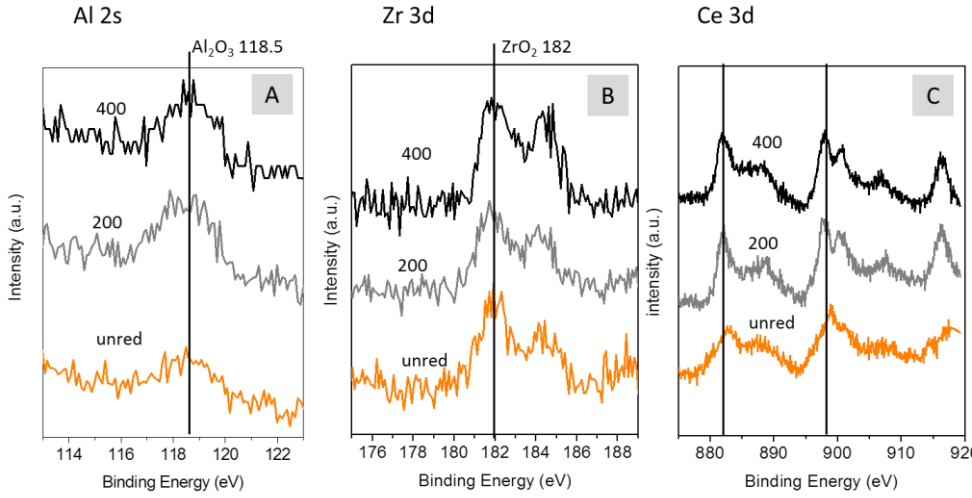

***Figure 8**. XPS profiles of Cl-dp-ME-Al (A), Cl-dp-ME-Zr (B) and Cl-dp-ME-Ce (C) unreduced and reduced at 200ºC and 400ºC in the XPS Al(2s). Zr(3d) and Ce(3d) regions, respectively.*

TPD profiles of pre-adsorbed pyridine are depicted in Figure 9 and acidity data are summarized in Table 2. From Figure 9 it is evident that the incorporation of platinum using H_2PtCl_6 as the precursor led to the creation of acidity. Therefore, there are two main pyridine desorption peaks centered at ca. 100ºC and 300ºC, respectively. Reduction of the solids at 200ºC results in the disappearance of the high-temperature peak whereas the low-temperature one remains even after reduction at 400ºC. In the case of N-dp-com solid, on the contrary, incorporation of platinum did not result in new acid sites, thus confirming that new acid sites are somehow associated to the presence of chlorine. In order to cast further light on the nature (Lewis or Brønsted) of acid sites, acidity tests were complemented with DRIFT studies. Figure 10 presents the DRIFT spectra of pyridine chemisorbed on Cl-dp-com solids at different temperatures (100-400ºC) though similar results are obtained for the other systems coming from H_2PtCl_6 precursor. In all cases, the spectra of pyridine adsorbed at 100ºC on unreduced Pt-containing solids exhibit two main bands centered at ca 1454 and 1610 cm^{-1} which are associated to Lewis acid sites, together with some other minor ones at ca. 1486 (Brønsted + Lewis), 1547 (Brønsted) [41, 42]. Acidity of solids reduced at 200ºC is lower (as evidenced by the decrease in intensity of all bands) whereas subsequent reduction at 400ºC hardly changes acidity (which is consistent with Figure 9). Interestingly, N-dp-com-unred solid also exhibited in DRIFT studies the above-mentioned Lewis acid sites which retained pyridine up to 100ºC whereas no bands due to pyridine adsorption were observed for reduced systems (not shown). All these results suggest that on introduction of platinum (either using H_2PtCl_6 or $Pt(NO_3)_4$ as the precursor) some new acid sites, mainly Lewis-type, are created. In the case of Cl-series some of those sites are kept in reduced solids (probably associated to the presence of chlorine) whereas for N-dp-com reduction at 200ºC leads to their disappearance, which could be due to reduction of Pt(II) and Pt(IV) to Pt^0 as evidenced by XPS and H_2 TPR studies.

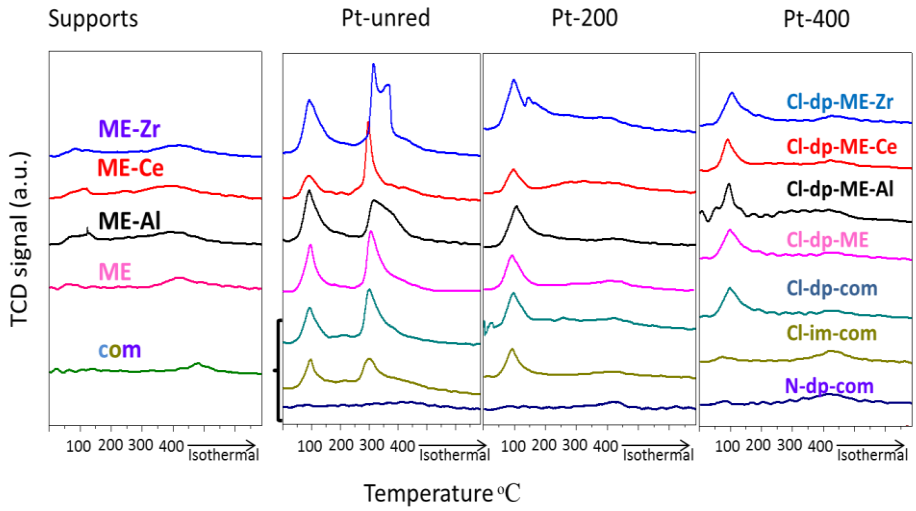

***Figure 9**. Temperature-programmed desorption (TPD) profiles of pyridine pre-adsorbed at 50ºC for supports and Pt/ZnO systems (unreduced and reduced at 200ºC and 400ºC).*

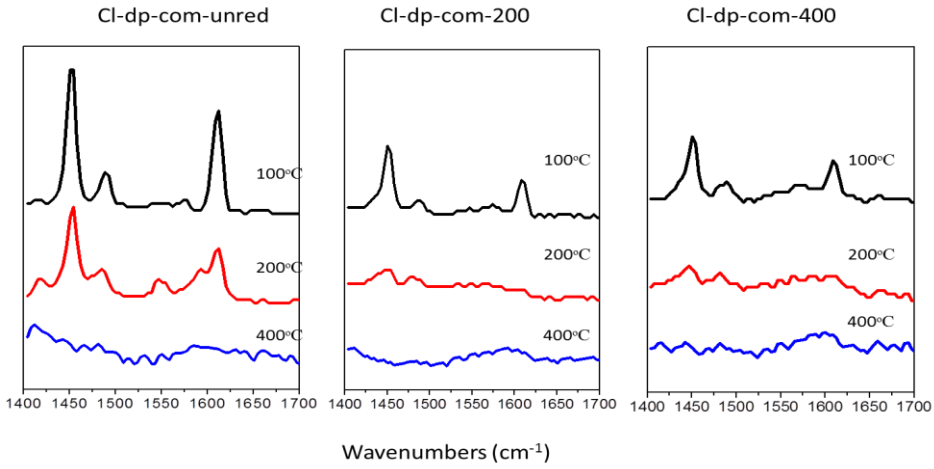

***Figure 10**. Diffuse reflectance infrared Fourier transformed spectra (DRIFT) of Cl-dp-com systems saturated with pyridine at 50ºC upon thermal treatment at different temperatures (100, 200 and 400ºC).*

3.3.Catalytic activity

Production of 1,2-PDO from glycerol is known to occur via intermediate production of acetol. Therefore, dehydration of primary hydroxyl group in glycerol yields acetol whose hydrogenation leads to 1,2-PDO (Scheme 1). The different catalysts were tested for their activity for glycerol transformation into 1,2-PDO. Under standard conditions (see section 2.4.), supports (unred or reduced at 200ºC or 400ºC) were not active in the process. As for the Pt-containing solids, results obtained for conversion and selectivity after 15h reaction are summarized in Figure 11. In terms of conversion, values achieved with unreduced samples are in general quite similar to those obtained for solids reduced at 200ºC. This is hardly surprising since at the working temperature (180ºC) platinum can be in-situ reduced (remember TPR profiles). Subsequent reduction at 400ºC led to a dramatic decrease in conversion. Increase in particle size (as evidenced by TEM, Table 2) and formation of Pt-Zn alloy (remember XRD results) could account for that. An additional point to take into account is that total acidity decreases with reduction temperature (see Table 2) which will be further commented in the mechanistic discussion. It is also worth noting that conversion values for N-dp-com systems are significantly lower than those of their Cl-dp-com counterparts which again could be related to the larger particles. In fact, if TOF values (expressed as moles of glycerol converted per mole of Pt per hour) are represented (Figure 12), N-dp-com and Cl-dp-com perform quite similarly either unreduced and reduced at 200ºC.

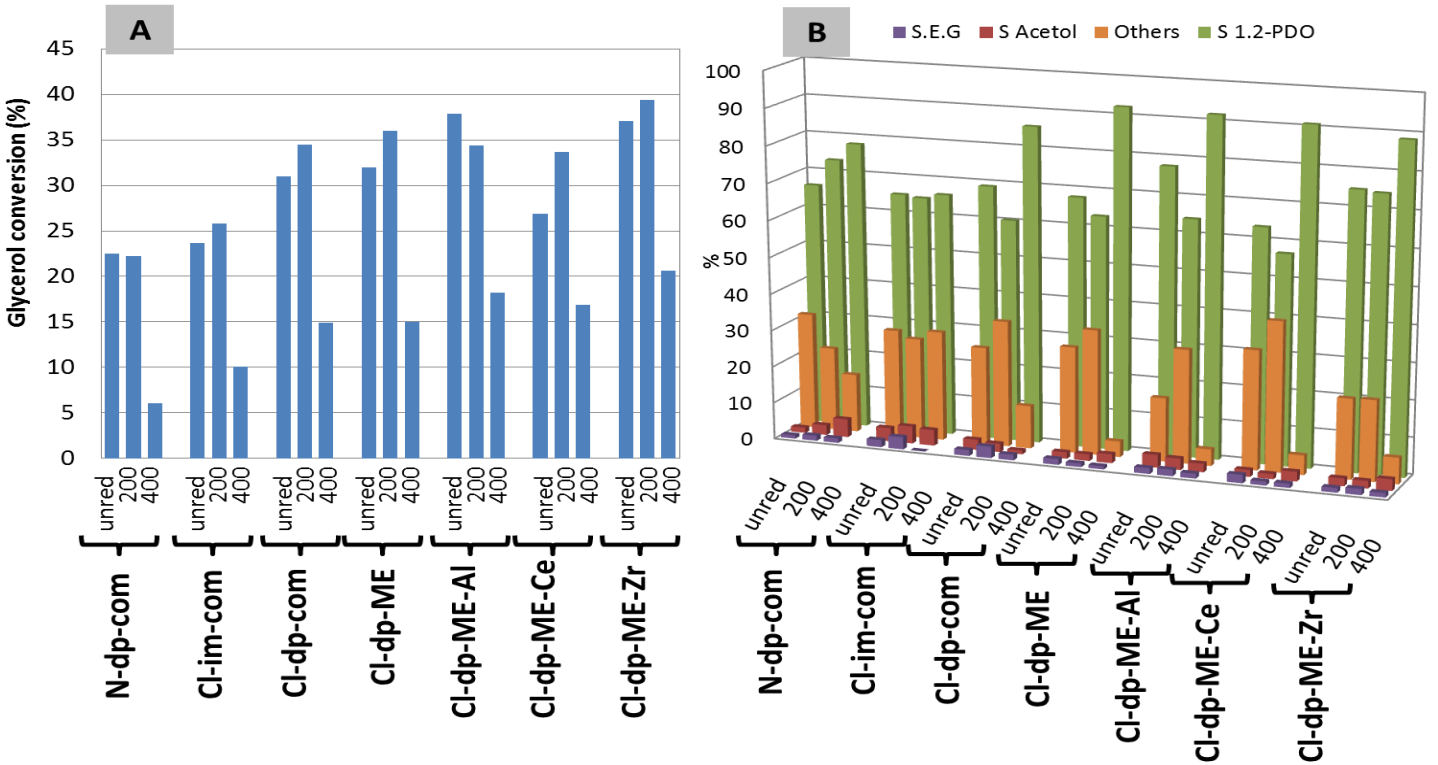

Figure 11*. Results for catalytic transformation of glycerol expressed in terms of conversion (A) and selectivity to ethylene glycol (EG), acetol, 1,2-PDO or others (B) for t=15h. Reaction conditions: 100 mg catalysts, 10 mL 1.36 M water solution of glycerol. 180ºC and 6 bar of initial hydrogen pressure. Reaction time: 15h*

In terms of TOF, Cl-dp-ME-Zr-unred and Cl-dp-Al-unred (the most acidic solids, as determined by TPD of pre-adsorbed pyridine) are the systems exhibiting the highest values whereas Cl-dp-ME-Ce-unred, for which some kind of Pt-support interaction had already been detected by XRD in unred system and Cl-im-com (which apparently also evidenced Pt-support interaction at lower temperatures than its ME counterparts) are the least active solids. Figure 13 shows a dependence of conversion on acidity and platinum average particle size. From that figure it is evident that the presence of the metal is necessary for the reaction since supports, despite exhibiting some acidity, are inactive in the reaction. This backs the idea of the metal participating in dehydration of glycerol to acetol.

As far as selectivity to 1,2-PDO is concerned (Figure 11B), reduction at 400ºC resulted in a significant increase up to values of ca. 90%, the exception being N-dp-com and Cl-im-com. However, appropriate study of effect of reduction temperature on selectivity to 1,2-PDO requires the performance of reactions with unred and 200 systems at lower reaction times in order to get similar conversions to those achieved with solids reduced at 400ºC after 15h (i.e. selectivity values must be compared at iso-conversions). This will be performed in the following section.

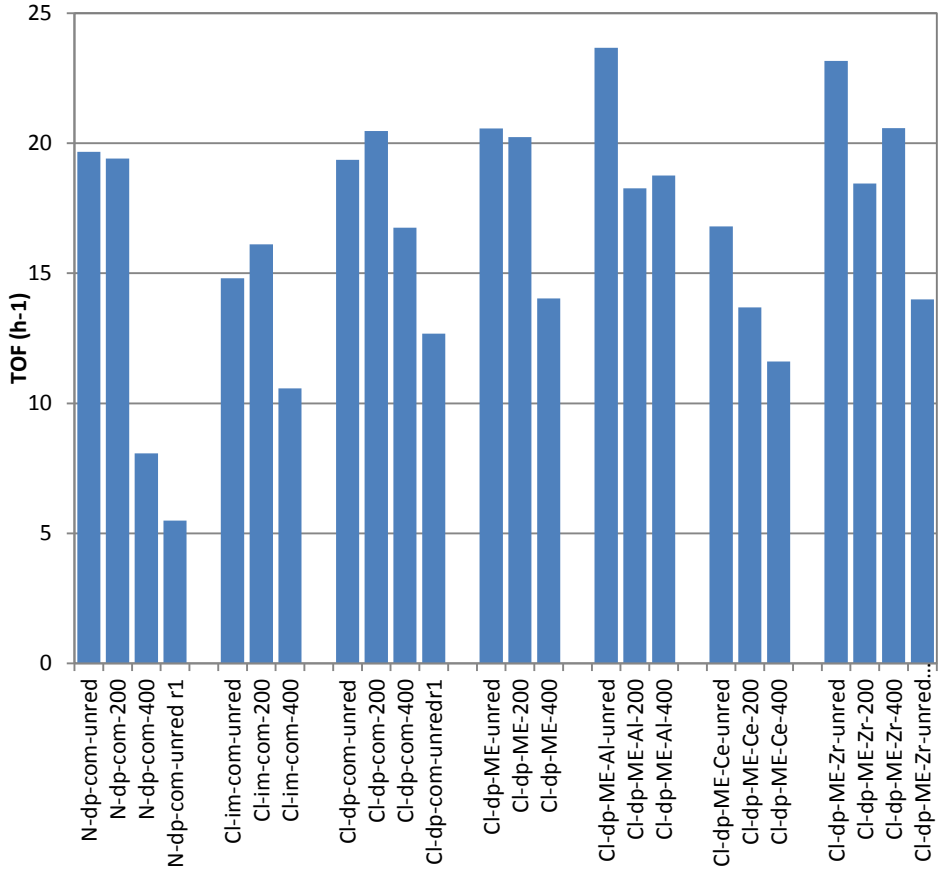

Figure 12. *Results obtained for catalytic transformation of glycerol expressed in terms of turnover frequencies (TOF) for t=15h. Reaction conditions: 100 mg catalysts, 10 mL 1.36 M water solution of glycerol. 180ºC and 6 bar of initial hydrogen pressure. Reaction time: 15h. Data correspond to systems unreduced, reduced at 200ºC and 400ºC. In some cases results for the first reutilisation of unreduced solids have been included (r1 suffix).*

Mechanistic discussion

In order to cast further light on the process, some further studies were performed and a reaction mechanism suggested (Scheme 1). Firstly, experiments at variable reaction times (1-15h) were conducted starting from glycerol. The results showed that for Cl-containing solids, the selectivity to 1,2-PDO was particularly low during the first hours of reaction (see data for Cl-dp-com-unred in Table 3). This could be due to the presence of Cl ions on the surface favoring excessive hydrogenolysis and C-C cleavage [17, 18]. Moreover, aqueous phase reforming (APR) is known to be favored on highly-dispersed catalysts as it is the case [16] (Scheme 1).

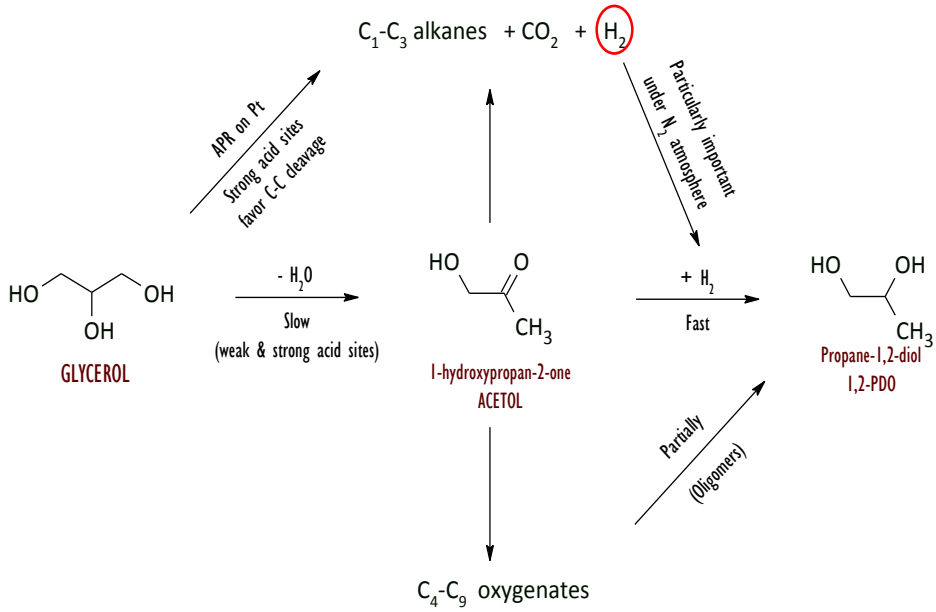

Scheme 1. Mechanism proposed for transformation of glycerol under our experimental conditions.

Apparently, after 5 hours of reaction the extent of C-C cleavage decreased thus resulting in an increase in selectivity to 1,2-PDO. Complementary XPS and TPD studies of pre-adsorbed pyridine (Table 3) showed that chlorine was almost lost from the catalyst surface within 1 hour of reaction and that acidity had significantly decreased. These results suggest the possibility of acidic cracking occurring on strong acid sites which deactivate as reaction proceeds thus resulting in an increase in selectivity to 1,2-PDO. Interestingly, reutilization studies (Table 3) showed a drop in conversion which could be associated to the deactivation of those strong acid sites which could catalyze both C-C cleavage and dehydration of glycerol into acetol. The drop in conversion is accompanied by a significant increase in selectivity to 1,2-PDO. From Table 3 it is also evident that as reaction proceeds, there is a catalyst restructuration involving chlorine leaching and decoration of platinum particles by Zn (see decrease in Pt/Zn ratio), whereas Pt particle size remains constant. In the case of N-dp-com system, initial selectivity to 1,2-PDO is higher than that achieved on Cl-series, which again could be related to the absence of strong acid sites associated to chlorine as well as the higher Pt particle size which is detrimental to APR . Reuse of the systems led to a significant decrease in conversion which could be associated to the Pt leaching (compare %Pt as determined by ICP-MS of N-dp-com unred (fresh) and N-dp-com unred (15 h), Table 3), and decoration of Pt particles by Zn. The increase in selectivity with reuses could suggest some Pt-Zn strong metal-support interaction leading to active sites more selective to 1,2-PDO.

***Table 3**. Results obtained for glycerol transformation on Cl-dp-com and N-dp-com under standard conditions expressed as glycerol conversion % and selectivity to 1,2-PDO, acetol, ethylene glycol (EG) and other products. In some cases, results for characterization of the solids have been included.*

Catalyst	GC-FID					ICP-MS		XPS		TPD pyridine	TEM
	gly conv	Selectivity 1.2-PDO	Selectivity acetol	Selectivity EG	Selectivity others	%Pt	Pt/Zn	Cl/Pt	Cl/Zn	Acidity (µmol/mg cat)	Particle size (nm)
Cl-dp-com unred (fresh)	--	--	--	--	--	4.2	0.42	0.72	0.29	0.23	1.9
Cl-dp-com unred (1h)	2.3	35.8	6.5	0.0	57.7	ND	0.28	0.11	0.03	0.11	ND
Cl-dp-com unred (5h)	10.5	35.0	4.0	2.5	58.5	ND	ND	ND	ND	ND	ND
Cl-dp-com unred (10h)	24.5	63.0	4.3	1.7	25.5	ND	ND	ND	ND	ND	ND
Cl-dp-com unred (15h)	31.0	69.1	3.8	1.6	25.5	4.3	0.24	0.11	0.03	0.11	1.9
Cl-dp-com unred r1 (15h)	20.3	71.9	2.7	0.6	24.5	ND	ND	ND	ND	ND	ND
Cl-dp-com unred r2 (15h)	18.0	79.2	3.2	1.0	16.5	ND	ND	ND	ND	ND	ND
N-dp-com unred (fresh)	--	--	--	--	--	4.3	0.25	0	0	0.06	2.8
N-dp-com unred (5h)	11.3	53.9	4.8	1.6	39.7	ND	ND	ND	ND	ND	ND
N-dp-com unred (15h)	22.5	66.0	1.5	0.9	31.6	3.3	0.14	0	0	0.06	2.8
N-dp-com unred r1	8.8	80.7	5.3	0.3	13.7	ND	ND	ND	ND	ND	ND
N-dp-com unred r2	7.3	87.3	4.8	0.0	7.9	ND	ND	ND	ND	ND	ND

For similar conversion values, solids reduced at 400ºC exhibited a higher selectivity to 1,2-PDO than unred systems (Figure 11 and Table 3). This suggests that changes occurring in the catalyst as reduction temperature is increased (Pt-Zn alloy formation, loss of acidity, increase in Pt particle size) leads to the prevalence or the formation of specific active sites for 1,2-PDO generation.Some other experiments were conducted starting from acetol. Production of 1,2-PDO from glycerol is known to occur through acetol, via dehydration of a primary hydroxyl group in glycerol. Moreover, dehydration of glycerol to acetol is slower than hydrogenation of acetol to 1,2-PDO [19]. In fact, if we start from 1.36 M acetol (the same concentration as for glycerol studies), conversion after 15h is total, with selectivity to 1,2-PDO in the 83-86% range. The exception is Cl-im-com (91% conversion, 68% selectivity). Taking the example of Cl-dp-com-unred, selectivity at full conversion is 85.2%. When the reaction time is decreased to 3h, the conversion and selectivity values on Cl-dp-com-unred are lower (74% and 85.5%, respectively). Reducing acetol initial concentration to 1/3 of its value, conversion after 3h is 93% and selectivity 97%. In the case of acetol, GC-MS studies evidenced the formation of several C_4-C_9 liquid oxygenates, their relative percentage increasing with the reduction of hydrogen pressure or the increase in acetol initial concentration.

Finally, some reactions were carried out under nitrogen atmosphere. Activity order was coincident with that obtained under H_2 atmosphere (e.g. the most acidic solids, Cl-dp-com-Al-unred and Cl-dp-com-Zr-unred, were also the most active ones) though selectivity to 1,2-PDO decreased significantly because of APR and formation of C_4-C_9 liquid oxygenates.

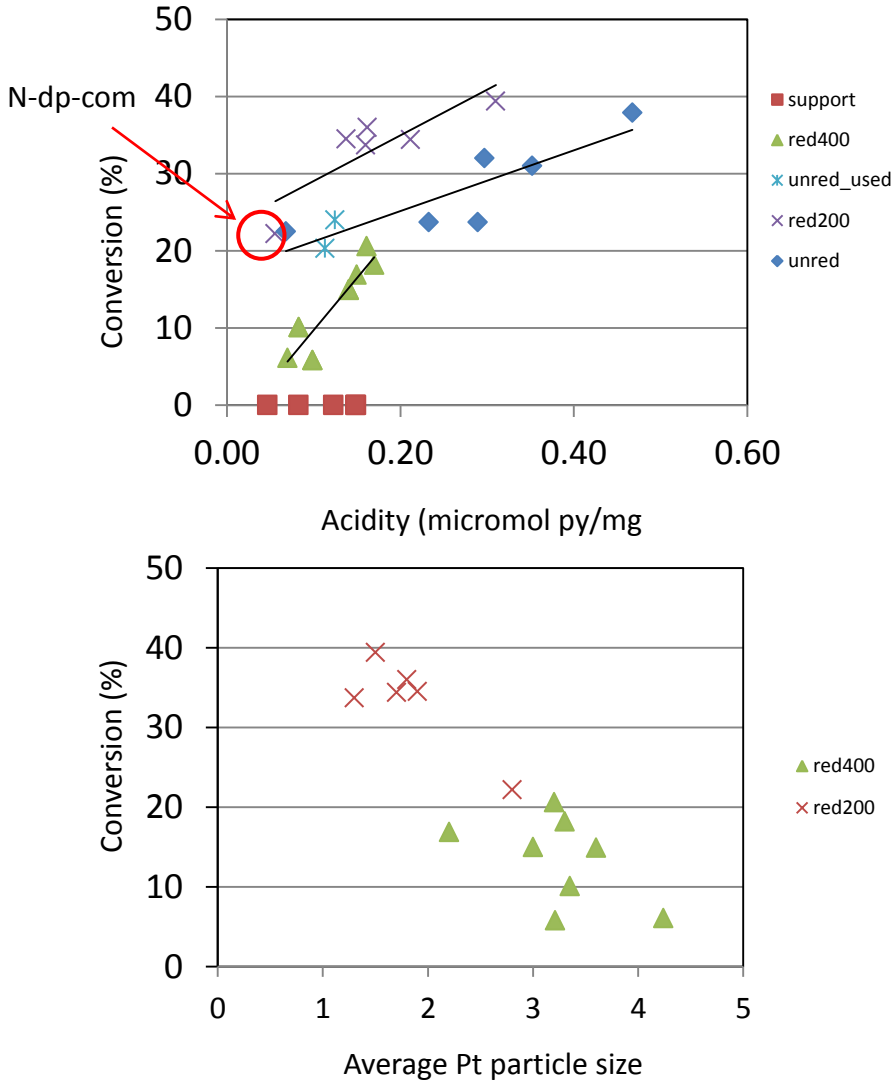

Figure 13. *Glycerol conversion as a function of acidity (micromoles of pyridine per mg of catalyst) or average particle size (in nm, as determined by TEM) for the different catalysts used in the present manuscript. Reaction conditions: 100 mg catalysts, 10 mL 1.36 M water solution of glycerol. 180ºC and 6 bar of initial hydrogen pressure. Reaction time: 15h.*

4. Conclusions

Different ZnO solids (either alone or doped with Al, Zr or Ce) were synthesized through the microemulsion technique which allowed us to obtain similar particle sizes and textural properties. Platinum was subsequently incorporated from H_2PtCl_6 through deposition-precipitation or impregnation method. For comparative purposes, a system from $Pt(NO_3)_4$ was also obtained through deposition-precipitation method. Incorporation of platinum led to the creation of new (mainly Lewis) acid sites, particularly important in the case of chlorine-containing solids. Moreover, acidity is partly lost during reduction treatment or as the reaction proceeds which could be ascribed to both chlorine release and platinum decoration by the support (as evidenced by XPS). A direct relationship between acidity and glycerol conversion was found. Interestingly, supports were not active in the process which evidences the participation of the metal in the dehydration of glycerol to acetol. As regards selectivity to 1,2-PDO, it increases as reaction proceeds and acidity of solids decreases to the detriment of acidic cracking. This suggests that strong acid sites associated to chlorine are responsible for C-C cleavage and excessive hydrogenolysis, whereas dehydration of glycerol into acetol requires moderate acidity. Moreover, formation of Pt-Zn strong metal interaction is beneficial to 1,2-PDO selectivity.

Acknowledgements

The authors are thankful to Junta de Andalucia and FEDER funds (P08-FQM-3931 and P09-FQM-4781 projects) for financial support. SCAI at the University of Cordoba is also acknowledged for ICP-MS measurements and the use of TEM and XPS. Finally, the authors are grateful to COST Action CM0903 for financial support, including a short-term scientific mission (STSM) of V.Montes.

References

1. Z. Yuan, P. Wu, J. Gao, X. Lu, Z. Hou, X. Xheng, Catal. Lett. 130 (2009) 261–265.
2. A. Marinas, P. Bruijnincx, J. Ftouni, F. J. Urbano, C. Pinel, Catal. Today 239 (2015) 31-37.
3. R. Rodrigues, N. Isoda, M. Gonçalves, F.C.A. Figueiredo, D. Mandelli, W.A. Carvalho, Chem. Eng. J. 198/199 (2012) 457–467.
4. M. Checa, F. Auneau, J. Hidalgo-Carrillo, A. Marinas, J.M. Marinas, C. Pinel, F.J.Urbano, Catal. Today 196 (2012) 91–100.
5. T. Miyazawa, Y. Kusunoki, K. Kunimori, K. Tomishige, J. Catal. 240 (2006) 213–221.
6. F. Auneau, C. Michel, F. Delbecq, C. Pinel, P. Sautet, Chem. Eur. J. 17 (2011) 14288–14299.
7. J. Chaminand, L. Djakovitch, P. Gallezot, P. Marion, C. Pinel, C. Rosier, Green Chem. 6 (2004) 359–361.
8. F. Auneau, S. Noël, G. Aubert, M. Besson, L. Djakovitch, C. Pinel, Catal. Commun. 16 (2011) 144–149.
9. F. Vila, M. López Granados, M. Ojeda, J.L.G. Fierro, R. Mariscal, Catal. Today 187 (2012) 122–128.
10. Z. Huang, F. Cui, J. Xue, J. Zuo, J. Chen, C. Xia, Catal. Today 183 (2012) 42–51
11. I. Gandarias, P.L. Arias, J. Requies, M. El Doukkali, M.B. Güemez, J. Catal. 282 (2011) 237–247.
12. L. Ma, D. He, Catal. Today 149 (2010) 148–156.
13. A. Iriondo, J.F. Cambra, V.L. Barrio, M.B. Guemez, P.L. Arias, M.C. Sanchez-Sanchez, R.M. Navarro, J.L.G. Fierro, Appl. Catal. B: Environ. 106 (2011) 83– 93.

14. J. Ten Dam, F. Kapteijn, K. Djanashvili, U. Hanefeld, Catal. Commun. 13 (2011) 1–5.
15. A. Wawrzetz, B. Peng, A. Hrabar, A. Jentys, A.A. Lemonidou, J.A. Lercher, J. Catal. 269 (2010) 411–420.
16. M. L. Barbelli, F. Pompeo, G. F. Santori, N.N. Nichio, Catal. Today 213 (2013) 58– 64.
17. S. N. Delgado, D. Yap, L. Vivier, C. Especel, J. Mol. Catal. A: Chem. 367 (2013) 89– 98.
18. E.S. Vasiliadou, E. Heracleous, I.A. Vasalos, A.A. Lemonidou, Appl. Catal. B: Environ. 92 (2009) 90–99.
19. J. ten Dam, U. Hanefeld, ChemSusChem, 4 (2011) 1017 – 1034.
20. S. Zhu, Y. Qiu, Y. Zhu, S.Hao, H. Zheng, Y.Li , Catal. Today 212 (2013) 120– 126.
21. B. Peng, C. Zhao, I. Mejía-Centeno, G. A. Fuentes, A. Jentys, J. A. Lercher, Catal. Today 183 (2012) 3– 9.
22. Y. Feng, H. Yin, A.Wang, L. Shen, L. Yu, T. Jiang, Chem. Eng. J. 168 (2011) 403–412.
23. I. Gandarias, P.L. Arias, J. Requies, M.B. Güemez, J.L.G. Fierro, Appl. Catal. B: Environ. 87 (2010) 248–256.
24. V. Montes, M. Checa, A. Marinas, M. Boutonnet, J.M. Marinas, F.J. Urbano, S. Järas, C. Pinel, Catal. Today 223 (2014) 129– 137.
25. M. Sanchez-Dominguez, K. Pemartin, M. Boutonnet, Current Op. Colloid Interf. Sci. 17 (2012) 297-305.
26. M. Sanchez-Dominguez, L. F. Liotta, G. Di Carlo, G. Pantaleo,A. M. Venezia, C. Solans, M. Boutonnet, Catal. Today 158 (2010) 35–43.
27. A. S. Shaporev, V. K. Ivanov, A. E. Baranchikov, O. S. Polezhaeva, Y. D. Tretyakov, Russian J. Inorg. Chem. 52 (2007) 1811-1816.

28. G. Patrinoiu, J. M. Calderón-Moreno, D. C. Culita, R. Birjega, R. Ene, O. Carp, Solid State Sci. 23 (2013) 58-64.
29. F. Xiao, B. Zhang, C. Lee, , J. Environ. Sci. 20(2008) 907–914.
30. M.A. Aramendía, V. Boráu, C. Jiménez, A. Marinas, J. M. Marinas, J. A. Navío, J. R. Ruiz, F. J. Urbano, Colloids Surf. A: Physicochem. Eng. Aspects 234 (2004) 17–25.
31. D. Raoufi, T.Raoufi, Appl. Surf. Sci. 255 (2009) 5812–5817.
32. Y. Wei, Z. Zhao, T. Li, J. Liu, A. Duan, G. Jiang, Appl. Catal. B: Environ.146 (2014) 57– 70.
33. J. Hidalgo-Carrillo, A. Marinas, J. M. Marinas, J. J. Delgado, R. Raya-Miranda, F. J. Urbano, Appl. Catal.s B: Environ. 154–155 (2014) 369–378.
34. M. Abid, V. Paul-Boncour, R. Touroude, Appl. Catal. A: Gen. 297 (2006) 48–59.
35. S. Subramanian, Platinum Metals Rev. 36 (1992) 98-103.
36. J. Silvestre-Albero, F. Coloma, A. Sepúlveda-Escribano, F. Rodríguez-Reinoso, Appl. Catal. A: Gen. 304 (2006) 159–167.
37. P. S. Querino, J. R. C. Bispo, M. do Carmo Rangel, Catal. Today 107–108 (2005) 920–925.
38. J. Hidalgo-Carrillo, M. A. Aramendía, A. Marinas, J. M. Marinas, F. J. Urbano, Appl. Catal. A: Gen. l 385 (2010) 190–200.
39. G. E. McGuire, G. K. Schweitzer, Thomas A. Carlson, Inorg. Chem. 12 (1973) 2450-2453.
40. A. Salaün, M. Veillerot, F. Pierre, E. Souchier, V. Jousseaume, ECS J. Solid State Sci. Technol. 3 (2014) N39-N45.
41. G. Berhault, M. Lacroix, M.Breysse, F.Maugé, J.-C. Lavalley, H. Nie, L. Qu, J. Catal. 178 (1998) 555-565.
42. B. Li, R. D. Gonzalez, Catal. Today 46 (1998) 55-67

Chapter 3

Preparation and characterization of Pt-modified Co-based catalyst through the microemulsion technique: Preliminary results on the Fischer–Tropsch synthesis

Paper III

Preparation and characterization of Pt-modified Co-based catalysts through the microemulsion technique. Preliminary results on the Fischer-Tropsch synthesis

V. Montes[1], M. Boutonnet[2] S. Järas[2], M. Lualdi[2], A, Marinas[*1], J.M. Marinas[1], F. J. Urbano[1], M. Mora[1]

[1]*Organic Chemistry Department, Campus de Excelencia Internacional CeiA3, University of Córdoba, Campus de Rabanales, Marie Curie Building, E-14014 Córdoba, Spain.*

[2]*KTH (Royal Institute of Technology), Chemical Technology, Teknikringen 42, SE-100 44 Stockholm, Sweden.*

Keywords: Fischer-Tropsch synthesis; microemulsion technique; Pt-modified cobalt catalysts; Co-TiO_2 interaction

*Corresponding author. Tel.: +34 957218622; fax: +34 957212066. E-mail address: alberto.marinas@uco.es

Abstract

The influence of the addition of small amounts of platinum (0.1-0.25% wt) to cobalt-based systems on Fischer-Tropsch synthesis was investigated. The solids were synthesized through microemulsion technique using TiO_2 as the support. The best catalytic performance was achieved using Synperonic 13/6.5 as the surfactant. In all cases, the presence of platinum led to an increase in CO conversion which could be ascribed to the promotion of cobalt reducibility as evidenced by XPS. Moreover, the simultaneous reduction of cobalt and platinum precursors during synthetic procedure (ME1) was preferable to the consecutive one (ME2) probably as a result of a better Co-Pt interaction in the former case, as evidenced by TPR. TPR, Raman and XPS data also suggested that not only the presence of Co^0 but also the appearance of Co-TiO_2 interactions favor the catalytic performance and that in general those interactions are stronger for ME1 solids.

Graphical abstract

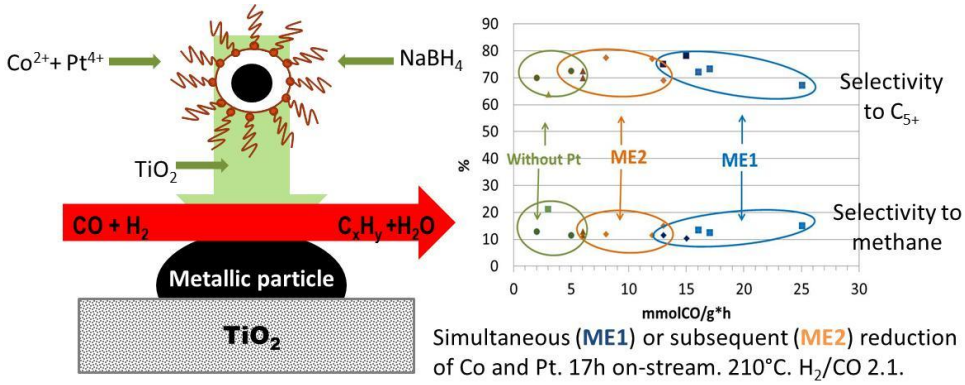

Simultaneous (ME1) or subsequent (ME2) reduction of Co and Pt. 17h on-stream. 210°C. H_2/CO 2.1.

1. Introduction

Fischer–Tropsch synthesis (FTS) is one major step for the transformation of non-petroleum feedstocks, such as natural gas, coal, and biomass, into a wide number of hydrocarbons, such as light hydrocarbons, gasoline, diesel fuel and waxes [1]. The reaction process, normally conducted at 200-350 ºC and under a pressure of 20-40 bars, involves mono- or bimetallic catalysts. Several metals (e.g. Co, Fe and Ru) have been reported as catalysts, though only Co and Fe are industrially applicable due to the high price of Ru. Fe is used in the production of short chain hydrocarbons at high temperature and low H_2/CO ratio whereas Co-based catalyst are chosen when the target is the production of hydrocarbons of the middle-distillate fraction and waxes. Typically, Co based catalysts operate with a H_2/CO ratio slightly over 2 [2].

Once a metal has been selected, the support could also play an important role in FT catalytic performance (influencing the metal dispersion, generation of metal-support interactions, deactivation…). Iglesia et al. [3] reported that the FTS activity was almost independent of support (SiO_2, Al_2O_3, TiO_2, ZrO_2) and proportional to metal dispersion. In another study using SBA-15 and Ti-doped SBA-15 as the support, Lualdi et. al [4] found that the final particle size of Co_3O_4 synthesized through impregnation of cobalt nitrate was dependent on the nature of the support. This suggests that the support effect is indirect (i.e. influence on metal particle size and thus on conversion).

Venezia and co-workers [5] reported that a catalyst of Co over titania-modified silica, exhibited better catalytic performance than another catalyst consisting in Co on pure silica in spite of the similar cobalt particle size in both fresh systems. They explained it in terms of CoO interacting strongly with titania thus avoiding the particle mobility and therefore the deactivation by sintering during FTS.

Focusing on Co catalysts, particle size, dispersion and reducibility of cobalt are some key features in the activity and selectivity performance. It is widely accepted that cobalt particle sizes should not be too low. Otherwise, production of methane increases to the detriment of selectivity to long chain hydrocarbons (S_{C5+}) probably as a result of the much lower reducibility of very small nanoparticles [6-9]. Iglesia et al [10] found that the intrinsic site reaction rate does not depend on Co particle size in the range of ca. 10-200 nm. In contrast, Wang et al. [11] studied the FTS on different Co/SiO_2 catalysts with cobalt particle sizes in the 1.4–10.5 nm range. The authors concluded that no intrinsic particle size effect was observed for the metallic Co particles in the range of 3.5–10.5 nm.

Most of the papers on FT process use impregnation technique as the synthetic method [12]. However, microemulsion (ME) technique allows a better control of cobalt particle size as reported by Lödgberg et al [13, 14]. The authors synthesized Co particles on TiO_2 through both ME and impregnation methods [14], the particle size being significantly lower in the former case (10 and 22 nm, respectively). Furthermore, such smaller particle size resulted in a greater activity and selectivity to high hydrocarbons (C_{5+}). When using the ME method, in order to avoid the formation of amorphous Co species due the presence of boron (coming from the reduction agent, sodium borohydride), the authors had to resort to six depositions of 2wt% of Co each (to a total content of 12wt % Co), with intermediate washing of the catalytic powder to properly eliminate the rest of boron and also surfactant.

The addition of small amounts of other elements (ZnO, MnO, alkaline earth and especially noble metals [12, 15-21]) can lead to the promotion of FTS. The most common effect of the addition of some noble metals is the increase in the conversion rate of carbon monoxide (CO). It is well known that the reducibility of Co is improved in the presence of a small amount of noble metal [18-22] though the optimization of the metal content and the method of incorporation is a matter of

debate [23]. The improvement in the reducibility with the addition of a metal may occur with or without modification of Co dispersion [24]. The enhancement of Co reducibility on Pt incorporation have been reported for several supports (e.g. SiO_2, TiO_2, ZrO_2) though it seems especially pronounced in the case of Al_2O_3 [25]. Boron promotion effect is unclear yet. On the one hand, the presence of boron clearly decreases the degree of reduction of Co [26], but on the other hand it also decreases the deactivation rate through avoiding the deposition of carbon during the FT process [27].

The present study is aimed at going further on the optimization of the synthesis of cobalt-based systems through ME technique (Co incorporated in one step), including the addition of small amounts of platinum with a view to improve catalytic performance for FTS. For a better comparison of the different systems special care was taken to obtain similar cobalt particle sizes in all cases.

2. Experimental

2.1. Chemicals

The microemulsions were formed mixing 2,2,4-Trimethylpentane (99.9% Sigma Aldrich) or cyclohexane (99.0%, Sigma Aldrich) with Synperonic 13/6.5 (Croda) and Berol 02 (Akzo Nobel), respectively. The metal precursors were $CoCl_2 \cdot 6H_2O$ (99.9%, Alfa Aesar), and 8 wt% H_2PtCl_6 aqueous solution (Sigma Aldrich). $NaBH_4$ (98%, Sigma Aldrich) was used as the reducing agent. The supports were ZnO nanopowder (Sigma Aldrich) and TiO_2 (Degussa Evonik P25). The TiO_2 was calcined at 800 ºC with an air flow of 2 L/min in order to get mostly rutile phase. Acetone and ethanol (technical grade) were used during the washing process. Milli-Q water was used for the preparation of the solutions.

2.2. Synthesis of the systems

Figure 1 summarizes the steps followed to synthesize the Co-based nanoparticles. Two different water in oil microemulsions were prepared containing either Berol 02 or Synperonic 13/6.5 as the surfactant. Under optimized conditions, composition of microemulsion (ME) is as follows:

a) Berol 02/cyclohexane/2% wt Water solution of precursor: 18/71/11 wt% (hereinafter referred to as B series)
b) Synperonic13/6.5/2,2,4-Trimethylpentane/2% wt Water solution of precursor: 28/64/8 wt % (hereinafter referred to as S series).

Once the optimum composition of ME had been determined, Co-based systems were synthesized. Firstly the microemulsion was put in a N_2 atmosphere inside a glove bag, and deoxygenated by bubbling N_2 for a couple of minutes. Then, two different approaches were adopted depending on the incorporation of Pt. ME1 method involved the simultaneous reduction of Co and Pt whereas in ME2 method Co was reduced first and then Pt was incorporated. In both cases, the amount of reducing agent was calculated to have a B/Co molar ratio of 3. Therefore, in ME1 the appropriate amount of Pt was added as an aqueous solution of 8 wt % H_2PtCl_6 to the water solution of $CoCl_2$, and then both cobalt and Pt were reduced with a 10M $NaBH_4$ water solution. In contrast, in ME2, cobalt was reduced first with the 10M $NaBH_4$ solution and after 15 minutes the corresponding amount of Pt was added as an aqueous solution of 8 wt % H_2PtCl_6. In both, ME1 and ME2 methods reduction step was allowed for 2 hours under vigorous stirring.

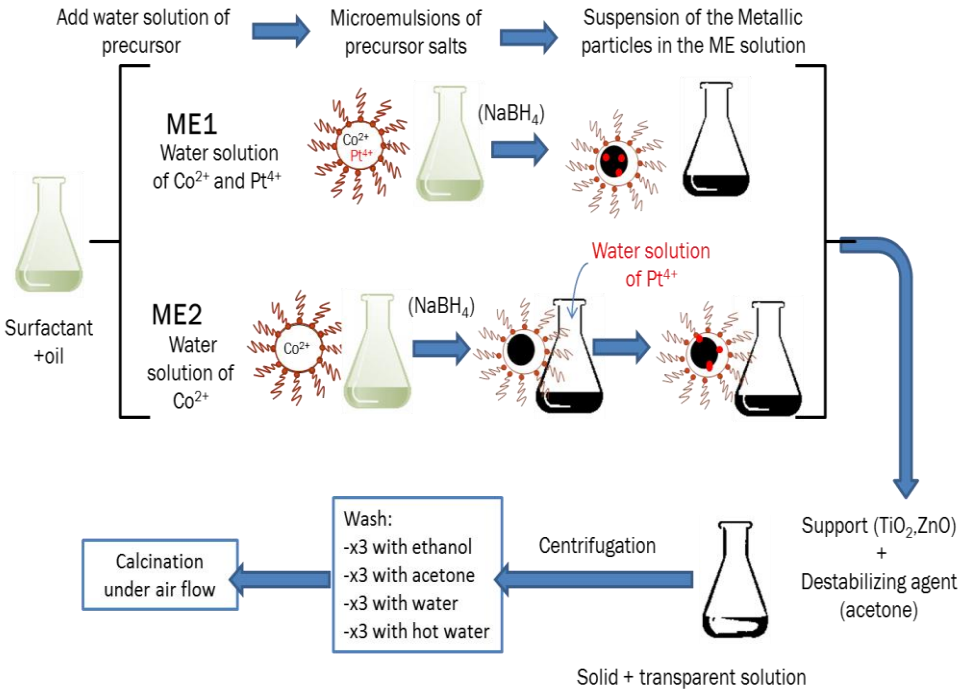

Figure 1. *Schematic representation of synthetic procedure to obtain the different Pt-modified cobalt-based systems through microemulsion technique.*

After the reduction step, the metal particles were deposited onto the TiO_2 support by destabilization of the organosol (Metallic particles stabilized by surfactant and dispersed in the oil phase) with acetone (1 g acetone/1 g ME) in the presence of the support under vigorous stirring for 1h. After 1 hour, the inert atmosphere was broken opening the plastic bag and it was kept stirring one additional hour. Then the solid powders were centrifuged and washed with ethanol, acetone, water and boiling water three times each, using a washing solution/ME ratio of 1:1 by weight. Finally, the catalysts were dried for 12 h at 120 ºC and then calcined with 2 L/min synthetic air flow at 300 ºC or 500 ºC during 16 hours with a temperature ramp of 1 ºC/min.

The nominal content of cobalt was in all cases 12 wt %, whereas platinum was incorporated in a 0.1 or 0.25 wt %. For comparative purposes, the corresponding systems without platinum were also synthesized.

The nomenclature of the solids includes an S or B prefix indicating the surfactant (Synperonic 13/6.5 or Berol 02, respectively), the support (TiO_2 or ZnO) and, when applicable, the corresponding nominal amount of Pt. The name is followed by the approach to incorporate platinum (ME1 or ME2) and finally the calcination temperature. For instance a catalyst synthesized with Synperonic 13/6.5 on TiO_2 containing 0.25 % of Pt incorporated through ME1 method and calcined at 300 ºC is called ´S-TiO_2-0.25%Pt ME1-cal300´ whereas S-TiO_2-cal300 denotes the 12 wt % Co/TiO_2 synthesized from the microemulsion using Synperonic as the surfactant and calcined at 300 ºC. In total, 11 systems were synthesized as shown in Table 1.

2.3. Characterization

Elemental analysis of metal-containing samples was carried out by the staff at the Central Service for Research Support (SCAI) of the University of Córdoba. It was performed using inductively coupled plasma mass spectrometry (ICP-MS). Measurements were made on a Perkin-Elmer ELAN DRC-e instrument following dissolution of the sample in a 1:3 HNO_3/HCl mixture with a soft heating. Calibration was done by using PE Pure Plus atomic spectroscopy standards, also from Perkin-Elmer.

Surface areas of the solids were determined from nitrogen adsorption–desorption isotherms obtained at liquid nitrogen temperature on a Micromeritics ASAP-2010 instrument, using the Brunnauer–Emmett–Teller (BET) method. All samples were degassed to 0.1 Pa at 120 ºC prior to measurement.

Transmission electron microscopy (TEM) images were obtained using a Philips CM-10 microscope. All samples were mounted on 3 mm holey carbon copper grids.

EDX measurements were performed on a JEOL JSM-6300 scanning electron microscope (SEM) equipped with an energy-dispersive X-ray (EDX) detector. It was operated at an acceleration voltage of 20 keV with a resolution of 65 eV.

X-ray diffraction (XRD) was performed on the samples after destabilization using a Siemens D5005 X-ray diffractometer with Cu Kα radiation. A secondary monochromator was used. Particle sizes were estimated by using the Scherrer formula assuming spherical crystallites.

X-ray photoelectron spectroscopy (XPS) data were recorded on 4 mm × 4 mm pellets 0.5 mm thick that were obtained by gently pressing the powdered materials following outgassing to a pressure below about 2×10^{-8} Torr at 150 ºC in the instrument pre-chamber to remove chemisorbed volatile species. The main chamber of the Leibold–Heraeus LHS10 spectrometer used, capable of operating down to less than 2×10^{-9} Torr, was equipped with an EA-200MCD hemispherical electron analyser with a dual X-ray source using MgKα (hv = 1253.6 eV) or Al K_α (hv = 1486.6 eV) at 120 W, at 30 mA, with C(1s) as energy reference (284.6 eV). Measurements with the Mg anode were performed at University of Cordoba whereas those with the Al anode were carried out at University of Sevilla although with similar equipments. Nevertheless, the equipment in Cordoba is newer and thus more sensitive.

Hydrogen Temperature-Programmed-Reduction (TPR) of catalysts was performed on a Micromeritics Autochem 2910. A 5% H_2 in Ar flow was passed through the catalyst and the temperature increased from ambient to 800 ºC (10 ºC/min) while monitoring the H_2 consumption with a thermal conductivity detector (TCD).

Raman spectra were performed on a Renishaw inVia Raman microscope with laser of 785 nm and a grating of 1200 lines/mm. The laser power was adjusted at 1% with an exposure time of 10 s after 10 accumulations.

2.4. Catalytic tests

The FT synthesis experiments were carried out in stainless steel fixed bed reactor (0.93 cm i.d). Approximately 0.5 g of calcined Co catalyst was passed through a sieve of 53 – 90 μm, and then diluted with 5 g of SiC (75 - 150 μm) as inert solid to achieve an isothermal bed temperature profile. Reduction of catalyst was made *in situ* in a H_2 flow of 250 Ncm^3/min at atmospheric pressure, 400 ºC for 16 hours with a heating rate of 1 ºC/min from 70 ºC. Then, the catalyst was cooled down to 170 ºC in flowing H_2 and flushed with He for another hour before the reactor system was pressurized to 20 bar. Afterwards, the feed of syngas flow was introduced with a H_2/CO molar ratio of 2.1, also containing 3 mol% of N_2 as internal standard. The reactor temperature was then slowly increased up to 210 ºC. The heavy hydrocarbons and the liquid products were collected in a heated trap (90 ºC). The gas products also passed through a ‘‘cold” trap at room temperature in order to condense residual liquid products. The gas products were analyzed on line with a HP 5890 gas chromatograph equipped with a thermal conductivity (TCD) and a flame ionization (FID) detectors. H_2, CH_4, CO_2, internal standard N_2, and unconverted CO were quantified with the TCD whereas light hydrocarbons (C1–C4) were quantified with the FID. The selectivity to high hydrocarbons (S_{C5+}) was calculated as follows:

$$S_{C5+} = 100 - (S_{C1} + S_{C2} + S_{C3} + S_{C4} + S_{CO2})$$

3. Results and discussion

3.1. Screening of catalysts for FTS

Firstly, a screening of catalysts for FTS was carried out. In total 11 solids were obtained and tested for the reaction under standard conditions (17 h on stream, see section 2.4.). Then the most catalytically active systems would be selected for further characterization studies, searching for some structure-activity relationships.

Initially, berol 02 (ethoxylated nonylphenol, see structure in Table 1) was used as the surfactant and two partially-reducible solids (TiO_2 and ZnO) were chosen as the support trying to induce some metal-support interaction favorable to FTS (e.g. avoiding cobalt sintering as the reaction proceeds) [5]. Moreover, 0.25% platinum was incorporated through two different methods (simultaneously or subsequently to cobalt) in order to favor cobalt reducibility [12]. In total, 6 solids were obtained from berol 02.

Table 1 summarizes the activity expressed as mmol CO converted per gram of catalyst per hour (mmol CO/g·h) after 17 h on stream. From that table it is evident that in all cases the incorporation of platinum resulted in higher activity as compared to the corresponding unmodified solids (B-TiO_2 and B-ZnO). This is particularly evident for B-TiO_2-0.25%Pt ME1 which exhibited the highest activity values. This prompted us to select TiO_2 as the support for a new synthesis using an environmentally-friendlier surfactant, Synperonic 13/6.5 (see structure in Table 1). Moreover, on this occasion two different Pt contents (0.1 and 0.25% weight) were chosen. This resulted in 5 new solids.

Table 1. *Some catalytic results obtained for the different systems synthesized in the present study for FTS together with the estimated Co_3O_4 particle size from XRD (311 diffraction peak at 2θ of 36.9º)*

Surfactant	Incorporation method	Calcined 300		Calcined 500	
		mmolCO/g*h[(a)]	Co_3O_4 XRD particle size[(b)]	mmolCO/g*h[(a)]	Co_3O_4 XRD particle size[(b)]
Berol 02 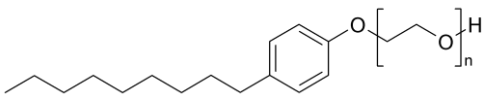	B-TiO_2	5.2	12.3	2.3	15.2
	B-TiO_2-0.25%Pt ME1	13.4	11.7	15.8	19.4
	B-TiO_2-0.25%Pt ME2	6.9	10.9	5.4	18.7
	B-ZnO	3.4	12.6	-	19.3
	B-ZnO-0.25%Pt ME1	6.5	12.1	-	18.6
	B-ZnO-0.25%Pt ME2	6.9	13.4	-	18.7
Synperonic13/6.5 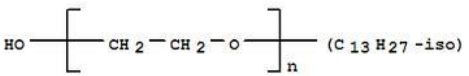	S-TiO_2	3.0	12.5	1.9	13.7
	S-TiO_2-0.1%PtME1	17.8	13.8	-	16.5
	S-TiO_2-0.25%PtME1	25.4	13.3	16.3	16.4
	S-TiO_2-0.1%PtME2	13.2	13.3	-	16.2
	S-TiO_2-0.25%PtME2	12.9	14.8	8.7	18.9

(a) mmol of CO consumed per gram of catalyst and per hour after 17 hours on stream. 210ºC, 20 bar; H_2/CO molar ratio 2.1

(b)This particle size is subjected to error due to overlapping of signals corresponding to Co_3O_4 and the support (TiO_2 or ZnO)

Again, catalytic results shown in Table 1 evidence the increase in activity with the incorporation of platinum (which is even more marked than for berol 02, with a 4-8 fold increase as compared to S-TiO_2). Furthermore, the enhancement is generally more pronounced for ME1 than for ME2. Moreover, systems calcined at 500 °C are normally less active than the corresponding counterparts calcined at 300 °C. All in all, the best results were obtained for S-TiO_2 solids. This is the reason why at this point attention was focused on S-TiO_2 systems.

Figure 2 summarizes the results obtained for all tested catalysts corresponding to B-TiO_2 or S-TiO_2 series for a time-on-stream of 17 h. From that Figure it is clearly evident that incorporation of platinum does not seem to change selectivity values (i.e. reaction mechanism) though it leads to higher conversions and that this effect is more marked for ME1 than for ME2. Moreover, S series exhibit better catalytic performance than B-series.

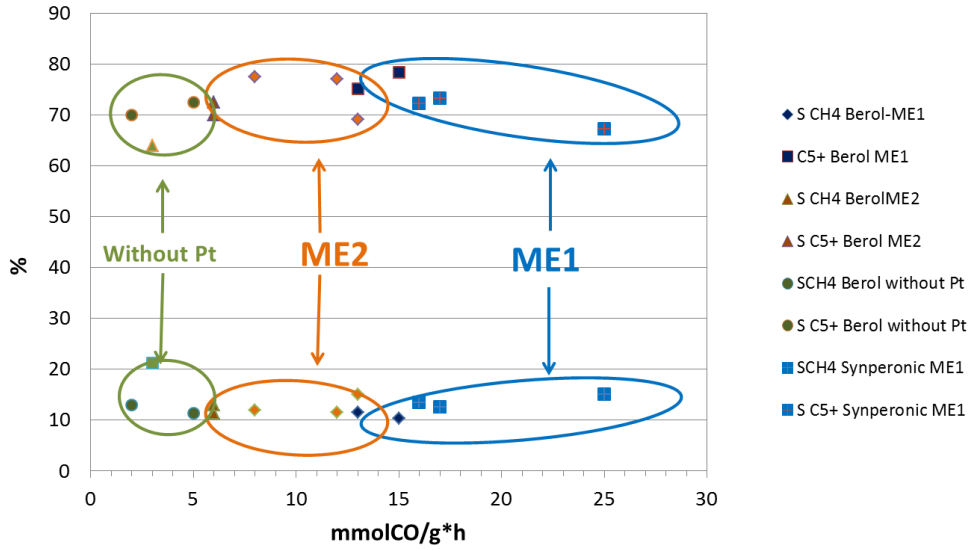

***Figure 2**. Comparison of activity (expressed as mmol CO/g·h) and selectivity to CH_4 and C_{5+} for all the solids for a time-on-stream of 17 h. Standard conditions (i.e. 20 bar, 170ºC, H_2/CO molar ratio 2.1).*

Figure 3 shows the evolution of activity (expressed as mmol CO/g cat·h) with time-on-stream. Regarding S-TiO_2 series (Figure 3A), there seems to be two clear trends. On one hand, ME1 systems for which there is a continuous increase in conversion with time-on-stream (in particular for the systems with 0.25% Pt). On the other hand, ME2 solids for which a maximum appears to be reached at ca. 4-5 h after which conversion hardly changes or even decreases as it is the case of the catalyst containing 0.25 wt % of Pt. As for B-TiO_2 solids (Figure 3B), all systems exhibit the maximum at ca. 4-5 h followed by the decrease in activity.

A more in-depth description of catalytic behavior of S-TiO_2 solids for a time on stream of 17 hours is summarized in Table 2. That table includes a more detailed description of selectivities as well as the corresponding TOF values considering Co^0 content estimated from TPR profile and particle size as determined by TEM. From TOF values, activity of systems with 0.1% Pt is quite similar irrespective of the ME method. However, for solids containing 0.25% Pt activity of ME1 solids is ca. 3 times that of ME2 systems. Moreover, increase in Pt content from 0.1 to 0.25% resulted in an increase in activity for ME1 whereas it was detrimental for ME2.

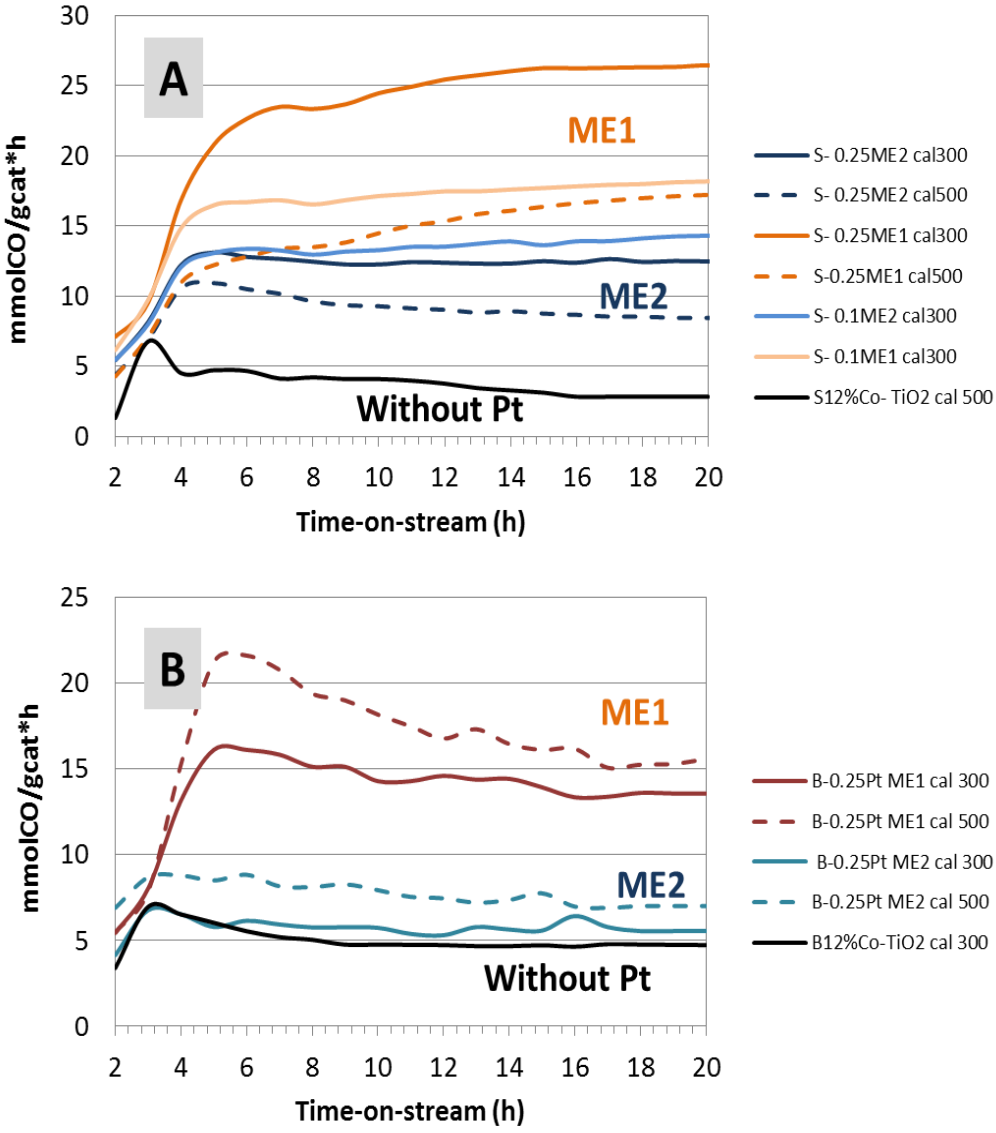

Figure 3. *Evolution of activity (expressed as mmol CO/g·h) for the different solids. A) S-TiO_2 series and B) B-TiO_2 series. Temperature was slowly increased from 170ºC up to 210ºC and then kept at the final temperature. 20 bar and H_2/CO molar ratio 2.1.*

Table 2. *Some catalytic results obtained for S-TiO_2 systems in FTS for a time on stream of 17 h, 210ºC, 20 bar; H_2/CO molar ratio 2.1*

Catalyst	Space velocity[(a)]	Conv (%)	mmolCO/g*h	S(CO_2)[(b)]	S(CH_4)[(c)]	S(C_2-C_4)[(d)]	S(C_{5+})[(e)]	TOF (s^{-1})
S-TiO_2 cal300	10018.6	2.11	3.0	2.61	21.17	12.2	64.02	0.0061
S-TiO_2-0.1%PtME1 cal300	10588.2	11.7	17.8	0.18	12.56	13.8	73.46	0.023
S-TiO_2-0.1%PtME2 cal300	10027.9	9.5	13.2	0.4	15.07	15.3	69.23	0.021
S-TiO_2-0.25%PtME1 cal300	8797.6	21.1	25.4	0.18	14.95	17.51	67.36	0.030
S-TiO_2-0.25%PtME2 cal300	10644.6	8.1	12.9	0.56	11.42	10.80	77.22	0.009
S-TiO_2-0.25%PtME1 cal500	6940.4	17	16.3	0.23	13.43	13.94	72.40	0.034
S-TiO_2-0.25%PtME2 cal500	7020.2	8.3	8.7	0.37	11.92	10.09	77.62	0.012

[(a)] Space velocity (NmL of syngas/h*gcat)

[(b)] Selectivity to CO_2, [(c)] Selectivity to CH_4, [(d)] Selectivity to compounds with 2-4 carbons, [(e)] Selectivity to compounds with 5 or more carbons

3.1. Characterization of the systems

Figures 4A and 4B represent the X-Ray diffractograms of S-TiO_2 and B-TiO_2 systems, respectively. The support (TiO_2) calcined at 800 ºC consisted in rutile and anatase in a 74%/26% ratio with particle sizes of 51.1 and 30.2 nm, respectively (as determined from Scherrer formula using 110 and 101 reflections for rutile and anatase, respectively). As can be seen, signals for anatase overlap with those corresponding to cobalt. It was also the case of ZnO (not shown) which consisted in wurtzite particles with average particle sizes of 45 nm as estimated from 101 reflection at ca. 36.5º. Nevertheless, an attempt at estimating Co_3O_4 particle size by XRD analysis, applying Scherrer equation on the 311 diffraction peak at 2θ of 36.9º [28] was made trying to subtract the contribution of anatase or wurtzite to such a peak. Estimated values for Co_3O_4 are also given in Table 1. Though much less reliable than those obtained from TEM (see below) obtained results evidence quite a similar Co_3O_4 particle size for all the solids calcined at the same temperature and the increase in particle size on increasing calcination temperature from 300 ºC to 500 ºC, which could account for the decrease in activity expressed as mmol CO/g*h (see Table 1).

It it is possible to estimate the metallic particle size of Co^0 from the values measured for Co_3O_4 using the formula [29]:

$d(Co^0)= 0.75* d(Co_3O_4)$

With this calculation the estimated metallic (Co^0) particles size for systems calcined at 300 ºC are in the range of 8.2 to 11.1 nm.

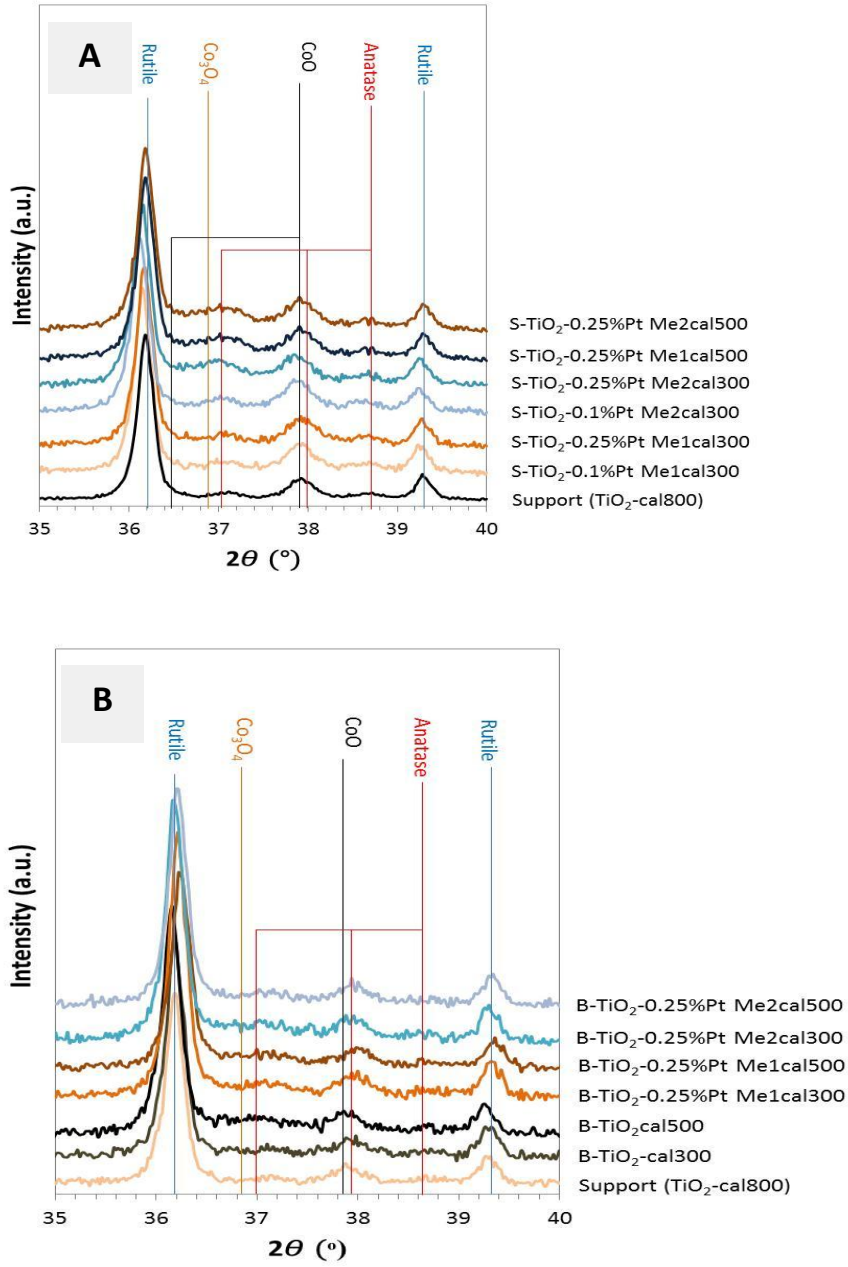

Figure 4. *X-Ray diffractograms of the different systems corresponding to S-TiO_2 (A) and B-TiO_2 (B) series. For the sake of comparison, that of the support has also been included.*

TEM micrographs of Pt-modified catalysts after reduction at 400 ºC during 16 hours are represented in Figure 5. A first conclusion from that study is that overlapping of Co_3O_4 and TiO_2 signals led to a significant overestimation of cobalt particle sizes. In fact, for S-series systems calcined at 300 ºC, average particle sizes are in the 3.8-4.7 nm range. Calcination at 500 ºC resulted in an increase in particle size (e.g. from 4.1 to 5.5 nm for S-TiO_2-0.25%Pt ME1). The similar cobalt particle sizes obtained for the different systems confirms the suitability of microemulsion technique to obtain a good control of particle size and will allow us a better comparison of catalytic performance.

BET areas measured for all catalysts are in the 20-25 m^2/g range similar to that of the support (TiO_2) after calcination (22 m^2/g). Table 3 includes elemental analysis of systems by ICP-MS, EDAX and XPS (using the Mg anode). Co composition as measured by EDAX is slightly higher than that obtained by ICP-MS, always below the nominal content (12 wt %). It is noteworthy that XPS with the Mg anode are subjected to error due to the interference of O_{KLL} Auger in Co2p signal. That is probably the reason why Co content as determined by XPS is so high. In fact, using the Al anode, all systems exhibit Co contents in the 10-12% range. In contrast, XPS data collected in Table 3 were registered with a more sensitive equipment than that possessing the Al anode which allowed us to detect Pt despite its low content.

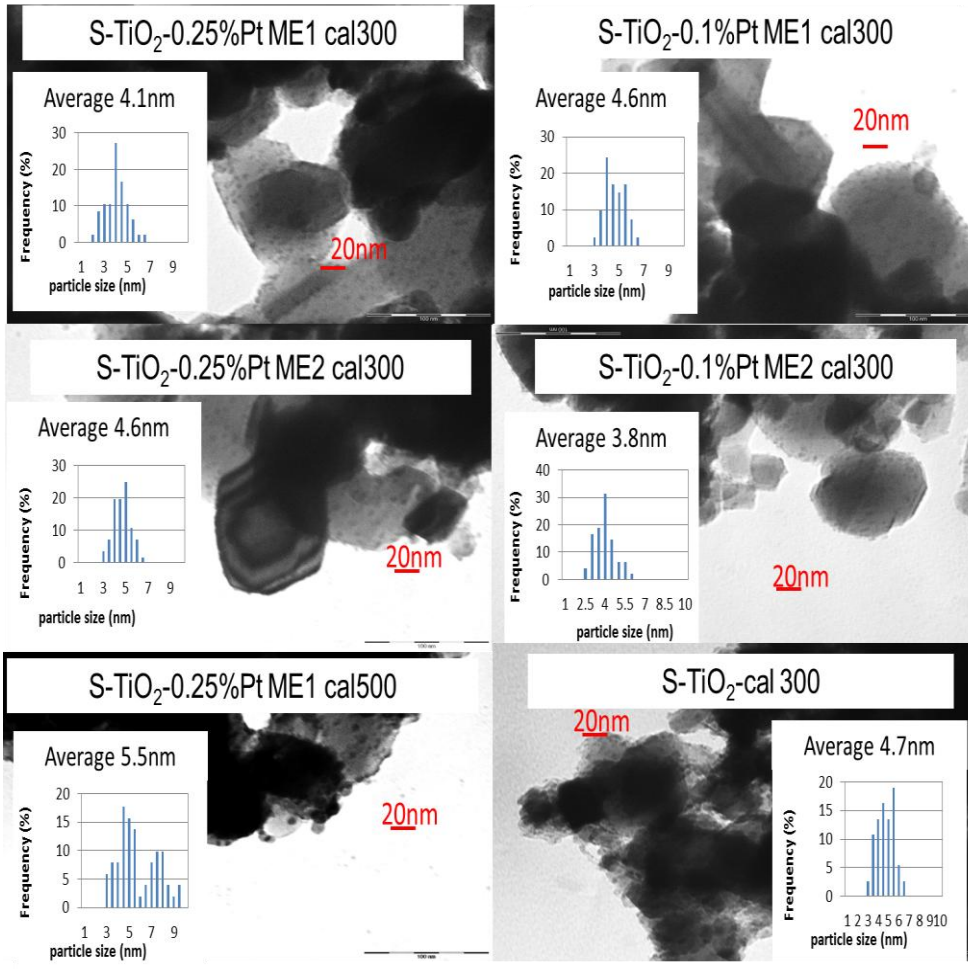

Figure 5. *TEM micrographs of the different S-TiO_2 systems after reduction at 400 ºC during 16 h*

Even though the Pt incorporation method differed in ME1 and ME2 (simultaneous or subsequent to Co) Pt content as measured by EDAX was quite similar for both methods and close to the nominal content, thus confirming the success of the incorporation method. However, Pt/Ti ratio as measured by XPS was especially low for the catalyst S-TiO_2 0.25%Pt ME2 as compared to S-TiO_2 0.25%Pt ME1. This could suggest a lower dispersion of platinum in the former solid which in turn could be ascribed to the synthetic method. In fact, assuming similar micelle sizes in both synthetic methods, there will be probably more micelles containing only platinum in ME2 systems thus leading to bigger platinum particles as compared to ME1 solids. This will be more marked for the systems with the highest Pt content (0.25% wt) whereas for the solids with 0.1% wt Pt, this could be somehow compensated by the favoring of Pt^0 nucleation over growth since Pt^{4+} is added to a medium with an excess of reduction agent ($NaBH_4$).

Finally, according to EDAX and XPS results, the amount of chloride is negligible. This confirms the successful removal of chlorine (which is known to be a catalyst poison) coming from platinum and cobalt precursors during the synthetic procedure (through washing and/or release as HCl) [30]. Boron was not detected by EDAX. This species can also act as poison or promoter depending on its concentration [31]. The higher the boron content of Pt-containing systems as determined from XPS (Table 3) the higher the CO conversion (see Table 1 or 2) which could suggest a possible promotion effect of such species. Tan et al. [31] found that the presence of Co_2B species reduced the stability of carbon formed during FT process which prevented to a certain extent deactivation of the catalyst.

***Table 3**. Elemental analysis of some of the systems synthesized in the present study*.

Catalyst	weight composition (%)									
	ICP-MS			EDAX				XPS[(a)]		
	Co	Pt	B	Co	Pt	B	C	Co	Pt	B
S-TiO_2 cal300	8.82	0	0.31	9.32	0	-	45.04	10.03	0	1.34
S-TiO_2-0.1%PtME1 cal 300	8.66	0.14	1.05	9.31	0.14	-	19.71	18.50	0.48	3.20
S-TiO_2-0.25%PtME1 cal300	8.54	0.17	1.37	10.2	0.35	-	18.69	19.63	0.92	3.96
S-TiO_2-0.1%PtME2 cal300	9.39	0.05	0.84	10.4	0.13	-	23.55	20.52	0.51	3.00
S-TiO_2-0.25%PtME2 cal300	8.40	0.21	0.88	10.8	0.29	-	16.93	18.89	0.37	3.00

Catalyst	XPS data based on atomic composition[(a)]			
	Fresh		Reduced 400	
	Pt/Ti	Co/Ti	Co/Ti	Co^0/Co (ox)[(b)]
S-TiO_2 cal300	0	0.87	0.52	0.12
S-TiO_2-0.1%PtME1 cal 300	0.0055	0.76	0.76	0.29
S-TiO_2-0.25%PtME1 cal300	0.0138	0.99	0.59	0.34
S-TiO_2-0.1%PtME2 cal300	0.0075	0.98	0.64	0.18
S-TiO_2-0.25%PtME2 cal300	0.0039	0.63	0.26	0.34
S-TiO_2-0.25%PtME1 cal500	0.0036	0.33	Not det	Not det
S-TiO_2-0.25%PtME2 cal500	0.0021	0.32	Not det	Not det

(a) XPS signals used were C1s, O1s, Co2p, Pt4f, Ti2p and B1s. These XPS data (in particular Co content and Co/Ti ratio) can be subjected to error since they were determined with the Mg anode and thus Co2p photoelectron spectrum presents a contribution of the O_{KLL} Auger. In fact, Co content obtained using Al anode was in the 10-12% range for all systems

(b) $Co^0/(Co^{2+} + Co^{3+})$ ratio

In order to study the reducibility of the catalysts, Hydrogen Temperature-Programmed-Reduction (TPR) studies were conducted (Figure 6). For comparative purposes, all TPR profiles were normalized per gram of catalyst. In all cases the green line represents the Co catalysts without platinum used as the reference (S-TiO_2 or B-TiO_2).

For S-TiO_2 systems two main peaks centered at 289 and 444 ºC can be observed, which could correspond to the two-step reduction $Co_3O_4 \rightarrow CoO$ and $CoO \rightarrow Co^0$ [28, 32].

The small shoulder at ca. 520 ºC could be due to Co-TiO_x interactions which shift the profile to higher temperatures [33, 34]. As far as ME1 series is concerned, the incorporation of Pt results in the shift of the first reduction peak to lower temperatures particularly for calcination temperature of 300 ºC (see the peak at ca. 160 ºC) which is consistent with the expected promotion of Co reduction on incorporation of platinum [12]. In contrast, the relative intensity of the peak appearing at ca. 444 ºC in S-TiO_2 seems to decrease in favor of the shoulder at higher temperatures (now centered at ca. 520 ºC) which could be indicative of a stronger Co-support interaction. Regarding ME2 series, the different Pt content led to significant changes in TPR profile. Therefore, the solids containing 0.1% Pt presented a shift to higher reduction temperatures whereas the opposite holds true for systems with 0.25% wt Pt. This could suggest a higher Co-support interaction in the former case. Interestingly, TPR profiles of S-TiO_2 0.1% PtME1 cal300 and S-TiO_2 0.1% PtME2 cal300 are very similar at temperatures over 200ºC which could account for their similar TOF values (ca. 0.020 s^{-1}, Table 2). In contrast, the absence of the TPR peak at high temperatures in S-TiO_2 0.25% PtME2 could indicate the absence of Co-support interaction which could explain its much lower TOF values as compared to S-TiO_2 0.25% PtME1 (0.009 and 0.030 s^{-1}, respectively, Table 2).

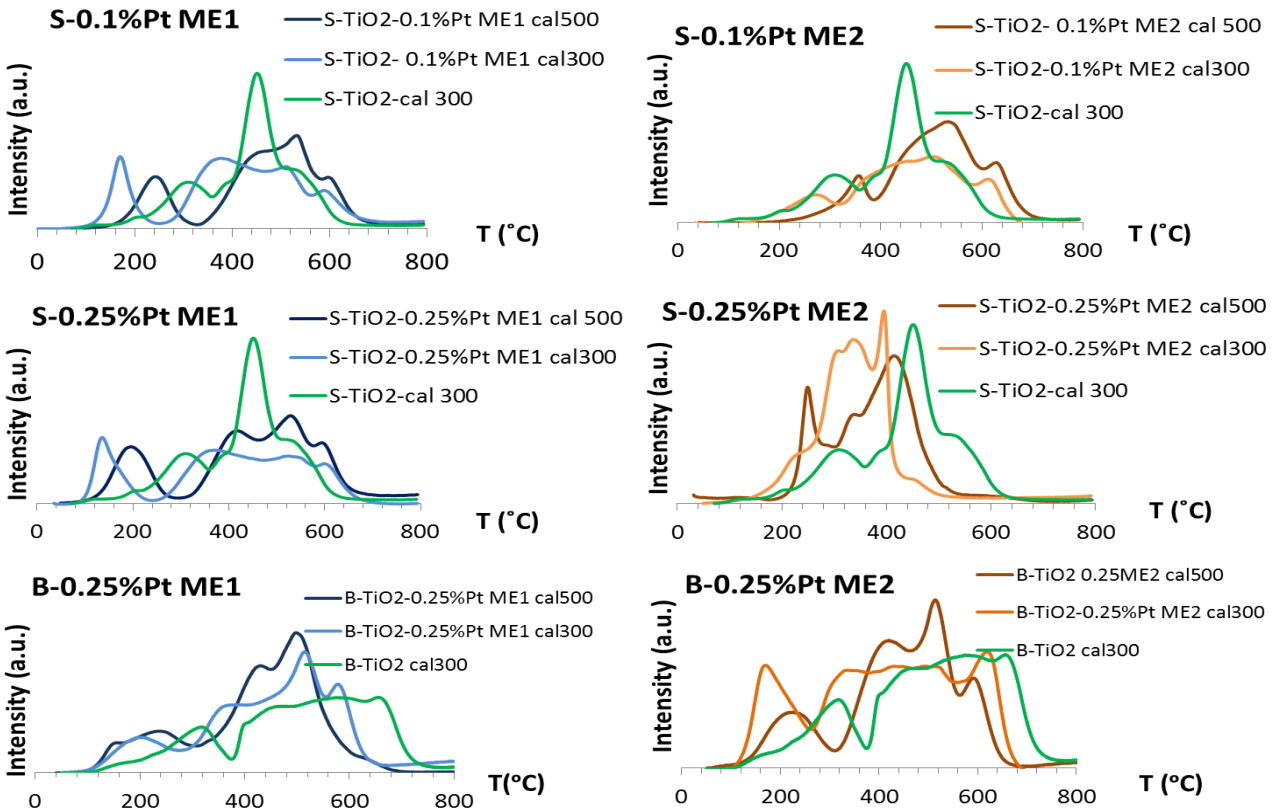

Figure 6*. TPR profiles of S-TiO_2 and B-TiO_2 systems.*

Furthermore, the observed promotion effect of Pt on cobalt reducibility in ME1 series unlike ME2 systems could be explained in terms of the synthetic method. For ME1 cobalt and platinum were simultaneously added and then reduced by sodium borohydride. On the contrary, in ME2 method cobalt was added first, reduced by sodium borohydride and platinum precursor was subsequently added. This means that, in principle, a better cobalt-platinum interaction would be expected from ME1 method which is the one for which TPR profiles evidenced the shift of the first reduction peak to lower temperatures.

Finally, in all cases the increase in calcination temperature resulted in a shift of TPR profiles to higher temperatures which led to the decrease in activity expressed as mmol CO/g*h though not in TOF (Table 2) which could be ascribed to the increase in cobalt particle size with calcination temperature (Figure 5).

Regarding B-TiO_2 systems, TPR profiles evidence the promotion effect of Pt on cobalt reducibility (as evidenced by the shift of the peak at ca. 300ºC to lower temperatures on Pt addition) though unlike S-series, irrespective of the method (ME1 or ME2), no Co-support interaction is observed (i.e. no shift of peak at ca. 700ºC at higher temperatures). This could be one of the reasons for the lower catalytic performance of B-series as compared to S-solids. Nevertheless, this requires further studies. In any case, given the better catalytic performance of S-series and that alcohol ethoxylates (as it is the case of Synperonic) has been described as environmentally-friendlier substitutes for nonylphenol ethoxylates (e.g. berol) [35] attention was focused on the characterization of S-series systems.

All in all, TPR profiles just give us some evidences on the structural differences of the solids which could account for the observed catalytic performance. However, some complementary information from other techniques is needed. In this sense, another important point to consider is the crystallographic form of cobalt in the different solids. To cast further light on that, Raman and XPS spectroscopies were used.

Unlike XRD where Co_3O_4 and TiO_2 signals overlap, Raman spectra of both systems differ. Co_3O_4 Raman spectra exhibits typical bands at ca. 193, 478, 520, 618 and 686 cm^{-1} which can be ascribed to T2g, Eg, F2g, F2g and A1g vibrational modes, respectively [34, 36]. CoO also presents these bands though their intensity is comparatively lower [12]. Raman spectra of samples calcined at 300 ºC (Figure 7) exhibit most of these bands. However, in general, (the exception being the band at ca. 620 cm^{-1}) their intensity is lower for ME1 than for ME2 which assuming similar crystallinity (and taking into account that cobalt content and particle size is similar for all samples) could suggest a higher CoO content in ME1 series.

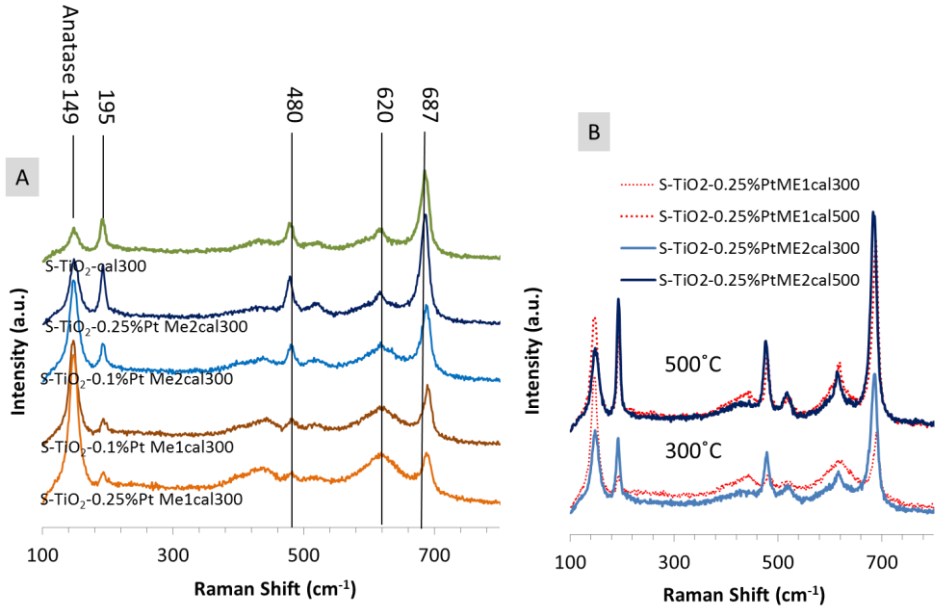

Figure. 7. *Raman spectra of the different S-TiO2 systems. (A) Solids calcined at 300 ◦C. (B) Comparison of solids containing 0.25% Pt calcined at 300 and 500 ◦C.*

Moreover, A1g band at 687 cm^{-1} for S-TiO_2 cal300 and S-TiO_2-0.25%Pt-ME2 cal 300 is shifted around 3-4 cm^{-1} to higher frequencies for the other systems which were more active in FTS (Table 2). Some authors explain the shift of Raman bands as a result of interactions of cobalt oxides with the support [34].

This stronger Co-support interaction for ME1 could also be the reason for the higher intensity of the band at ca. 620cm^{-1}. Finally, as expected, increase in calcination temperature from 300 to 500 ºC (Figure 7B) resulted in an increase in the intensity of Raman Bands probably as a result of a higher crystallinity and particle sizes (as evidenced by TEM).

In order to confirm the presence of different cobalt species distribution in ME1 and ME2 solids (higher proportion of CoO in the former), XPS was utilized. Co^0 exhibits a Co2p3/2 signal at ca. 778 eV. As for Co_3O_4 and CoO they exhibit Co2p3/2 peaks at ca. 779.6 and 780.0 eV, respectively, what makes the differentiation of both species difficult [37].

XPS profiles obtained for our solids in the Co2p region are represented in Figure 8. As can be seen reduction at 400°C for 16h results in the appearance of the Co^0 peak centered at 777.5 eV. Moreover, results reveal the promotion effect of platinum on cobalt reduction (see the increase in the relative intensity of the signal attributed to Co^0 for Pt-containing solids as compared to S-TiO_2-cal300 and the Co^0/Co(ox) ratio in Table 3). However, no clear correlation between such a ratio and catalytic activity is observed. This could suggest that not only the presence of Co^0 but also the distribution of Co^{2+} and Co^{3+} should be considered. It is important to note that Co2p photoelectron spectrum measured with Mg anode presents a contribution of the O_{KLL} Auger [38].

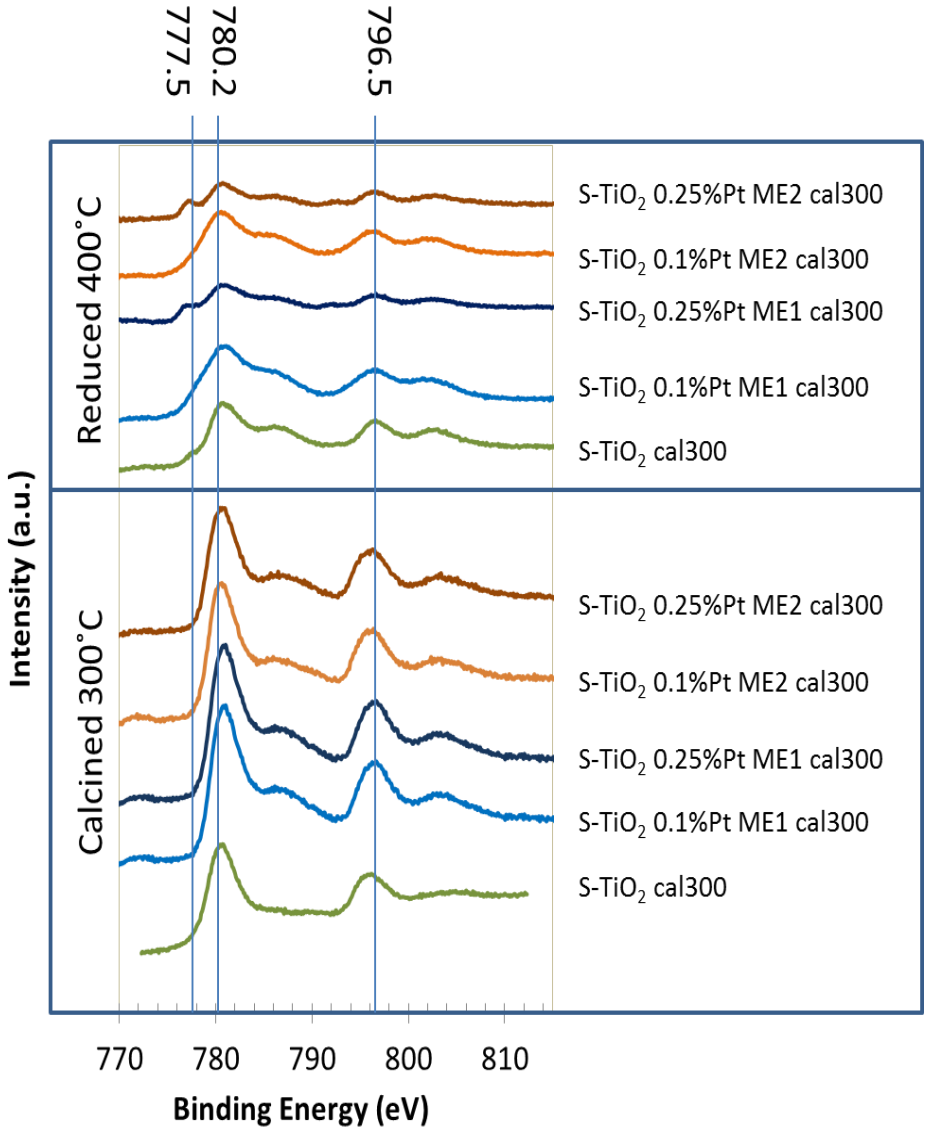

Figure 8. *Co 2p XPS spectra of the different S-TiO_2 solids registered with the Mg anode.*

Therefore, experiments were repeated for S-TiO_2, S-TiO_2-0.25% PtME1 and S-TiO_2-0.25% PtME2 using the Al anode. Moreover, Auger signal was registered since it is more sensitive to changes in the chemical state of cobalt than the Co2p signal.

Figure 9 represents the Auger signal for the solids containing 0.25% Pt. For the sake of comparison the signal of S-TiO_2 system has also been included. Two peaks corresponding to Co_{LMN} Auger lines are observed in these curves at 712.3 and 719.1 eV (Figure 9A). From those values the modified Auger parameter (α′) can be calculated using the following equation:

$\alpha' = 1486.6 + KE\ (Co_{LMM}) - KE\ (Co\ 2p3/2)$

where KE (Co_{LMM}) is the kinetic energy of the Co_{LMM} Auger electron, KE (Co 2p3/2) is the kinetic energy of Co 2p3/2 photoelectron and 1486.6 is the energy of the Al Kα X-ray excitation in eV. Therefore, values of 1554.5 and 1547.7 eV are obtained which can be attributed to Co_3O_4 and CoO, respectively [38].

Results shown in Figure 9A confirm that the system synthesized through ME1 method contain a higher proportion of Co^{2+} species than those obtained through ME2. This is consistent with Raman results: all solids contain CoO and Co_3O_4 but CoO phase is more important in ME1 than in ME2. Moreover, 0.25%PtME1 system exhibits a more intense O1s signal at ca. 531.3 eV (Figure 9B) which could be ascribed to the generation of the above-mentioned metal-support interactions [39]. This Co-support interaction, more important in ME1 systems as compared to ME2 solids could avoid cobalt sintering as the reaction proceeds and thus account for the observed higher activity of ME1 as compared to ME2 and deactivation of the latter solids with time-on-stream (Figure 3A). In fact, TEM micrographs of spent catalysts (Figure 10) confirm that ME2 solids are more prone to sintering as the reaction proceeds. Assuming that particles in that figures were Co_3O_4 mainly, it would result in average particle sizes of 4.7 and 5.9 nm for

S-TiO_2-0.25%PtME1 cal 300 and S-TiO_2-0.25%PtME2 cal 300, respectively. The possible influence of some other factors in activity and deactivation, in particular different nature of carbonaceous deposits in ME1 and ME2 solids, is currently under investigation.

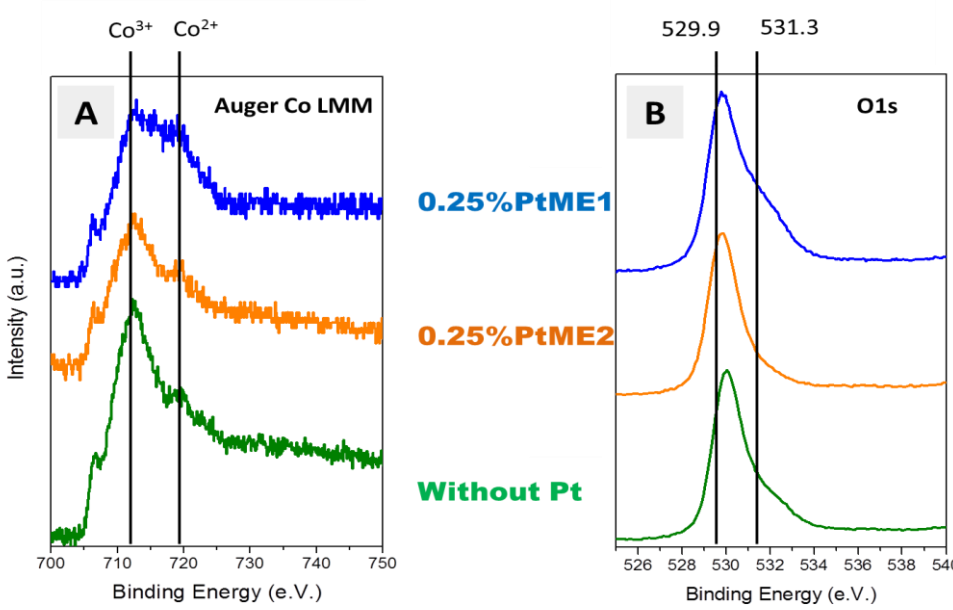

***Figure 9**. XPS results with the Al anode of solids reduced at 400ºC. Co_{LMM} Auger (A) and O1s (B) signals*

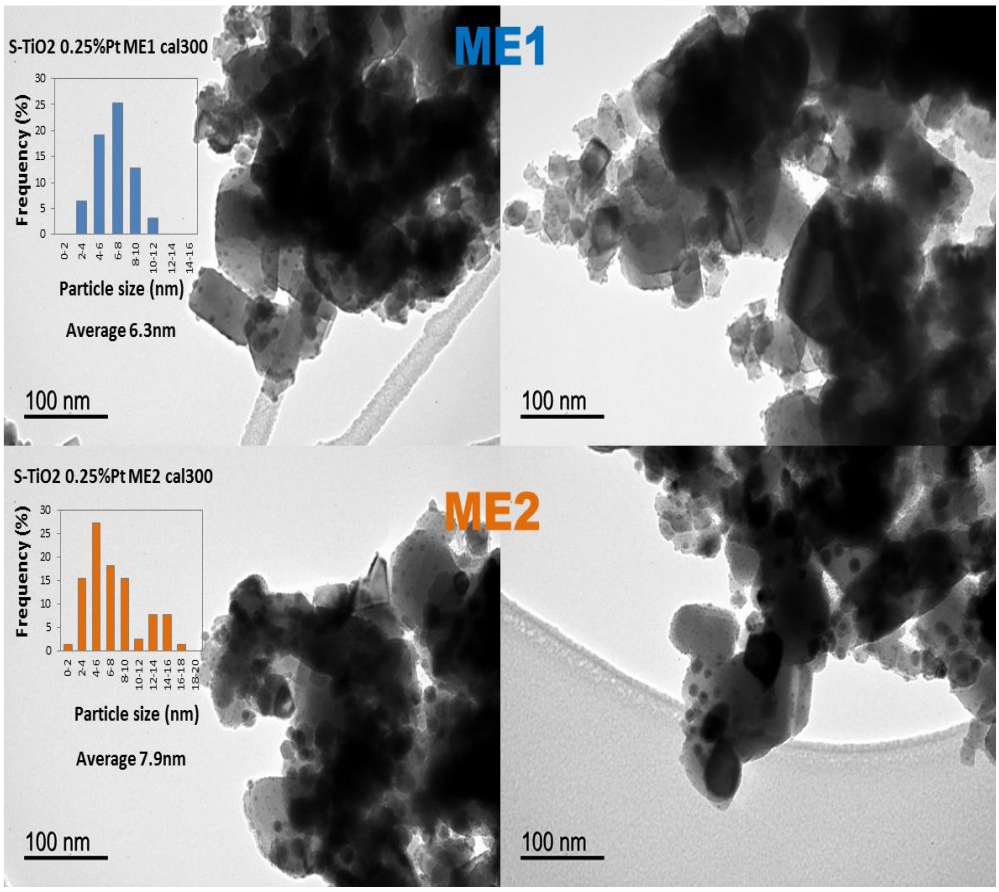

Fgure 10. *TEM micrographs of some spent systems. Particle sizes were calculated assuming all particles corresponded to* Co_3O_4.

4. Conclusion

Several Pt-modified cobalt catalysts containing 0-0.25 wt % platinum and 12 wt % cobalt were synthesized through microemulsion technique (ME) using TiO_2 as the support. Moreover, Berol 02 and Synperonic 13/6.5 were used as surfactants. Two incorporation methods involving simultaneous (ME1) or consecutive (ME2) reduction of cobalt and platinum with sodium borohydride were essayed. A first screening of catalysts for Fischer-Tropsch synthesis led us to select S-TiO_2 series (TiO_2 as the support and Synperonic 13/6.5 as the surfactant) for subsequent characterization studies. In all cases ME technique led to quite comparable cobalt particle sizes (averaging in the range of 3.8-4.7 nm for catalysts calcined at 300 ºC as determined by TEM). Moreover, ME1 solids led to higher conversions than their ME2 counterparts. The higher Pt-Co and Co-support interaction in the former case (as evidenced by TPR profile) could account for that. Raman spectra evidenced the presence of Co_3O_4 and CoO in all solids though CoO proportion is higher in ME1 as compared to ME2. There results were confirmed by XPS which together with the increase in the O1s XPS signal at ca. 531.2 eV with the reduction treatment, more significant for ME1 as compared to ME2 solids, is supportive of the existence of a greater Co-support interaction in the former systems. All in all, results showed that both the presence of reduced cobalt species (Co^0) and Co-TiO_2 interactions were responsible for the different behavior of the systems.

Acknowledgements

The authors are thankful to Spanish Junta de Andalucia and FEDER funds (P08-FQM-3931 and P09-FQM-4781 projects) for financial support. SCAI at the University of Cordoba is also acknowledged for ICP-MS measurements and the use of TEM and XPS. SGI at the University of Sevilla is also acknowledged for

XPS analyses with Al anode. Finally, the authors are grateful to COST Action CM0903 for financial support and short-term scientific mission (STSM) of V. Montes.

References

[1] E. van Steen, M. Claeys, Chem. Eng. Technol. 31 (2008) 655–666.

[2] C. Perego, R. Bortolo, R. Zennaro, Catal. Today 142 (2009) 9–16.

[3] E. Iglesia, S. C. Reyes, R. J. Madon, S. L. Soled, Adv. Catal. 39 (1993) 221-235.

[4] M. Lualdi, G. Di Carlo, S. Lögdberg, S. Järås, M. Boutonnet, V. La Parola, L.F. Liotta , G. M. Ingob, A.M. Venezia, Appl. Catal. A 443– 444 (2012) 76– 86.

[5] A. M. Venezia, V. La Parola, L. F. Liotta , G. Pantaleo, M. Lualdi, M. Boutonnet, S. Järås, Catal. Today, 197 (2012) 18– 23.

[6] R.C. Reuel, C.H. Bartholomew, J. Catal. 85 (1984) 78-88.

[7] A. Barbier, A. Tuel, I. Arcon, A. Kodre, G.A. Martin, J. Catal. 200 (2001) 106-116.

[8] G.L. Bezemer, J.H. Bitter, H.P.C.E. Kuipers, H. Oosterbeek, J.E. Holewijn, X. Xu, F. Kapteijn, A.J. Van Dillen, K.P. De Jong, J. Am. Chem. Soc. 128 (2006) 3956-3964.

[9] Ø. Borg, P.D.C. Dietzel, A.I. Spjelkavik, E.Z. Tveten, J.C. Walmsley, S. Diplas, S. Eri, A. Holmen, E. Rytter, J. Catal. 259 (2008) 161-164.

[10] E. Iglesia, S.L. Soled, R.A. Fiato, J. Catal. 137 (1992) 212.

[11] Z.-J. Wang, S. Skiles, F. Yang, Z. Yan, D. W. Goodman, Catal. Today 181 (2012) 75– 81

[12] Y. Khodakov, W. Chu, P. Fongarland, Chem. Rev. 107 (2007) 1692-1744

[13] S. Järås, S. Lögdberg, M. Boutonnet, European Patent Application Number EP07106863.9 (2007).

[14] S. Lögdberg, M.Boutonnet, J. C. Walmsley, S. Järås, A. Holmen, E.A. Blekkan, Appl.Catal. A 393 (2011) 109–121.

[15] H. Wanga, Y. Yang, J. Xu, H. Wang, M. Ding, Y. Li, J. Mol. Catal. A 326 (2010) 29–40.

[16] F. Morales, E. Smit, F. Groot, T. Visser, B.M. Weckhuysen, J. Catal. 246 (2007) 91–99.

[17] A.R. de la Osa, A. De Lucas, A. Romero, J.L. Valverde, P. Sánchez, Fuel 90 (2011) 1935–1945.

[18] A. Kogelbauer, J. G. Goodwin Jr., R. Oukaci, J. Catal. 160 (1996) 125-133.

[19] K. Okabe, X. Li, M. Wei, H. Arakawa, Catal. Today 89 (2004) 431-438.

[20] M. Reinikainen, M.K. Niemelä, N. Kakuta, S. Suhonen, Appl. Catal. A 174 (1998) 61-75.

[21] Xu, D., W. Li, H. Duan, Q. Ge, H. Xu, Catal. Lett 102 (2005) 229-235.

[22] K. M. Cook, S. Poudyal, J. T. Miller, C. H. Bartholomew, W. C. Hecker, Appl. Catal. A. 449 (2012) 69– 80.

[23] F. Diehl, A.Y. Khodakov, Oil Gas Sci. Technol. 64 (2009) 11-24.

[24] E. Iglesia, S.C. Reyes, Rostam J. Madon, Stuart L. Soled, Advances Catal. 39 (1993) 221-235.

[25] Z. Zsoldos, F. Garin, L. Hilaire, L. Guczi. J. Mol. Catal. A 111 (1996) 113-122.

[26] J. Li, N.J. Coville, Appl. Catal. A 181 (1999) 201-208.

[27] K. F. Tan, J. Chang, A. Borgna, M. Saeys, J. Catal. 280 (2011) 50-59.

[28] G. Prieto, A. Martínez, P. Concepción, R. Moreno-Tost, J. Catal. 266 (2009) 129–144.

[29] D. Schanke, S. Vada, E.A. Blekkan, A.M. Hilmen, A. Hoff, A. Holmen, J. Catal. 156 (1995) 85–95.

[30] M. S. Spencer, M. V. Twigg, Annual Rev Mater. Res. 35 (2005) 427-464.

[31] K. F. Tan, J. Chang, A. Borgna, M. Saeys, J. Catal. 280 (2011) 50-59.

[32] A.R. de la Osa, A. De Lucas, A. Romero, J.L. Valverde, P. Sánchez, Catal. Today 176 (2011) 298– 302.

[33] R. Riva, H. Miessner, R.Vitali, G. Del Piero, Appl.Catal. A 196 (2000) 111–123.

[34] J. Łojewska, A. Kołodziej, T. Łojewski, R. Kapica, J. Tyczkowski, Appl. Catal. A 366 (2009) 206-211.

[35] US EPA Nonylphenol (NP) and Nonylphenol Ethoxylates (NPEs) Action Plan, available at http://www.epa.gov/oppt/existingchemicals/pubs/actionplans/np-npe.html).

[36] D. Gallant, M. Pézolet, S. Simard, J. Phys. Chem. B 110 (2006) 6871-6880.

[37] M.C. Biesinger, B. P. Payne, A. P. Grosvenor, L. W.M. Lau, A. R. Gerson, R. St.C. Smart, Appli. Surf. Sci. 257 (2011) 2717–2730.

[38] R. Moreno-Tost, J. Santamaría-González, P. Maireles-Torres, E. Rodríguez-Castellón, A. Jiménez-López, Appl. Catal. B, 38 (2002) 51-60.

[39] E. van Steen, M. Claeys, D. Nabaho, A.P. Petersen, R. Stracey, C. Change, J.W. Niemantsverdriet, Proceedings to 15th ICC, Munich, 2012. Available at http://events.dechema.de/events/en/Events/Materials+for+Energy+_+EnMat+II/Congress+Planer/Datei_Handler-tagung-564-file-7246-p-127866.html

Chapter 4

Enantioselective hydrogenation of ethyl pyruvate to ethyl lactate on several Pt-based systems modified with cinchona-alkaloids

Abstract

This chapter deals with the enantioselective hydrogenation of ethyl pyruvate to ethyl lactate on Pt-based catalysts. USY zeolites and MCM-41 were used as the supports for Pt in order to have a homogeneous distribution of pore sizes and high surface area which would also result in a high Pt dispersion. Furthermore, the use of microporous and mesoporous materials could inform us on potential diffusion problems. Moreover, two different calcination rates (1 or 10°C/min) were used in order to study the influence of this parameter on Pt particle size and finally on catalytic performance.

Under standard conditions, cinchonidine was used as a chiral modifier to induce enantioselectivity.

4.1. Brief introduction

Enantioselective catalysis is very important in fragrance and drugs industry. One of the approaches to induce chirality consists in the co-adsorption of a chiral molecule (referred to as chiral modifier) together with the substrate. In the case of Pt, cinchona alkaloids are commonly used. In general, it is commonly accepted that the chiral modifier of platinum should possess the following characteristics [1-3]:

1) An extended aromatic system for anchoring onto the Pt surface.
2) Stereogenic center (s) responsible for enantiodiferentiation.
3) Nitrogen heteroatom to interact with the substrate through hydrogen-bonding.

However, Baiker and co-workers [4] found the first modifier of platinum which did not possess the nitrogen atom but an oxygen one.

There are several factors influencing the catalytic activity of Pt-based systems such as the precursor, support, solvent and the presence of additives, just

to cite some of them [3-5,9]. One of the reference catalysts is 5% Pt/Al_2O_3 (Engelhard Art. 4759) modified with cinchonidine (CD) whereas toluene and acetic acid are the solvents commonly used.

In this chapter synthesized solids are first tested for the process in 3 different solvents (isopropanol, toluene and acetic acid) using CD as the chiral modifier. Then, several commercial chiral molecules are tested as additives in order to study their effect on catalytic performance. Finally, factorial design of experiments is applied to further study one of these chiral molecules which was found to enhance reaction rate and enantioselectivity. The study is completed with some UV-Vis experiments to look for some modifier-additive-solvent interaction.

4.2. Experimental

4.2.1. Materials

8% weight H_2PtCl_6 aqueous solution, Pt(II) acetylacetonate [$Pt(acac)_2$], aluminosilicate mesostructured MCM-41(hexagonal), acetic acid, toluene and ethyl pyruvate were purchased from Sigma-Aldrich. MilliQ water was used for the preparation of water solutions. Ultra Stable Zeolites type Y, USY780 and USY300 was obtained from Zeolist international. Cinchonidine (CD), and Cinchonine (CN) from Fluka with a purity over 98% were used as chiral modifiers. Figure 4.1 shows the different chiral molecules tested as additives (apart from CD or CN): D-(-)-α-Phenyl 1-2 ethanediol (puriss >99% Fluka), L (+) α Phenylglycinol (>98% Fluka), R-(-)- Mandelic acid (>99% Aldrich), D(-)- α-Phenylglycine (>99% Fluka), L(+)- α-Phenylglycine (>99% Fluka), 4-Hydroxy- D(-)-α-phenylglycine (>99% Fluka), (1R 2S)-(+)-cis-1-Amino-2-indanol (99% Aldrich), (3R 4R)-(-)-Benzyl-3-4-pyrrolidindiol (97% Fluka), (S)-(+)-Phenyl-2-oxazolidinone (>97%Aldrich), Fmoc-ser-OH (>97% Fluka).

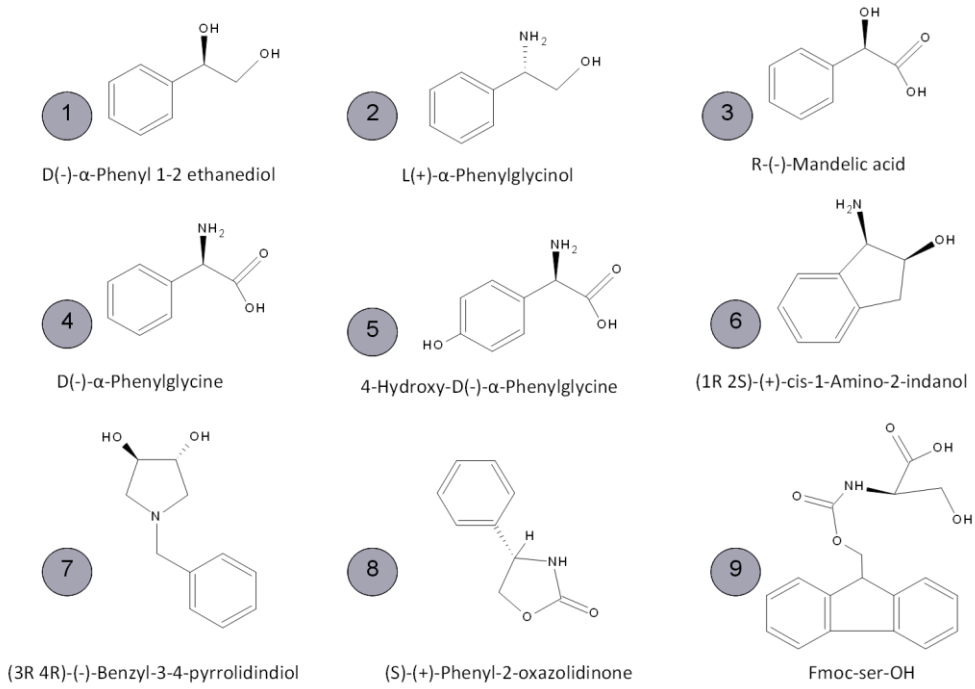

Figure 4.1. *Different commercial chiral molecules tested in the present chapter both as chiral modifiers of platinum and as co-additives in CD-modified platinum systems. Additive Nr. 4 was tested both in the R and S forms.*

4.2.2. Synthesis of Pt based solids

Before each synthesis the support was calcined at 550ºC during 24 h with a flow of N_2. In a typical synthesis 4.75g of support (in order to obtain 5wt% Pt/support in final systems) was suspended in 200mL of milli-Q water containing the inorganic metal precursor (H_2PtCl_6). In the case of using the organic metal precursor, the addition of 5 ml of iso-propanol and the use of an ultra-sound bath

was necessary to dissolve it. The suspensions were stirred for 5h at room temperature and then the solvent was rota-evaporated under vacuum at 80ºC. The solids were then dried overnight at 120ºC and subsequently calcined at 500ºC during 5 h under a synthetic air flow. Two calcination rates (10ºC/min and 1ºC/min) were used. Prior to each reaction the catalysts were reduced for 2 hours at 400ºC under hydrogen flow (20 mL/min).

The nomenclature of the solids includes the support, the platinum precursor and finally the calcination rate. Therefore, for instance, the catalyst synthesized using USY780 as the support, chloroplatinic acid as the metal precursor and calcined at 1ºC/min is named USY780-H_2PtCl_6-1ºC/min.

4.2.3. Characterization

Elemental analysis of metal-containing samples was performed by the staff at the Central Service for Research Support (SCAI) of the University of Córdoba. It was performed using inductively coupled plasma-mass spectrometry (ICP-MS). Measurements were made on a Perkin-Elmer ELAN DRC-e instrument following dissolution of the sample in a 1:1:3 of HF/HNO_3/HCl mixture with a soft heating. Calibration was done by using PE Pure Plus atomic spectroscopy standards, also from Perkin-Elmer.

EDX measurements were performed on a JEOL JSM-6300 scanning electron microscope (SEM) equipped with an energy-dispersive X-ray (EDX) detector. It was operated at an acceleration voltage of 20keV with a resolution of 65eV.

Surface areas of the solids were determined from nitrogen adsorption–desorption isotherms obtained at liquid nitrogen temperature on a Micromeritics ASAP-2010 instrument, using the Brunnauer–Emmett–Teller (BET) method. All samples were degassed to 0.1 Pa at 120ºC prior to measurement.

Transmission electron microscopy (TEM) images were obtained using a JEOL JEM 1400 microscope. All samples were mounted on 3 mm holey carbon copper grids. In order to make histogram of particles over 100 particles were used.

X-ray patterns of the samples were obtained on a Siemens D-5000 diffractometer equipped with a DACO-MP automatic control and data acquisition system. The instrument was equipped with a graphite monochromator and used Co Kα radiation. Metal particle sizes were calculated using Scherrer equation.

Temperature-programmed reduction (TPR) measurements were made with a Micromeritics TPD-TPR 2920 analyser. An amount of 100 mg of catalyst was placed in the sample holder and reduced in a 10:90 H_2/Ar stream flowing at 20 mL/min. The temperature was ramped from 313 to 1073 K at 10 ºC/min .

Diffuse reflectance UV–vis spectra were performed on a Cary 1E (Varian) instrument using as reference the solvent, acetic acid or toluene.

4.2.4. Catalytic tests

Two different devices (a IKA multi-reactor with 12 quartz vials of 20 mL, operating at 1bar H_2 pressure, and magnetic stirrer) or a FIKE type PSTFS stainless steel high-pressure autoclave equipped with a 50 mL PTFE vessel and a magnetic stirrer (for higher pressures) were used.

Before each reaction the solvent and the reagent were distilled. Under standard conditions, 20 mL of solvent, 2 mg of modifier (or the required amount to have 1:1.3:272 Pt:modifier:ethyl pyruvate molar ratio), 20mg of catalyst (reduced at 400ºC during 2h with a flow of H_2) and 400µL of ethyl pyruvate were introduced in the vessel. Reactor was purged first with N_2 three times, then with H_2 x 3 and finally the pressure adjusted with H_2. The stirring rate was 1200 rpm and the temperature kept at 20ºC. At the desired time stirring was stopped, the pressure reduced and the system purged with N_2. The catalyst was spin-dried and the liquid

passed through a filter of PTFE 0.45µm. Then it was analyzed by GC-FID (HP5890) equipped with a Chrompack Capillary Colum CP-Chirasil-DEX. Quantification was carried out through the corresponding calibration curves. Enantiomeric excess (e.e.) was calculated according to:

$$\text{e.e. } [\%] = ([R] - [S])/([R] + [S]) \times 100$$

4.2.5.Multifactorial design of experiments

These experiments were performed in the above-described autoclave. The effect of process parameters (temperature, hydrogen pressure, modifier amount and additive amount) on conversion and selectivity to (R)-ethyl lactate on USY780-$Pt(acac)_2$-10ºC/min was studied using a multifactorial design of experiments run by the software StatGraphics® version 5.1. Matrix design was randomized in order to eliminate the influence of any other no observed covariables on obtained results. Three factors were included in the factorial design: initial hydrogen pressure at three levels (5, 30 and 55 bar) mg of CD (0.1, 2 and 3.9 mg) and mg of additive (OHDF, Nr. 5 in Figure 4.1, 0, 2 and 4 mg). Acetic acid was used as the solvent, temperature kept 20ºC and reaction time was 17h.

4.3. Results and discussion

Table 4.1 shows some of the main features of the Pt-containing systems. For comparative purposes, supports have also been included. Some of the main conclusions are:

1) there was a good incorporation of Pt;
2) incorporation of Pt led to a decrease in surface area though in any case the values remained high;
3) calcination temperature had a great influence on Pt particle size. As expected, smaller particle sizes were obtained for calcination rates of 1ºC/min as compared to 10ºC/min;
4) the influence of Pt precursor is not clear from the table.

TEM micrographs and particle size histograms (Fig. 4.2) confirm that calcination at 1ºC/min leads to smaller and more homogeneous in size Pt particles. This is also consistent with XRD results (Fig. 4.3) the solids calcined at 1ºC/min not exhibiting Pt peaks despite the high metal content.

H_2-TPR profiles (Fig. 4.4) show that at the selected reduction temperature (400ºC) Pt has been reduced for all the systems, the exception being USY300-H_2PtCl_6-1ºC/min. In this latter case, the peak appearing at 550ºC could suggest some metal-support interaction.

***Table 4.1**. Some features concerning characterization of Pt-containing solids.*

	BET area (m^2/g)	Si/Al (mole ratio)			Pt (wt %)			Average Pt particle size (nm)
		Nominal	(ICP-MS)	(EDAX)	Nominal	(ICP-MS)	(EDAX)	(TEM)
MCM41	993	39.5	39.0	59		-		-
MCM41-$Pt(acac)_2$-10°C/min	815	39.5	34.0	57	5	5.2	4.6	6.7
MCM41-$H_2PtCl_6$10°C/min	610	39.5	25.0	57	5	4.4	4.4	4.7
MCM41-H_2PtCl_6 1°C/min	857	39.5	36.6	50	5	4.8	4.6	3.9
USY780	782	40	55.0	62		-		-
USY780-$Pt(acac)_2$ 10°C/min	716	40	43.3	59	5	4.2	4.5	3.6
USY78- H_2PtCl_6 10°C/min	645	40	67.1	57	5	4.8	3.9	6.9
USY780-H_2PtCl_6 1°C/min	589	40	39.1	49	5	5.4	4.2	3.1
USY300	754	2.5	3.0	4.2		-		-
USY300-$Pt(acac)_2$ 10°C/min	561	2.5	3.3	3.3	5	3.9	3.7	6.3
USY30- H_2PtCl_6 10°C/min	607	2.5	3.5	3.3	5	4.2	4.2	8.3
USY300-H_2PtCl_6 1°C/min	444	2.5	3.0	3.1	5	4.4	4.8	2.3

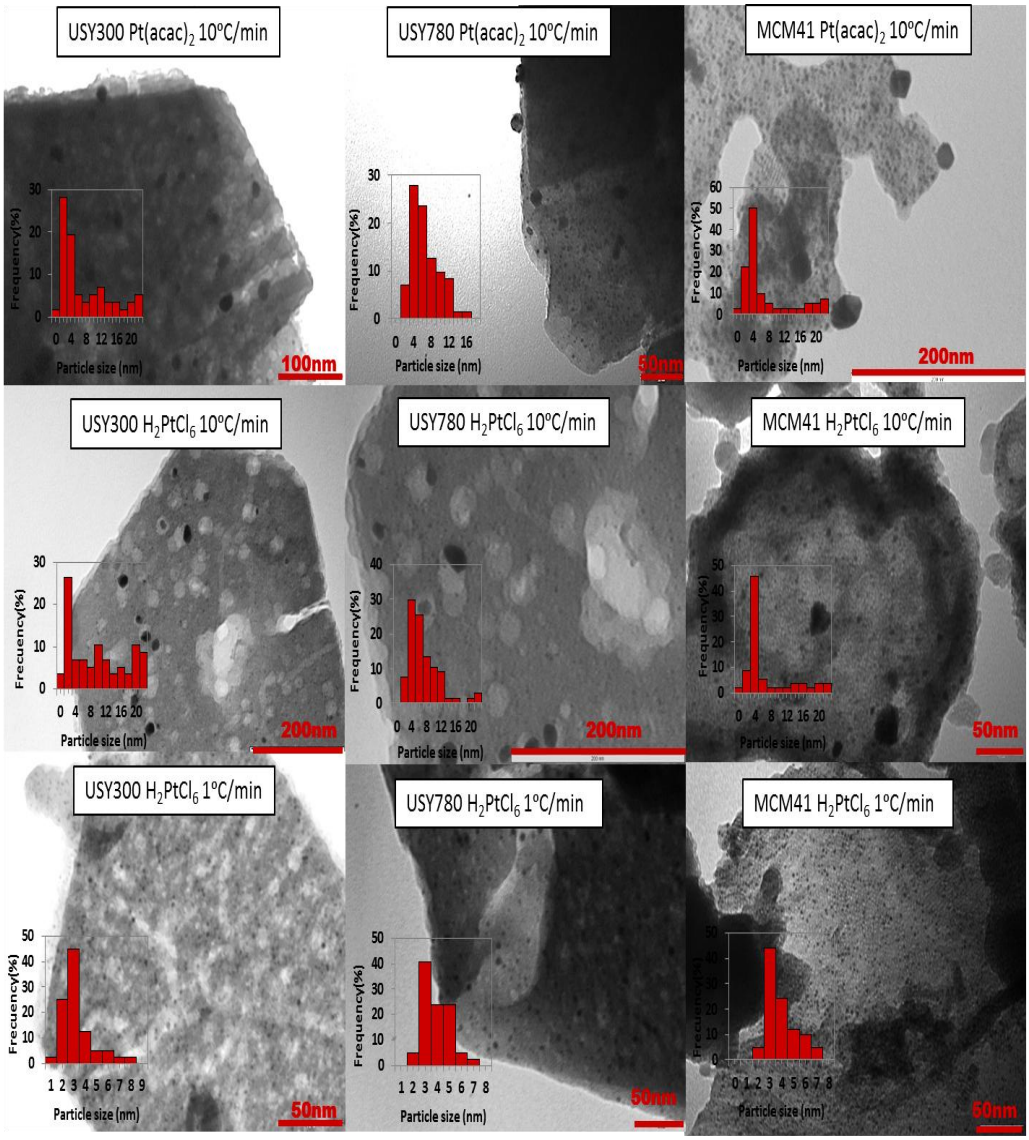

Figure 4.2. *TEM micrographs of the Pt-containing systems*.

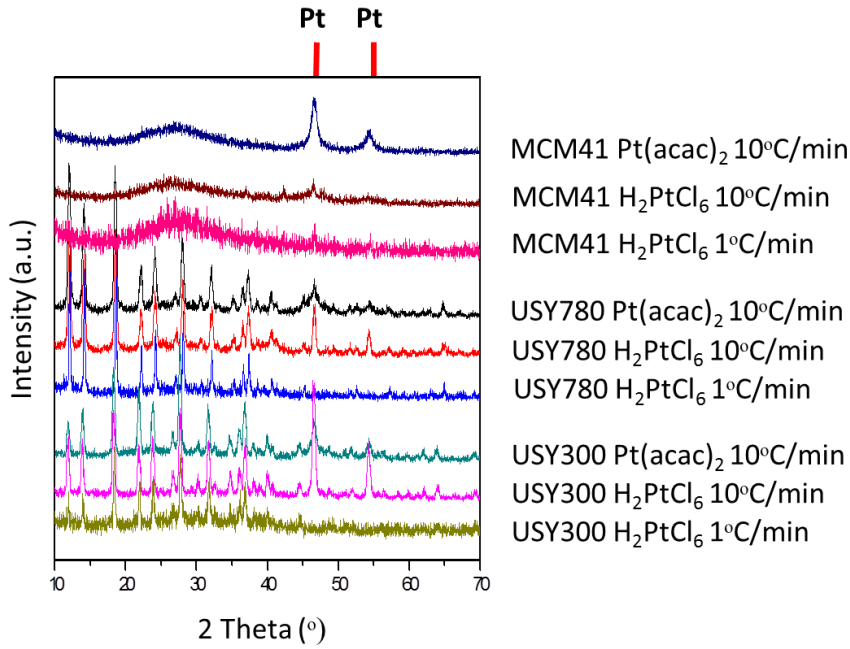

Figure 4.3. *X-ray diffractograms of the Pt-containing solids.*

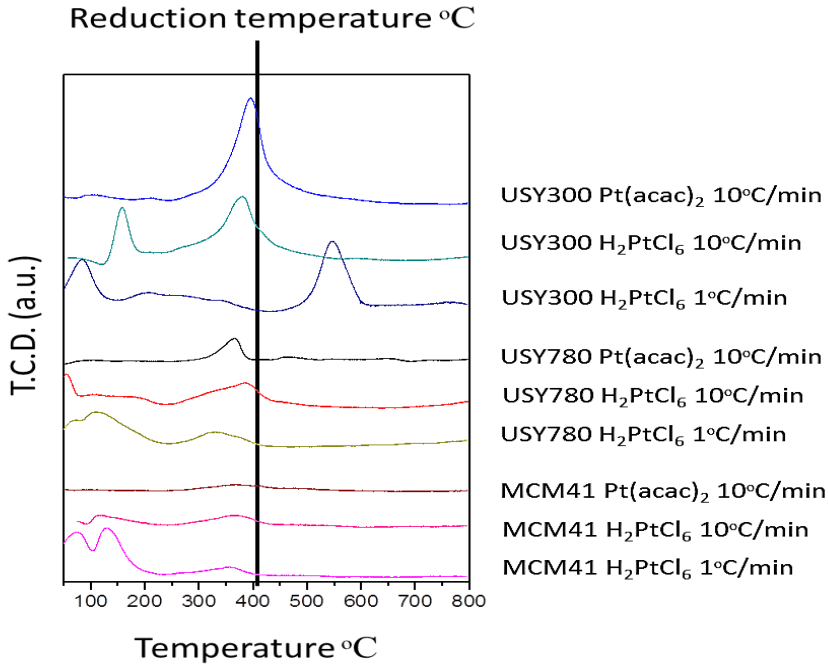

Figure 4.4. *H_2-TPR profiles of the Pt-containing solids.*

4.3.1. Study of the different catalysts using CD as the chiral modifier

Figure 4.5, shows the results obtained for the different catalysts for hydrogenation of ethyl pyruvate to (R)-ethyl lactate. Reactions were performed under standard conditions using CD as the modifier, 1bar H_2 and 17h of reaction.

Having a look at Figure 4.5A, one can see that ee values followed the trend USY300<USY780<MCM-41. This seems to suggest that higher Si/Al ratios (and thus higher hydrophobicity) is preferable to high hydrophilicity and that due to steric hindrance mesoporous (MCM-41) are better than microporous materials. Moreover, calcination at 1ºC/min led to higher conversions and enantiomeric excess values as compared to 10ºC/min. The lower Pt particle size, and the higher fraction of particles in the 3-5 nm range which has been found to be the optimum in the reaction [5] , could account for that.

As far as the solvent is concerned, isopropanol led to the lowest e.e. values (see Pt/Al_2O_3 Engelhard 4759 for which in all cases 100% conversion was achieved), whereas, in general, the highest e.e. values were obtained when acetic acid was used as the solvent. Toluene resulted in the highest e.e. values only for MCM-41. This could be related to diffusion problems in microporous materials. Though not represented, the reaction was performed without modifier exhibiting the lowest conversion values. In fact, the use of chiral modifiers which favors the e.e. is normally accompanied by an increment in reaction rate.

Finally, under these working conditions, the best results corresponded to the reference catalyst (Pt/Al_2O_3 Engelhard Art. 4759) in acetic acid which exhibited 69.7 % e.e. at 100% conversion followed by MCM41-H_2PtCl_6-1ºC/min (87.4 % conv., 65.5% e.e.).

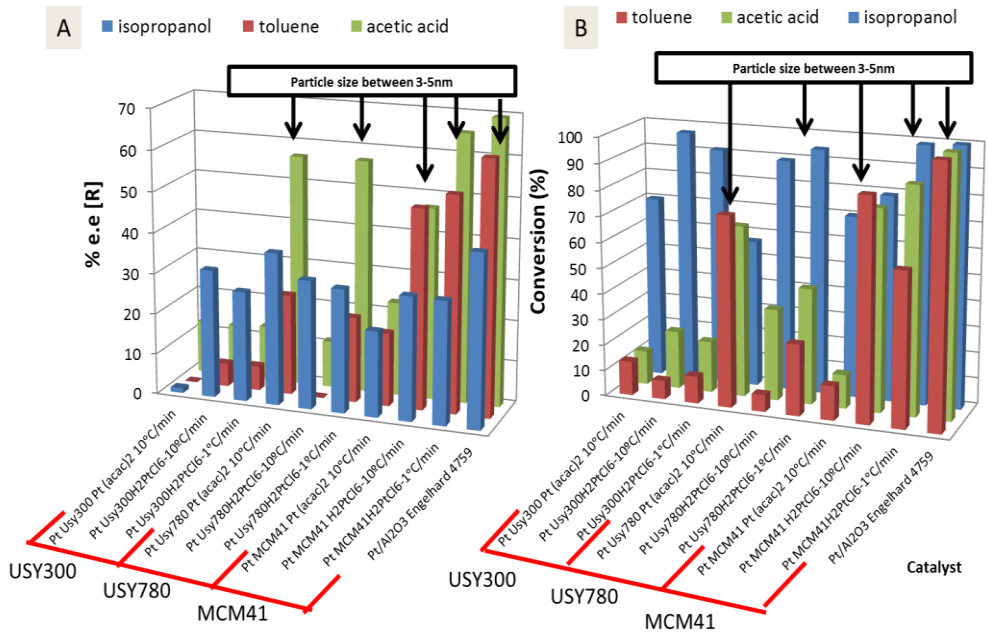

Figure 4.5. *Conversion and enantiomeric excess obtained for the different Pt-containing solids for 1bar H_2 and 17 h of reaction under standard conditions.*

4.3.2. Effect of the presence of chiral molecules as co-additives

Chiral molecules shown in Figure 4.1 were tested as chiral modifiers of Pt. None of them exhibited enantiomeric excess. This is hardly surprising, considering that the typical extended aromatic ring should possess at least 2 condense aromatic rings [6,10] for good anchoring to Pt and the low solubility of such molecules in polar solvents (such as acetic acid).

However, some authors have reported the improvement in ee and conversion through the presence of other molecules co-adsorbed, especially for low modifier concentration values, typically under 10^{-5}M. For instance, Tálas et al. [7] found that addition of achiral tertiary and secondary amines improved both reaction rate and e.e. values in hydrogenation of ethyl pyruvate. Circular dichroism experiments prompted them to ascribe the observed results to the increase of the virtual concentration of the modifier in accordance with the shift of dimer-monomer equilibrium of cinchonidine.

Therefore, we decided to study the effect of these chiral molecules as co-additives.

Figure 4.6 shows the results (in terms of conversion and e.e.) obtained for three different catalysts at 55 bar of hydrogen pressure and using CD and additive concentrations of 10^{-5}M and 10^{-3}M, respectively. For comparative purposes, results achieved with pure CD (without additive) are also shown. As can be seen, co-additives Nr 4 (R and S) and 5 led in all cases to an improvement both in conversion and enantioselectivity as compared to pure CD. Molecule Nr 5 has basically the same structure as 4 but with an OH in *para* position in the aromatic ring in order to increase its solubility in polar solvents.

In fact, as shown in Figure 4.6D, the presence of molecule Nr. 5 led to the highest improvement in ee (up to 130%). Interestingly, both 4R and 4S leads to a similar improvement to R-lactate which suggests that the effect of this additive is somehow associated to the adsorption process and not to enantiodifferentiation.

Modifier Nr 5 (OHDF) was then selected for further studies. In this case a set of experiment were performed mixing CD or CN and additive Nr. 5 at 25 bar H_2, and always keeping modifier+additive concentration at 10^{-3}M. These types of experiments are usually done to study the so- called non-linear effect. Several catalysts were used and all of then showed an improvement of the e.e. and the conversion when the OHDF is present in the system and the concentration of CD and CN are low (Figure 4.7), specially below 10% of the normal ratio described in the experimental part (1 mole catalyst, 1.3 mole modifier, 272 mole ethyl pyruvate). Again, interestingly, addition of OHDF leads to an improvement of e.e. achieved with both CD and CN (to R or S lactate, respectively).

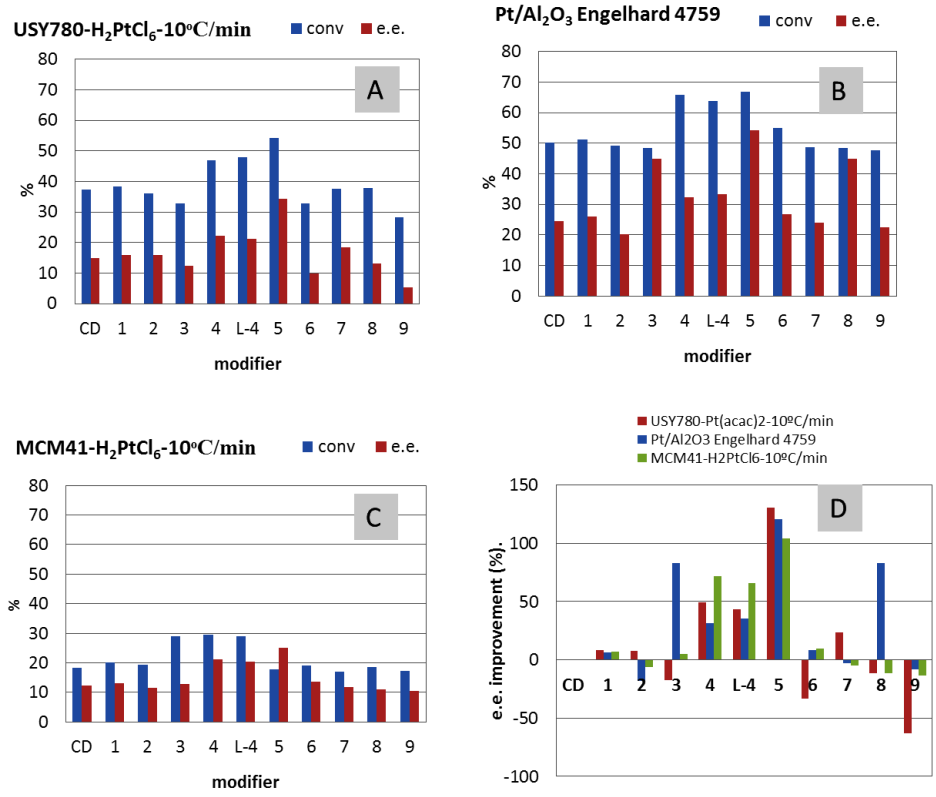

Figure 4.6. *Results obtained for enantioselective hydrogenation of ethyl pyruvate to (R)-ethyl lactate on several Pt-containing catalysts using the molecules of Figure 4.1 as additives and CD as the co-modifier.*

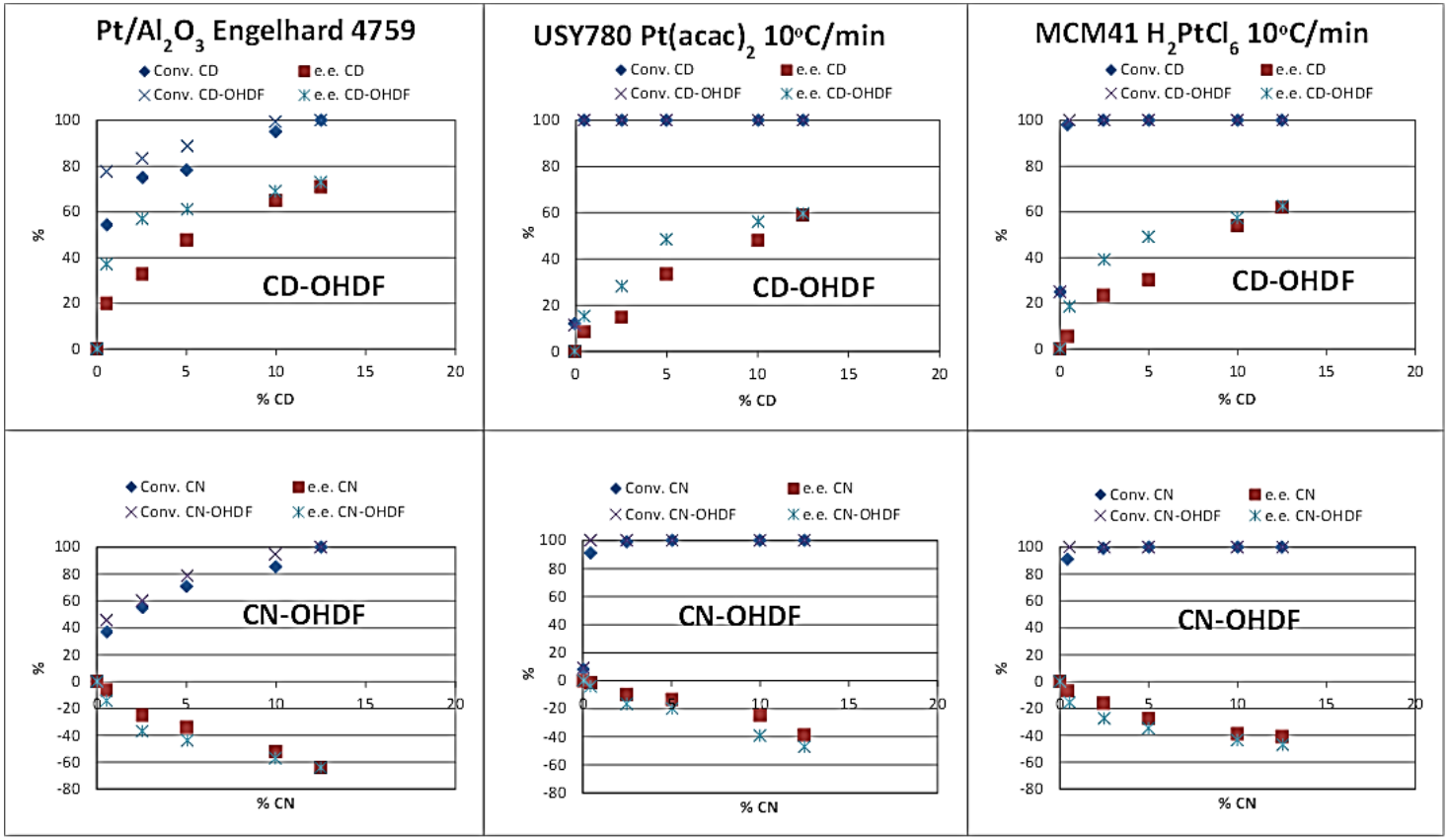

Figure 4.7*. Study of non-lineal effect in enantioselective hydrogenation of ethyl pyruvate to ethyl lactate on several Pt-containing solids, using CD or CN as the modifier and additive Nr 5 (OHDF) in acetic acid.*

4.3.3. UV study of modifier-additive-solvent interaction

In order to cast further light on the reason for the enhancement in both reaction rate and enantioselectivity obtained for Additives Nrs 4 and 5, several experiments were performed using UV-Vis spectroscopy. Results are shown in Figure 4.8 for 6 different additives, CD as the chiral modifier, Pt/Al_2O_3 Engelhard 4759 as the catalyst and acetic acid as the solvent. All experiments were performed in the liquid phase using pure acetic acid spectrum as the reference.

Therefore, the experiment started recording the UV-Vis spectra of the CD+modifier mixture (black line), the intensity being very low in all cases. Then, the substrate (ethyl pyruvate) was added (red spectrum) and the system stirred for 50 min (see blue spectrum). As can be seen, only when additives Nrs. 4 and 5 were used, the spectrum after the addition of ethyl pyruvate changed with time, thus evidencing some kind of interaction occurring in solution. Finally, the catalyst was added, stirred for 15 min, filtered and a new UV-Vis spectrum recorded. Once again, the only difference is observed for addtives Nrs. 4 and 5.

Similar experiments were performed in toluene (not shown) obtaining the same results which suggest that the observed interaction is independent of the solvent.

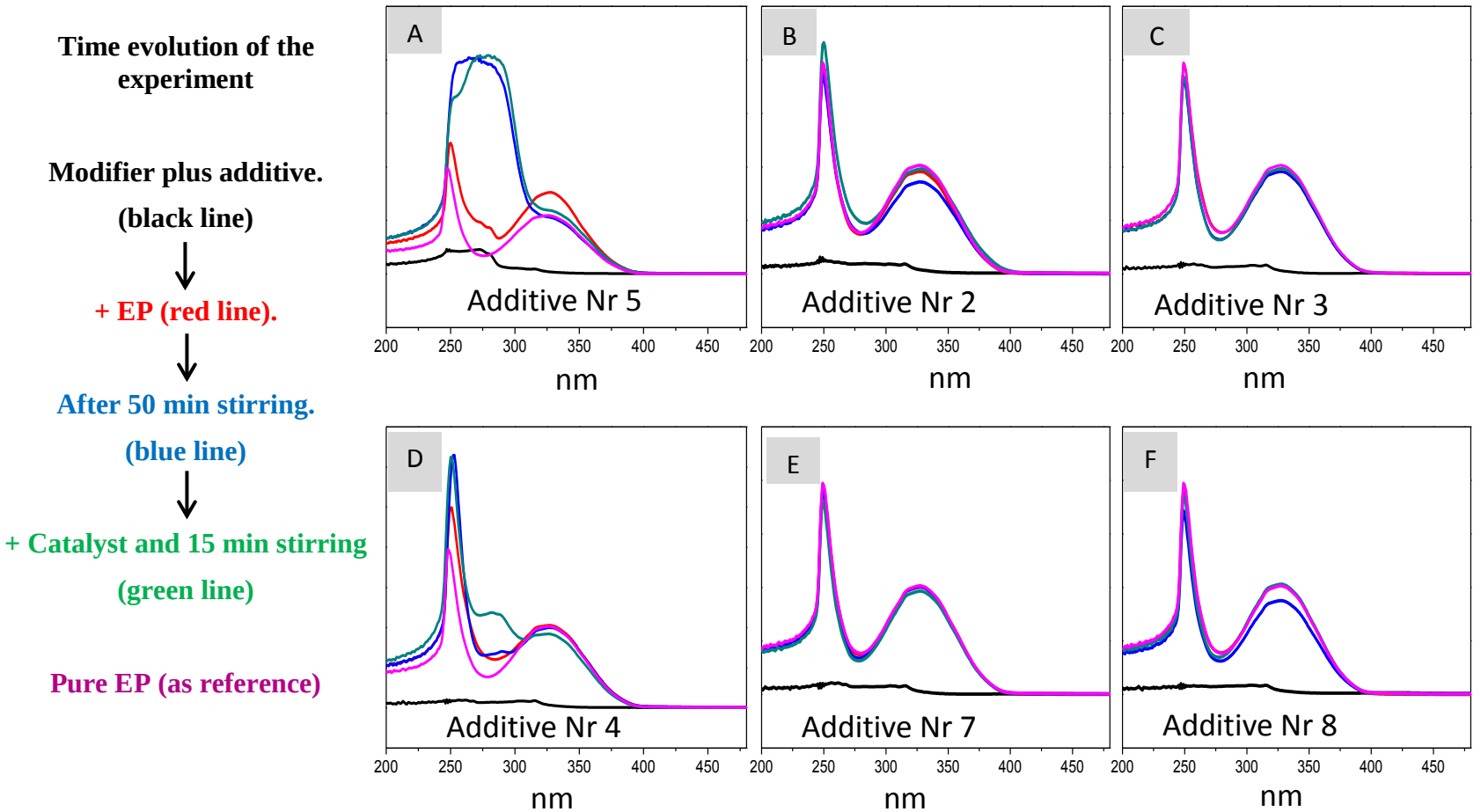

Figure 4.8. *UV-Vis study of EP-modifier-additive interaction in the liquid phase (acetic acid).*

4.3.4. Multivariable study

The last part of this chapter was devoted to the study of the possibility to improve reaction rate and e.e. values for a given catalyst (USY780-H_2PtCl_6-10ºC/min) using factorial design of experiments. Hydrogen pressure, amount of CD and additive Nr 5 (OHDF) were used as the variables.

Results are summarized in Table 4.2 and Figure 4.9. A first conclusion from Table 4.2 is that for CD contents of 2 or 3.9 mg conversion was always total and e.e. values hardly changed. On the contrary, for experiments starting from 0.1 mg conversion was in the 36.1-60.6% range and selectivity varied between 14.5 and 42.7%, e.e. increasing with the increase in the amount of additive Nr 5. This is consistent with results previously described and confirms the positive effect of the presence of additive Nr 5, specially at low CD contents. As regards the effect of hydrogen pressure (Figure 4.9A), the highest e.e. values are obtained between 30 and 40 bars whereas subsequent increase result in a decrease in e.e. probably as a consequence of the hydrogenation of the aromatic ring in modifier and/or additive which is detrimental to adsorption on Pt.

Standardized Pareto chart is depicted in Figure 4.9B evidencing the positive effect of both CD and additive content in e.e.

From the multivariable study, the optimum conditions correspond to 30.4 bar of H_2, 2.91 mg CD and 2.46 mg of OHDF resulting in 100% conversion and 79% e.e., the maximum achieved in the present chapter.

Table 4.2. *Results obtained for the 27 experiments of the factorial design of experiments.*

Entry	Temperature °C	Pressure (H_2 bar)	mg CD	mg OHDF	Conv. (%)	e.e. (%)
1	20	5	0.1	0	38.1	17.3
2	20	5	0.1	2	44.2	28.9
3	20	5	0.1	4	42.5	29.6
4	20	5	2	0	100	65.4
5	20	5	2	2	100	68.8
6	20	5	2	4	100	68.2
7	20	5	3.9	0	100	67.6
8	20	5	3.9	2	100	69.2
9	20	5	3.9	4	100	70.1
10	20	30	0.1	0	43.7	24.9
11	20	30	0.1	2	57.9	39.5
12	20	30	0.1	4	60.6	42.6
13	20	30	2	0	100	69.7
14	20	30	2	2	100	71.8
15	20	30	2	4	100	70
16	20	30	3.9	0	100	69.4
17	20	30	3.9	2	100	71.2
18	20	30	3.9	4	100	69.9
19	20	55	0.1	0	36.1	14.5
20	20	55	0.1	2	55.5	32.5
21	20	55	0.1	4	53.2	33.7
22	20	55	2	0	100	68.9
23	20	55	2	2	100	69.7
24	20	55	2	4	100	69.3
25	20	55	3.9	0	100	68.3
26	20	55	3.9	2	100	68.4
27	20	55	3.9	4	100	69.1

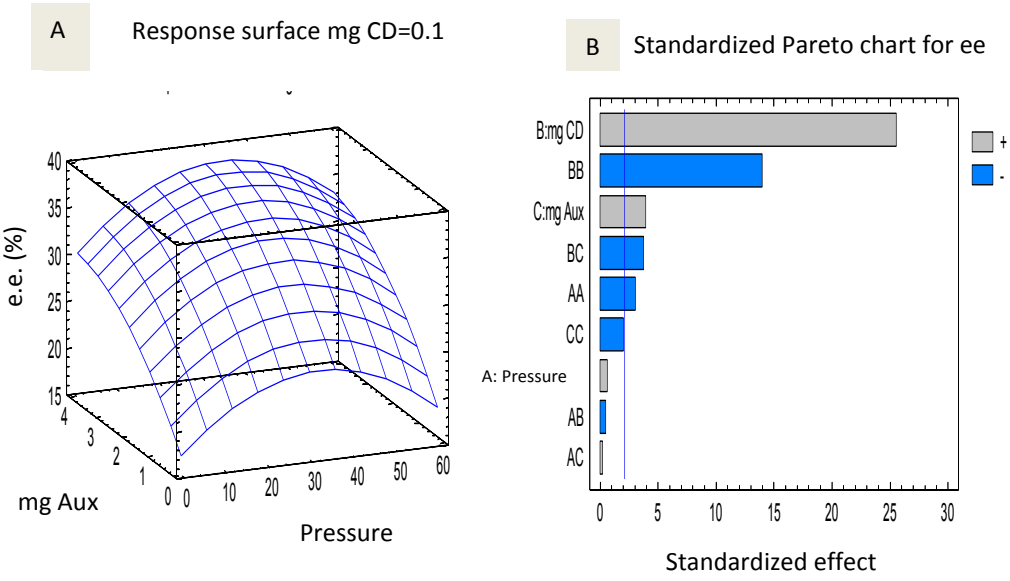

Figure 4.9. *Response surface (A) and standardized Pareto chart (B) for e.e.*

4.4. Conclusions

Different systems consisting in Pt supported on several porous-ordered materials (MCM-41 and USY zeolite) were synthesized and tested for enantioselective hydrogenation of ethyl pyruvate to ethyl lactate using cinchona-alkaloids as the chiral modifiers. The best results in terms of conversion and enantiomeric excess (e.e.) corresponded to the solids exhibiting the highest fraction of Pt particles in the 3-5 nm range. Three different solvents were used (isopropanol, toluene and acetic acid), acetic acid affording the highest e.e. values. Several commercial chiral molecules were tested as additives in order to favor e.e., 4-hydroxy-D-(-)-phenylglycine (OHDF) exhibiting a positive effect for low CD contents thus increasing e.e. The fact that the additive increases both e.e. to R or S-

lactate depending on the presence of cinchonidine or cinchonine, respectively evidenced that its synergistic effect must be somehow associated to an enhancement in adsorption and not in enantiodifferentiation. In fact, UV-Vis studies evidenced that this additive was the only one showing some kind of substrate-modifier-additive interaction in the liquid phase. A multivariable study on one of the catalysts (USY780-H2PtCl6-10ºC/min) varying the hydrogen pressure, amount of CD and OHDF, allowed us to obtain 79% e.e. at total conversion and confirmed the above-mentioned positive effect of OHDF on enantioselectivity.

References

[1] A. Baiker, J. Mol. Catal. A:Chem. 115 (1997) 473-493.

[2] J.T. Wehrli, A. Baiker, D.M. Monti, H.U. Blaser, J. Mol. Catal. 49 (1989) 195-203.

[3] H.U. Blaser, H.P. Jalett, D.M. Monti, A. Baiker, J.T. Wehrli, in: R.K. Grasselli, A.W. Sleight (Eds.), Stud. Surf. Sci. Catal. Elsevier, 1991, pp. 147-155.

[4] A. Marinas, T. Mallat, A. Baiker, J. Catal. 221 (2004) 666-669.

[5] J. Wehrli, A. Baiker, D. Monti, H. Blaser, J. Mol. Catal. 61 (1990) 207-226.

[6] C. Exner, A. Pfaltz, M. Studer, H.U. Blaser, Adv. Synth. Catal. 345 (2003) 1253-1260.

[7] E. Tálas, F. Zsila, P. Szabó, J.L. Margitfalvi, J. Mol. Catal. A: Chem., 357 (2012) 87-94.

[8] N. Maeda, K. Hungerbühler, A. Baiker, JACS 133 (2011) 19567-19569.

[9] J. de Graaf, A.J. van Dillen, K.P. de Jong, D.C. Koningsberger,J. Catal. 203 (2001) 307-321.

[10] T. Mallat, A. Baiker, Appl. Catal. A: Gen. 200 (2000) 3-22.

Chapter 5

Chemoselective hydrogenation of crotonaldehyde to crotyl alcohol on several Pt-based catalysts

Abstract

This chapter deals with the chemoselective hydrogenation of crotonaldehyde to crotyl alcohol on the solids consisting in supported noble metals (Pt-based systems mainly) described in the other chapters. Several Alumino-silicates (USY 300, USY 780 and MCM41) and ZnO systems were used as the supports. The hydrogenation of crotonaldehyde was performed in a gas flow reaction system.

5.1. Brief Introduction

Chemoselective hydrogenation of unsaturated aldehydes is an important reaction from the industrial point of view. The most important product is unsaturated alcohol. However, unfortunately, hydrogenation of C=C is thermodynamically favored over that of C=O. Crotonaldehyde is one of the most studied probe molecules for the process (scheme 5.1).

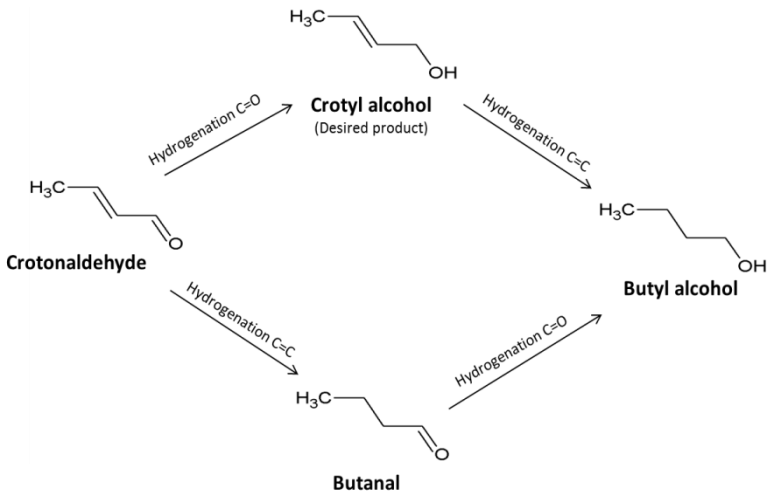

Scheme 5.1. *Crotonaldehyde hydrogenation pathways.*

In order to perform the process, there are two main approaches: i) Reduction of the carbonyl group by hydrogen transfer from an alcohol through the so-called Meerwein–Ponndorf–Verley (MPV) reduction. Some of the catalysts effectively used in this process include magnesium oxides and hydroxides or zirconium oxides [1-2]; ii) reduction with H_2 using a noble metal, typically group VIII metals, platinum being the most widely used [3-5]. Furthermore, in order to enhance activity and selectivity to the unsaturated alcohol, different strategies have been described such as the addition of a second 3d metal [6,7], or the use of (partially) reducible supports (TiO_2, ZnO, etc.) to promote strong metal-support interactions (SMSI) and eventually alloy formation [8-13]. All the strategies are aimed at weakening the C=O bond and/or avoiding the adsorption through C=C bond.

In this chapter, all the noble metal-based solids synthesized during the PhD for different purposes (glycerol hydrogenolysis, enantioselective catalysis…) are tested for selective transformation of crotonaldehyde to crotyl alcohol. It will allow us to study the effect on the process of some features such as diffusion limitations (e.g. use of microporous and mesoporous ordered materials), metal precursor (in particular the presence of chlorine) or reduction temperature. The use of several supports, in particular partially reducible ones such as zinc oxides, will also allow us to explore the effect of the so-called strong metal-support interaction (SMSI) on the catalytic performance.

5.2..Experimental

5.2.1.Catalyst synthesis

The synthesis of the catalysts was performed by three different methods: microemulsion (ME), impregnation (im) and deposition-precipitation (dp). Further details are given in chapters 2 and 4.

5.2.2.Characterization

Elemental analysis of metal-containing samples was performed by the staff at the Central Service for Research Support (SCAI) of the University of Córdoba. It was performed using inductively coupled plasma mass spectrometry (ICP-MS). Measurements were made on a Perkin-Elmer ELAN DRC-e instrument following dissolution of the sample in a 1:3 HNO_3/HCl mixture with a soft heating. Calibration was done by using PE Pure Plus atomic spectroscopy standards, also from Perkin-Elmer.

Thermogravimetric analyses (TGA–DTA) were performed on a Setaram SetSys 12 instrument. An amount of 20 mg of sample was placed in an alumina crucible and heated at temperatures from 30 to 1000ºC at a rate of 10ºC/min under a stream of synthetic air at 40 mL/min in order to measure weight loss, heat flow and derivative weight loss.

EDX measurements were performed on a JEOL JSM-6300 scanning electron microscope (SEM) equipped with an energy-dispersive X-ray (EDX) detector. It was operated at an acceleration voltage of 20keV with a resolution of 65eV.

Surface areas of the solids were determined from nitrogen adsorption–desorption isotherms obtained at liquid nitrogen temperature on a Micromeritics ASAP-2010 instrument, using the Brunnauer–Emmett–Teller (BET) method. All samples were degassed to 0.1 Pa at 120ºC prior to measurement.

Transmission electron microscopy (TEM) images were obtained using a JEOL JEM 1400 microscope. All samples were mounted on 3 mm holey carbon copper grids.

X-ray patterns of the samples were obtained on a Siemens D-5000 diffractometer equipped with a DACO-MP automatic control and data acquisition system. The instrument was equipped with a graphite monochromator and used Cu Kα radiation. Metal particle sizes were calculated using Scherrer equation.

X-ray photoelectron spectroscopy (XPS) data were recorded on 4 mm × 4 mm pellets 0.5 mm thick that were obtained by gently pressing the powdered materials following outgassing to a pressure below about 2×10^{-8} Torr at 150ºC in the instrument pre-chamber to remove chemisorbed volatile species. The main chamber of the Leibold–Heraeus LHS10 spectrometer used, capable of operating down to less than 2×10^{-9} Torr, was equipped with an EA-200MCD hemispherical electron analyser with a dual X-ray source using AlKα (hv = 1486.6 eV) at 120 W, at 30 mA, with C(1s) as energy reference (284.6 eV).

Temperature-programmed reduction (TPR) measurements were made with a Micromeritics TPD-TPR 2920 analyser. An amount of 100 mg of catalyst was placed in the sample holder and reduced in a 10:90 H_2/Ar stream flowing at 20 mL min^{-1}. The temperature was ramped from 50 to 350ºC.

5.2.3. Catalytic test

The solids were tested for hydrogenation of crotonaldehyde. The system used was a stainless steel (1/8´´) gas phase flow system of Micrometric equipped with a mass flow controller for N_2 and H_2. The effluent flow was analyzed on line connecting the system to a HP 5890 series II gas chromatograph equipped with a capillary column (Supel Cowax 10 of 60mX0.25mm with a 0.25μm film). The reactions were performed loading the reactor with 50mg of catalyst and 2 grams of

inert SiO_2. The catalysts were reduced *in situ*. First, the system was purged with N_2 flow (20mL/min) during 5 minutes at room temperature. Then, a flow of 20 mL/min of H_2 was passed through the reactor and the temperature risen up to the selected reduction temperature (100ºC, 200ºC or 400ºC). The temperature was kept during 1 hour and then it was cooled down until the reaction temperature (100º or 150ºC). While catalyst was reduced, the crotonaldehyde gas phase flow was stabilized passing a flow of 20 ml/min of H_2 through a bottle with the reagent at 0ºC.

Figure 5.1. *Picture of the gas flow reactor system used for hydrogenation of crotonaldehyde.*

5.3. Results and discussion

5.3.1. Catalysts characterization.

The synthesis and characterization of the solids have been described elsewhere (Chapter 2 and 4) and the main features are summarized in Tables 5.1-5.3.

Table 5.1. *Some features concerning characterization of Pt-based solids using porous-ordered materials as the supports (further details are given in chapter 4).*

	% wt Pt			Average Pt particle size (nm)	Surface (m^2/g)
	Nominal	(ICP-MS)	(EDAX)	(TEM)	(Isotherm)
MCM41		-		-	993
MCM41 $Pt(acac)_2$ 10°C/min	5	5.2	4.6	6.7	815
MCM41 H_2PtCl_6 10°C/min	5	4.4	4.4	4.7	610
MCM41 H_2PtCl_6 1°C/min	5	4.8	4.6	3.9	857
USY780		-		-	782
USY780 $Pt(acac)_2$ 10°C/min	5	4.2	4.5	3.6	716
USY780 H_2PtCl_6 10°C/min	5	4.8	3.9	6.9	645
USY780 H_2PtCl_6 1°C/min	5	5.4	4.2	3.1	589
USY300		-		-	754
USY300 $Pt(acac)_2$ 10°C/min	5	3.9	3.7	6.3	561
USY300 H_2PtCl_6 10°C/min	5	4.2	4.2	8.3	607
USY300 H_2PtCl_6 1°C/min	5	4.4	4.8	2.3	444

***Table 5.2**. Some features concerning characterization of Pt-based solids using ZnO as the support (I). Further details are given in chapter 2, paper I.*

Catalyst*	Metal/ZnO weight %				BET surface	Mean particle size (nm)	
	Nominal	ICP-MS	EDAX	XPS	(m^2/g)	TEM	XRD
Pt-ME-ZnO-B			0.8	0.8	16	2.2	NS
Pt-ME-ZnO-B calc300	5	1.2	0.6	0.6	16	-	-
Pt-ME-ZnO-B calc500			-	0.7	16	-	-
Pt-dp-ZnO red200	5	5.2	-	5.3	19	3.1	NS
Pd-ME-ZnO-B			5.3	3.6	16	3.0	NS
Pd-ME-ZnO-B calc 300	5	4.4	4.8	3.4	16	-	7.4
Pd-ME-ZnO-B calc 500			5.7	3.4	16	-	14.2
Pd-dp-ZnO red200	5	4.1	-	0.9	17	-	15.0
Rh-ME-ZnO-B	5	0.3	0.6	0.4	16	2.1	NS
Rh-ME-ZnO-B calc 300			0.4	0.4	16	-	-
Rh-ME-ZnO-B calc 500			-	0.3	16	-	-
Rh-dp-ZnO red200	5	2.4	-	3.2	25	3.7	-

**For simplification, in Fig. 5.4. , the catalysts synthesized by microemulsion do not include the suffix B.*

Table 5.3. *Some features concerning characterization of Pt-based solids using ZnO as the support (II). Further details are given in chapter 2, paper II.*

Catalyst	Pt weight %		Average Pt particle size (TEM, nm)		Surface (m^2/g)
	ICP-MS	EDX	200	400	(Isotherm)
Pt-Cl-dp-com	4.2	2.7	1.9	3.6	15
Pt-Cl-dp-ME	4.7	3.0	1.8	3.0	29
Pt-Cl-dp-ME-Al	4.5	3.9	1.7	3.3	27
Pt-Cl-dp-ME-Ce	6.1	4.0	1.3	2.2	31
Pt-Cl-dp_ME-Zr	4.8	5.5	1.5	3.2	36
Pt-Cl-im-com	4.5	2.9	2.0	3.3	15
Pt-N-dp-com	4.3	6.0	2.8	4.2	15

5.3.2. Experiments using porous-ordered materials (MCM-41 and USY zeolites) as the supports.

The typical reaction profile for the catalysts is represented in Figure 5.2 whereas results for all systems are represented in Table 5.4. In all cases there is an initial deactivation period followed by the stabilization for reaction time of 150-200 min (see Fig. 5.2). Catalysts reduced at 200ºC were those exhibiting the lowest activity what could be ascribed to the fact that such reduction temperature is not enough as to have all Pt as Pt^0 (see Figure 4.4). The most active systems were those reduced at 300ºC whereas subsequent reduction at 400ºC was detrimental to activity. XRD (Figure 5.3) did not show any shift in Pt^0 signal with reduction temperature which would have been indicative of metal-support interaction.

Apart from the expected products considering the reaction pathways in scheme 5.1, propene was also detected. Formation of propene involves a secondary non desired reaction in which the four carbon chain of the molecule is broken to give two compounds: propene plus CO. The mechanistic route to decarbonylation of crotonaldehyde over acid centers giving CO and propene have been reported elsewhere [14]. The initial deactivation could be partly ascribed to this process, in which CO is produced and subsequently irreversible absorbed onto Pt.

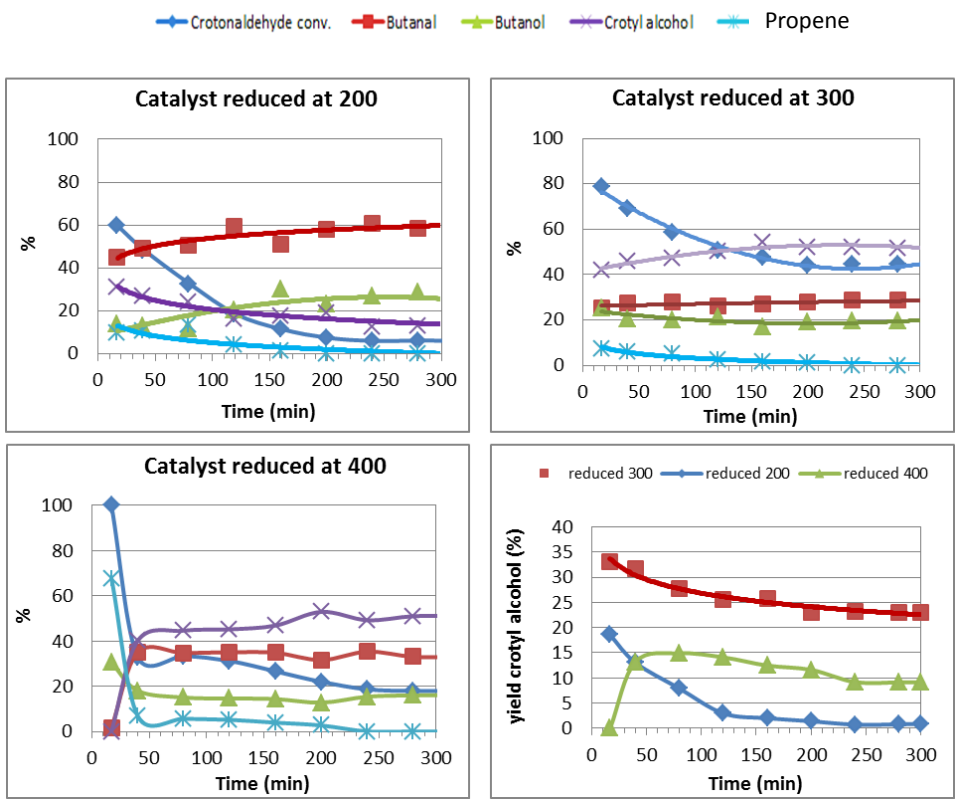

Figure 5.2. *Typical reaction profile for hydrogenation of crotonaldehyde on MCM41 H_2PtCl_6 1°C/min under standard conditions.*

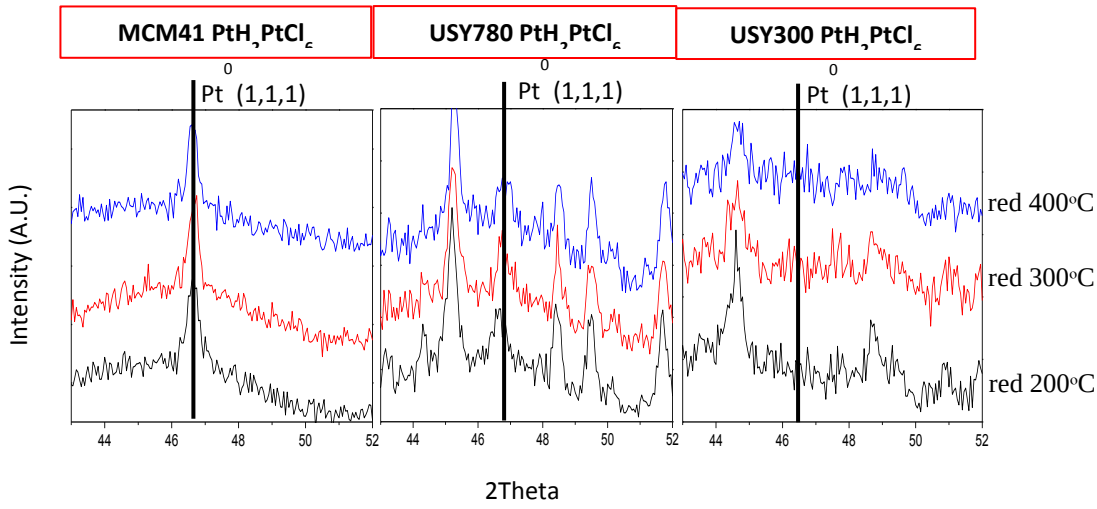

***Figure 5.3**. Detail of X-Ray diffractogram of several solids.*

***Table 5.4**. Conversion and selectivity obtained on the different solids under standard conditions after 200 min.*

200 min	**Red Tem (ºC)**	**Crot. conv.**	**S. Butanal**	**S. Butanol**	**S. Butenol**	**S. Propene**	**BET surface (m^2/g)**
MCM41	200	6.4	84.2	0.0	15.8	0.0	-
$Pt(acac)_2$	300	31.6	63.6	17.7	17.2	1.5	-
10ºC/min	400	22.7	83.5	4.2	12.3	0.0	-
MCM41	200	5.9	64.0	23.5	12.5	0.0	-
H_2PtCl_6	300	47.3	39.5	15.3	45.1	0.0	-
10ºC/min	400	16.4	51.8	13.1	35.1	0.0	-
MCM41	200	7.5	57.8	23.2	19.0	0.0	830
H_2PtCl_6	300	44.2	27.7	19.0	51.9	1.3	692
1ºC/min	400	22.0	31.6	12.8	52.9	2.7	839

200 min	Red Tem (°C)	Crot. conv.	S. Butanal	S. Butanol	S. Butenol	S. Propene	BET surface (m^2/g)
USY780	200	0.0	0.0	0.0	0.0	0.0	-
$Pt(acac)_2$	300	41.9	60.4	13.9	25.8	0.0	-
10°C/min	400	27.6	65.9	8.3	25.8	0.0	-
USY780	200	0.0	0.0	0.0	0.0	0.0	-
H_2PtCl_6	300	35.8	37.2	21.9	40.9	0.0	-
10°C/min	400	20.2	37.6	36.6	25.8	0.0	-
USY780	200	0.0	0.0	0.0	0.0	0.0	598
H_2PtCl_6	300	41.3	32.0	30.7	35.6	1.7	556
1°C/min	400	16.3	37.3	24.6	38.1	0.0	678
USY300	200	0.0	0.0	0.0	0.0	0.0	-
$Pt(acac)_2$	300	18.6	64.0	27.0	7.8	1.2	-
10°C/min	400	19.2	63.2	26.7	10.2	0.0	-
USY300	200	0.0	0.0	0.0	0.0	0.0	-
H_2PtCl_6	300	28.4	62.4	17.0	17.9	2.7	-
10°C/min	400	19.0	54.6	32.7	12.7	0.0	-
USY300	200	0.0	0.0	0.0	0.0	0.0	393
H_2PtCl_6	300	30.1	57.6	22.4	18.8	1.3	338
1°C/min	400	15.2	66.7	13.8	19.4	0.0	421

As far as conversion is concerned, the most active systems are those using MCM-41 which could be ascribed to diffusion limitations.

As regards the selectivity to crotyl alcohol, it is higher for solids obtained using H_2PtCl_6 as the precursor as compared to the utilization of $Pt(acac)_2$. This is consistent with results reported in the literature in which favoring of adsorption of the substrate onto the catalyst though the C=O bond for Cl-containing solids has been described [15-16] .

All in all, the best selectivity to crotyl alcohol on porous ordered materials was 52% on Pt MCM41 H_2PtCl_6 1ºC/min for a conversion of ca. 44%.

5.3.3 Catalytic activity of metallic nanoparticles synthesized by ME and dp (paper I)

In chapter 2 (paper Nr 1) the synthesis and characterization of several solids consisting in Pt, Pd, Rh or Au on ZnO synthesized either through microemulsion (ME) or deposition-precipitation method (ME) was described. These solids were tested for gas-phase crotonaldehyde hydrogenation.

Unlike the use of porous-ordered materials as the supports, no propene was detected on this occasion. Figure 5.4 summarizes the activity of the systems after 200 min on stream.

In general, the solids synthesized by ME led to higher conversions of crotonaldehyde as compared to their dp-counterparts, even though the metallic incorporation was lower (Table 5.2).

Among the different metals, Au was not active under our reaction conditions whatever the preparation method. Pd nanoparticles led to 100% conversion but 100% selectivity to C=C hydrogenation (butanal). Further studies were not performed on Pd-containing solids because the target compound was the unsaturated alcohol.

The best yields to crotyl alcohols were achieved with Pt and Rh catalysts, especially after reduction of the solids at 200º and 400ºC when the major product was crotyl alcohol for solids synthesized through DP. The highest selectivity to unsaturated alcohol (82.9%) was afforded by Pt_{dp} ZnO reduced at 400ºC though conversion was very low (ca. 3%).

Comparing Pt and Rh-containing systems, in the case of solids synthesized through DP method, catalytic performance, both in terms of conversion and selectivity, is quite similar despite the different mean metal particle sizes and metal contents. In the case of ME systems, the synthetic procedure allowed us to obtain comparable metal particle sizes.

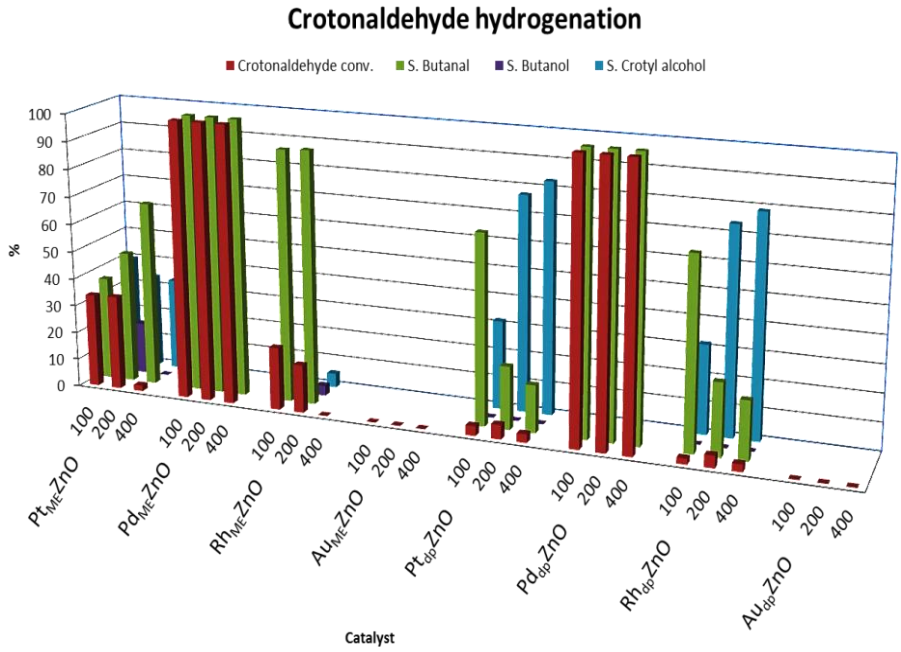

Figure 5.4. *Catalytic results after 200min of the metals over metal supported on ZnO commercial.*

Results showed that Pt systems are more selective to the unsaturated alcohol for comparative metal particle sizes. The presence of some remaining surfactant on metal particles could lead to lower selectivities to the desired alcohol as compared to DP-solids.

5.3.4 Catalytic activity of Pt synthesized by deposition-precipitation on different ZnO (paper II)

Finally, different Pt-based solids synthesized over diverse ZnO-based solids were tested. ZnO was modified with Al, Ce, and Zr. The supports were synthesized by ME technique and then Pt incorporated by deposition precipitation method (solids described in chapter 2, paper Nr 2).

The main results obtained for t=200 min are depicted in Figure 5.5. Firstly, reactions were performed at 100ºC (Figure 5.5A). Under standard reaction conditions catalytic performance is quite similar, the exception being the solid containing cerium. Reduction of the solids at 200ºC results in an increase in selectivity to crotyl alcohol which is even higher for solids reduced at 400ºC.

XPS analyses described in paper Nr 2 (see Chapter 2) evidenced that oxidation state of Ce changes with the reduction temperature. Ceria is known to exhibit SMSI and XPS results evidenced the formation of a Pt-Ce alloy. Abid et al reported that for Pt/ CeO_2 the high reduction temperatures favor the selectivity to unsaturated alcohol. They also observed that the performance of Pt supported over CeO_2 depends of the particle size, with an optimum for the selectivity to unsaturated alcohol for metal particles of 3-4 nm, which are the values observed by TEM for the Pt_{dp}ZnCe catalyst after reduction at 400ºC [16] .

Similarly, XRD analysis of all ZnO-based solids showed that the SMSI started to appear at 200ºC and eventually Pt-Zn alloy was formed at 400ºC. So the selectivity to crotyl alcohol could be somehow related to this interaction.

In fact, selectivities to crotyl alcohol for solids supported on ZnO are significantly higher than those achieved for Pt solids supported on porous-ordered

materials synthesized from the same Pt-precursor for which no SMSI was observed.

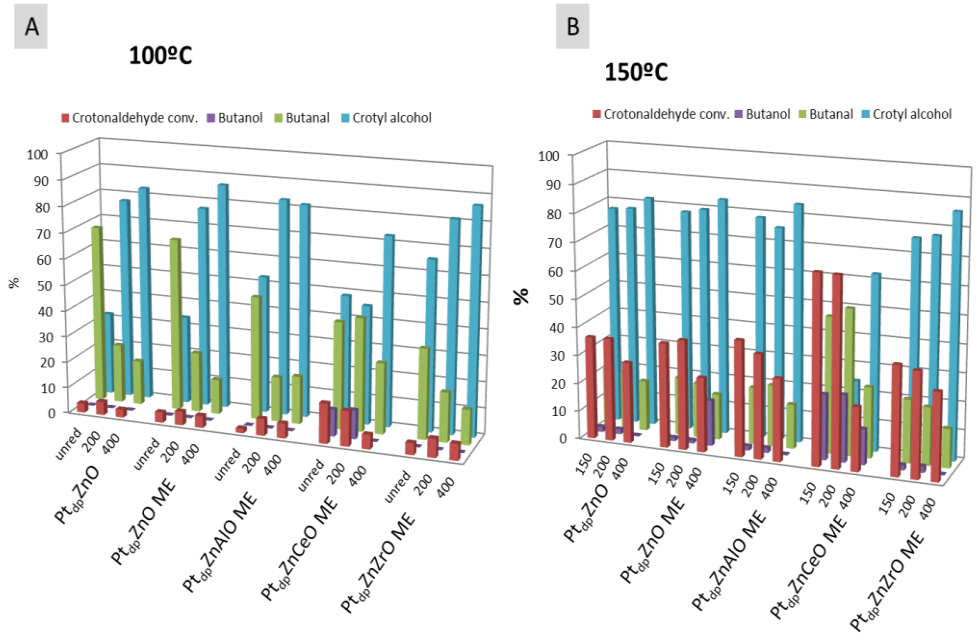

Figure 5.5. *Results obtained for gas-phase hydrogenation of crotonaldehyde.*

Given the low conversion values achieved with these solids, reaction temperature was increase from 100ºC up to 150ºC. Results are depicted in Figure 5.5B.

Again PtdpZnCeOME led to different results compared with the others. The conversion was 60% for the catalyst reduced at 150 and 200ºC and butanal was the major product with selectivities of 45% and 50% respectively. After reduction at 400ºC the catalytic behavior was more similar to the rest of catalysts

thus leading to lower conversion than lower reduction temperatures and crotyl alcohol as the major product.

Figure 5.6 shows the reaction profile of the PtdpZnO reduced at 200ºC and 400ºC at both reaction temperatures (100 and 150ºC). It allows us to show the general trend in the different systems. First, increase in reaction temperature from 100ºC to 150ºC resulted in a 4-10 fold increase in conversion whereas selectivity to crotyl alcohol remained quite high (over 75%, the exception being again PtdpZnCeO ME). The increase in selectivity is accompanied by a slight decrease in conversion.

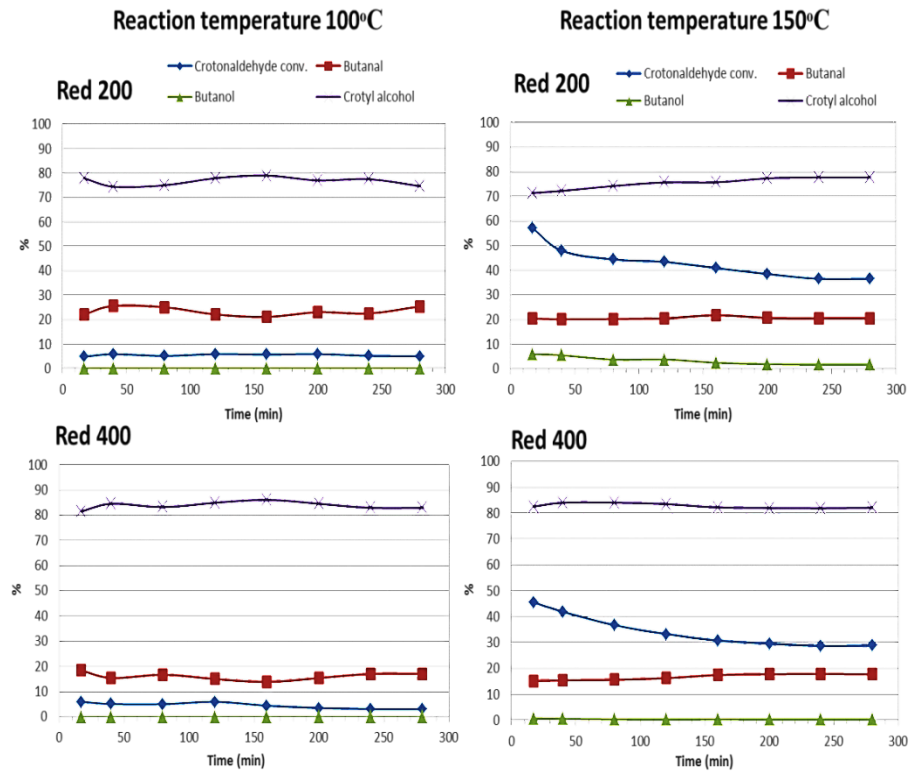

Figure 5.6. *Reaction profile obtained for gas-phase hydrogenation of crotonaldehyde on* $Pt_{dp}ZnO$.

As commented above, comparing the systems using porous-ordered materials as the supports to those utilizing ZnO-based solids, it is worth noting that the latter systems exhibit higher selectivities to crotyl alcohol. SMSI could account for that. Moreover, deactivation of the ZnO-based solids is lower than that for solids based on aluminosilicates what together with the non-observed formation of propene as a by-product could indicate that deactivation follows different mechanisms in both cases. Nevertheless, this requires further studies.

5.4. Conclusions

All the solids consisting in supported noble metals were tested for gas-phase selective hydrogenation of crotonaldehyde to crotyl alcohol. As regards the use of porous-ordered materials as the supports, higher conversions were obtained for MCM-41 as compared to USY zeolite which evidenced the existence of diffusion problems. Moreover, if Pt-precursors (H_2PtCl_6 and $Pt(acac)_2$) are compared, the former leads to higher selectivities to crotyl alcohol thus confirming that the presence of chlorine favors adsorption of crotonaldehyde through C=O. As far as ZnO solids are concerned, high selectivities to the unsaturated alcohol were achieved specially at high reduction temperatures which has been ascribed to Pt-Zn interactions.

References

[1]. S. Axpuac, M.A. Aramendia, J. Hidalgo-Carrillo, A. Marinas, J.M. Marinas, V. Montes-Jimenez, F.J. Urbano, V. Borau, Catal. Today 187 (2012) 183– 190.

[2]. J. F. Miñambres, A. Marinas, J. M. Marinas, F. J. Urbano, Appl.Catal. B: Environ.140– 141 (2013) 386– 395.

[3]. U.K. Singh, M.A. Vannice, J. Catal. 199 (2001) 73–84.

[4]. F. Ammari, C. Milone, R. Touroude, J. Catal. 235 (2005) 1–9.

[5]. J. Kaspar, M. Graziani, G.P. Escobar, A. Trovarelli, J. Mol. Catal. 72 (1992) 243–251.

[6]. R. Zheng, M.D. Porosoff, J.L. Weiner, S. Lu, Y. Zhu, J.G. Chen, Appl. Catal. A 419/420(2012) 126–132.

[7]. E.V. Ramos-Fernandez, A. Sepulveda-Escribano, F. Rodriguez-Reinoso, Catal.Commun. 9 (2008) 1243–1246.

[8]. Z.G. Szabó, F. Solymosi in "Proceedings, 2nd International Congress on Catalysis", p. 1627, Technip, Paris, 1961.

[9]. S.J. Tauster, S.C. Fung, R.L. Garten, J. Am. Chem. Soc. 100 (1978) 170–175.

[10]. J. Hidalgo-Carrillo, M.A. Aramendia, A. Marinas, J.M. Marinas, F.J. Urbano, Appl.Catal. A 385 (2010) 190–200.

[11]. J.C. Serrano-Ruiz, J. Luettich, A. Sepulveda-Escribano, F. Rodriguez-Reinoso, J.Catal. 241 (2006) 45–55.

[12]. M. Abid, V. Paul-Boncour, R. Touroude, Appl. Catal. A 297 (2006) 48–59.

[13]. A.M. Ruppert, T. Paryjczak, Appl. Catal. A 320 (2007) 80–90.

[14]. M.E. Grass, R.M. Rioux, G.A. Somorjai, Catal. Lett. 128 (2009) 1-8.

[15]. F. Ammari, J. Lamotte, R. Touroude, J. Catal. 221 (2004) 32-42.

[16]. M. Abid, G. Ehret, R. Touroude, Appl. Catal. A: Gen. 217 (2001) 219-229.

Conclusiones generales/

General conclusions

Conclusiones

El objetivo general de la Tesis era sintetizar y caracterizar diversos sólidos mediante diferentes métodos y estudiar su comportamiento catalítico en diversos procesos de hidrogenación de interés industrial.

Para ello se sintetizaron diversos catalizadores heterogéneos consistentes en nanopartículas metálicas soportadas buscando establecer relaciones estructura-actividad.

Los catalizadores fueron sintetizados empleando diferentes métodos tales como deposición-precipitación, impregnación y microemulsión. El precursor metálico escogido, el soporte o el método sintético fueron determinantes en aspectos tales como el tamaño final de partícula o la existencia de interacción metal-soporte y, en definitiva, en el comportamiento catalítico. Cada proceso de hidrogenación estudiado mostró unos requerimientos propios, lo que indica la necesidad de llevar a cabo una síntesis del catalizador "a medida" en cada caso, con el fin de optimizar los resultados.

Seguidamente se detallan los resultados encontrados en cada uno de los capítulos (a excepción del primero dedicado a la introducción) organizados en función de cada artículo publicado.

Capítulo 2 – Hidrogenolisis del glicerol sobre diversos sistemas metálicos soportados sobre ZnO

Artículo 1 – *Síntesis de diferentes sistemas metálicos soportados sobre ZnO mediante la técnica de microemulsión y su aplicación como catalizadores a la transformación catalizada del glicerol en acetol y 1,2-propanodiol*

La técnica de microemulsión (ME) es un método adecuado para controlar el tamaño de la partícula metálica, si bien requiere la optimización de diversos

parámetros. El método nos permitió sintetizar sistemas de Pt, Pd y Rh con tamaños de partícula similares (2-4 nm, serie B).

Cuando se empleó $NaBH_4$ como agente reductor, se obtuvieron tamaños de partícula más pequeños que al utilizar hidracina, lo que explica el mejor comportamiento catalítico de los sistemas de la serie B en la transformación de glicerol en acetol y 1,2-PDO.

Los sistemas obtenidos mediante la técnica de microemulsión contenían partículas en estado metálico, si bien su tratamiento a temperaturas en el intervalo 200-300ºC condujo a una mejora en la actividad catalítica.

A medida que se eleva la temperatura de tratamiento de los sistemas se producen dos efectos contrarios. Por un lado, se va eliminando paulatinamente el surfactante, lo que es positivo para la actividad. Por otro, la progresiva eliminación del surfactante favorece la sinterización de las partículas metálicas y a 400ºC se forma una aleación Pt-Zn, lo que va en detrimento de la actividad. Así, parece que a temperaturas de 200-300ºC se produce un compromiso entre ambas tendencias opuestas.

El orden de reactividad siguió la secuencia Rh > Pt > Pd y los sistemas sintetizados mediante microemulsión (ME) fueron comparativamente más selectivos a acetol que los obtenidos mediante deposición-precipitación (DP). Esto puede deberse a la presencia de restos de surfactante rodeando a las partículas metálicas, lo que podría limitar su actividad hidrogenante. Además, el metal parece participar tanto en el proceso de deshidratación del glicerol a acetol como en la posterior hidrogenación de éste a 1,2-PDO.

Artículo 2- *Transformación selectiva del glicerol a 1,2-PDO sobre diversos sistemas Pt/ZnO: estudio del papel y origen de la acidez del catalizador*

Se sintetizaron diversos sólidos basados en ZnO (bien solo o dopado con Al, Zr ó Ce) mediante la técnica de microemulsión, lo que nos permitió obtener tamaños de partícula y propiedades texturales similares. Posteriormente, se incorporó platino empleando H_2PtCl_6 como precursor metálico, mediante los métodos de deposición-precipitación o microemulsión. A efectos comparativos, también se obtuvo un sistema incorporando $Pt(NO_3)_4$ mediante el método de deposición-precipitación.

La incorporación de platino condujo a la creación de nuevos centros ácidos (fundamentalmente de tipo Lewis), especialmente cuando se empleó el precursor clorado. Además, la acidez se pierde parcialmente durante el tratamiento reductor del catalizador o a medida que avanza la reacción, lo que puede atribuirse a la pérdida de cloro y a la decoración de las partículas de platino por el soporte (evidenciado mediante XPS).

Se encontró una relación directa entre la acidez del catalizador y la conversión del glicerol. Resulta interesante comprobar que los soportes no fueron activos en el proceso, lo que prueba la participación del metal en la deshidratación del glicerol a acetol. En lo que se refiere a la selectividad a 1,2-PDO, aumenta a medida que avanza la reacción y disminuye la acidez de los sólidos, en detrimento del craqueo catalítico. Esto sugiere que los centros ácidos fuertes asociados al cloro son los responsables de la ruptura C-C e hidrogenolisis excesiva, mientras que la deshidratación del glicerol a acetol requiere una acidez moderada. Además, la aparición de una interacción fuerte Pt-Zn es beneficiosa para la selectividad a 1,2-PDO.

Capítulo 3- Síntesis de Fischer-Tropsch

Artículo 3- *Preparación y caracterización de catalizadores basados en cobalto modificado con Pt mediante la técnica de microemulsión: estudios preliminares en la síntesis de Fischer-Tropsch*

Se sintetizaron diversos catalizadores de cobalto modificado con platino soportados sobre TiO_2 con unos contenidos de 0–0,25% en peso en Pt y 12% en peso de Co, mediante el método de microemulsión. Además, se utilizó Berol 02 y Synperonic 13/6.5 como surfactantes. Se ensayaron dos métodos de incorporación diferentes consistentes en la reducción simultánea (ME1) o consecutiva (ME2) de cobalto y platino con borohidruro sódico.

Un primer *screening* (o rastreo) de catalizadores para la síntesis de *Fischer-Tropsch* nos llevó a seleccionar la serie S-TiO_2 (TiO_2 como soporte y Synperonic 13/6.5 como surfactante) para llevar a cabo estudios de caracterización en profundidad. En todos los casos, la técnica ME condujo a tamaños de partícula de cobalto comparables (tamaño medio determinado por TEM de 3,8-4,7 nm para los catalizadores calcinados a 300ºC).

Además, los sólidos ME1 condujeron a mayores conversiones que sus homólogos de la serie ME2. Esto puede deberse a la mayor interacción Pt-Co y Co-soporte en la serie ME1 (evidenciada mediante el perfil TPR). Los espectros Raman mostraron la presencia de Co_3O_4 y CoO en todos los sólidos, si bien la proporción de CoO es mayor en la serie ME1. Estos resultados fueron confirmados mediante XPS, lo que unido al aumento de la señal de O1s a alrededor de 531,2 eV con el tratamiento de reducción, más importante en el caso de los sistemas ME1 que los ME2, apoya la existencia de una mayor interacción Co-soporte en los primeros.

En resumen, los resultados mostraron que la presencia de especies reducidas de cobalto (Co^0) e interacciones Co-TiO_2 fueron las responsables del diferente comportamiento catalítico observado en los sistemas.

Capítulo 4- Hidrogenación enantioselectiva del piruvato de etilo a lactato de etilo sobre diversos sistemas basados en platino modificado con alcaloides de la familia de la cinchona

Se sintetizaron diversos sistemas de Pt soportado sobre varios materiales de poro controlado (MCM-41 y zeolita USY) y se probaron en la hidrogenación enantioselectiva del piruvato al lactato de etilo empleando alcaloides de la familia de la cinchona como modificadores quirales. Los mejores resultados en términos de conversión y exceso enantiomérico (e.e.) se lograron con los sólidos que mostraron la mayor fracción de partículas de Pt en el intervalo 3-5 nm.

De los tres disolvente ensayados (isopropanol, tolueno y ácido acético), el acético fue el que condujo a mayores excesos enantioméricos.

Se probaron diversas moléculas quirales comerciales como aditivos, con el fin de favorecer el exceso enantiomérico, siendo la 4-hidroxi-(D)-(-)-fenilglicina (OHDF) la que mostró un efecto más positivo (incremento del e.e.) a contenidos bajos en cinchonidina (CD). El hecho de que la adición de dicha molécula conduzca a un aumento en el e.e. tanto a R-lactato como a S-lactato (según esté en presencia de cinchonidina o cinchonina, respectivamente) prueba que el efecto sinérgico está asociado a algún tipo de mejora en la adsorción más que a la enantiodiferenciación propiamente dicha. De hecho, mediante estudios de espectroscopia UV-Vis se demostró que la OHDF era el único aditivo que presentaba algún tipo de interacción sustrato-modificador-aditivo en fase líquida.

Un estudio multivariante realizado empleando uno de los catalizadores (USY780-H_2PtCl_6-10ºC/min) y variando la presión de hidrógeno y las cantidades

de CD y OHDF, nos permitió obtener un e.e. del 79% a conversión total y confirmó el efecto positivo de la OHDF anteriormente comentado.

Capítulo 5- Hidrogenación quimioselectiva del crotonaldehido a alcohol crotílico sobre diversos catalizadores basados en Pt

Todos los sistemas consistentes en metales nobles soportados descritos en la presente Memoria fueron ensayados en la hidrogenación selectiva de crotonaldehido a alcohol crotílico en fase gas. En lo que respecta al uso de soportes de tamaño de poro controlado (USY y MCM-41) los sistemas basados en MCM-41 condujeron a mayores conversiones que los que emplearon la zeolita USY, lo que evidencia la existencia de problemas de difusión.

Además, si se comparan los precursores metálicos (H_2PtCl_6 y $Pt(acac)_2$), los primeros conducen a mayores selectividades hacia el alcohol crotílico, lo que confirma que la presencia de cloro favorece la adsorción del crotonaldehido a través del enlace C=O.

En cuanto a los sistemas soportados sobre ZnO, se obtuvieron altas selectividades al alcohol insaturado, en especial a altas temperaturas de reducción del catalizador, lo que se atribuye a la existencia de interacciones Pt-Zn.

Conclusions

The general goal of the PhD was to synthesize and characterize various solids by several methods and to study their catalytic activity in diverse industrially-relevant hydrogenation processes.

To this end it was decided to synthesize several heterogeneous catalysts consisting of supported metal nanoparticles and try to establish some structure-performance relationships.

The catalysts were synthesized by various methods such as deposition-precipitation, impregnation and microemulsion. Metal precursor, support and synthetic method of choice played a crucial role in several features such as the final particle size or metal-support interaction and thus on catalytic performance. Each hydrogenation reaction showed some specific catalytic needs, necessitating the custom design of the catalyst for optimizing the results.

Below are detailed the findings from each chapter (chapter one devoted to introduction excluded) and published article.

Chapter 2 – Glycerol hydrogenolysis on different ZnO-supported metal systems

Paper I - *Synthesis of different ZnO-supported metal systems through microemulsion technique and application to catalytic transformation of glycerol to acetol and 1,2-propanediol*

Microemulsion (ME) technique is an adequate method to control metal particle size though it requires optimization of several parameters. The method allowed us to synthesize Pt, Pd and Rh systems with similar metal particle sizes (2–4 nm, B-series).

$NaBH_4$ used as reducing agent gave smaller particle sizes than hydrazine thus accounting for the better catalytic performance in glycerol transformation to acetol and 1,2-PDO of B-series. Systems obtained through ME technique contained particles in the metal state though thermal treatment to temperatures in the 200–300ºC range led to an improvement of catalytic performance. As temperature rises there are two opposite effects. On the one hand, surfactant is removed which is positive to activity. On the other, progressive loss of surfactant favors sintering of metal particles and at 400ºC a metal-Zn alloy is formed both being detrimental to activity. In this sense, a compromise between both trends seems to be reached at temperatures of 200–300ºC.

Reactivity order followed the sequence Rh > Pt > Pd and ME systems were found to be comparatively more selective to acetol than DP solids. This could be due to some remaining surfactant in the surroundings of metallic particles thus limiting their hydrogenation activity. Moreover, metal seems to participate both in dehydration of glycerol to acetol and the subsequent reduction to 1,2-PDO.

Paper II- *Selective transformation of glycerol into 1,2-propanediol on several Pt/ZnO solids: Further insight into the role and origin of catalyst acidity*

Different ZnO solids (either alone or doped with Al, Zr or Ce) were synthesized through the microemulsion technique which allowed us to obtain similar particle sizes and textural properties. Platinum was subsequently incorporated from H_2PtCl_6 through deposition–precipitation or impregnation method. For comparative purposes, a system from $Pt(NO_3)_4$ was also obtained through deposition–precipitation method.

Incorporation of platinum led to the creation of new (mainly Lewis) acid sites, particularly important in the case of chlorine-containing solids. Moreover, acidity is partly lost during reduction treatment or as the reaction proceeds which

could be ascribed to both chlorine release and platinum decoration by the support (as evidenced by XPS).

A direct relationship between acidity and glycerol conversion was found. Interestingly, supports were not active in the process which evidences the participation of the metal in the dehydration of glycerol to acetol. As regards selectivity to 1,2-PDO, it increases as reaction proceeds and acidity of solids decreases to the detriment of acidic cracking. This suggests that strong acid sites associated to chlorine are responsible for C-C cleavage and excessive hydrogenolysis, whereas dehydration of glycerol into acetol requires moderate acidity. Moreover, formation of Pt–Zn strong metal interaction is beneficial to 1,2-PDO selectivity.

Chapter 3- Fischer–Tropsch synthesis

Paper III- *Preparation and characterization of Pt-modified Co-based catalysts through the microemulsion technique: Preliminary results on the Fischer–Tropsch synthesis*

Several Pt-modified cobalt catalysts containing 0–0.25 wt% platinum and 12 wt% cobalt were synthesized through microemulsion technique (ME) using TiO_2 as the support. Moreover, Berol 02 and Synperonic 13/6.5 were used as surfactants. Two incorporation methods involving simultaneous (ME1) or consecutive (ME2) reduction of cobalt and platinum with sodium borohydride were essayed. A first screening of catalysts for Fischer–Tropsch synthesis led us to select S-TiO_2 series (TiO_2 as the support and Synperonic 13/6.5 as the surfactant) for subsequent characterization studies. In all cases ME technique led to quite comparable cobalt particle sizes (averaging in the range 3.8–4.7 nm for catalysts calcined at 300 ◦C as determined by TEM).

Moreover, ME1 solids led to higher conversions than their ME2 counterparts. The higher Pt–Co and Co–support interaction in the former case (as evidenced by TPR profile) could account for that. Raman spectra evidenced the presence of Co_3O_4 and CoO in all solids though CoO proportion is higher in ME1 as compared to ME2. There results were confirmed by XPS which together with the increase in the O1s XPS signal at ca. 531.2 eV with the reduction treatment, more significant for ME1 as compared to ME2 solids, is supportive of the existence of a greater Co–support interaction in the former systems. All in all, results showed that both the presence of reduced cobalt species (Co^0) and Co–TiO_2 interactions were responsible for the different behavior of the systems.

Chapter 4- Enantioselective hydrogenation of ethyl pyruvate to ethyl lactate on several Pt-based systems modified with cinchona alkaloids

Different systems consisting in Pt supported on several porous-ordered materials (MCM-41 and USY zeolite) were synthesized and tested for enantioselective hydrogenation of ethyl pyruvate to ethyl lactate using cinchona-alkaloids as the chiral modifiers. The best results in terms of conversion and enantiomeric excess (e.e.) corresponded to the solids exhibiting the highest fraction of Pt particles in the 3-5 nm range.

Three different solvents were used (isopropanol, toluene and acetic acid), acetic acid affording the highest e.e. values.

Several commercial chiral molecules were tested as additives in order to favor e.e., 4-hydroxy-D-(-)-phenylglycine (OHDF) exhibiting a positive effect for low cinchonidine (CD) contents thus increasing e.e. The fact that the additive increases both e.e. to R or S-lactate depending on the presence of cinchonidine or cinchonine, respectively, evidenced that its synergistic effect must be somehow associated to an enhancement in adsorption and not in enantiodifferentiation. In

fact, UV-Vis studies evidenced that this additive was the only one showing some kind of substrate-modifier-additive interaction in the liquid phase.

A multivariable study on one of the catalysts (USY780-H_2PtCl_6-10ºC/min) varying the hydrogen pressure, amount of CD and OHDF, allowed us to obtain 79% e.e. at total conversion and confirmed the above-mentioned positive effect of OHDF on enantioselectivity.

Chapter 5- Chemoselective hydrogenation of crotonaldehyde to crotyl alcohol on several Pt-based catalysts

All the solids consisting in supported noble metals were tested for gas-phase selective hydrogenation of crotonaldehyde to crotyl alcohol. As regards the use of porous-ordered materials as the supports, higher conversions were obtained for MCM-41 as compared to USY zeolite which evidenced the existence of some diffusion problems.

Moreover, if Pt-precursors (H_2PtCl_6 and $Pt(acac)_2$) are compared, the former leads to higher selectivities to crotyl alcohol thus confirming that the presence of chlorine favors adsorption of crotonaldehyde through C=O.

As far as ZnO solids are concerned, high selectivities to the unsaturated alcohol were achieved specially at high reduction temperatures which have been ascribed to Pt-Zn interactions.

Resumen /Summary

Resumen de la tesis de D. Vicente Montes Jiménez

1. Introducción o motivación de la Tesis

La importancia de la Catálisis queda reflejada en el hecho de que más del 90% de los procesos químicos industriales presenta algún paso catalizado. En la presente Tesis Doctoral se planteó la síntesis y caracterización de diversos sólidos mediante distintos procedimientos así como el estudio de su actividad catalítica en procesos de interés industrial mediados por H_2, tales como la hidrogenolisis del glicerol, la síntesis tipo *Fischer-Tropsch* (FT), la reducción enantioselectiva del grupo carbonilo o la reducción quimioselectiva del grupo C=O frente al C=C. De modo genérico se buscaba arrojar más luz acerca de determinadas variables influyentes en estos tipos de procesos, con vistas a aumentar la conversión y selectividad hacia el producto deseado.

La hidrogenolisis del glicerol busca la valorización de dicho subproducto procedente de la bio-refinería. La catálisis heterogénea es una alternativa viable, usando diferentes metales nobles soportados. No obstante, existe cierta controversia en cuanto al orden de actividad de los metales en la reacción, así como la influencia del tamaño de la partícula metálica [1-2].

La síntesis tipo *Fischer-Tropsch* (FT) es un proceso implicado en la obtención de combustible desde fuentes alternativas al petróleo y persigue la síntesis de hidrocarburos de cadena larga a partir de una mezcla gaseosa de H_2/CO (gas de síntesis). Un tema de debate en este campo es el método de actuación del metal noble incorporado a los principales catalizadores, Co y Fe. Existe una discusión sobre si el metal noble actúa sólo mejorando la temperatura de reducción del metal o juega otro papel [3].

En lo que se refiere a las reacciones quirales, dentro de ellas sobresalen las hidrogenaciones enantioselectivas mediante inducción quiral [4-6]. Ésta se realiza

mediante adsorción en la fase metálica (a base de un metal noble, como platino) de un compuesto quiral. Aún existen aspectos que resolver, como por ejemplo la necesidad de un grupo amino en el modificador quiral [4] o el efecto del uso de aditivos o el soporte [7].

En lo que respecta a la reducción quimioselectiva del grupo C=O frente al C=C, en la bibliografía aparecen continuamente nuevos catalizadores, más activos, selectivos y menos contaminantes, formados por metales depositados sobre soportes [8-10]. No obstante, aún existen aspectos por resolver como el papel específico del soporte, su interacción con el metal o la importancia de la dispersión metálica.

2. Contenido de la investigación

De este modo, en la presente Tesis Doctoral, en una visión global de la catálisis, se aborda la secuencia síntesis-caracterización-actividad catalítica tratando de establecer relaciones estructura-actividad. Los catalizadores sintetizados están constituidos por nanopartículas metálicas soportadas.

Se presta especial atención al control de variables de síntesis como el método empleado (microemulsión, deposición-precipitación o impregnación) o el precursor metálico (con o sin cloro). Entre los soportes empleados se encuentran óxidos parcialmente reducibles (como el ZnO o el TiO_2), con el fin de estudiar el efecto en la actividad catalítica de las interacciones metal-soporte, o sistemas de tamaño de poro controlado (zeolitas tipo USY y material mesoporoso MCM-41) con el fin de favorecer la adsorción debido a su elevada superficie específica y estudiar los posibles problemas difusionales (al pasar de mesoporos a microporos). Mención aparte merece la optimización de diversas variables en el método de microemulsión, con vistas a conseguir sintetizar nanopartículas metálicas soportadas de Pt, Pd o Rh con tamaño semejante o el ensayo de diversas moléculas

quirales comerciales con el fin de explorar el efecto de su adición al medio de reacción en la hidrogenación enantioselectiva del piruvato a lactato de etilo sobre sistemas de Pt soportado modificado con alcaloides de la familia de las cinchonas.

3. Conclusiones

Cada proceso de hidrogenación estudiado mostró unos requerimientos propios, lo que indica la necesidad de llevar a cabo una síntesis del catalizador "a medida" en cada caso, con el fin de optimizar los resultados. Seguidamente se incluyen algunas de las conclusiones extraídas para cada proceso ensayado.

En el caso de la *hidrogenolisis del glicerol* sobre sistemas metálicos (Pt, Pd, Rh) soportados sobre ZnO, se logró mediante el método de microemulsión obtener un tamaño de partícula metálica similar (2-4 nm).

Si bien las partículas metálicas sintetizadas se encuentran en estado de oxidación cero, su mayor actividad se produce tras su tratamiento a temperaturas de 200-300ºC. Esto parece deberse a la presencia de restos de surfactante, favoreciendo el tratamiento térmico su pérdida y con ello, el acceso del sustrato a la partícula metálica.

Asimismo, la presencia de surfactante favorece la selectividad hacia acetol, al limitar, de algún modo, la actividad hidrogenante del metal.

Estudios posteriores centrados en sistemas de Pt/ZnO mostraron que el metal interviene no sólo en el paso de acetol a 1,2-PDO sino también en la deshidratación previa del glicerol a acetol. Además, la reacción requiere una acidez moderada ya que una acidez elevada favorece procesos secundarios como el craqueo catalítico, lo que va en detrimento de la selectividad a 1,2-PDO.

Para el proceso *Fischer-Tropsch*, se consiguió mediante microemulsión obtener sistemas de Co soportado sobre TiO_2 modificado con Pt, con tamaño de partícula de cobalto en el intervalo 3,8-4,7 nm.

La reducción simultánea de Co y Pt condujo a mayores conversiones que la consecutiva. Esto se atribuyó a una posible mayor interacción Pt-Co y Co-soporte en el primer caso, evidenciada por TPR, Raman y XPS.

En lo que respecta a la *reducción enantioselectiva de piruvato a lactato de etilo*, empleando sistemas de Pt/USY y Pt/MCM-41 se encontró que el tamaño de partícula de platino óptimo está en el intervalo 3-5 nm.

Ensayando diferentes compuestos quirales comerciales como aditivos, se consiguió al adicionar 4-hidroxi-D-(-)-fenilglicina (OHDF) un aumento del exceso enantiomérico a R o S-lactato de etilo (según se emplease cinchonidina o cinchonina como modificador quiral del platino) a bajas concentraciones del modificador quiral. Estudios mediante UV-Vis evidenciaron la existencia de algún tipo de interacción sustrato-modificador-aditivo en disolución.

Un estudio multivariante realizado empleando uno de los catalizadores (USY780-H_2PtCl_6-10ºC/min) y variando la presión de hidrógeno y las cantidades de CD y OHDF, nos permitió obtener un e.e. del 79% a conversión total y confirmó el efecto positivo de la OHDF anteriormente comentado.

Finalmente, el estudio de la reacción de *hidrogenación quimioselectiva del crotonaldehido a alcohol crotílico en fase gaseosa* puso de manifiesto la existencia de problemas de difusión al emplear como soporte materiales microporosos (zeolita USY).

La existencia de cloro residual proveniente del precursor metálico clorado favorece la selectividad hacia el alcohol insaturado.

Los sistemas que emplearon ZnO como soporte presentaron una mayor selectividad hacia el alcohol crotílico a altas temperaturas de reducción, lo que parece sugerir que la interacción fuerte Pt-Zn es favorable para la reacción.

4. Bibliografía

[1] M. Checa, F. Auneau, J. Hidalgo-Carrillo, A. Marinas, J. M. Marinas, C. Pinel, F. J. Urbano, *Catal. Today*, 196 (2012) 91-100.

[2] J. Chaminand, L. Djakovitch, P. Gallezot, P. Marion, C. Pinel, C. Rosier, *Green Chem.*, 6 (2004) 359–361.

[3] F. Diehl, A.Y. Khodakov, *Oil Gas Sci. Technol.*, 64 (2009) 11-24.

[4] A. Marinas, T. Mallat, A. Baiker, *J. Catal*., 221 (2004) 666.

[5] M. Heitbaum, F. Glorius, I. Escher, *Angew. Chem. Int. Ed*., 45 (2006) 4732. (revisión general sobre catálisis quiral heterogénea)

[6] E. Schmidt, A. Vargas, T. Mallat, A. Baiker., *J.A.C.S.* 131 (2009) 12358-12367.

[7] F. Hoxha, B. Schimmoeller, Z. Cakl, A. Urakawa, T. Mallat, S.E. Pratsinis, A. Baiker , *J. Catal.*, 271 (2010) 115–124.

[8] M. Lashdaf, A. O. I. Krause, M. Lindblad, M. Tiitta, T. Venalainen, *Appl. Catal. A, 241 (2003) 65.*

[9] P.G.N. Mertens, H. Poelman, X. Ye, I.F.J. Vankelecom, P.A. Jacobs, D.E. De Vos, *Catal. Today*, 122 (2007) 352.

[10] F. Alonso, P. Riente, F. Rodríguez-Reinoso, J. Ruiz-Martínez, A. Sepúlveda-Escribano, M. Yus, *J. Catal*., 260 (2008) 113.

Summary of PhD report by Vicente Montes Jiménez

1. Introduction/Motivation of the PhD

The importance of Catalysis is evidenced by the fact that over 90% of industrial chemical processes requires the use of some catalyzed step. This PhD was aimed at synthesizing and characterizing several solids though diverse methods as well as testing them as catalysts in several industrially relevant hydrogen-mediated processes. More specifically, studied processes were glycerol hydrogenolysis, Fischer-Tropsch synthesis (FTS), enantioselective reduction of carbonyl group and chemoselective reduction of C=O in the presence of C=C.

All in all, the goal was to cast further light on some specific variables influencing the processes in order to increase conversion and selectivity to the desired product.

Glycerol hydrogenolysis is a viable way to valorize glycerol (a by-product in the biorefinery) using several supported noble metals as heterogeneous catalysts. Nevertheless, there is currently some controversy on the activity order of the metals as well as on the influence of metal particle size on catalytic performance [1-2].

Fischer-Tropsch (FT) synthesis is a process implied in the obtaining of fuel from alternative sources to oil and look for the synthesis of some long-chain hydrocarbons from a H_2/CO gas mixture (the so-called synthesis gas). The way the presence of a noble metal used as an additive to Co or Fe influences the process is a current matter of debate. There is some controversy on whether the noble metal just favors the other metal reducibility or plays any additional role [3].

As regards chiral reactions, one interesting available alternative is enantioselective hydrogenation through chiral induction [4-6]. It consists in the adsorption on the metal phase (e.g. platinum) of a chiral compound. There are still

some features to clarify such as the need for an amino group in the chiral modifier [4] or the effect of the use of additives or the support on the process [7].

As far as chemoselective reduction of C=O in the presence of C=C is concerned, some new, more active, selective and environmentally-friendlier supported metal catalysts are continuously described in the literature [8-10]. Nevertheless, some aspects such as the role of the support, its interaction with the metal or the effect of metal dispersion on the catalytic activity require further studies.

2. Content of the research

In the present PhD, a global vision of catalysis is adopted following the sequence synthesis-characterization-catalytic activity with a view to stablish some structure-performance relationships for the catalysts. Synthesized systems consist in several supported metal nanoparticles. Special attention is paid to the control of diverse synthetic variables such as the method (microemulsion, deposition-precipitation or impregnation), or the metal precursor of choice (with or without chlorine). Some of the solids used as the supports include several partially-reducible oxides (such as ZnO or TiO_2), with a view to study the effect of metal-support interaction on catalytic performance. Several porous ordered materials (USY zeolites and MCM-41) are also tested in order to favor adsorption (due to their high surface area) and evidence potential diffusional problems (when microporous instead of mesoporous systems are used).

Two additional points which worth mentioning are the optimization of diverse variables in microemulsion technique or the exploration of several commercial chiral molecules as additives in enantioselective hydrogenation. In the first case, the final goal is the synthesis of diverse supported metal (Pt, Pd or Rh) nanoparticles of similar sizes. In the second case, those molecules are added to the

reaction medium to study their effect on enantioselective hydrogenation of ethyl pyruvate to ethyl lactate on cinchona-modified supported Pt systems.

3. Conclusions

Each hydrogenation process exhibited some particular requirements thus evidencing the need for a taylor-made synthesis of the catalyst to optimize the results. Some of the conclusions drawn from the study are going to be commented now for each process.

Regarding glycerol hydrogenolysis on several ZnO-supported metal (Pt, Pd, Rh) systems, similar metal particle sizes (in the 2-4 nm range) were obtained through microemulsion technique.

Even though synthesized metal particles were already in the zero oxidation state, their highest activity was obtained on thermal treatment at 200-300ºC. The presence of some remaining surfactant could account for that, thermal treatment favoring its loss and thus the access of substrate to the metal particle. Moreover, the presence of surfactant favors selectivity to acetol since it somehow limits hydrogenation activity of the metal.

Further studies on Pt/ZnO systems evidenced the role of the metal not only on the hydrogenation of acetol to 1,2-PDO but also on the previous dehydration of glycerol into acetol. Moreover, the reaction requires a moderate acidity whereas strong acid sites favors some secondary reactions such as catalytic cracking, to the detriment of selectivity to 1,2-PDO.

As regards Fischer-Tropsch synthesis, microemulsion technique allowed us to obtain several Pt-modified TiO-supported cobalt systems with cobalt particle sizes in the 3.8-4.7 nm range. Simultaneous reduction of Co and Pt led to higher conversions than consecutive reduction. This was explained as a result of the higher Pt-Co and Co-support interaction in the former case, as evidenced by TPR, Raman and XPS.

As far as enantioselective reduction of ethyl pyruvate to ethyl lactate is concerned, a study on Pt/USY and Pt/MCM-41 solids showed that the optimum platinum particle size is in the 3-5 nm range. A screening of several commercial chiral molecules as additives resulted in the increase in e.e. values (R or S) through the addition to the reaction medium of 4-hydroxy-D-(-)-phenylglycine (OHDF) in the presence of low concentration of cinchonidine or cinchonine, respectively. UV-Vis studies evidenced the existence of some substrate-modifier-additive interaction in the liquid phase.

A multivariable study on one of the catalysts (USY780-H_2PtCl_6-10ºC/min) varying the hydrogen pressure, amount of CD and OHDF, allowed us to obtain 79% e.e. at total conversion and confirmed the above-mentioned positive effect of OHDF on enantioselectivity.

Finally, the study of gas-phase chemoselective hydrogenation of crotonaldehyde to crotyl alcohol showed the existence of some diffusion problems when microporous (USY zeolite) materials were used as the support.

The presence of some residual chlorine coming from the metal precursor used favors selectivity to the unsaturated alcohol.

Furthermore, those solids using ZnO as the support exhibited the highest selectivity values to crotyl alcohol upon reduction at high temperatures which seems to suggest that strong Pt-Zn interaction is positive to the reaction.

4. References

[1] M. Checa, F. Auneau, ,J. Hidalgo-Carrillo, A. Marinas, J. M. Marinas, C. Pinel, F. J. Urbano, *Catal. Today*, 196 (2012) 91-100.

[2] J. Chaminand, L. Djakovitch, P. Gallezot, P. Marion, C. Pinel, C. Rosier, *Green Chem.*, 6 (2004) 359–361.

[3] F. Diehl, A.Y. Khodakov, *Oil Gas Sci. Technol.*, 64 (2009) 11-24.

[4] A. Marinas, T. Mallat, A. Baiker, *J. Catal*., 221 (2004) 666.

[5] M. Heitbaum, F. Glorius, I. Escher, *Angew. Chem. Int. Ed*., 45 (2006) 4732. (general review on heterogeneous chiral catalysis).

[6] E. Schmidt, A. Vargas, T. Mallat, A. Baiker., *J.A.C.S.* 131 (2009) 12358-12367.

[7] F. Hoxha, B. Schimmoeller, Z. Cakl, A. Urakawa, T. Mallat, S.E. Pratsinis, A. Baiker , *J. Catal.,* 271 (2010) 115–124.

[8] M. Lashdaf, A. O. I. Krause, M. Lindblad, M. Tiitta, T. Venalainen, *Appl. Catal. A, 241 (2003) 65.*

[9] P.G.N. Mertens, H. Poelman, X. Ye, I.F.J. Vankelecom, P.A. Jacobs, D.E. De Vos, *Catal. Today*, 122 (2007) 352.

[10] F. Alonso, P. Riente, F. Rodríguez-Reinoso, J. Ruiz-Martínez, A. Sepúlveda-Escribano, M. Yus, *J. Catal*., 260 (2008) 113.

Otras aportaciones científicas

Articles

Authors*:* Suárez París R., Montes V., Boutonnet M., Järås S.

Title: Higher alcohol synthesis over nickel-modified alkali-doped molybdenum sulfide catalysts prepared by conventional coprecipitation and coprecipitation in microemulsions

Catalysis Today, doi:10.1016/j.cattod.2014.12.003

Authors*:* L. Ilieva, P. Petrova, T. Tabakova, G. Pantaleo, V. Montes, J.W. Sobczak, W. Lisowski,Z. Kaszkur, M. Boutonnet, A.M. Venezia.

Title: Pure hydrogen production via PROX over gold catalysts supported on Pr-modified ceria

Fuel 134 (2014) 628–635

Authors: Francesco Regali, Leonarda Francesca Liotta, Anna Maria Venezia, Vicente Montes, Magali Boutonnet, Sven Jaras.

Title: Effect of metal loading on activity, selectivity and deactivation behavior of Pd/silica–alumina catalysts in the hydroconversion of n-hexadecane

Catalysis Today 223 (2014) 87– 96

Authors: S. Axpuac, M.A. Aramendía, J. Hidalgo-Carrillo, A. Marinas, J.M. Marinas, V. Montes-Jiménez, F.J. Urbano and V. Borau

Title: Study of structure performance relationships in Meerwein-Ponndorf-Verley reduction of crotonaldehyde on several magnesium and zirconium-based systems

Catalysis Today 187 (2012) 183-190

Communications to Congresses

Authors: Suárez-París, Rodrigo; Montes-Jiménez, Vicente; Boutonnet, Magali; Järas, Sven

Title: Mixed alcohols synthesis over K-Ni-MoS2 catalysts prepared by conventional coprecipitation and by microemulsion. Effect of alcohols co-feeding.

Name: NSC2014 - 16th Nordic Symposium on Catalysis

Type of presentation: Oral communication

Date: 15-06-2014

Authors: Montes-Jiménez, Vicente; Boutonnet, Magali; Järas, Sven; Lualdi, Matteo ; Marinas-Aramendía,Alberto.

Title: Catalizadores de Co/TiO_2 dopados con Pt: actividad en la reacción de Fischer-Tropsch e influencia del metal noble

Name: I Encuentro de Jóvenes Investigadores de la SECAT

Type of presentation: Poster communication

Date: 18-6-2014

Authors: Montes-Jiménez, Vicente; Marinas-Aramendía, Alberto; Boutonnet, Magali; Marinas-Rubio, Jose Maria; Urbano-Navarro, Francisco Jose

Title: Pt supported on ZnO doped with Al, Ceand Zr and their activity in glycerol hydrogenolysis

Name: UBIOCHEM. 4th international workshop: utilization of biomass for sustainable fuels and chemicals

Type of presentation: Oral communication

Date: 02-10-2013

Authors: Pardo, Fatima; Montes-Jiménez, Vicente; Marinas-Aramendía, Alberto; Cabrera, Saul; Järas, Sven; Boutonnet, Magali

Title: The effect of mesoporous silicas with different pore size on cobalt based catalyst for Fischer-Tropsch Synthesis

Name: UBIOCHEM. 4th international workshop: utilization of biomass for sustainable fuels and chemicals

Type of presentation: Oral communication

Date: 02-10-2013

Authors: Pardo, Fatima; Montes-Jiménez, Vicente; Marinas-Aramendía, Alberto; Cabrera, Saúl; Boutonnet,Magali

Title: Cobalt on ordered mesoporous supports for Fischer Tropsch Synthesis

Name: Catalysis for Renewable Sources: fuels, energy, chemicals

Type of presentation: Oral communication

Date: 02-10-2013

Authors: Montes-Jiménez, Vicente; Boutonnet, Magali; Sven, Jaras; Marinas-Aramendía, Alberto; Marinas-Rubio, Jose Maria; Urbano-Navarro, Francisco Jose

Title: Fischer-Tropsch synthesis on Pt-modified cobalt catalysts synthesized through microemulsion technique

Name: XIth european congress on catalysis (EUROPACAT XI)

Type of presentation: Poster communication

Date: 11-09-2013

Authors:. Montes-Jiménez, Vicente; Marinas-Aramendía, Alberto; Marinas-Rubio, Jose Maria; Borau-Bolós, Victoriano; Urbano-Navarro, Francisco Jose
Title:. A comparative sudy of two selective hydrogenation processes on Pt/USY and Pt/MCM41 systems
Type of presentation: Oral communication
Name: 5th Czech-Italian-Spanish Conference on Molecular Sieves and Catalysis
Date: 16-06-2013

Authors: Montes-Jiménez, Vicente; Marinas-Aramendía, Alberto; Marinas-Rubio, Jose Maria; Borau-Bolós, Victoriano; Urbano-Navarro, Francisco Jose
Title:. **:** Enantioselective Hydrogenation of Ethylpyruvate on Pt supported on USY Zeolite and MCM-41: Optimization of the Process Through Factorial Design
Type of presentation: Poster communication
Name: 5th Czech-Italian-Spanish Conference on Molecular Sieves and Catalysis
Date:16- 06-2013

Authors: V. Montes, A. Marinas, J.M. Marinas, F.J. Urbano.
Title:. Sistemas metálicos soportados como catalizadores heterogéneos en procesos químicos.
Type of presentation: Oral communication.
Name: III meeting of young researchers (Cordoba,Spain)
Date: 09-04-2013

Authors: V. Montes, A. Marinas, J.M. Marinas, F.J. Urbano.

Title:. Síntesis de nanopartículas metálicas y oxidos a través de microemulsión.

Type of presentation: Oral communication.

Name: IV NanoUCO (Cordoba, Spain)

Date: 08-02-2013

Authors: V. Montes, A. Marinas, J.M. Marinas, F.J. Urbano.

Title:. Selective hydrogenation on Pt/USY and Pt/MCM41 systems

Type of presentation: Poster communication

Name: Zeoforum (Valencia, Spain)

Date: 03-12-2012

Authors: V. Montes, M. Checa, A. Marinas, J.M. Marinas, F. J. Urbano, M. Boutonnet, S. Järas, C. Pinel

Title: Synthesis of different ZnO-supported metal systems through microemulsion technique and application to selective hydrogenation processes

Type of presentation: Oral communication.

Name: UBIOCHEM III Sustainable production of fuels/energy, materials and chemicals from Biomass (3rd joint meeting COST Action CM0903, UBIOCHEM)

Date: 01-11-2012

Authors: V. Montes, M. Boutonnet, S. Järas, A, Marinas, J.M. Marinas, F. J. Urbano

Title: Fischer-Tropsch synthesis on different platinum-modified Co catalysts
Type of presentation: Oral communication.
Name: UBIOCHEM III Sustainable production of fuels/energy, materials and chemicals from Biomass (3rd joint meeting COST Action CM0903, UBIOCHEM)
Date: 01-11-2012

Authors: Petrova, Petya; Boutonnet, Magali; Montes-Jiménez, Vicente; Tabakova, Tatyana; Ivanov, Ilieva. Lyuba
Title: **:** Differently prepared Pr-doped ceria supports of gold catalysts for WGSR
Type of presentation: Poster communication
Name: UBIOCHEM III Sustainable production of fuels/energy, materials and chemicals from Biomass (3rd joint meeting COST Action CM0903, UBIOCHEM)
Date: 01-11-2012

Authors: V. Montes, M.A. Aramendía, A. Marinas, J.M. Marinas, F.J. Urbano.
Title: Enantioselective hydrogenation of ethyl pyruvate on supported platinum systems: optimisation of reaction conditions through factorial design
Type of presentation: Poster communication
Name: FEZA 2011 (Valencia, Spain)
Date: 05-07-2011

Authors: V. Montes, M.A. Aramendía, A. Marinas, J.M. Marinas, F.J. Urbano.
Title: Influencia del soporte y precursor del metal en catalizadores de Pt para la hidrogenación enantioselectiva del piruvato de etilo.

Type of presentation: Oral communication.
Name: SECAT 2011 (Zaragoza, Spain)
Date: 29-06-2011

Authors: V. Montes, M.A. Aramendía, A. Marinas, J.M. Marinas, F.J. Urbano.
Title: Pt on mesoporous supports for enantioselective reduction of ethyl pyruvate
Type of presentation: Poster comunication
Name: III NANO-UCO (Cordoba, Spain)
Date:08-01-2011

Authors: V. Montes, M.A. Aramendía, A. Marinas, J.M. Marinas, F.J. Urbano.
Title: Enantioselective heterogeneous catalysis
Type of presentation: Oral communication
Name: 1st meeting of young researchers (Cordoba,Spain)
Date: 08-04-2010

Authors: V. Montes, M.A. Aramendía, A. Marinas, J.M. Marinas, F.J. Urbano.
Title: Platinum systems as catalysts for enantioselective reduction of ethyl pyruvate
Type of presentation: Poster communication
Name: II NANO-UCO (Cordoba, Spain)
Date:16-01-2010

Indicios de Calidad

CLAVE:	Artículo
TÍTULO:	Synthesis of different ZnO-supported metal systems through microemulsion technique and application to catalytic transformation of glycerol to acetol and 1,2-propanediol
AUTORES:	V. Montes, M. Checa, A. Marinas, M. Boutonnet , J.M. Marinas, F. J. Urbano, S. Järas, C. Pinel
NOMBRE DE LA REVISTA	Catalysis today
AÑO, VOLUMEN, PÁGINA:	2014, 223, 129
EDITORIAL:	ELSEVIER SCIENCE BV
REVISTA INCLUIDA EN JOURNAL CITATION REPORTS (JCR):	Si
ÍNDICE DE IMPACTO (2013)	3.309
CATEGORÍA:	Engineering, Chemical
LUGAR QUE OCUPA LA REVISTA EN LA CATEGORÍA:	15 de 133
CUARTIL:	Primer Cuartil (Q1)

CLAVE:	Artículo
TÍTULO:	Selective transformation of glycerol into 1,2-propanediol onseveral Pt/ZnO solids: Further insight into the roleand origin of catalyst acidity
AUTORES:	V. Montes, M. Boutonnet, S. Järås, A. Marinas, J.M. Marinas, F.J. Urbano
NOMBRE DE LA REVISTA	Catalysis today
AÑO, VOLUMEN, PÁGINA:	http://dx.doi.org/10.1016/j.cattod.2014.11.014
EDITORIAL:	ELSEVIER SCIENCE BV
REVISTA INCLUIDA EN JOURNAL CITATION REPORTS (JCR):	Si
ÍNDICE DE IMPACTO (2013)	3.309
CATEGORÍA:	Engineering, Chemical
LUGAR QUE OCUPA LA REVISTA EN LA CATEGORÍA:	15 de 133
CUARTIL:	Primer Cuartil (Q1)

CLAVE:	Artículo
TÍTULO:	Preparation and characterization of Pt-modified Co-based catalysts through the microemulsion technique: Preliminary results on the Fischer–Tropsch synthesis
AUTORES:	V. Montes, M. Boutonnet, S. Ja¨ra˚s, M. Lualdi, A. Marinas, J.M. Marinas, F.J. Urbano, M. Mora
NOMBRE DE LA REVISTA	Catalysis today
AÑO, VOLUMEN, PÁGINA:	2014, 223, 66
EDITORIAL:	ELSEVIER SCIENCE BV
REVISTA INCLUIDA EN JOURNAL CITATION REPORTS (JCR):	Si
ÍNDICE DE IMPACTO (2013)	3.309
CATEGORÍA:	Engineering, Chemical
LUGAR QUE OCUPA LA REVISTA EN LA CATEGORÍA:	15 de 133
CUARTIL:	Primer Cuartil (Q1)

Anexo I

Copia de las publicaciones incluidas en la Tesis

Catalysis Today 223 (2014) 129–137

Contents lists available at ScienceDirect

Catalysis Today

journal homepage: www.elsevier.com/locate/cattod

Synthesis of different ZnO-supported metal systems through microemulsion technique and application to catalytic transformation of glycerol to acetol and 1,2-propanediol

V. Montes[a], M. Checa[a], A. Marinas[a,*], M. Boutonnet[b], J.M. Marinas[a], F.J. Urbano[a], S. Järas[b], C. Pinel[c]

[a] Organic Chemistry Department, University of Córdoba. Campus de Excelencia Internacional Agroalimentario, ceiA3, Marie Curie Building, E-14014 Córdoba, Spain
[b] KTH (Royal Institute of Technology), Chemical Technology, Teknikringen 42, SE-100 44 Stockholm, Sweden
[c] IRCELYON, UMR 5256 CNRSAJCBL, 2 Avenue Albert Einstein, 69626 Villeurbanne Cedex, France

ARTICLE INFO

Article history:
Received 6 February 2013
Received in revised form 19 August 2013
Accepted 5 September 2013
Available online 12 October 2013

Keywords:
Glycerol hydrogenolysis
Platinum catalyst
Rhodium catalyst
Palladium catalyst
1,2-Propanediol (1,2-PDO)
Hydroxyacetone (acetol)

ABSTRACT

Different systems consisting of diverse metals (Au, Pt, Pd, Rh) supported on ZnO (5% by weight) were synthesized through the microemulsion technique (ME) and tested for glycerol hydrogenolysis, the main products being hydroxyacetone (acetol) and 1,2-propanediol (1,2-PDO). The solids synthesized using sodium borohydride as the reducing agent (B series) had smaller particle sizes as compared to the use of hydrazine (H series) which, in turn, resulted in a better catalytic performance. This synthetic method allowed us to obtain similar metal particle sizes (2–4 nm) for Pt, Pd and Rh solids in B series, whereas average gold metal particle was higher (>8 nm) which probably accounts for Au-containing systems being inactive under our experimental conditions. Reactivity order followed the sequence Rh > Pt > Pd. A comparison of the systems synthesized in the present paper through ME technique with those obtained in a previous work through the deposition–precipitation process revealed a higher activity and selectivity to acetol for the former solids which could be related to the presence of surfactant. Moreover, results suggested that metal sites could participate not only in hydrogenation of acetol to 1,2-propanediol but also in the previous dehydration step of glycerol to acetol.

1. Introduction

Glycerol is a byproduct obtained during production of biodiesel through transesterification of vegetable oils. Approximately 10% weight of the converted feedstock is released as glycerol which makes its possible valorization an interesting issue. One possibility is its catalytic transformation on different metals under hydrogen or inert atmosphere. One of the chemicals produced from glycerol in neutral medium is 1,2-propanediol (PDO) resulting from a dehydration process (leading to hydroxyacetone or acetol) followed by a hydrogenation step. 1,2-PDO can be used as antifreeze, in food industry or as feedstock in the preparation of polyester resins for film and fiber manufacture [1]. As for acetol, it is used as an interesting organic intermediate to produce polyols and acrolein, in food industry to give aroma to food, in textiles or in cosmetic industry as skin tanning agent [2]. Some of the metals used in the transformation of glycerol into 1,2-PDO include Cu [3–5], and noble metals such as Ir [6], Ru [7–9], Rh [10,11], Pd [10,12] or Pt [13,14].

In a previous study [14], different reducible oxides (TiO_2, ZnO, SnO_2 and ZrO_2) were screened as support for platinum and tested for glycerol hydrogenolysis, ZnO being the solid with the highest selectivity to 1,2-PDO. This prompted us to select ZnO as the support for diverse metals (Pt, Rh, Pd and Au) which were incorporated through the deposition–precipitation technique in a nominal content of 5% by weight. All the solids exhibited the best catalytic performance on reduction treatment at 200 °C whereas higher temperatures led to the formation of a metal-Zn alloy which under our experimental conditions was detrimental to activity. Catalytic activity followed the sequence Pt > Rh > Pd >> Au. However, XRD and TEM studies revealed quite different metal particle sizes, for Pt and Rh as compared to Pd and Au (3.1, 3.7, 15 and 12 nm, respectively). Therefore, it was not clear to what extent catalytic results had been influenced by the different metal particle size. In order to cast further light on that, in the present study a new synthesis under similar conditions (same metal precursor, support and metal content) is carried out by the microemulsion technique.

A microemulsion (ME) is a thermodynamically stable colloidal dispersion in which two immiscible liquids (polar and non-polar) form nanosized droplets dispersed in a continuous phase and stabilized by a third component: the surfactant. These nanodroplets

* Corresponding author. Tel.: +34 957218622; fax: +34 957212066.
E-mail addresses: alberto.marinas@uco.es, qo2maara@uco.es (A. Marinas).

0920-5861/$ – see front matter © 2013 Elsevier B.V. All rights reserved.
http://dx.doi.org/10.1016/j.cattod.2013.09.021

can be used as nanoreactors to synthesize metal particles in a very narrow particle size range. There are several reviews on the preparation of nanoparticles of noble metals through this technique and their application as catalyst to several processes [15–18]. Basically, some of the crucial parameters to be considered are the type of surfactant (anionic, cationic or non-ionic, the latter normally being less sensitive to temperature), the oil phase (oil–surfactant interaction influences the shape and size of microemulsion) or the concentration of metal solution (normally high concentrations lead to larger final metal particle sizes). The internal structure of the ME is determined by the relative fractions of these three constituents: surfactant, oil and water solution. The ME is only formed for certain ratios of the constituents, outside which a two-phase system is formed. The ratios for which the ME exists depend on the system, nature and polarity of the components, and changing these ratios the size of droplets are controlled and hence the final particle size. Another important point to be considered is the reducing agent which will lead to the formation of metallic particles, the most commonly used being hydrazine (N_2H_4) and sodium borohydride ($NaBH_4$). Typically a stoichiometric excess is used in order to ensure the full reduction of precursor salt. Furthermore, such an excess results in smaller metal particle sizes because the nucleation is favored over particle growth [19]. Others parameters influencing the process are temperature, speed of stirring or atmosphere, just to cite some of them.

2. Experimental

2.1. Materials

Synperonic 13/6.5 was a gift from Croda. All the other chemicals (2,2,4-trimethylpentane (99.9%, TMP), hydrazine monohydrate 98%, sodium borohydride 96%, 8 wt% H_2PtCl_6 aqueous solution, $HAuCl_4$, $Pd(NO_3)_2$, $RhCl_3$, ZnO nanopowder, acetone (technical grade), tetrahydrofuran (99.9%, THF), glycerol 99%, 1,2-propanediol 99.5%, 1,3-propanediol 98%, hydroxyacetone (acetol, 95%), ethylene glycol 99.5%, n-propanol 99.5%, acrolein (≥95%) and lactic acid ≥85%) were purchased from Sigma–Aldrich. MilliQ water was used for preparation of the aqueous solutions of metal salts.

2.2. Synthesis of ZnO-supported systems

Fig. 1A summarizes the main steps for the preparation of the catalysts from a water in oil microemulsion (reverse micelle). The total amounts of reagents were calculated in order to obtain a nominal content of 5 wt% metal in 2 g of catalyst.

Under optimized conditions, the composition of microemulsions (ME) was surfactant: synperonic 13/6.5 (28.6 wt%), oil: trimethylpentane (TMP) (66.8 wt%), water: 2 wt% metal precursor salt (4.6 wt%).

As depicted in Fig. 1A, the synthesis began mixing the corresponding amounts of Synperonic 13/6.5 and TMP in a flask. The mixture was kept under vigorous stirring (1000 rpm) and then the water solution of precursor was added dropwise resulting in a transparent solution of microemulsion encapsulating the dissolved metallic precursor. ME was then deoxygenated bubbling N_2 for a couple of minutes and for the rest of the process an inert atmosphere was created with N_2. Afterwards, the reducing agent ($NaBH_4$ or N_2H_2), in a 1:5 molar ratio (metal: reducing agent) was added as a fresh water solution 10 M (maximum 1 min old). The color of solution changed from yellow (Pt, Pd and Au), red (Rh) to black just with the first drop of reducing agent solution. At that point, the metallic particle had already been formed and stabilized by surfactant. In order to ensure a full reduction of precursor the mixture was kept under stirring for 1 h. The inert atmosphere was then removed and the system was kept stirred one additional hour. The next step was the addition of the support (1.8 g ZnO) directly followed by acetone (50% weight of total ME) as destabilizing agent all at once. The suspension was kept stirring for 2 h for a full destabilization of the ME.

The suspension was then centrifuged (3000 rpm) for 15 min. A good indicative of a successful reduction and destabilization was that after separation of the solid, the liquid was transparent and colorless.

Then the solids were carefully washed with ethanol, acetone, cold water (at room temperature) and hot water (boiling water), three times each with half the weight of acetone employed for destabilization. Finally, the systems were dried for 12 h at 120 °C and when applicable calcined at 300 °C or 500 °C for 16 h (ramp of 1 °C/min) with a flow of synthetic air of 2 L/h.

Catalyst nomenclature includes the metal, the support (ZnO), the reducing agent (B or H for sodium borohydride or hydrazine, respectively) and the thermal treatment. Therefore, for instance, 'Pt/ZnO-H unred' denotes the platinum system synthesized through reduction with hydrazine and tested as synthesized (unreduced) whereas 'Pd/ZnO-B calc500 red 200' refers to the palladium solid obtained through reduction with $NaBH_4$ and submitted to calcination at 500 °C first followed by reduction at 200 °C.

For comparative purposes, the corresponding systems synthesized through the deposition–precipitation method using the same precursor salt, support and nominal metal content (5 wt%) were also tested in this study. Fig. 1B summarizes the main synthetic steps whereas full details on the synthesis and characterization of the catalysts can be found elsewhere [14]. The nomenclature of these systems is M/ZnO dp 200 where M refers to the metal, dp to the synthetic method (deposition–precipitation) and 200 to the reduction temperature (200 °C).

2.3. Characterization

Elemental analysis of metal-containing samples was performed by the staff at the Central Service for Research Support (SCAI) of the University of Córdoba. It was performed using inductively coupled plasma mass spectrometry (ICP-MS). Measurements were made on a Perkin-Elmer ELAN DRC-e instrument following dissolution of the sample in a 1:3 HNO_3/HCl mixture with a soft heating. Calibration was done by using PE Pure Plus atomic spectroscopy standards, also from Perkin-Elmer.

Surface areas of the solids were determined from nitrogen adsorption–desorption isotherms obtained at liquid nitrogen temperature on a Micromeritics ASAP-2010 instrument, using the Brunnauer–Emmett–Teller (BET) method. All samples were degassed to 0.1 Pa at 120 °C prior to measurement.

Transmission electron microscopy (TEM) images were obtained using a Philips CM-10 microscope. All samples were mounted on 3 mm holey carbon copper grids.

EDX measurements were performed on a JEOL JSM-6300 scanning electron microscope (SEM) equipped with an energy-dispersive X-ray (EDX) detector. It was operated at an acceleration voltage of 20 keV with a resolution of 65 eV.

X-ray patterns of all M/ZnO-B and M/ZnO-H samples (Fig. 3) were obtained on a Siemens D5005 X-ray diffractometer utilizing Cu Kα radiation. A secondary monochromator was used. The metallic particle sizes were estimated by using the Scherrer formula assuming spherical crystallites. X-ray diffractograms of Pd/ZnO-B calcined/reduced at different temperatures (Fig. 8) were recorded on a Siemens D-5000 diffractometer equipped with a DACO-MP automatic control and data acquisition system. The instrument was equipped with a graphite monochromator and used Co Kα radiation.

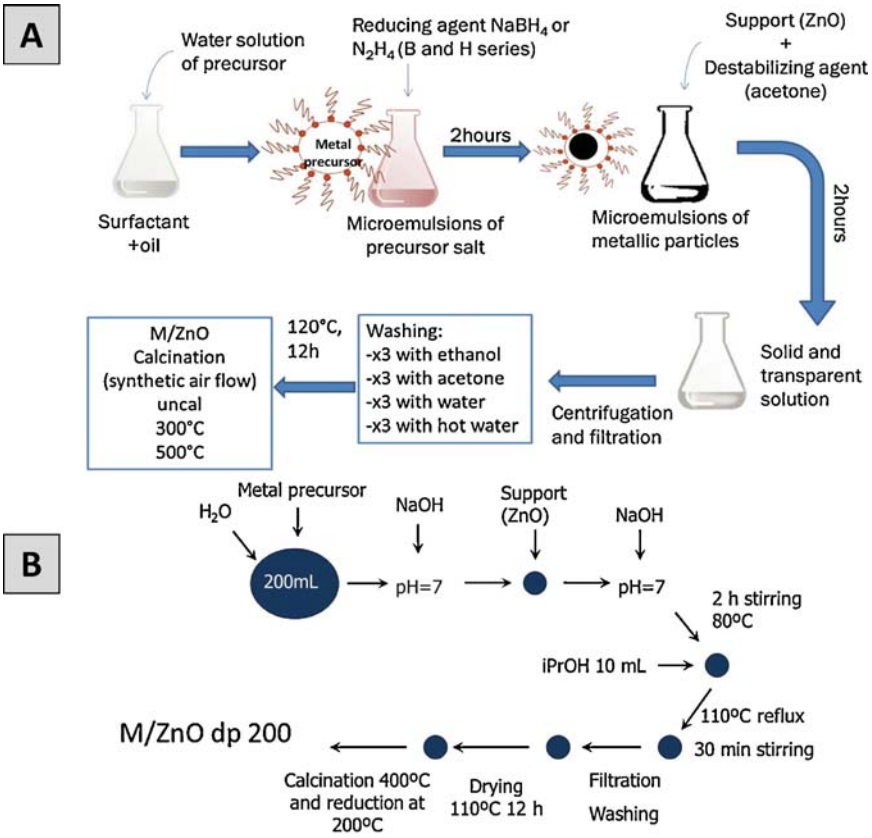

Fig. 1. Schematic representation of the synthetic procedure followed to obtain the different ZnO-supported metal systems through microemulsion technique (A) and deposition–precipitation method (B).

X-ray photoelectron spectroscopy (XPS) data were recorded on 4 mm × 4 mm pellets 0.5 mm thick that were obtained by gently pressing the powdered materials following outgassing to a pressure below about 2×10^{-8} Torr at 150 °C in the instrument pre-chamber to remove chemisorbed volatile species. The main chamber of the Leibold-Heraeus LHS10 spectrometer used, capable of operating down to less than 2×10^{-9} Torr, was equipped with an EA-200MCD hemispherical electron analyser with a dual X-ray source using Mg Kα ($h\nu$ = 1253.6 eV) at 120 W, at 30 mA, with C(1s) as energy reference (284.6 eV).

Surface acidity was determined by thermal programmed desorption (TPD) of pyridine previously adsorbed on the solids monitored by TCD. An amount of 50 mg of sample was placed under a He stream flowing at 10 mL/min in a reactor 10 mm in diameter that was placed inside an oven. The He stream was used to clean the solids by heating to 350 °C at a rate of 10 °C/min and then cooling by thermal inertia to room temperature. At that point, the surface of the solid was saturated with the probe molecule for 30 min. Pyridine was supplied by bubbling the He stream through liquid pyridine at room temperature. After saturation, excess physisorbed probe substance was removed by passing a He stream at 10 mL/min for 1 h. Then, desorption was started by raising the temperature to 400 °C at 10 °C/min and holding the final level for 30 min.

2.4. Catalytic tests

Hydrogenolysis of glycerol was conducted in a Berghof HR-100 stainless steel high-pressure autoclave equipped with a 75 mL PTFE vessel and a magnetic stirrer. Under standard conditions, 20 mL of a 1.36 M solution of glycerol in water and 50 mg of catalyst were introduced in the vessel. Reactor was then purged with hydrogen and temperature (180 °C) and hydrogen pressure (6 bar) adjusted. The stirring rate was 1200 rpm. After 15 h of reaction, stirring was stopped and the vessel cooled in an ice bath. The catalyst was spin-dried and the liquid passed through a filter of PTFE 0.45 μm. Then it was analyzed by GC-FID (Agilent Technologies 7890, with a Supelco 25357 NukolTM capillary column). Quantification was carried out through the corresponding calibration curves.

3. Results and discussion

As indicated in Section 2, the optimized composition of ME system was surfactant: Synperonic13/6.5 (28.6%), oil: trimethylpentane (66.8%), water: 2 wt% of precursor salt (4.6%). In order to find such a composition, different experiments were performed. It is important to point out that the relative fraction of the constituents of ME is a key feature to control the size of micelles and thus the final

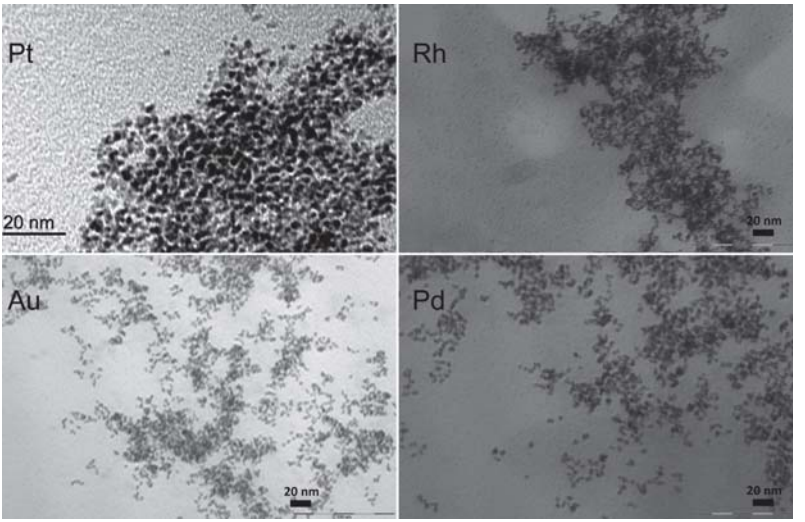

Fig. 2. TEM micrographs of the different microemulsions after the addition of sodium borohydride.

metal particle size. With a view to optimize the process, different mixtures of surfactant and oil at room temperature were prepared. Then an aqueous solution of 1% and 2% weight (wt) of precursor was added dropwise in order to know the solubility limit. Determination of this limit is easy because the microemulsions are isotropic and transparent, and when they destabilize the transparent solution turns into a cloudy system. These experiments determined the region of relative fractions of constituents to form stable reverse micelles. Finally in order to simplify the process, the same system of microemulsion was applied to synthesize all catalysts once ensured that ME was stable for all metal precursors. Also in order to minimize the environmental impact, the system of choice was that in which less amount of surfactant and oil was required.

Fig. 2 shows the TEM micrographs of microemulsions of metallic particles (precursor reduced using $NaBH_4$). As can be seen, at this point the synthetic method ensured metal particles in the 2–4 nm range. Support (ZnO) was then added and microemulsions were destabilized using acetone. The solid was centrifuged and washed to obtain the different M/ZnO systems (M = Pt, Pd, Rh and Au). Some features concerning characterization of the systems are depicted in Table 1. Surface areas of all the systems are in the 15–17 m^2/g range, quite similar to that of the support, ZnO (15 m^2/g). Moreover, a comparison of metal nominal contents (5 wt%) with the values determined by ICP-MS evidences that the synthesis of metal particles through ME technique led to a low incorporation of rhodium (0.3%), a higher incorporation of platinum (1.2 and 2.9% for Pt/ZnO-B and Pt/ZnO-H, respectively) and the almost quantitative incorporation of palladium (4.4 and 4.5% for Pd/ZnO-B and Pd/ZnO-H, respectively). It is possible that the washing process of the solids resulted in the partial dissolution of the metals. In fact, ICP-MS monitoring of the washing process of Pt/ZnO-B solid confirmed that there was a progressive loss of platinum, especially during washing with cold water (that step accounts for ca. 53% Pt loss). However, subsequent treatment with hot water did not lead to any further loss thus confirming that the noble metal remained stabilized thereafter on the catalyst surface. Consequently, no significant metal leaching was observed during catalytic studies.

X-ray diffractograms of the systems are depicted in Fig. 3 and mean particle sizes, as determined from Scherrer equation are indicated in Table 1. From Fig. 3 and Table 1 it is clearly evident that the use of sodium borohydride as the reducing agent (B series) led to smaller metal particles as compared to the utilization of hydrazine (H series). Furthermore, hydrazine was not able to reduce rhodium which was clearly evident during the synthetic method, since unlike the other cases no change in the color of the microemulsion of $RhCl_3$ was observed when hydrazine was added. Finally, in all cases, and particularly for H series, destabilization of ME with acetone resulted in an increase in metal particle size which was especially dramatic in the case of gold. This testifies to the importance of the different steps (and in particular of ME destabilization) in the synthesis of metal nanoparticles through microemulsion. In order to try to obtain smaller gold metal particle sizes, different modifications were applied to the destabilization step, including the substitution of acetone by THF as the

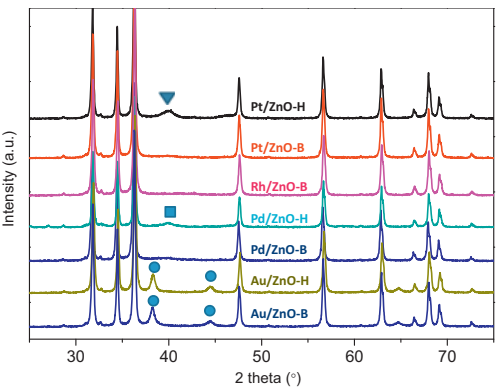

Fig. 3. X-ray diffractograms of the different systems. Symbols indicate the signal corresponding to the metal: Au (circle), Pd (square) and Pt (triangle).

Table 1
Some features concerning characterization of the different ZnO-supported metal systems.

Catalyst[a]	Metal/ZnO weight%				BET surface[b] (m^2/g)	Mean particle size (nm)	
	Nominal	ICP-MS	EDAX	XPS		TEM	XRD[c]
Pt/ZnO-H	5	2.9	3.4	1.2	15	5.3	5.5
Pt/ZnO-H calc300			2.9	1.3	15	–	–
Pt/ZnOH calc500			–	1.3	15	–	–
Pt/ZnO-B			0.8	0.8	16	2.2	NS
Pt/ZnO-B calc300	5	1.2	0.6	0.6	16	–	–
Pt/ZnO-B calc500			–	0.7	16	–	–
Pt/ZnO dp 200	5	5.2	–	5.3	19	3.1	NS
Pd/ZnO-H			4.1	4.6	15	9.0	6.8
Pd/ZnO-H calc 300	5	4.5	2.8	–	15	–	12.2
Pd/ZnO-H calc 500			3.5	–	15	–	17.7
Pd/ZnO-B			5.3	3.6	16	3.0	NS
Pd/ZnO-B calc 300	5	4.4	4.8	3.4	16	–	7.4
Pd/ZnO-B calc 500			5.7	3.4	16	–	14.2
Pd/ZnO dp 200	5	4.1	–	0.9	17	–	15.0
Rh/ZnO-B	5	0.3	0.6	0.4	16	2.1	NS
Rh/ZnO-B calc 300			0.4	0.4	16	–	–
Rh/ZnO-B calc 500			–	0.3	16	–	–
Rh/ZnO dp 200	5	2.4	–	3.2	25	3.7	–

[a] Rh/ZnO-H does not exist since hydrazine was not able to reduce Rh.
[b] The support (ZnO) has a surface area of 15 $m^2\ g^{-1}$.
[c] The measurement of particle sizes of calcined Pd samples corresponded to the peak of PdO at 2θ 39.9°. NS denotes that no signal of the metal was observed by XRD. Au/ZnO-B, Au/ZnO-H and Au/ZnO dp 200 exhibited average particle sizes of 19, 22 and 12 nm, respectively and were inactive for glycerol conversion under our experimental conditions. Therefore, no further characterization was performed.

destabilization agent and the modification of the order of addition of such an agent and ME. All in all, the smaller particle sizes (8 nm) were obtained when ME was added dropwise into a suspension of the support of acetone under vigorous stirring.

TEM micrographs of the different solids after destabilization, filtration and calcination confirmed XRD results. Therefore, B series (Fig. 4 and Table 1) presented metal particle sizes in the 2–4 nm range, the exception being gold in which case bigger particles were obtained. It is also interesting to note the relatively low particle size interval obtained by ME synthetic method (see inset of Fig. 4 for Pt/ZnO-B).

The systems were then tested for glycerol hydrogenolysis. Results expressed as mol of glycerol converted per mol of metal and selectivity to 1,2-PDO after 15 h are summarized in Figs. 5 and 6. For comparative purposes, catalytic performance of the corresponding system synthesized through the deposition–precipitation method and reduced at 200 °C (M/ZnO dp 200) is also included. As can be seen, data for Rh/ZnO-H and Au/ZnO-B and Au/ZnO-H are absent. In the first case, as explained above, hydrazine was unable to reduce rhodium particles whereas gold systems were inactive for the reaction, probably as a result of their big particle size (above 8 nm).

Conversion of glycerol into 1,2 or 1,3-propanediol on bifunctional catalysts has been described to occur via dehydration followed by hydrogenation. Depending on the hydroxyl group in glycerol involved in the dehydrogenation (either primary or secondary), 1,2-PDO or 1,3-PDO are obtained, respectively (Scheme 1). Moreover, some other liquid (e.g. ethylene glycol, 1-propanol) and gaseous (e.g. methane, ethane and propane) by-products could be obtained [14]. In our case, under standard conditions (15 h of reaction, 180 °C, 6 bar H_2) all catalysts yielded acetol or 1,2-PDO mainly,

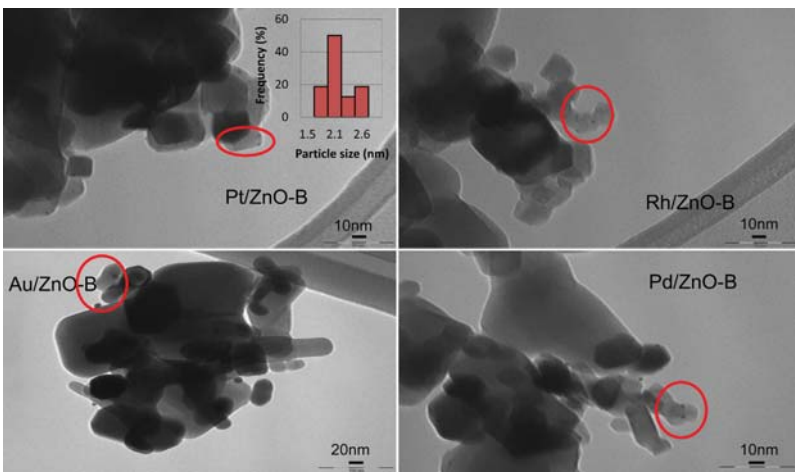

Fig. 4. TEM micrographs of the different M/ZnO-B solids.

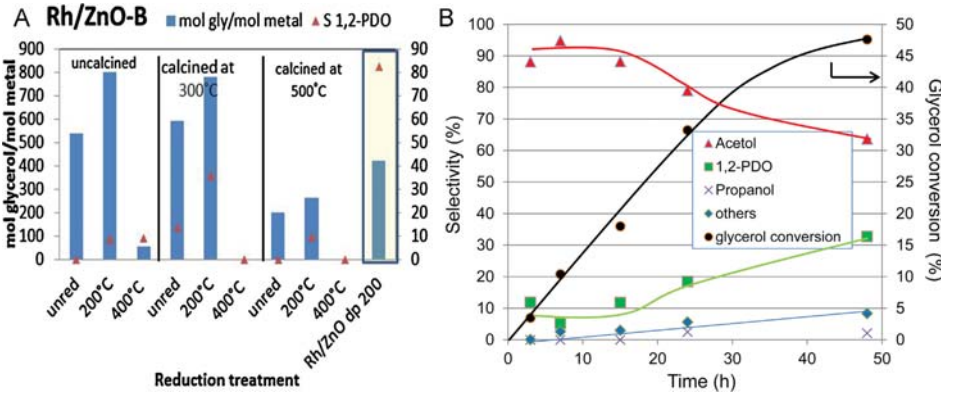

Fig. 5. (A) Catalytic transformation of glycerol on Rh/ZnO-B solid (A) results for $t = 15$ h. (B) Kinetic profile for Rh/ZnO-B uncalc 200. Reaction conditions: 50 mg catalysts, 5 mL 1.36 M water solution of glycerol. 180 °C and 6 bar of initial hydrogen pressure.

accounting for ca. 100% selectivity (Figs. 5 and 6) which confirms the dehydration through primary OH. For longer reaction times (i.e. conversions over ca. 20%), some other by-products were obtained though still 1,2-PDO and acetol accounted for over 90% selectivity (Fig. 5B).

The formation of dehydration products in water environment has already been described not only for glycerol transformation into acrolein or acetol [20] but also for some other processes (e.g. dehydration of fructose to 5-hydroxymethylfurfural (HMF)) [21]. There is some controversy in the literature concerning the nature

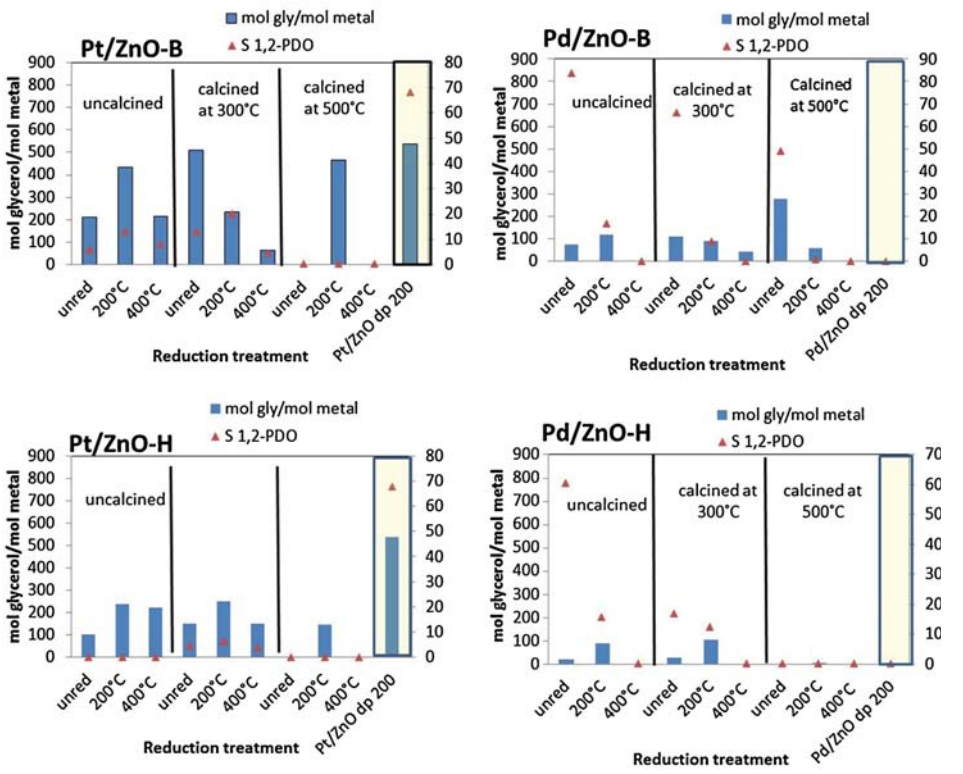

Fig. 6. Catalytic transformation of glycerol on several Pt and Pd solids. Reaction conditions: 50 mg catalysts, 20 mL 1.36 M water solution of glycerol. 180 °C and 6 bar of initial hydrogen pressure.

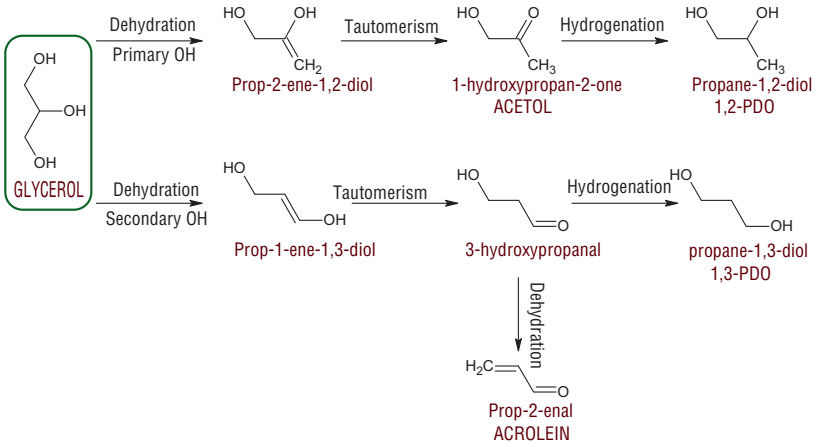

Scheme 1. Transformation routes of glycerol into 1,2-PDO or 1,3-PDO through an initial dehydration step.

of the active sites responsible for acetol formation. On the one hand, most of the papers report that dehydration of glycerol to acetol occurs on acid sites [10] although some other works describe the acetol formation on basic sites by a dehydrogenation process followed by dehydration and enolization [22]. In addition, redox properties of metal oxide catalysts could also influence the performance of those solids in the gas-phase dehydration of glycerol [23,24]. Subsequent hydrogenation of acetol on the metal catalysts gives 1,2-propanediol. Kim et al. [25] studying the gas-phase dehydration of glycerol over silica–alumina catalysts concluded that acrolein was formed on Brønsted acid sites whereas acetol yield was proportional to the concentration of Lewis acid sites. However, in batch processes and in an aqueous environment, Brønsted acid sites will be responsible for both acrolein and acetol production [26]. Moreover, a study of glycerol dehydration based on quantum mechanical calculations reported that neutral glycerol showed a high barrier to dehydration whereas protonated glycerol exhibited a much lower barrier for dehydration to acetol [27]. Density functional calculations indicate that glycerol dehydrates to either acetol or acrolein through alkoxide species formed by competitive adsorption of the primary or secondary glycerol OH groups, respectively (Scheme 1). The stronger adsorption mode of glycerol through the secondary OH group was responsible for the higher selectivity to acrolein at moderated temperatures [26]. On the other hand, some other authors conclude that the metal could be involved in the dehydration of glycerol to acetol. Sato et al. [28] found that dehydration of glycerol in gas phase occurred via Cu-alkoxide species formed by the release of an OH radical from the primary OH group. Similarly, Bienholz et al. [29] prepared a set of different silica supported copper catalysts and found a linear relationship between the specific copper surface and the catalytic activity not only in the hydrogenation of acetol to 1,2-PDO but also in the dehydration of glycerol to acetol thus suggesting that both processes occurred at the copper surface. The influence of the metal in the dehydration step has been suggested for some other metals (e.g. Pt [30]). Nevertheless, Wang and Liu [31] working with Cu–ZnO catalysts in the batch conversion of glycerol to 1,2-PDO found that the dehydration step to acetol was carried out on the ZnO acidic surface and the subsequent hydrogenation of acetol to 1,2-PDO takes place in the Cu domains. Furthermore, the activation energy for acetol hydrogenation is about 30 kJ lower than that of glycerol dehydration [32] and therefore dehydration step determines the overall glycerol conversion while hydrogenation by Cu is responsible for the final selectivity to 1,2-PDO [31,32].

In our study, different preliminary experiments were conducted in order to ensure that M/ZnO solids catalyzed the formation of both acetol and 1,2-PDO. First of all, a blank experiment (1.36 M glycerol, no catalyst) showed that glycerol was stable under reaction conditions. Pure ZnO was then tested as the catalyst and again glycerol was not transformed evidencing that, even though transformation of glycerol into acetol is a simple dehydration process, ZnO cannot catalyze the process under our experimental conditions. Finally, a 1.36 M solution of acetol in water was submitted to the reaction conditions and acetol did not rehydrate. These results seems to support the hypothesis of metal sites participating in both dehydration to acetol and subsequent hydrogenation to 1,2-PDO or, at least, that incorporation of the metal to the ZnO creates a new population of acid sites able to dehydrate the glycerol to acetol.

In order to cast further light on the nature of active sites responsible for formation of acetol, acidity of several systems was determined by thermal programmed desorption (TPD) of pre-adsorbed pyridine (Fig. 7). As can be seen, the support (ZnO) did not exhibit any peak which could account for its inactivity in

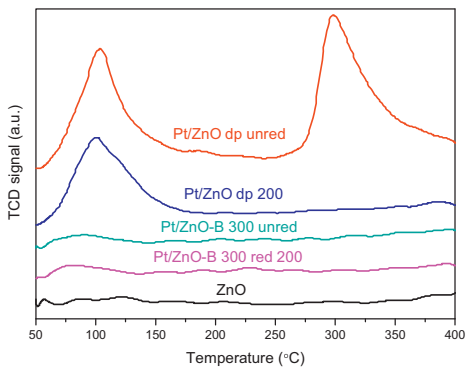

Fig. 7. TPD profile of pre-adsorbed pyridine for some of the Pt-based solids.

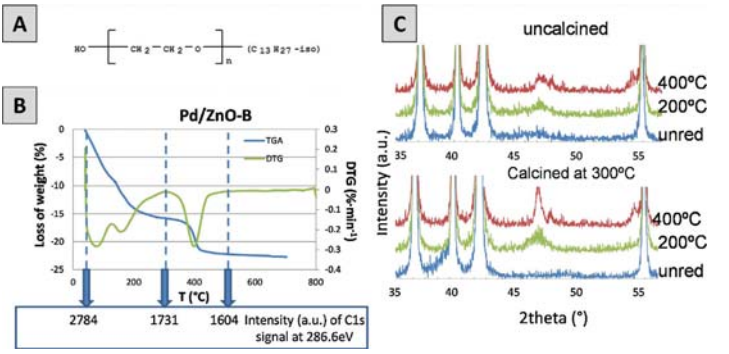

Fig. 8. (A) Chemical structure of the surfactant (Synperonic 13/6.5). (B) TG analysis of Pd/ZnO-B and relative percentage of carbon associated to C—O species (from C1s signal by XPS). (C) X-ray diffractograms of Pd/ZnO-B under different thermal treatments.

the process. On the contrary, Pt/ZnO systems synthesized through deposition–precipitation technique, exhibited well-defined pyridine desorption peaks which evidences the existence of acid sites which in turn could result in their observed activity. Those acid sites could originate from the platinum precursor (chloroplatinic acid) [33]. In fact, a comparison of Pt/ZnO dp unred and Pt/ZnO dp 200 systems shows the loss of the peak appearing at higher temperature (ca. 300 °C) in the latter which could be due to the release of chloride during reduction pretreatment as HCl.

Interestingly, despite the fact that Pt/ZnO solids obtained through microemulsion technique did not exhibit any pyridine peak, they were active in glycerol conversion. This could be supportive of the above-mentioned role of metal sites in dehydration of glycerol to acetol. Nevertheless, the possibility of some influence of remaining surfactant or even the existence of low-acidity active sites (not titrated with pyridine) cannot be ruled out.

Results achieved for platinum (Pt/ZnO-B and Pt/ZnO-H), palladium (Pd/ZnO-B and Pd/ZnO-H) and rhodium (Rh/ZnO-B) solids are summarized in Figs. 5 and 6. In all cases B series led to better catalytic results as compared to H series. The lower metal particle sizes (as evidenced by XRD and TEM, see Table 1) in the former case can account for that. Focusing on B series, reactivity order follows the sequence Rh > Pt > Pd. In our previous study on systems synthesized through the deposition–precipitation method [14], palladium was also found to be the least active system though its greater particle size as compared to that of Rh and Pt (22 nm and 3–4 nm, respectively) could explain such catalytic results. In the present work ME technique allowed us to better control metal particle sizes (2–4 nm for all Pt, Pd and Rh in M/ZnO-B series) which confirms that under our experimental conditions Pd is less active.

Focusing on B-series, the best catalytic results for each metal corresponds to Pt/ZnO-B calc300 unred (510 mol glycerol/mol of metal, 87% selectivity to acetol), Pd/ZnO-B calc500 unred (279 mol glycerol/mol of metal, 51% selectivity acetol) and Rh/ZnO-B uncalc red 200 (800 mol glycerol/mol of metal, 91% selectivity to acetol). In the first case, catalytic activity is quite close to that of the corresponding DP counterpart (Pt/ZnO dp 200, 538 mol glycerol/mol Rh) whereas in the other two cases, synthesis through the ME method led to a significant improvement in activity (see Figs. 5A and 6). Furthermore, ME systems are comparatively more selective to acetol than their DP counterparts. If we assume a separate function of catalyst components (acidic and metallic) this would mean that in ME systems the metallic function is lower than in DP catalysts in which acetol is readily hydrogenated to 1,2-PDO. Some remaining surfactant in the surrounding of metallic particles could be the reason for the low hydrogenating activity of the ME systems. Moreover, interestingly, despite the fact that as-synthesized M/ZnO-B systems consist of metal particles in the zero oxidation state, their optimum catalytic performance is achieved upon thermal pretreatment (calcination and/or reduction) normally at ca. 200–300 °C. In order to cast further light on the reason for that, different characterization studies were carried out. Fig. 8 shows the results for Pd/ZnO-B system. First, a thermogravimetric study (TG) of the system revealed that the solid exhibited a weight loss of ca. 22% upon calcination at temperatures up to 400 °C. This is probably due to decomposition of remaining surfactant. In fact, an XPS study of Pd/ZnO-B as synthesized and calcined at 300 °C and 500 °C in the C1s region (not shown) revealed the progressive decrease in the signal at 286.6 eV assigned to C—O species in alcohol and ether groups [34]. More interestingly, an XRD study of the system showed that smaller metal particles were obtained upon reduction for uncalcined systems as compared to previously calcined ones suggesting that the remaining surfactant prevents to a certain extent sintering of metal particles. Therefore, thermal treatment has two opposite effects on catalytic performance of M/ZnO-B solids. On the one hand, as temperature rises less surfactant remains which should be positive since metal particles are more accessible. On the other, thermal treatment results in an increase in particle size and appearance of strong metal-support interaction (SMSI) effect (at ca. 400 °C) which is detrimental to activity. It seems that there is an optimum temperature (ca. 200–300 °C) for which a compromise is reached.

4. Conclusions

ME technique is an adequate method to control metal particle size though it requires optimization of several parameters. The method allowed us to synthesize Pt, Pd and Rh systems with similar metal particle sizes (2–4 nm, B-series). $NaBH_4$ used as reducing agent gave smaller particle sizes than hydrazine thus accounting for the better catalytic performance in glycerol transformation to acetol and 1,2-PDO of B-series. Systems obtained through ME technique contained particles in the metal state though thermal treatment to temperatures in the 200–300 °C range led to an improvement of catalytic performance. As temperature rises there are two opposite effects. On the one hand, surfactant is removed which is positive to activity. On the other, progressive loss of surfactant favors sintering of metal particles and at 400 °C a metal-Zn alloy is formed both being detrimental to activity. In this sense, a compromise between both trends seems to be reached at

temperatures of 200–300 °C. Reactivity order followed the sequence Rh > Pt > Pd and ME systems were found to be comparatively more selective to acetol than DP solids. This could be due to some remaining surfactant in the surroundings of metallic particles thus limiting their hydrogenation activity. Moreover, metal seems to participate both in dehydration of glycerol to acetol and the subsequent reduction to 1,2-PDO.

Acknowledgements

The authors are thankful to Junta de Andalucia and FEDER funds (P07-FQM-02695, P08-FQM-3931 and P09-FQM-4781 projects) for financial support. SCAI at the University of Cordoba is also acknowledged for ICP-MS measurements and the use of TEM and XPS. Finally, the authors are grateful to COST Action CM0903 for financial support, including a short-term scientific mission (STSM) of V. Montes.

References

[1] Z. Yuan, P. Wu, J. Gao, X. Lu, Z. Hou, X. Xheng, Catal. Lett. 130 (2009) 261–265.
[2] M.H. Mohamad, R. Awang, W.M.Z.W. Yunus, Am. J. Appl. Sci. 8 (2011) 1135–1139.
[3] F. Vila, M. López Granados, M. Ojeda, J.L.G. Fierro, R. Mariscal, Catal. Today 187 (2012) 122–128.
[4] Z. Huang, F. Cui, J. Xue, J. Zuo, J. Chen, C. Xia, Catal. Today 183 (2012) 42–51.
[5] I. Gandarias, P.L. Arias, J. Requies, M. El Doukkali, M.B. Güemez, J. Catal. 282 (2011) 237–247.
[6] F. Auneau, S. Noël, G. Aubert, M. Besson, L. Djakovitch, C. Pinel, Catal. Commun. 16 (2011) 144–149.
[7] N. Hamzah, N.M. Nordin, A.H.A. Nadzri, Y.A. Nik, M.B. Kassim, M.A. Yarmo, Appl. Catal. A 419/420 (2012) 133–141.
[8] C. Montassier, J.C. Ménézo, L.C. Hoang, C. Renaud, J. Barbier, J. Mol. Catal. 70 (1991) 99–110.
[9] K. Tomishige, Catal. Sci. Technol. 1 (2011) 179–190.
[10] T. Miyazawa, Y. Kusunoki, K. Kunimori, K. Tomishige, J. Catal. 240 (2006) 213–221.
[11] F. Auneau, C. Michel, F. Delbecq, C. Pinel, P. Sautet, Chem. Eur. J. 17 (2011) 14288–14299.
[12] J. Chaminand, L. Djakovitch, P. Gallezot, P. Marion, C. Pinel, C. Rosier, Green Chem. 6 (2004) 359–361.
[13] R. Rodrigues, N. Isoda, M. Gonçalves, F.C.A. Figueiredo, D. Mandelli, W.A. Carvalho, Chem. Eng. J. 198/199 (2012) 457–467.
[14] M. Checa, F. Auneau, J. Hidalgo-Carrillo, A. Marinas, J.M. Marinas, C. Pinel, F.J. Urbano, Catal. Today 196 (2012) 91–100.
[15] M. Boutonnet, Curr. Opin. Colloid Interface Sci. 13 (2008) 270–286.
[16] M. Boutonnet, J. Kizling, P. Stenius, Colloids Surf. 5 (1982) 209–225.
[17] C. Destrée, J.B. Nagy, Adv. Colloid Interface Sci. 123–126 (2006) 353–367.
[18] I. Capek, Adv. Colloid Interface Sci. 110 (2004) 49–74.
[19] J.B. Nagy, A. Gourgue, E.G. Derouane, Stud. Surf. Sci. Catal. 16 (1983) 193–202.
[20] W. Suprun, M. Lutecki, T. Haber, H. Papp, J. Mol. Catal. A 309 (2009) 71–78.
[21] P. Carniti, A. Gervasini, M. Marzo, Catal. Commun. 12 (2011) 1122–1126.
[22] A.K. Kinage, P.P. Upare, P. Kasinathan, Y.K. Hwang, J.S. Chang, Catal. Commun. 11 (2010) 620–623.
[23] W. Suprun, M. Lutecki, R. Gläser, H. Papp, J. Mol. Catal. A 342/343 (2011) 91–100.
[24] W. Suprun, M. Lutecki, H. Papp, Chem. Eng. Technol. 34 (2011) 134–139.
[25] Y.T. Kim, K.-D. Jung, E.D. Park, Appl. Catal. B 107 (2011) 177–187.
[26] K. Kongpatpanich, T. Nanok, B. Boekfa, M. Probst, J. Limtrakul, Phys. Chem. Chem. Phys. 13 (2011) 6462–6470.
[27] M.R. Nimlos, S.J. Blanksby, X. Qian, M.E. Himmel, D.K. Johnson, J. Phys. Chem. A 110 (2006) 6145–6156.
[28] S. Sato, M. Akiyama, R. Takahashi, T. Hara, K. Inui, M. Yokota, Appl. Catal. A 347 (2008) 186–191.
[29] A. Bienholz, H. Hofmann, P. Claus, Appl. Catal. A 391 (2011) 153–157.
[30] I. Gandarias, P.L. Arias, J. Requies, M.B. Güemez, J.L.G. Fierro, Appl. Catal. B 87 (2010) 248–256.
[31] S. Wang, H. Liu, Catal. Lett. 117 (2007) 62–67.
[32] Z. Zhou, X. Li, T. Zeng, W. Hong, Z. Cheng, W. Yuan, Chin. J. Chem. Eng. 18 (2010) 384–390.
[33] J. Hidalgo-Carrillo, M.A. Aramendía, A. Marinas, J.M. Marinas, F.J. Urbano, Appl. Catal. A 385 (2010) 190–200.
[34] K.S. Kim, C.M. Ryu, C.S. Park, G.S. Sur, C.E. Park, Polymer 44 (2003) 6287–6295.

Catalysis Today xxx (2014) xxx–xxx

Contents lists available at ScienceDirect

Catalysis Today

journal homepage: www.elsevier.com/locate/cattod

Selective transformation of glycerol into 1,2-propanediol on several Pt/ZnO solids: Further insight into the role and origin of catalyst acidity

V. Montes[a], M. Boutonnet[b], S. Järås[b], A. Marinas[a,*], J.M. Marinas[a], F.J. Urbano[a]

[a] Organic Chemistry Department, University of Córdoba, Campus de Excelencia Internacional Agroalimentario, ceiA3, Marie Curie Building, E-14014 Córdoba, Spain
[b] KTH (Royal Institute of Technology), Chemical Technology, Teknikringen 42, SE-100 44 Stockholm, Sweden

ARTICLE INFO

Article history:
Received 9 May 2014
Received in revised form
11 September 2014
Accepted 3 November 2014
Available online xxx

Keywords:
Glycerol transformation
Microemulsion technique
Pt/ZnO
1,2-Propanediol
Role of acid sites
Effect of chlorine

ABSTRACT

Microemulsion technique allowed us to synthesize different ZnO solids with similar particle sizes and textural properties. Platinum was subsequently incorporated by deposition–precipitation and impregnation methods and solids tested for glycerol selective transformation into 1,2-PDO. Incorporation of platinum led to the creation of new (mainly Lewis) acid sites. A good correlation between conversion and acidity of Pt/ZnO solids was obtained. Interestingly, despite exhibiting some acidity, supports alone were inactive in the process which evidenced the role of the metal in dehydration of glycerol into acetol. Furthermore, as the reaction proceeded some chlorine coming from the precursor (H_2PtCl_6) was leached which led to the disappearance of the strongest acid sites, associated to side reactions (catalytic cracking) thus resulting in an increase in selectivity to 1,2-PDO. Eventual formation of Pt–Zn alloy upon reduction of the systems at ca. 400 °C was beneficial to 1,2-PDO selectivity.

1. Introduction

Glycerol is a by-product from biodiesel production (ca. 100 kg of glycerol per ton of biodiesel produced). Therefore, its valorization through transformation into other valuable chemicals is of great interest. One of those valuable products is 1,2-propanediol (1,2-PDO), which is used in food industry, as a less toxic alternative to 1,2-ethanediol in antifreeze and as a deicer or as a feedstock in the preparation of polyester resins, just to cite some examples of applications [1]. This chemical is traditionally obtained through the petrochemical route via hydration of propylene oxide. Alternatively, 1,2-PDO could be produced through a biomass route from glycerol via dehydration of primary hydroxyl group (thus forming acetol) followed by hydrogenation of acetol into 1,2-PDO [2].

There are different features affecting activity and selectivity of glycerol transformation on metals, such as the metal of choice (e.g. Pt [3,4], Rh [5,6], Pd [5,7], Ir [8], Cu [9–11]) the addition of a second metal [12,13], of acid or basic additives [5,14], the metal particle size [15,16] or the support [17,18], just to cite some of them.

As for the mechanistic studies, there are some discrepancies in the literature concerning the nature of active sites responsible for selective transformation of glycerol into 1,2-PDO, in particular for initial dehydration of glycerol into acetol. Selective dehydroxylation of polyols can proceed through 3 different mechanisms. (i) E1 (acid-catalyzed), involving protonation of a hydroxyl group which is then expelled as water, the resulting carbocation being neutralized by the elimination of a neighboring proton; (ii) E2 (base-catalyzed) involving simultaneous H^+ removal, loss of the OH and formation of C=C bond and (iii) homolytic cleavage of a C—O bond on a metallic surface (hydrogenolysis). Therefore, on acidic systems E1 mechanism is followed. In principle, dehydration of glycerol could take place through the primary or the secondary hydroxyl group, the former being thermodynamically favored [19].

According to Zhu et al. [20] Brønsted acid sites catalyze 1,3-propanediol formation whereas Lewis acid sites lead to 1,2-propanediol. On the contrary, Peng et al. [21] speculate on Brønsted acid sites being responsible for glycerol dehydration processes in aqueous medium given the fact that Lewis acid sites would be converted into Brønsted centers. As for the strength needed for the process, in a study on gas phase hydrogenolysis of glycerol

* Corresponding author. Tel.: +34 957218622; fax: +34 957212066.
E-mail address: alberto.marinas@uco.es (A. Marinas).

http://dx.doi.org/10.1016/j.cattod.2014.11.014
0920-5861/

catalyzed by Cu/ZnO/MO*x* (MO*x* = Al_2O_3, TiO_2, and ZrO_2) solids, Feng et al. [22] concluded that strong acid sites were responsible for 1,2-PDO formation whereas weak acid sites led to 1,3-PDO. In the liquid phase, Vasiliadou et al. [18] found that moderate acid sites are sufficient to activate glycerol dehydration. Finally, some studies give support to the role of the metal not only in hydrogenation of acetol but also in glycerol activation [18,23,24].

In a previous paper, a screening of different partially reducible oxides to be used as supports for platinum was described, ZnO being selected for subsequent studies [4]. Moreover, systems reduced at 200 °C exhibited better catalytic performance than those reduced at 400 °C, a temperature at which Pt–Zn alloy was formed which was detrimental to activity. In a follow-up study [24], different solids consisting in a noble metal supported on ZnO were synthesized through the microemulsion method. This allowed us to obtain quite similar metal (Pt, Rh, Pd) particle sizes. Under our experimental conditions, reactivity followed the order Rh > Pt > Pd. Furthermore, the presence of some remaining surfactant seemed to somehow hinder hydrogenation activity of the metal, thus leading to an unusually high selectivity to acetol.

In the present paper, the good control of particle size ensured through microemulsion (ME) technique is used to synthesize diverse ZnO solids (either alone or modified with Al, Ce or Zr) with a view to tune acidity of the support. Platinum is subsequently incorporated onto the systems through deposition–precipitation technique or impregnation from H_2PtCl_6 aqueous solutions. For comparative studies, a system starting from a different precursor (platinum nitrate) was also synthesized. The final goal is to cast further light on the nature and origin of active sites responsible for the initial dehydration step of glycerol into acetol.

2. Experimental

2.1. Materials

Synperonic 13/6.5 was a gift from Croda. Zn(II)-2-ethylhexanoate (89%) dissolved in mineral spirit, Al(III)-2-ethylhexanoate, Zr(IV)-2-ethylhexanoate, Ce(IV)-2-ethylhexanoate, and 15% (w/w) Pt(IV) nitrate solution were purchased from Alfa Aesar. 8 wt% of H_2PtCl_6 aqueous solution, ZnO nanopowder, acetone (technical grade), glycerol 99%, 1,2-propanediol 99.5%, 1,3-propanediol 98%, (hydroxyacetone) acetol 95%, ethylenglycol 99.5%, *n*-propanol 99.5%, *n*-hexane > 99%, HCl 33% in water, and NaOH > 99% were purchased from Sigma–Aldrich. Milli-Q water was used for preparation of water solutions.

2.2. Synthesis of the solids

2.2.1. Synthesis of ZnO solids through ME technique

The solids, ZnO (either alone or doped with 5 wt% of Al, Zr or Ce) were synthesized using the commonly known method of oil in water (O/W) microemulsion (ME) [25]. The internal structure of the ME is determined by the relative fractions of three constituents: surfactant, oil and water. The ME is only formed for certain ratios of the constituents, outside which a two-phase system is formed. The first step was to determine the relative fractions of components where the ME was stable. So, different composition mixtures of surfactant and water were prepared at different temperatures. Then a solution of organometallic precursor was added dropwise in order to know the maximum soluble amount. Determination of this amount is easy because the microemulsions are isotropic and transparent, and when they destabilize the transparent dissolution turns into a cloudy system. These experiments allowed us to determine the region of relative fractions of constituents to form microemulsion. Under optimized conditions, the composition of microemulsions (ME) was surfactant: synperonic 13/6.5 (18.8 wt%), oil: organic precursor of metal (10 wt% of Zn) dissolved in *n*-hexane (24.5%), water: 56.7 wt%. In the case of doping of ZnO with Al, Ce or Zr, the oil is formed by 10 wt% Zn + (Al, Ce or Zr). Moreover, Al, Ce or Zr content was calculated to have 5 wt% of these metals in the resulting ZnO solid.

Once the microemulsion had been obtained in the presence of the Zn(II) ethylhexanoate aqueous solution, pH was increased up to 11 with NH_4OH in order to precipitate ZnO [26]. Resulting solids were aged under stirring for 7 h, centrifuged and carefully washed with 3 portions of 100 mL *n*-hexane. The solids were dried at 70 °C for 12 h and calcined at 400 °C for 2 h at a rate of 10 °C/min with a synthetic air flow of 2 L/h.

For comparative purposes, a commercial ZnO solid was also used as the support in the present study.

2.2.2. Incorporation of platinum

2.2.2.1. Deposition precipitation method. The synthetic procedure was as follows: a volume of 6.57 mL of chloroplatinic acid solution (or 1.67 mL of $Pt(NO_3)_4$ solution) was diluted to 200 mL with Milli-Q water and adjusted to pH 7 by adding 0.1 M NaOH. Then, an amount of 4.75 g of support was added and the mixture readjusted to pH 7 with 0.1 M HCl. The solution containing the support was refluxed at 70 °C under vigorous stirring for 2 h. Then, a volume of 10 mL of isopropanol was added, the temperature raised to 110 °C and refluxing continued for 30 min, after which the mixture was vacuum filtered and the filtrate washed with 3 portions of 25 mL of water each. The resulting solid was dried in a muffle furnace at 110 °C for 12 h, ground and calcined at 400 °C for 4 h with a rate of 1 °C/min. After calcination, the solid was ground again, sieved through a mesh of 0.149 mm pore size and stored in a flask.

2.2.2.2. Impregnation method. 200 mL of water containing the metal precursor (chloroplatinic acid) was adjusted to pH 7 with NaOH. Then, the corresponding amount of ZnO solid (in order to obtain 5 wt% Pt/ZnO in final systems) was suspended and pH readjusted to 7 with HCl. Suspensions were stirred for 5 h at room temperature and then the solvent was rota-evaporated and calcined at 400 °C. After calcination, the solid was ground, sieved through a mesh of 0.149 mm pore size and stored in a flask.

The nomenclature of the solids includes an N or Cl prefix indicating the platinum precursor (platinum nitrate or chloroplatinic acid, respectively), followed by the method of incorporation (dp or im for deposition–precipitation or impregnation, respectively) and the origin of the ZnO used (com or ME for commercial or synthesized through microemulsion, respectively). In the latter case, when applicable, Al, Ce or Zr refers to the metal doping ZnO. Finally, the name is followed by the reduction treatment. Therefore, for instance, a catalyst synthesized by deposition–precipitation method from chloroplatinic acid on an Al-doped ZnO solid synthesized through microemulsion and pre-reduced at 200 °C is denoted as Cl-dp-ME-Al-200 whereas N-dp-com-unred would indicate that platinum nitrate was incorporated on a commercial ZnO through deposition–precipitation method and tested in the reaction without any reduction pre-treatment.

2.3. Characterization

Elemental analysis of metal-containing samples was performed by the staff at the Central Service for Research Support (SCAI) of the University of Córdoba. It was performed using inductively coupled plasma mass spectrometry (ICP-MS). Measurements were made on a Perkin-Elmer ELAN DRC-e instrument following dissolution of the sample in a 1:3 HNO_3/HCl mixture with a soft heating. Calibration was done by using PE Pure Plus atomic spectroscopy standards, also from Perkin-Elmer.

Please cite this article in press as: V. Montes, et al., Selective transformation of glycerol into 1,2-propanediol on several Pt/ZnO solids: Further insight into the role and origin of catalyst acidity, Catal. Today (2014), http://dx.doi.org/10.1016/j.cattod.2014.11.014

Thermogravimetric analyses (TGA–DTA) were performed on a Setaram SetSys 12 instrument. An amount of 20 mg of sample was placed in an alumina crucible and heated at temperatures from 30 to 1000 °C at a rate of 10 °C/min under a stream of synthetic air at 40 mL/min in order to measure weight loss, heat flow and derivative weight loss.

EDX measurements were performed on a JEOL JSM-6300 scanning electron microscope (SEM) equipped with an energy-dispersive X-ray (EDX) detector. It was operated at an acceleration voltage of 20 keV with a resolution of 65 eV.

Surface areas of the solids were determined from nitrogen adsorption–desorption isotherms obtained at liquid nitrogen temperature on a Micromeritics ASAP-2010 instrument, using the Brunnauer–Emmett–Teller (BET) method. All samples were degassed to 0.1 Pa at 120 °C prior to measurement.

Transmission electron microscopy (TEM) images were obtained using a JEOL JEM 1400 microscope. All samples were mounted on 3 mm holey carbon copper grids. Particle sizes were obtained by counting 100 particles.

X-ray patterns of the samples were obtained on a Siemens D-5000 diffractometer equipped with a DACO-MP automatic control and data acquisition system. The instrument was equipped with a graphite monochromator and used Cu Kα radiation. Metal particle sizes were calculated using Scherrer equation.

X-ray photoelectron spectroscopy (XPS) data were recorded on 4 mm × 4 mm pellets 0.5 mm thick that were obtained by gently pressing the powdered materials following outgassing to a pressure below about 2×10^{-8} Torr at 150 °C in the instrument pre-chamber to remove chemisorbed volatile species. The main chamber of the Leibold–Heraeus LHS10 spectrometer used, capable of operating down to less than 2×10^{-9} Torr, was equipped with an EA-200MCD hemispherical electron analyser with a dual X-ray source using AlKα ($h\nu$ = 1486.6 eV) at 120 W, at 30 mA, with C (1s) as energy reference (284.6 eV).

Temperature-programmed reduction (TPR) measurements were made with a Micromeritics TPD-TPR 2920 analyser. An amount of 100 mg of catalyst was placed in the sample holder and reduced in a 10:90 H_2/Ar stream flowing at 20 mL/min. The temperature was ramped from 50 to 350 °C.

Surface acidity in the catalysts were determined by thermal programmed desorption (TPD) of a pre-adsorbed probe molecule, pyridine (Py) monitored by TCD. An amount of 50 mg of sample was placed under a He stream flowing at 75 mL/min in a reactor 10 mm in diameter that was placed inside an oven. The He stream was used to clean the solids by heating to 350 °C at a rate of 10 °C/min and then cooling to 50 °C. At that point, the surface of the solid was saturated with the Py for 30 min. Pyridine was supplied by bubbling the He stream through liquid pyridine at room temperature over the samples. After saturation, excess physisorbed Py was removed increasing the temperature up to 50 °C and passing a He stream at 75 mL/min for 60 min. Then temperature was increased up to 400 °C at 10 °C/min, holding the final level for 30 min. Desorbed pyridine was quantified against a calibration graph previously constructed from variable injected volumes of pyridine.

The above-described overall acidity study by TPD-Py was supplemented with one by diffuse reflectance infrared (DRIFT) spectroscopy of the pyridine-saturated solids intended to identify the specific types of acid sites present. Measurements were made with an ABB Bomen MB Series IR spectrophotometer equipped with a SpectraTech P/N 0030-100 environmental chamber including a diffuse reflectance device capable of performing 258 scans at 8 cm^{-1} resolution at an adjustable temperature. Prior to analysis, each catalyst was thermally cleaned at 400 °C for 30 min. The last few minutes of the thermal treatment were used to record reference spectra.

2.4. Catalytic tests

Hydrogenolysis of glycerol was conducted in a Berghof HR-100 stainless steel high-pressure autoclave equipped with a 75 mL PTFE vessel and a magnetic stirrer. Under standard conditions, 10 mL of a 1.36 M solution of glycerol in water and 100 mg catalysts were introduced in the vessel. Reactor was then purged with the selected atmosphere (H_2 or N_2), and temperature (180 °C) and pressure (2 or 6 bar) adjusted. The stirring rate was 1200 rpm. After 15 h of reaction, stirring was stopped and the vessel cooled with an ice bath. The reaction mixture was centrifuged to separate the catalyst and the liquid passed through a filter of PTFE 0.45 μm. Then it was analyzed by GC-FID (Agilent Technologies 7890, with a Supelco 25357 NukolTM capillary column). Quantification was carried out through the corresponding calibration curves.

3. Results and discussion

3.1. Characterization of support

TG-DTA profiles of all uncalcined solids obtained through ME method are quite similar. Fig. 1 shows that of ME system. There are two main weight losses centered at ca. 140 °C and 330 °C, respectively. The first one could be due to water whereas the second one could be attributed to the decomposition of remaining organic compounds (e.g. surfactant, organic precursor) [27,28]. In fact, the loss weight % (41.6%) is much higher than the theoretical one corresponding to the conversion of $Zn(OH)_2$ into ZnO (ca. 18.1%) thus evidencing the presence of remaining organics. Interestingly, there is no significant weight loss at temperatures above calcination temperature (400 °C). In fact, TG-DTA profile of the solid calcined at 400 °C (Fig. 1) did not exhibit any weight loss thus ensuring thermal stability of the obtained solid.

The main features concerning characterization of the supports are given in Table 1. As can be seen, and as expected, ME method ensured quite similar particle sizes (22–26 nm) for all ZnO-based solids, BET surface areas being in the 27–36 m^2/g range. For comparative purposes, commercial ZnO solid has also being included in Table 1, its surface area being significantly lower (15 m^2/g). In all

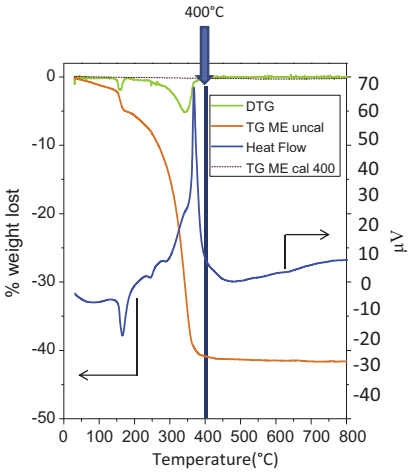

Fig. 1. TG-DTA profile obtained in synthetic air for the ME uncalcined system. Dotted line corresponds to weight loss of ME calcined at 400 °C.

Please cite this article in press as: V. Montes, et al., Selective transformation of glycerol into 1,2-propanediol on several Pt/ZnO solids: Further insight into the role and origin of catalyst acidity, Catal. Today (2014), http://dx.doi.org/10.1016/j.cattod.2014.11.014

Table 1
Some features concerning characterization of ZnO supports.

Support	N_2 isotherms		Particle size diameter (XRD)	Metal content (%)			Acidity (μmol py per mg catalyst)
	BET area (m^2/g)	Mean pore diameter (nm)		ICP-MS	EDX	XPS	
Com	15	11	50	–	–	–	0.05
ME	29	8	26	–	–	–	0.08
ME-Al	27	9	23	0.36	0.46	1.65	0.15
ME-Ce	31	7	22	0.53	3.67	3.44	0.15
ME-Zr	36	8	24	0.19	1.26	1.61	0.12

cases, ZnO-systems are mesoporous solids, with mean pore diameters ranging 7–11 nm. As regards elemental analyses of samples, bulk analyses (ICP-MS and EDX) reveal that the metals (Al, Ce or Zr) have been incorporated below the nominal value (5 wt%). One possible reason could be the partial re-dissolution of precipitated hydroxides at the high pH (11) used in the synthesis [29,30]. X-ray diffractograms of ZnO supports (not shown) revealed that in all cases ZnO have a zincite (wurzite) structure with the typical peaks at 2θ values of 31.7, 34.4, 36.2° corresponding to (1 0 0), (0 0 2) and (1 0 1) reflections, respectively [31]. No signals corresponding to ceria, zirconia or alumina were observed which is hardly surprising considering the above-mentioned low incorporation. Acidity of the solids was determined by TPD of pre-adsorbed pyridine (Table 1). Interestingly, despite the relatively low metal-doping content, incorporation of Al, Ce or Zr led to a significant increase in acidity, in the 50–88% range. Moreover, acidity of commercial ZnO solid is lower than that of the pure ZnO system obtained through microemulsion technique. No change in acidity of the supports was observed after treatment under H_2 flow for 2 h at 200 °C or 400 °C.

3.2. Characterization of platinum-containing solids

Some features concerning characterization of Pt-containing systems are summarized in Table 2. ICP-MS results confirm a good incorporation of platinum, quite close to the nominal content (5 wt%).

XRD profiles of the samples (Fig. 2) reveal that in general, reduction at 200 °C results in the appearance of a band at ca. 39.8° attributed to (1 1 1) crystal plane of the Pt^0 face-centered-cubic phase [32] whereas subsequent reduction at 400 °C leads to the shift of the band to higher 2θ values (ca. 40.9°) which is indicative of the formation of Pt–Zn alloy [4,33]. The exceptions are Cl-dp-ME-Ce and Cl-im-com systems. In the former case, unred system already exhibits a signal at ca. 39.8° which could be indicative of some kind of Pt–support interaction (Pt–Zn or Pt–Ce [34]). In the latter case, Pt–Zn alloy seems to be already present in the solid reduced at 200 °C (see signal at ca. 45.9°). In any case, the influence of other factors on the appearance of Pt bands (e.g. metal particle size, oxidation state) should be studied by other techniques (e.g. TEM, XPS).

H_2 TPR profiles are shown in Fig. 3. There are different factors affecting reducibility of metal particles such as size, the metal environment (e.g. presence of chloride species coming from the precursor) or when using partially reducible oxides as the support, as it is the case of the present study, existence of strong metal–support interactions [35–37]. Therefore, smaller metal particles are more difficult to be reduced than larger ones thus resulting in a shift to higher temperatures in the TPR profile. Moreover, the presence of chloride ions at the metal–support interface has been described to hinder electron exchange between the metal and the oxide support thus leading to higher reduction temperatures. Finally, reduction peaks appearing at the highest reduction temperatures are typically associated to those platinum particles strongly interacting with the support. Fig. 3 confirms that at the temperature selected for catalytic experiments (180 °C) all systems are reduced. Furthermore, TPR signals of all the systems obtained through ME exhibit a single relatively narrow peak which suggests a homogeneous platinum particle size distribution. As regards the solids based on commercial ZnO, results suggest the influence of both the synthetic method and the metal precursor on metal dispersion. Therefore, a more homogeneous distribution of platinum particle sizes would be expected for Cl-dp-com than for Cl-im-com judging by the narrower TPR peak in the former case. Comparing the effect of the employed Pt precursors (Cl-dp-com vs N-dp-com), larger and more heterogeneous in size platinum particles seem to have been obtained from platinum nitrate, as suggested by the wider TPR profile appearing at lower reduction temperatures. The influence of chlorine residues shifting TPR peaks to higher temperatures in the case of Cl-dp-com, cannot be ruled out. TEM micrographs (Figs. 4–6) cast further light on these issues. The first conclusion that can be drawn from this study is that the average particle sizes for the samples reduced at 200 °C are quite similar for all types of solids (in the 1.3–2.0 nm range, Table 2), the exception being N-dp-com for which larger metal particles (2.8 nm, Fig. 6) were obtained. This could be ascribed to the different metal precursor used and is in line with TPR profiles which evidenced an easier reduction of platinum particles in that solid. If TEM figures of Cl-im-com-200 and Cl-dp-com-200 are compared (Fig. 5), quite similar particle size distributions are obtained. This suggests that above-commented observed differences in TPR and XRD profiles could be ascribed to different metal–support interactions. Finally, in all cases, increase in reduction temperature from 200 °C up to 400 °C resulted in metal sintering.

Table 2
Some features concerning characterization of the different Pt/ZnO solids.

Catalyst	Pt (wt%)		Average Pt particle size (TEM, nm)		Total acidity (μmol py/mg catalyst)			
	ICP-MS	EDX	200	400	Unred	200	400	Used
Cl-dp-com	4.2	2.7	1.9	3.6	0.23	0.14	0.14	0.11
Cl-dp-ME	4.7	3.0	1.8	3.0	0.29	0.20	0.14	0.15
Cl-dp-ME-Al	4.5	3.9	1.7	3.3	0.35	0.21	0.17	0.13
Cl-dp-ME-Ce	6.1	4.0	1.3	2.2	0.30	0.16	0.15	0.11
Cl-dp_ME-Zr	4.8	5.5	1.5	3.2	0.47	0.31	0.16	0.12
Cl-im-com	4.5	2.9	2.0	3.3	0.20	0.11	0.08	0.0
N-dp-com	4.3	6.0	2.8	4.2	0.07	0.06	0.07	0.0

Please cite this article in press as: V. Montes, et al., Selective transformation of glycerol into 1,2-propanediol on several Pt/ZnO solids: Further insight into the role and origin of catalyst acidity, Catal. Today (2014), http://dx.doi.org/10.1016/j.cattod.2014.11.014

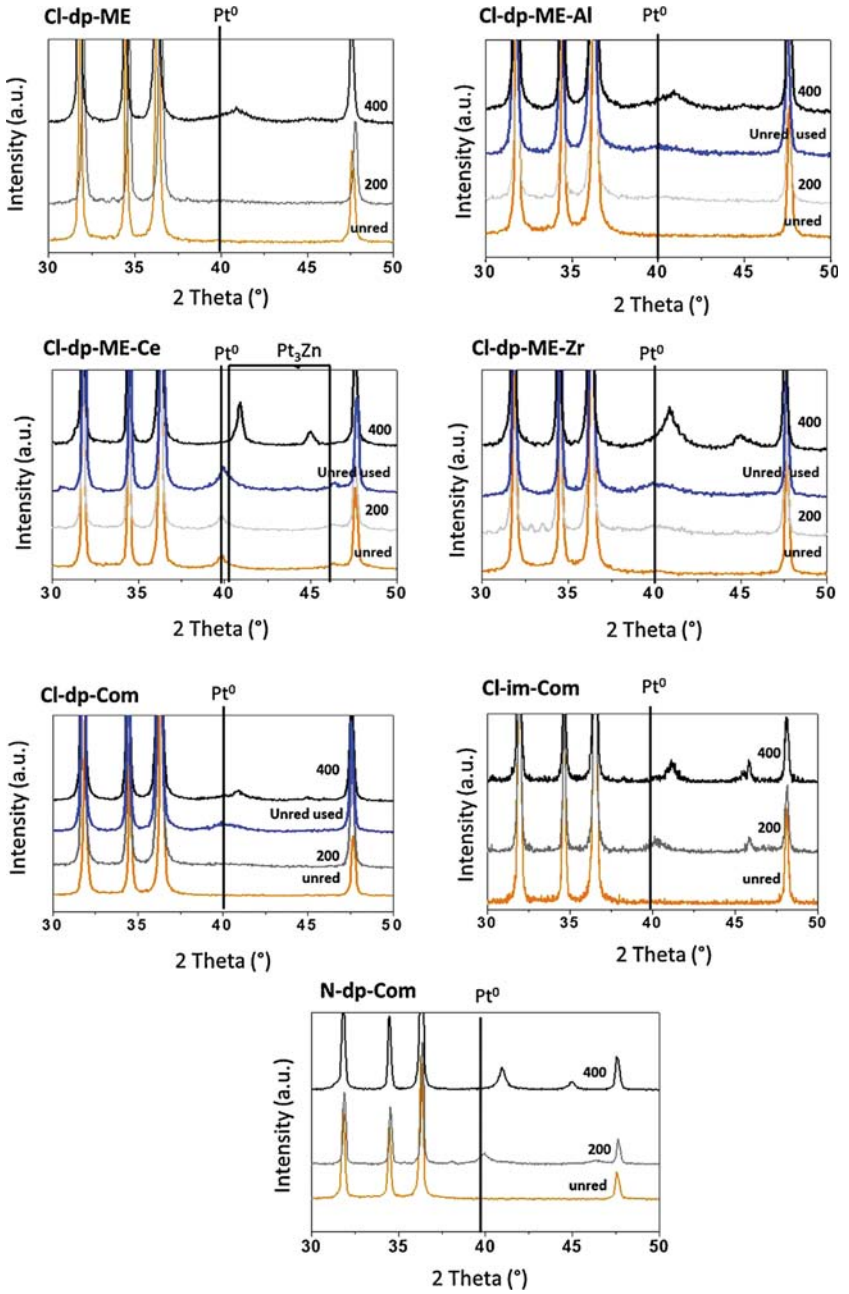

Fig. 2. X-ray diffractograms of the different Pt/ZnO systems unreduced or reduced at 200 °C and 400 °C. In some cases the profiles of unreduced systems after 15 h of reaction have also been included.

Please cite this article in press as: V. Montes, et al., Selective transformation of glycerol into 1,2-propanediol on several Pt/ZnO solids: Further insight into the role and origin of catalyst acidity, Catal. Today (2014), http://dx.doi.org/10.1016/j.cattod.2014.11.014

XPS spectra of unreduced samples in the Zn $2p_{3/2}$ region showed a peak centered at ca. 1022 eV which can be ascribed to ZnO. In the case of solids obtained from H_2PtCl_6, reduction at 200 °C resulted in the appearance of a second peak at ca. 1023 eV whose relative intensity decreased upon subsequent reduction at 400 °C (see Fig. 7). This second peak can be associated to oxychlorinated Zn^{2+} species [38]. As regards Pt $4f_{5/2}$, unreduced systems are formed by Pt^{2+} (72.4–72.8 eV) and Pt^{4+} (73.7–74.9 eV) whereas no signals corresponding to Pt^0 at ca. 70.6–71.0 eV were observed. Interestingly, the highest Pt^{2+} percentage (ca. 44%) corresponded to Cl-dp-ME-Ce solid which could be ascribed to Ce interacting with Pt (remember XRD profiles, Fig. 2). Reduction of the solids at 200 °C resulted in the formation of Pt^0 which is concordant with XRD and TPR profiles. As regards XPS spectra of metal-doping species (Fig. 8), Al 2s signals of Cl-dp-ME-Al unreduced and reduced at 200 and 400 °C remained at 118.5 eV which suggests an Al_2O_3 environment [39]. Similarly, Zr $3d_{5/2}$ signal of Cl-dp-ME-Zr-unred, 200 and 400 °C solids appeared at 182 eV which suggests the presence of ZrO_2 [40]. In contrast, Ce $3d_{5/2}$ signal of Cl-dp-ME-Ce-unred solid differed from those of the solid reduced at 200 °C and 400 °C thus suggesting different Ce(III)/Ce(IV) ratios in those samples depending on the reduction treatment [34].

TPD profiles of pre-adsorbed pyridine are depicted in Fig. 9 and acidity data are summarized in Table 2. From Fig. 9 it is evident that the incorporation of platinum using H_2PtCl_6 as the precursor led to the creation of acidity. Therefore, there are two main pyridine

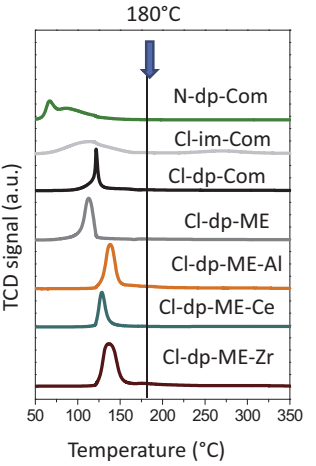

Fig. 3. TPR profiles of the different Pt/ZnO systems. The vertical line indicates reaction temperature in catalytic experiments of glycerol transformation (180 °C).

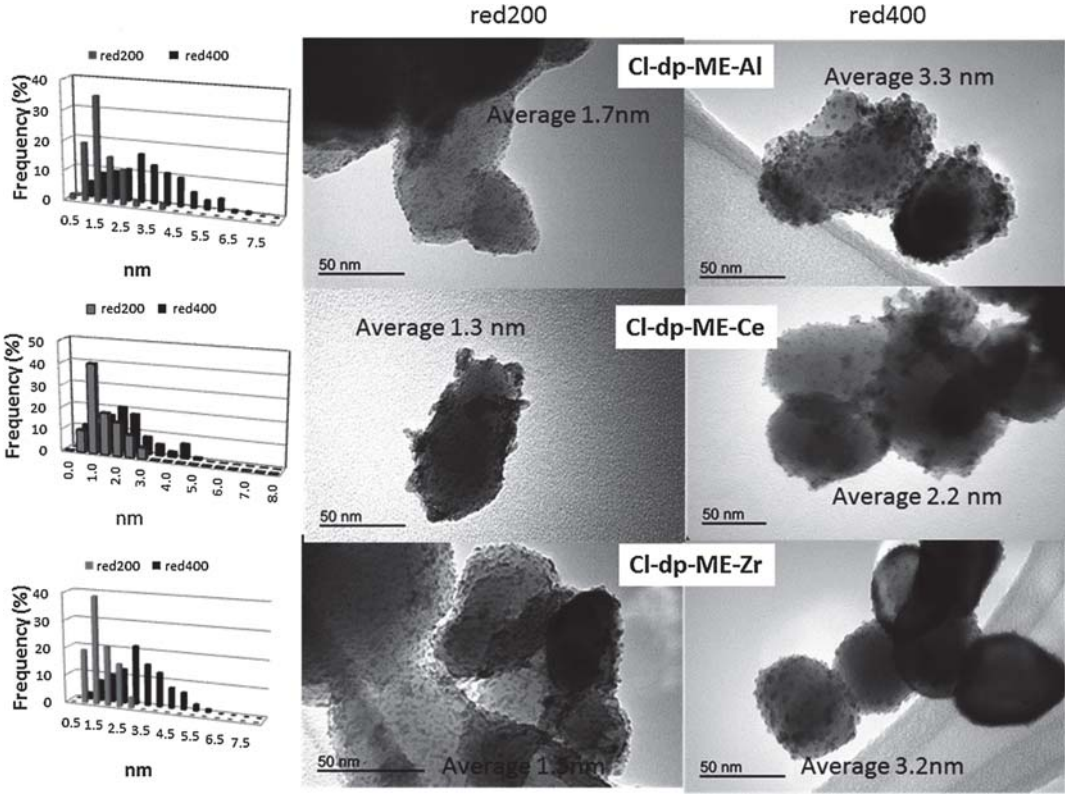

Fig. 4. TEM micrographs of Cl-dp-ME-Al, Cl-dp-ME-Ce and Cl-dp-ME-Zr reduced at 200 and 400 °C.

Please cite this article in press as: V. Montes, et al., Selective transformation of glycerol into 1,2-propanediol on several Pt/ZnO solids: Further insight into the role and origin of catalyst acidity, Catal. Today (2014), http://dx.doi.org/10.1016/j.cattod.2014.11.014

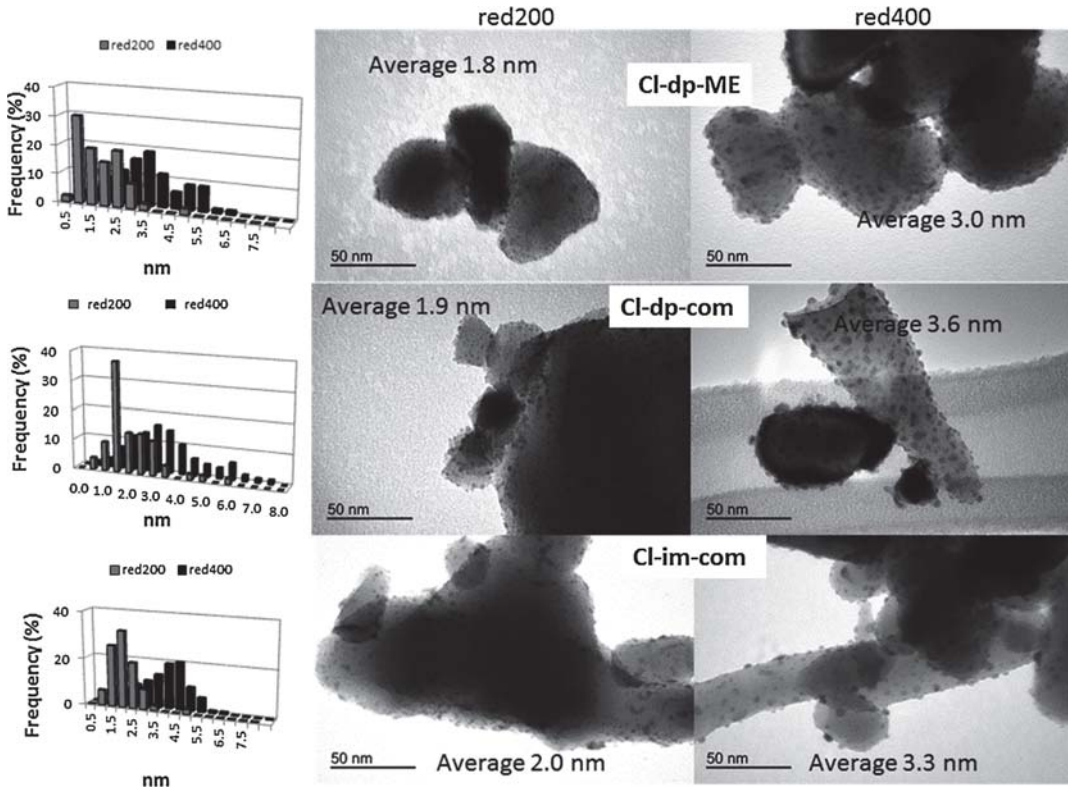

Fig. 5. TEM micrographs of Cl-dp-ME, Cl-dp -com and Cl-im-com reduced at 200 and 400 °C.

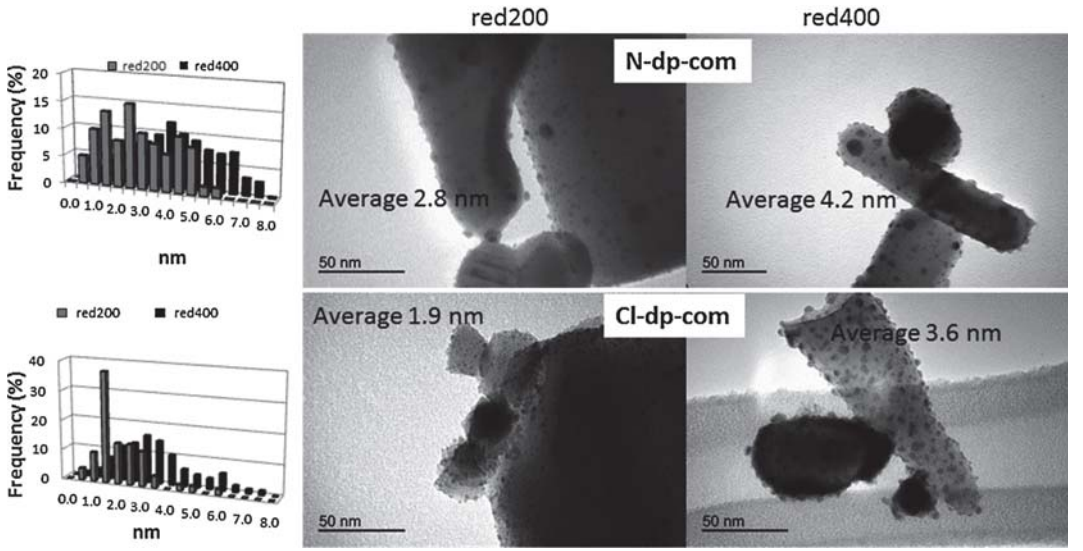

Fig. 6. TEM micrographs of N-dp-com and Cl-dp-com reduced at 200 and 400 °C.

Please cite this article in press as: V. Montes, et al., Selective transformation of glycerol into 1,2-propanediol on several Pt/ZnO solids: Further insight into the role and origin of catalyst acidity, Catal. Today (2014), http://dx.doi.org/10.1016/j.cattod.2014.11.014

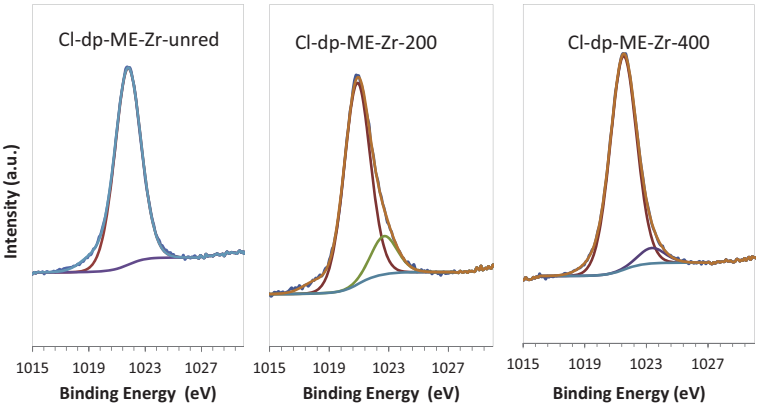

Fig. 7. XPS profiles in the Zn ($2p_{3/2}$) region of Cl-dp-ME-Zr system unreduced and reduced at 200 °C or 400 °C.

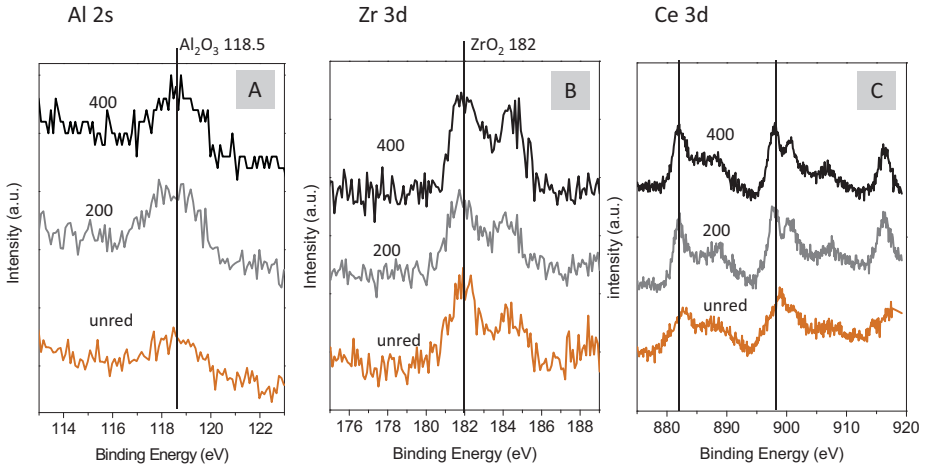

Fig. 8. XPS profiles of Cl-dp-ME-Al (A), Cl-dp-ME-Zr (B) and Cl-dp-ME-Ce (C) unreduced and reduced at 200 °C and 400 °C in the XPS Al (2s). Zr (3d) and Ce (3d) regions, respectively.

desorption peaks centered at ca. 100 °C and 300 °C, respectively. Reduction of the solids at 200 °C results in the disappearance of the high-temperature peak whereas the low-temperature one remains even after reduction at 400 °C. In the case of N-dp-com solid, on the contrary, incorporation of platinum did not result in new acid sites, thus confirming that new acid sites are somehow associated to the presence of chlorine. In order to cast further light on the nature (Lewis or Brønsted) of acid sites, acidity tests were complemented with DRIFT studies. Fig. 10 presents the DRIFT spectra of pyridine chemisorbed on Cl-dp-com solids at different temperatures (100–400 °C) though similar results are obtained for the other systems coming from H_2PtCl_6 precursor. In all cases, the spectra of pyridine adsorbed at 100 °C on unreduced Pt-containing solids exhibit two main bands centered at ca. 1454 and 1610 cm^{-1} which are associated to Lewis acid sites, together with some other minor ones at ca. 1486 (Brønsted + Lewis), 1547 (Brønsted) [41,42]. Acidity of solids reduced at 200 °C is lower (as evidenced by the decrease in intensity of all bands) whereas subsequent reduction at 400 °C hardly changes acidity (which is consistent with Fig. 9). Interestingly, N-dp-com-unred solid also exhibited in DRIFT studies the above-mentioned Lewis acid sites which retained pyridine up to 100 °C whereas no bands due to pyridine adsorption were observed for reduced systems (not shown). All these results suggest that on introduction of platinum (either using H_2PtCl_6 or $Pt(NO_3)_4$ as the precursor) some new acid sites, mainly Lewis-type, are created. In the case of Cl-series some of those sites are kept in reduced solids (probably associated to the presence of chlorine) whereas for N-dp-com reduction at 200 °C leads to their disappearance, which could be due to reduction of Pt(II) and Pt(IV) to Pt^0 as evidenced by XPS and H_2 TPR studies.

3.3. Catalytic activity

Production of 1,2-PDO from glycerol is known to occur via intermediate production of acetol. Therefore, dehydration of primary hydroxyl group in glycerol yields acetol whose hydrogenation leads

Please cite this article in press as: V. Montes, et al., Selective transformation of glycerol into 1,2-propanediol on several Pt/ZnO solids: Further insight into the role and origin of catalyst acidity, Catal. Today (2014), http://dx.doi.org/10.1016/j.cattod.2014.11.014

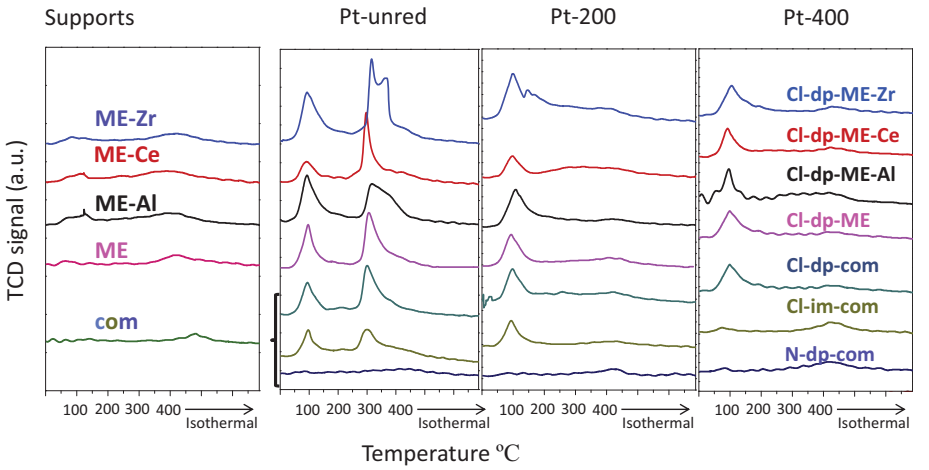

Fig. 9. Temperature-programmed desorption (TPD) profiles of pyridine pre-adsorbed at 50 °C for supports and Pt/ZnO systems (unreduced and reduced at 200 °C and 400 °C).

to 1,2-PDO (Scheme 1). The different catalysts were tested for their activity for glycerol transformation into 1,2-PDO. Under standard conditions (see Section 2.4), supports (unred or reduced at 200 °C or 400 °C) were not active in the process. As for the Pt-containing solids, results obtained for conversion and selectivity after 15 h reaction are summarized in Fig. 11. In terms of conversion, values achieved with unreduced samples are in general quite similar to those obtained for solids reduced at 200 °C. This is hardly surprising since at the working temperature (180 °C) platinum can be in situ reduced (remember TPR profiles). Subsequent reduction at 400 °C led to a dramatic decrease in conversion. Increase in particle size (as evidenced by TEM, Table 2) and formation of Pt–Zn alloy (remember XRD results) could account for that. An additional point to take into account is that total acidity decreases with reduction temperature (see Table 2) which will be further commented in the mechanistic discussion. It is also worth noting that conversion values for N-dp-com systems are significantly lower than those of their Cl-dp-com counterparts which again could be related to the larger particles. In fact, if TOF values (expressed as moles of glycerol converted per mole of Pt per hour) are represented (Fig. 12), N-dp-com and Cl-dp-com perform quite similarly either unreduced and reduced at 200 °C.

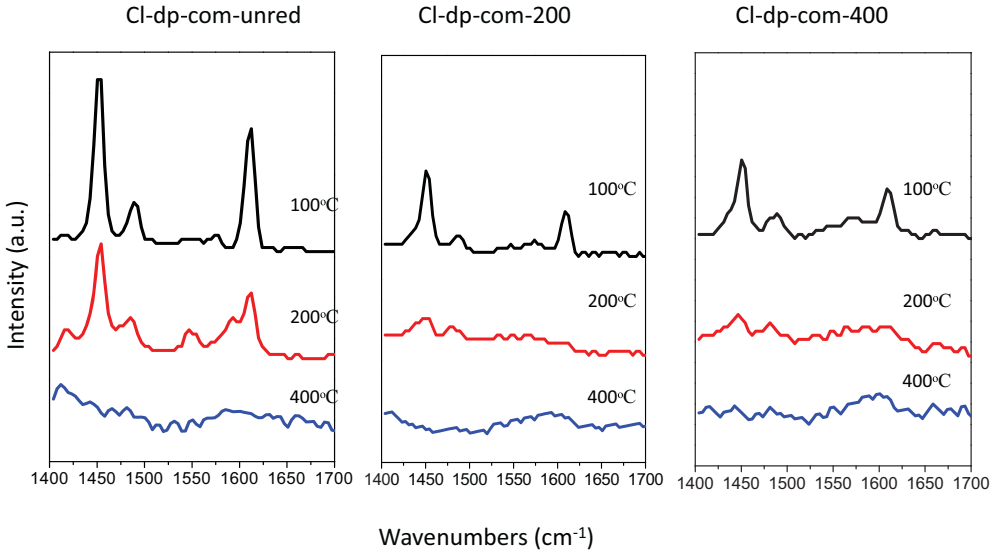

Fig. 10. Diffuse reflectance infrared Fourier transformed spectra (DRIFT) of Cl-dp-com systems saturated with pyridine at 50 °C upon thermal treatment at different temperatures (100, 200 and 400 °C).

Please cite this article in press as: V. Montes, et al., Selective transformation of glycerol into 1,2-propanediol on several Pt/ZnO solids: Further insight into the role and origin of catalyst acidity, Catal. Today (2014), http://dx.doi.org/10.1016/j.cattod.2014.11.014

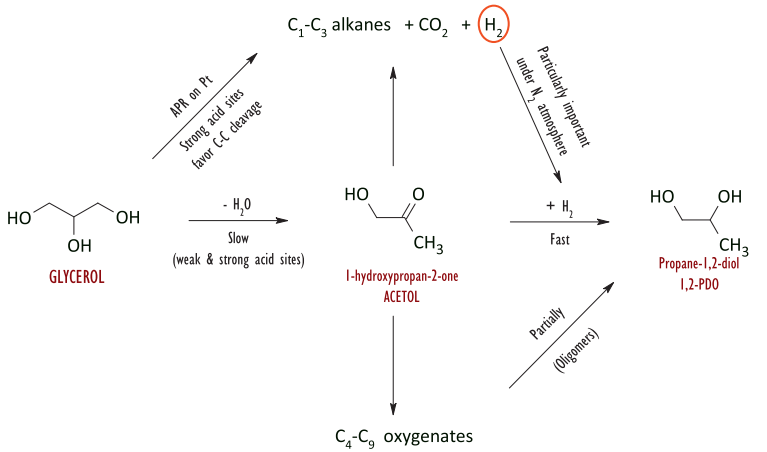

Scheme 1. Mechanism proposed for transformation of glycerol under our experimental conditions.

In terms of TOF, Cl-dp-ME-Zr-unred and Cl-dp-Al-unred (the most acidic solids, as determined by TPD of pre-adsorbed pyridine) are the systems exhibiting the highest values whereas Cl-dp-ME-Ce-unred, for which some kind of Pt–support interaction had already been detected by XRD in unred system and Cl-im-com (which apparently also evidenced Pt–support interaction at lower temperatures than its ME counterparts) are the least active solids. Fig. 13 shows a dependence of conversion on acidity and platinum average particle size. From that figure it is evident that the presence of the metal is necessary for the reaction since supports, despite exhibiting some acidity, are inactive in the reaction. This backs the idea of the metal participating in dehydration of glycerol to acetol.

As far as selectivity to 1,2-PDO is concerned (Fig. 11B), reduction at 400 °C resulted in a significant increase up to values of ca. 90%, the exception being N-dp-com and Cl-im-com. However, appropriate study of effect of reduction temperature on selectivity to 1,2-PDO requires the performance of reactions with unred and 200 systems at lower reaction times in order to get similar conversions to those achieved with solids reduced at 400 °C after 15 h (i.e. selectivity values must be compared at iso-conversions). This will be performed in the following section.

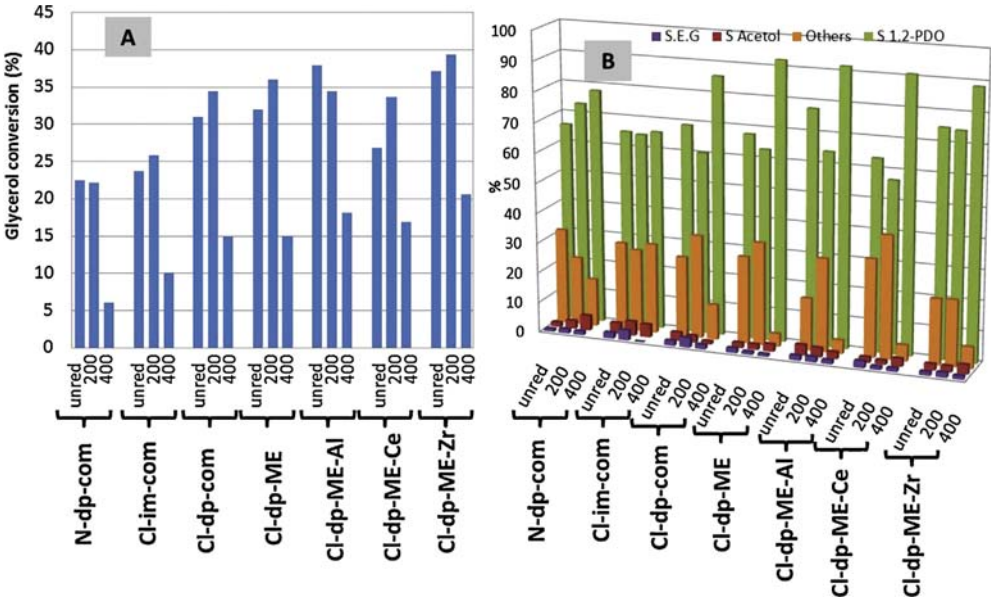

Fig. 11. Results for catalytic transformation of glycerol expressed in terms of conversion (A) and selectivity to ethylene glycol (EG), acetol, 1,2-PDO or others (B) for $t = 15$ h. Reaction conditions: 100 mg catalysts, 10 mL 1.36 M water solution of glycerol. 180 °C and 6 bar of initial hydrogen pressure. Reaction time: 15 h.

Please cite this article in press as: V. Montes, et al., Selective transformation of glycerol into 1,2-propanediol on several Pt/ZnO solids: Further insight into the role and origin of catalyst acidity, Catal. Today (2014), http://dx.doi.org/10.1016/j.cattod.2014.11.014

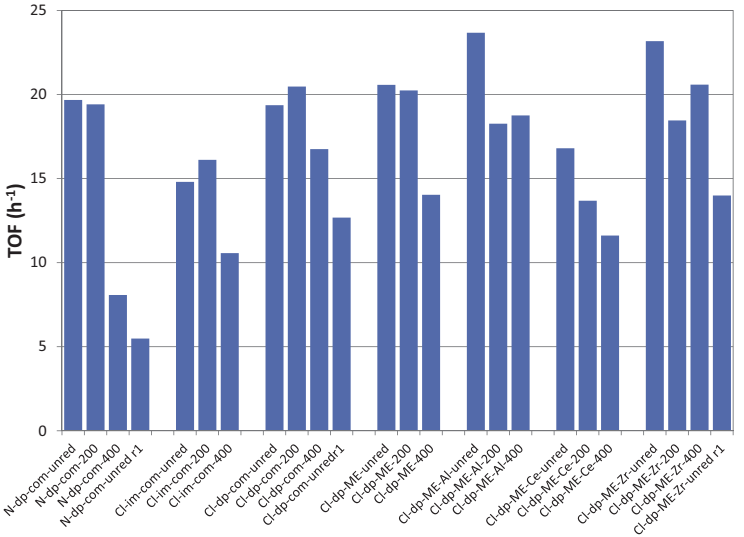

Fig. 12. Results obtained for catalytic transformation of glycerol expressed in terms of turnover frequencies (TOF) for $t = 15$ h. Reaction conditions: 100 mg catalysts, 10 mL 1.36 M water solution of glycerol. 180 °C and 6 bar of initial hydrogen pressure. Reaction time: 15 h. Data correspond to systems unreduced, reduced at 200 °C and 400 °C. In some cases results for the first reutilization of unreduced solids have been included (r1 suffix).

3.4. Mechanistic discussion

In order to cast further light on the process, some further studies were performed and a reaction mechanism suggested (Scheme 1). Firstly, experiments at variable reaction times (1–15 h) were conducted starting from glycerol. The results showed that for Cl-containing solids, the selectivity to 1,2-PDO was particularly low during the first hours of reaction (see data for Cl-dp-com-unred in

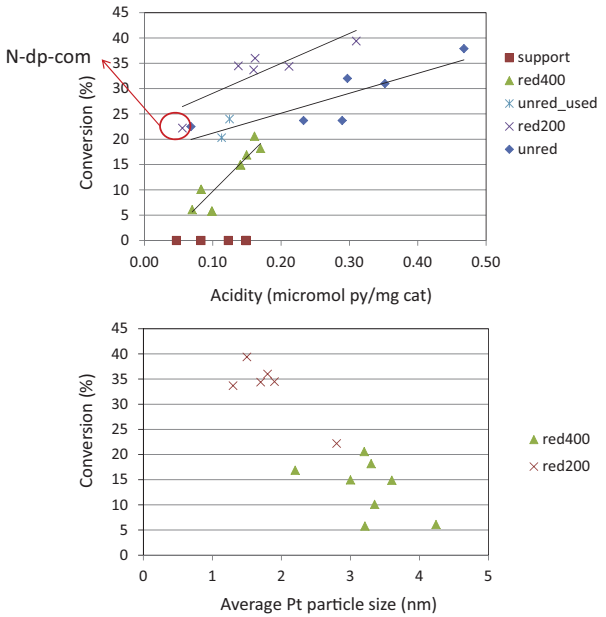

Fig. 13. Glycerol conversion as a function of acidity (micromoles of pyridine per mg of catalyst) or average particle size (in nm, as determined by TEM) for the different catalysts used in the present manuscript. Reaction conditions: 100 mg catalysts, 10 mL 1.36 M water solution of glycerol. 180 °C and 6 bar of initial hydrogen pressure. Reaction time: 15 h.

Please cite this article in press as: V. Montes, et al., Selective transformation of glycerol into 1,2-propanediol on several Pt/ZnO solids: Further insight into the role and origin of catalyst acidity, Catal. Today (2014), http://dx.doi.org/10.1016/j.cattod.2014.11.014

Table 3
Results obtained for glycerol transformation on Cl-dp-com and N-dp-com under standard conditions expressed as glycerol conversion % and selectivity to 1,2-PDO, acetol, ethylene glycol (EG) and other products. In some cases, results for characterization of the solids have been included.

Catalyst	GC-FID					ICP-MS	XPS			TPD pyridine	TEM
	Gly conv	Selectivity 1,2-PDO	Selectivity acetol	Selectivity EG	Selectivity others	% Pt	Pt/Zn	Cl/Pt	Cl/Zn	Acidity (μmol/mg cat)	Particle size (nm)
Cl-dp-com unred (fresh)	–	–	–	–	–	4.2	0.42	0.72	0.29	0.23	1.9
Cl-dp-com unred (1 h)	2.3	35.8	6.5	0.0	57.7	ND	0.28	0.11	0.03	0.11	ND
Cl-dp-com unred (5 h)	10.5	35.0	4.0	2.5	58.5	ND	ND	ND	ND	ND	ND
Cl-dp-com unred (10 h)	24.5	63.0	4.3	1.7	25.5	ND	ND	ND	ND	ND	ND
Cl-dp-com unred (15 h)	31.0	69.1	3.8	1.6	25.5	4.3	0.24	0.11	0.03	0.11	1.9
Cl-dp-com unred r1 (15 h)	20.3	71.9	2.7	0.6	24.5	ND	ND	ND	ND	ND	ND
Cl-dp-com unred r2 (15 h)	18.0	79.2	3.2	1.0	16.5	ND	ND	ND	ND	ND	ND
N-dp-com unred (fresh)	–	–	–	–	–	4.3	0.25	0	0	0.06	2.8
N-dp-com unred (5 h)	11.3	53.9	4.8	1.6	39.7	ND	ND	ND	ND	ND	ND
N-dp-com unred (15 h)	22.5	66.0	1.5	0.9	31.6	3.3	0.14	0	0	0.06	2.8
N-dp-com unred r1	8.8	80.7	5.3	0.3	13.7	ND	ND	ND	ND	ND	ND
N-dp-com unred r2	7.3	87.3	4.8	0.0	7.9	ND	ND	ND	ND	ND	ND

Table 3). This could be due to the presence of Cl ions on the surface favoring excessive hydrogenolysis and C—C cleavage [17,18]. Moreover, aqueous phase reforming (APR) is known to be favored on highly-dispersed catalysts as it is the case [16] (Scheme 1). Apparently, after 5 h of reaction the extent of C—C cleavage decreased thus resulting in an increase in selectivity to 1,2-PDO. Complementary XPS and TPD studies of pre-adsorbed pyridine (Table 3) showed that chlorine was almost lost from the catalyst surface within 1 h of reaction and that acidity had significantly decreased. These results suggest the possibility of acidic cracking occurring on strong acid sites which deactivate as reaction proceeds thus resulting in an increase in selectivity to 1,2-PDO. Interestingly, reutilization studies (Table 3) showed a drop in conversion which could be associated to the deactivation of those strong acid sites which could catalyze both C—C cleavage and dehydration of glycerol into acetol. The drop in conversion is accompanied by a significant increase in selectivity to 1,2-PDO. From Table 3 it is also evident that as reaction proceeds, there is a catalyst restructuration involving chlorine leaching and decoration of platinum particles by Zn (see decrease in Pt/Zn ratio), whereas Pt particle size remains constant. In the case of N-dp-com system, initial selectivity to 1,2-PDO is higher than that achieved on Cl-series, which again could be related to the absence of strong acid sites associated to chlorine as well as the higher Pt particle size which is detrimental to APR. Reuse of the systems led to a significant decrease in conversion which could be associated to the Pt leaching (compare %Pt as determined by ICP-MS of N-dp-com unred (fresh) and N-dp-com unred (15 h), Table 3), and decoration of Pt particles by Zn. The increase in selectivity with reuses could suggest some Pt–Zn strong metal–support interaction leading to active sites more selective to 1,2-PDO.

For similar conversion values, solids reduced at 400 °C exhibited a higher selectivity to 1,2-PDO than unred systems (Fig. 11 and Table 3). This suggests that changes occurring in the catalyst as reduction temperature is increased (Pt–Zn alloy formation, loss of acidity, increase in Pt particle size) leads to the prevalence or the formation of specific active sites for 1,2-PDO generation. Some other experiments were conducted starting from acetol. Production of 1,2-PDO from glycerol is known to occur through acetol, via dehydration of a primary hydroxyl group in glycerol. Moreover, dehydration of glycerol to acetol is slower than hydrogenation of acetol to 1,2-PDO [19]. In fact, if we start from 1.36 M acetol (the same concentration as for glycerol studies), conversion after 15 h is total, with selectivity to 1,2-PDO in the 83–86% range. The exception is Cl-im-com (91% conversion, 68% selectivity). Taking the example of Cl-dp-com-unred, selectivity at full conversion is 85.2%. When the reaction time is decreased to 3 h, the conversion and selectivity values on Cl-dp-com-unred are lower (74% and 85.5%, respectively). Reducing acetol initial concentration to 1/3 of its value, conversion after 3 h is 93% and selectivity 97%. In the case of acetol, GC–MS studies evidenced the formation of several C_4—C_9 liquid oxygenates, their relative percentage increasing with the reduction of hydrogen pressure or the increase in acetol initial concentration.

Finally, some reactions were carried out under nitrogen atmosphere. Activity order was coincident with that obtained under H_2 atmosphere (e.g. the most acidic solids, Cl-dp-com-Al-unred and Cl-dp-com-Zr-unred, were also the most active ones) though selectivity to 1,2-PDO decreased significantly because of APR and formation of C_4—C_9 liquid oxygenates.

4. Conclusions

Different ZnO solids (either alone or doped with Al, Zr or Ce) were synthesized through the microemulsion technique which allowed us to obtain similar particle sizes and textural properties. Platinum was subsequently incorporated from H_2PtCl_6 through deposition–precipitation or impregnation method. For comparative purposes, a system from $Pt(NO_3)_4$ was also obtained through deposition–precipitation method. Incorporation of platinum led to the creation of new (mainly Lewis) acid sites, particularly important in the case of chlorine-containing solids. Moreover, acidity is partly lost during reduction treatment or as the reaction proceeds which could be ascribed to both chlorine release and platinum decoration by the support (as evidenced by XPS). A direct relationship between acidity and glycerol conversion was found. Interestingly, supports were not active in the process which evidences the participation of the metal in the dehydration of glycerol to acetol. As regards selectivity to 1,2-PDO, it increases as reaction proceeds and acidity of solids decreases to the detriment of acidic cracking. This suggests that strong acid sites associated to chlorine are responsible for C—C cleavage and excessive hydrogenolysis, whereas dehydration of glycerol into acetol requires moderate acidity. Moreover, formation of Pt–Zn strong metal interaction is beneficial to 1,2-PDO selectivity.

Acknowledgements

The authors are thankful to Junta de Andalucia and FEDER funds (P08-FQM-3931 and P09-FQM-4781 projects) for financial support. SCAI at the University of Cordoba is also acknowledged for ICP-MS measurements and the use of TEM and XPS. Finally, the authors are

Please cite this article in press as: V. Montes, et al., Selective transformation of glycerol into 1,2-propanediol on several Pt/ZnO solids: Further insight into the role and origin of catalyst acidity, Catal. Today (2014), http://dx.doi.org/10.1016/j.cattod.2014.11.014

grateful to COST Action CM0903 for financial support, including a short-term scientific mission (STSM) of V. Montes.

References

[1] Z. Yuan, P. Wu, J. Gao, X. Lu, Z. Hou, X. Xheng, Catal. Lett. 130 (2009) 261–265.
[2] A. Marinas, P. Bruijnincx, J. Ftouni, F.J. Urbano, C. Pinel, Catal. Today 239 (2015) 31–37, http://dx.doi.org/10.1016/j.cattod.2014.02.048.
[3] R. Rodrigues, N. Isoda, M. Gonçalves, F.C.A. Figueiredo, D. Mandelli, W.A. Carvalho, Chem. Eng. J. 198/199 (2012) 457–467.
[4] M. Checa, F. Auneau, J. Hidalgo-Carrillo, A. Marinas, J.M. Marinas, C. Pinel, F.J. Urbano, Catal. Today 196 (2012) 91–100.
[5] T. Miyazawa, Y. Kusunoki, K. Kunimori, K. Tomishige, J. Catal. 240 (2006) 213–221.
[6] F. Auneau, C. Michel, F. Delbecq, C. Pinel, P. Sautet, Chem. Eur. J. 17 (2011) 14288–14299.
[7] J. Chaminand, L. Djakovitch, P. Gallezot, P. Marion, C. Pinel, C. Rosier, Green Chem. 6 (2004) 359–361.
[8] F. Auneau, S. Noël, G. Aubert, M. Besson, L. Djakovitch, C. Pinel, Catal. Commun. 16 (2011) 144–149.
[9] F. Vila, M. López Granados, M. Ojeda, J.L.G. Fierro, R. Mariscal, Catal. Today 187 (2012) 122–128.
[10] Z. Huang, F. Cui, J. Xue, J. Zuo, J. Chen, C. Xia, Catal. Today 183 (2012) 42–51.
[11] I. Gandarias, P.L. Arias, J. Requies, M. El Doukkali, M.B. Güemez, J. Catal. 282 (2011) 237–247.
[12] L. Ma, D. He, Catal. Today 149 (2010) 148–156.
[13] A. Iriondo, J.F. Cambra, V.L. Barrio, M.B. Guemez, P.L. Arias, M.C. Sanchez-Sanchez, R.M. Navarro, J.L.G. Fierro, Appl. Catal. B: Environ. 106 (2011) 83–93.
[14] J. Ten Dam, F. Kapteijn, K. Djanashvili, U. Hanefeld, Catal. Commun. 13 (2011) 1–5.
[15] A. Wawrzetz, B. Peng, A. Hrabar, A. Jentys, A.A. Lemonidou, J.A. Lercher, J. Catal. 269 (2010) 411–420.
[16] M.L. Barbelli, F. Pompeo, G.F. Santori, N.N. Nichio, Catal. Today 213 (2013) 58–64.
[17] S.N. Delgado, D. Yap, L. Vivier, C. Especel, J. Mol. Catal. A: Chem. 367 (2013) 89–98.
[18] E.S. Vasiliadou, E. Heracleous, I.A. Vasalos, A.A. Lemonidou, Appl. Catal. B: Environ. 92 (2009) 90–99.
[19] J. ten Dam, U. Hanefeld, ChemSusChem 4 (2011) 1017–1034.
[20] S. Zhu, Y. Qiu, Y. Zhu, S. Hao, H. Zheng, Y. Li, Catal. Today 212 (2013) 120–126.
[21] B. Peng, C. Zhao, I. Mejía-Centeno, G.A. Fuentes, A. Jentys, J.A. Lercher, Catal. Today 183 (2012) 3–9.
[22] Y. Feng, H. Yin, A. Wang, L. Shen, L. Yu, T. Jiang, Chem. Eng. J. 168 (2011) 403–412.
[23] I. Gandarias, P.L. Arias, J. Requies, M.B. Güemez, J.L.G. Fierro, Appl. Catal. B: Environ. 87 (2010) 248–256.
[24] V. Montes, M. Checa, A. Marinas, M. Boutonnet, J.M. Marinas, F.J. Urbano, S. Järas, C. Pinel, Catal. Today 223 (2014) 129–137.
[25] M. Sanchez-Dominguez, K. Pemartin, M. Boutonnet, Curr. Opin. Colloid Interface Sci. 17 (2012) 297–305.
[26] M. Sanchez-Dominguez, L.F. Liotta, G. Di Carlo, G. Pantaleo, A.M. Venezia, C. Solans, M. Boutonnet, Catal. Today 158 (2010) 35–43.
[27] A.S. Shaporev, V.K. Ivanov, A.E. Baranchikov, O.S. Polezhaeva, Y.D. Tret'yakov, Russian J. Inorg. Chem. 52 (2007) 1811–1816.
[28] G. Patrinoiu, J.M. Calderón-Moreno, D.C. Culita, R. Birjega, R. Ene, O. Carp, Solid State Sci. 23 (2013) 58–64.
[29] F. Xiao, B. Zhang, C. Lee, J. Environ. Sci. 20 (2008) 907–914.
[30] M.A. Aramendía, V. Boráu, C. Jiménez, A. Marinas, J.M. Marinas, J.A. Navío, J.R. Ruiz, F.J. Urbano, Colloids Surf. A: Physicochem. Eng. Aspects 234 (2004) 17–25.
[31] D. Raoufi, T. Raoufi, Appl. Surf. Sci. 255 (2009) 5812–5817.
[32] Y. Wei, Z. Zhao, T. Li, J. Liu, A. Duan, G. Jiang, Appl. Catal. B: Environ. 146 (2014) 57–70.
[33] J. Hidalgo-Carrillo, A. Marinas, J.M. Marinas, J.J. Delgado, R. Raya-Miranda, F.J. Urbano, Appl. Catal. B: Environ. 154–155 (2014) 369–378.
[34] M. Abid, V. Paul-Boncour, R. Touroude, Appl. Catal. A: Gen. 297 (2006) 48–59.
[35] S. Subramanian, Platin. Metals Rev. 36 (1992) 98–103.
[36] J. Silvestre-Albero, F. Coloma, A. Sepúlveda-Escribano, F. Rodríguez-Reinoso, Appl. Catal. A: Gen. 304 (2006) 159–167.
[37] P.S. Querino, J.R.C. Bispo, M. do Carmo Rangel, Catal. Today 107–108 (2005) 920–925.
[38] J. Hidalgo-Carrillo, M.A. Aramendía, A. Marinas, J.M. Marinas, F.J. Urbano, Appl. Catal. A: Gen. 385 (2010) 190–200.
[39] G.E. McGuire, G.K. Schweitzer, Thomas A. Carlson, Inorg. Chem. 12 (1973) 2450–2453.
[40] A. Salaün, M. Veillerot, F. Pierre, E. Souchier, V. Jousseaume, ECS J. Solid State Sci. Technol. 3 (2014) N39–N45.
[41] G. Berhault, M. Lacroix, M. Breysse, F. Maugé, J.-C. Lavalley, H. Nie, L. Qu, J. Catal. 178 (1998) 555–565.
[42] B. Li, R.D. Gonzalez, Catal. Today 46 (1998) 55–67.

Please cite this article in press as: V. Montes, et al., Selective transformation of glycerol into 1,2-propanediol on several Pt/ZnO solids: Further insight into the role and origin of catalyst acidity, Catal. Today (2014), http://dx.doi.org/10.1016/j.cattod.2014.11.014

Catalysis Today 223 (2014) 66–75

Contents lists available at ScienceDirect

Catalysis Today

journal homepage: www.elsevier.com/locate/cattod

Preparation and characterization of Pt-modified Co-based catalysts through the microemulsion technique: Preliminary results on the Fischer–Tropsch synthesis

V. Montes[a], M. Boutonnet[b], S. Järås[b], M. Lualdi[b], A. Marinas[a,*], J.M. Marinas[a], F.J. Urbano[a], M. Mora[a]

[a] Organic Chemistry Department, Campus de Excelencia Internacional CeiA3, University of Córdoba, Campus de Rabanales, Marie Curie Building, E-14014 Córdoba, Spain
[b] KTH (Royal Institute of Technology), Chemical Technology, Teknikringen 42, SE-100 44 Stockholm, Sweden

ARTICLE INFO

Article history:
Received 26 February 2013
Received in revised form
12 November 2013
Accepted 15 November 2013
Available online 20 December 2013

Keywords:
Fischer–Tropsch synthesis
Microemulsion technique
Pt-modified cobalt catalysts
Co–TiO_2 interaction

ABSTRACT

The influence of the addition of small amounts of platinum (0.1–0.25% wt) to cobalt-based systems on Fischer–Tropsch synthesis was investigated. The solids were synthesized through microemulsion technique using TiO_2 as the support. The best catalytic performance was achieved using Synperonic 13/6.5 as the surfactant. In all cases, the presence of platinum led to an increase in CO conversion which could be ascribed to the promotion of cobalt reducibility as evidenced by XPS. Moreover, the simultaneous reduction of cobalt and platinum precursors during synthetic procedure (ME1) was preferable to the consecutive one (ME2) probably as a result of a better Co–Pt interaction in the former case, as evidenced by TPR. TPR, Raman and XPS data also suggested that not only the presence of Co^0 but also the appearance of Co–TiO_2 interactions favor the catalytic performance and that in general those interactions are stronger for ME1 solids.

1. Introduction

Fischer–Tropsch synthesis (FTS) is one major step for the transformation of non-petroleum feedstocks, such as natural gas, coal, and biomass, into a wide number of hydrocarbons, such as light hydrocarbons, gasoline, diesel fuel and waxes [1]. The reaction process, normally conducted at 200–350 °C and under a pressure of 20–40 bar, involves mono- or bimetallic catalysts. Several metals (e.g. Co, Fe and Ru) have been reported as catalysts, though only Co and Fe are industrially applicable due to the high price of Ru. Fe is used in the production of short chain hydrocarbons at high temperature and low H_2/CO ratio whereas Co-based catalysts are chosen when the target is the production of hydrocarbons of the middle-distillate fraction and waxes. Typically, Co based catalysts operate with a H_2/CO ratio slightly over 2 [2].

Once a metal has been selected, the support could also play an important role in FT catalytic performance (influencing the metal dispersion, generation of metal–support interactions, deactivation, etc.). Iglesia et al. [3] reported that the FTS activity was almost independent of support (SiO_2, Al_2O_3, TiO_2, ZrO_2) and proportional to metal dispersion. In another study using SBA-15 and Ti-doped SBA-15 as the support, Lualdi et al. [4] found that the final particle size of Co_3O_4 synthesized through impregnation of cobalt nitrate was dependent on the nature of the support. This suggests that the support effect is indirect (i.e. influence on metal particle size and thus on conversion).

Venezia et al. [5] reported that a catalyst of Co over titania-modified silica, exhibited better catalytic performance than another catalyst consisting in Co on pure silica in spite of the similar cobalt particle size in both fresh systems. They explained it in terms of CoO interacting strongly with titania thus avoiding the particle mobility and therefore the deactivation by sintering during FTS.

Focusing on Co catalysts, particle size, dispersion and reducibility of cobalt are some key features in the activity and selectivity performance. It is widely accepted that cobalt particle sizes should not be too low. Otherwise, production of methane increases to the detriment of selectivity to long chain hydrocarbons (S_{C5+}) probably as a result of the much lower reducibility of very small nanoparticles [6–9]. Iglesia et al. [10] found that the intrinsic site reaction rate does not depend on Co particle size in the range of ca. 10–200 nm. In contrast, Wang et al. [11] studied the FTS on different Co/SiO_2 catalysts with cobalt particle sizes in the 1.4–10.5 nm range. The authors concluded that no intrinsic particle size effect was observed for the metallic Co particles in the range 3.5–10.5 nm.

* Corresponding author. Tel.: +34 957218622; fax: +34 957212066.
E-mail addresses: alberto.marinas@uco.es, qo2maara@uco.es (A. Marinas).

0920-5861/$ – see front matter © 2013 Elsevier B.V. All rights reserved.
http://dx.doi.org/10.1016/j.cattod.2013.11.053

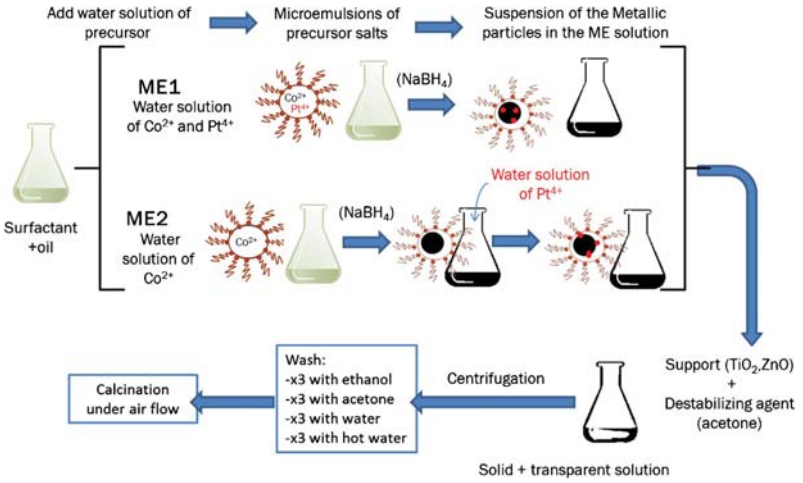

Fig. 1. Schematic representation of synthetic procedure to obtain the different Pt-modified cobalt-based systems through microemulsion technique.

Most of the papers on FT process use impregnation technique as the synthetic method [12]. However, microemulsion (ME) technique allows a better control of cobalt particle size as reported by Lödgberg et al. [13,14]. The authors synthesized Co particles on TiO_2 through both ME and impregnation methods [14], the particle size being significantly lower in the former case (10 and 22 nm, respectively). Furthermore, such smaller particle size resulted in a greater activity and selectivity to high hydrocarbons (C_{5+}). When using the ME method, in order to avoid the formation of amorphous Co species due the presence of boron (coming from the reduction agent, sodium borohydride), the authors had to resort to six depositions of 2 wt% of Co each (to a total content of 12 wt% Co), with intermediate washing of the catalytic powder to properly eliminate the rest of boron and also surfactant.

The addition of small amounts of other elements (ZnO, MnO, alkaline earth and especially noble metals [12,15–21]) can lead to the promotion of FTS. The most common effect of the addition of some noble metals is the increase in the conversion rate of carbon monoxide (CO). It is well known that the reducibility of Co is improved in the presence of a small amount of noble metal [18–22] though the optimization of the metal content and the method of incorporation is a matter of debate [23]. The improvement in the reducibility with the addition of a metal may occur with or without modification of Co dispersion [3]. The enhancement of Co reducibility on Pt incorporation has been reported for several supports (e.g. SiO_2, TiO_2, ZrO_2) though it seems especially pronounced in the case of Al_2O_3 [24]. Boron promotion effect is unclear yet. On the one hand, the presence of boron clearly decreases the degree of reduction of Co [25], but on the other hand it also decreases the deactivation rate through avoiding the deposition of carbon during the FT process [26].

The present study is aimed at going further on the optimization of the synthesis of cobalt-based systems through ME technique (Co incorporated in one step), including the addition of small amounts of platinum with a view to improve catalytic performance for FTS. For a better comparison of the different systems special care was taken to obtain similar cobalt particle sizes in all cases.

2. Experimental

2.1. Chemicals

The microemulsions were formed mixing 2,2,4-trimethylpentane (99.9% Sigma Aldrich) or cyclohexane (99.0%, Sigma Aldrich) with Synperonic 13/6.5 (Croda) and Berol 02 (Akzo Nobel), respectively. The metal precursors were $CoCl_2{\cdot}6H_2O$ (99.9%, Alfa Aesar), and 8 wt% H_2PtCl_6 aqueous solution (Sigma Aldrich). $NaBH_4$ (98%, Sigma Aldrich) was used as the reducing agent. The supports were ZnO nanopowder (Sigma Aldrich) and TiO_2 (Degussa Evonik P25). The TiO_2 was calcined at 800 °C with an air flow of 2 L/min in order to get mostly rutile phase. Acetone and ethanol (technical grade) were used during the washing process. Milli-Q water was used for the preparation of the solutions.

2.2. Synthesis of the systems

Fig. 1 summarizes the steps followed to synthesize the Co-based nanoparticles. Two different water in oil microemulsions were prepared containing either Berol 02 or Synperonic 13/6.5 as the surfactant. Under optimized conditions, composition of microemulsion (ME) is as follows:

(a) Berol 02/cyclohexane/2% wt water solution of precursor: 18/71/11 wt% (hereinafter referred to as B series)
(b) Synperonic13/6.5/2,2,4-trimethylpentane/2% wt water solution of precursor: 28/64/8 wt% (hereinafter referred to as S series).

Once the optimum composition of ME had been determined, Co-based systems were synthesized. Firstly the microemulsion was put in a N_2 atmosphere inside a glove bag, and deoxygenated by bubbling N_2 for a couple of minutes. Then, two different approaches were adopted depending on the incorporation of Pt. ME1 method involved the simultaneous reduction of Co and Pt whereas in ME2 method Co was reduced first and then Pt was incorporated. In both cases, the amount of reducing agent was calculated to have a B/Co molar ratio of 3. Therefore, in ME1 the appropriate amount of Pt was

Table 1
Some catalytic results obtained for the different systems synthesized in the present study for FTS together with the estimated Co_3O_4 particle size from XRD (311 diffraction peak at 2θ of 36.9°).

Surfactant	Incorporation method	Calcined 300		Calcined 500	
		mmol CO/g h[a]	Co_3O_4 XRD particle size[b]	mmol CO/g h[a]	Co_3O_4 XRD particle size[b]
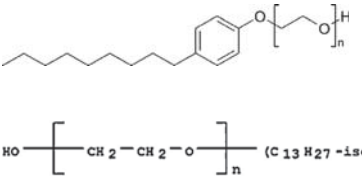	B-TiO_2	5.2	12.3	2.3	15.2
	B-TiO_2-0.25%Pt ME1	13.4	11.7	15.8	19.4
	B-TiO_2-0.25%Pt ME2	6.9	10.9	5.4	18.7
	B-ZnO	3.4	12.6	–	19.3
	B-ZnO-0.25%Pt ME1	6.5	12.1	–	18.6
	B-ZnO-0.25%Pt ME2	6.9	13.4	–	18.7
	S-TiO_2	3.0	12.5	1.9	13.7
	S-TiO_2-0.1%PtME1	17.8	13.8	–	16.5
	S-TiO_2-0.25%PtME1	25.4	13.3	16.3	16.4
	S-TiO_2-0.1%PtME2	13.2	13.3	–	16.2
	S-TiO_2-0.25%PtME2	12.9	14.8	8.7	18.9

[a] mmol of CO consumed per gram of catalyst and per hour after 17 h on stream. 210 °C, 20 bar; H_2/CO molar ratio 2.1.
[b] This particle size is subjected to error due to overlapping of signals corresponding to Co_3O_4 and the support (TiO_2 or ZnO).

added as an aqueous solution of 8 wt% H_2PtCl_6 to the water solution of $CoCl_2$, and then both cobalt and Pt were reduced with a 10 M $NaBH_4$ water solution. In contrast, in ME2, cobalt was reduced first with the 10 M $NaBH_4$ solution and after 15 min the corresponding amount of Pt was added as an aqueous solution of 8 wt % H_2PtCl_6. In both, ME1 and ME2 methods reduction step was allowed for 2 h under vigorous stirring.

After the reduction step, the metal particles were deposited onto the TiO_2 support by destabilization of the organosol (Metallic particles stabilized by surfactant and dispersed in the oil phase) with acetone (1 g acetone/1 g ME) in the presence of the support under vigorous stirring for 1 h. After 1 h, the inert atmosphere was broken opening the plastic bag and it was kept stirring one additional hour. Then the solid powders were centrifuged and washed with ethanol, acetone, water and boiling water three times each, using a washing solution/ME ratio of 1:1 by weight. Finally, the catalysts were dried for 12 h at 120 °C and then calcined with 2 L/min synthetic air flow at 300 °C or 500 °C during 16 h with a temperature ramp of 1 °C/min.

The nominal content of cobalt was in all cases 12 wt%, whereas platinum was incorporated in a 0.1 or 0.25 wt%. For comparative purposes, the corresponding systems without platinum were also synthesized.

The nomenclature of the solids includes an S or B prefix indicating the surfactant (Synperonic 13/6.5 or Berol 02, respectively), the support (TiO_2 or ZnO) and, when applicable, the corresponding nominal amount of Pt. The name is followed by the approach to incorporate platinum (ME1 or ME2) and finally the calcination temperature. For instance a catalyst synthesized with Synperonic 13/6.5 on TiO_2 containing 0.25% of Pt incorporated through ME1 method and calcined at 300 °C is called '-TiO_2-0.25%Pt ME1-cal300′ whereas S-TiO_2-cal300 denotes the 12 wt% Co/TiO_2 synthesized from the microemulsion using Synperonic as the surfactant and calcined at 300 °C. In total, 11 systems were synthesized as shown in Table 1.

2.3. Characterization

Elemental analysis of metal-containing samples was carried out by the staff at the Central Service for Research Support (SCAI) of the University of Córdoba. It was performed using inductively coupled plasma mass spectrometry (ICP-MS). Measurements were made on a Perkin-Elmer ELAN DRC-e instrument following dissolution of the sample in a 1:3 HNO_3/HCl mixture with a soft heating. Calibration was done by using PE Pure Plus atomic spectroscopy standards, also from Perkin-Elmer.

Surface areas of the solids were determined from nitrogen adsorption–desorption isotherms obtained at liquid nitrogen temperature on a Micromeritics ASAP-2010 instrument, using the Brunnauer–Emmett–Teller (BET) method. All samples were degassed to 0.1 Pa at 120 °C prior to measurement.

Transmission electron microscopy (TEM) images were obtained using a Philips CM-10 microscope. All samples were mounted on 3 mm holey carbon copper grids.

EDX measurements were performed on a JEOL JSM-6300 scanning electron microscope (SEM) equipped with an energy-dispersive X-ray (EDX) detector. It was operated at an acceleration voltage of 20 keV with a resolution of 65 eV.

X-ray diffraction (XRD) was performed on the samples after destabilization using a Siemens D5005 X-ray diffractometer with Cu Kα radiation. A secondary monochromator was used. Particle sizes were estimated by using the Scherrer formula assuming spherical crystallites.

X-ray photoelectron spectroscopy (XPS) data were recorded on 4 mm × 4 mm pellets 0.5 mm thick that were obtained by gently pressing the powdered materials following outgassing to a pressure below about 2×10^{-8} Torr at 150 °C in the instrument pre-chamber to remove chemisorbed volatile species. The main chamber of the Leibold–Heraeus LHS10 spectrometer used, capable of operating down to less than 2×10^{-9} Torr, was equipped with an EA-200MCD hemispherical electron analyser with a dual X-ray source using MgKα ($h\nu$ = 1253.6 eV) or Al K_α ($h\nu$ = 1486.6 eV) at 120 W, at 30 mA, with C(1s) as energy reference (284.6 eV). Measurements with the Mg anode were performed at University of Cordoba whereas those with the Al anode were carried out at University of Sevilla although with similar equipments. Nevertheless, the equipment in Cordoba is newer and thus more sensitive.

Hydrogen Temperature-Programmed-Reduction (TPR) of catalysts was performed on a Micromeritics Autochem 2910. A 5% H_2 in Ar flow was passed through the catalyst and the temperature increased from ambient to 800 °C (10 °C/min) while monitoring the H_2 consumption with a thermal conductivity detector (TCD).

Raman spectra were performed on a Renishaw inVia Raman microscope with laser of 785 nm and a grating of 1200 lines/mm. The laser power was adjusted at 1% with an exposure time of 10 s after 10 accumulations.

2.4. Catalytic tests

The FT synthesis experiments were carried out in stainless steel fixed bed reactor (0.93 cm i.d). Approximately 0.5 g of calcined Co catalyst was passed through a sieve of 53–90 μm, and then diluted

with 5 g of SiC (75–150 μm) as inert solid to achieve an isothermal bed temperature profile. Reduction of catalyst was made in situ in a H_2 flow of 250 Ncm^3/min at atmospheric pressure, 400 °C for 16 h with a heating rate of 1 °C/min from 70 °C. Then, the catalyst was cooled down to 170 °C in flowing H_2 and flushed with He for another hour before the reactor system was pressurized to 20 bar. Afterwards, the feed of syngas flow was introduced with a H_2/CO molar ratio of 2.1, also containing 3 mol% of N_2 as internal standard. The reactor temperature was then slowly increased up to 210 °C. The heavy hydrocarbons and the liquid products were collected in a heated trap (90 °C). The gas products also passed through a "cold" trap at room temperature in order to condense residual liquid products. The gas products were analyzed on line with a HP 5890 gas chromatograph equipped with a thermal conductivity (TCD) and a flame ionization (FID) detectors. H_2, CH_4, CO_2, internal standard N_2, and unconverted CO were quantified with the TCD whereas light hydrocarbons (C1–C4) were quantified with the FID. The selectivity to high hydrocarbons (S_{C5+}) was calculated as follows:

$$S_{C5+} = 100 - (S_{C1} + S_{C2} + S_{C3} + S_{C4} + S_{CO2})$$

3. Results and discussion

3.1. Screening of catalysts for FTS

Firstly, a screening of catalysts for FTS was carried out. In total 11 solids were obtained and tested for the reaction under standard conditions (17 h on stream, see Section 2.4). Then the most catalytically active systems would be selected for further characterization studies, searching for some structure–activity relationships.

Initially, berol 02 (ethoxylated nonylphenol, see structure in Table 1) was used as the surfactant and two partially reducible solids (TiO_2 and ZnO) were chosen as the support trying to induce some metal–support interaction favorable to FTS (e.g. avoiding cobalt sintering as the reaction proceeds) [5]. Moreover, 0.25% platinum was incorporated through two different methods (simultaneously or subsequently to cobalt) in order to favor cobalt reducibility [12]. In total, 6 solids were obtained from berol 02.

Table 1 summarizes the activity expressed as mmol CO converted per gram of catalyst per hour (mmol CO/g h) after 17 h on stream. From that table it is evident that in all cases the incorporation of platinum resulted in higher activity as compared to the corresponding unmodified solids (B-TiO_2 and B-ZnO). This is particularly evident for B-TiO_2-0.25%Pt ME1 which exhibited the highest activity values. This prompted us to select TiO_2 as the support for a new synthesis using an environmentally friendlier surfactant, Synperonic 13/6.5 (see structure in Table 1). Moreover, on this occasion two different Pt contents (0.1 and 0.25% weight) were chosen. This resulted in 5 new solids. Again, catalytic results shown in Table 1 evidence the increase in activity with the incorporation of platinum (which is even more marked than for berol 02, with a 4–8 fold increase as compared to S-TiO_2). Furthermore, the enhancement is generally more pronounced for ME1 than for ME2. Moreover, systems calcined at 500 °C are normally less active than the corresponding counterparts calcined at 300 °C. All in all, the best results were obtained for S-TiO_2 solids. This is the reason why at this point attention was focused on S-TiO_2 systems.

Fig. 2 summarizes the results obtained for all tested catalysts corresponding to B-TiO_2 or S-TiO_2 series for a time-on-stream of 17 h. From that Figure it is clearly evident that incorporation of platinum does not seem to change selectivity values (i.e. reaction mechanism) though it leads to higher conversions and that this effect is more marked for ME1 than for ME2. Moreover, S series exhibit better catalytic performance than B-series.

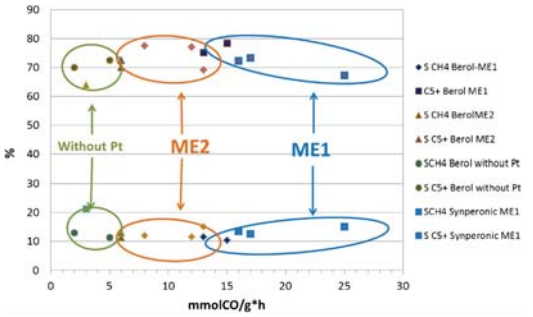

Fig. 2. Comparison of activity (expressed as mmol CO/g h) and selectivity to CH_4 and C_{5+} for all the solids for a time-on-stream of 17 h. Standard conditions (i.e. 20 bar, 170 °C, H_2/CO molar ratio 2.1).

Fig. 3 shows the evolution of activity (expressed as mmol CO/g cat h) with time-on-stream. Regarding S-TiO_2 series (Fig. 3A), there seems to be two clear trends. On one hand, ME1 systems for which there is a continuous increase in conversion with time-on-stream (in particular for the systems with 0.25% Pt). On the other hand, ME2 solids for which a maximum appears to be reached at ca. 4–5 h after which conversion hardly changes or even decreases as it is the case of the catalyst containing 0.25 wt % of Pt. As for B-TiO_2 solids (Fig. 3B), all systems exhibit the maximum at ca. 4–5 h followed by the decrease in activity.

A more in-depth description of catalytic behavior of S-TiO_2 solids for a time on stream of 17 h is summarized in Table 2. That table includes a more detailed description of selectivities as well as the corresponding TOF values considering Co^0 content estimated from TPR profile and particle size as determined by TEM. From TOF values, activity of systems with 0.1% Pt is quite similar irrespective

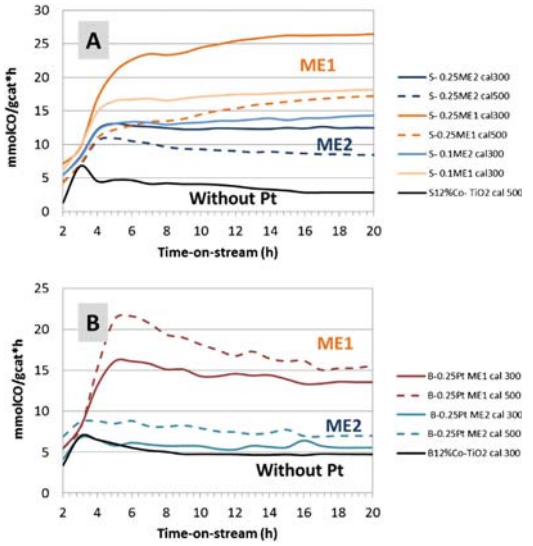

Fig. 3. Evolution of activity (expressed as mmol CO/g h) for the different solids. (A) S-TiO_2 series and (B) B-TiO_2 series. Temperature was slowly increased from 170 °C up to 210 °C and then kept at the final temperature. 20 bar and H_2/CO molar ratio 2.1.

Table 2
Some catalytic results obtained for S-TiO_2 systems in FTS for a time on stream of 17 h, 210 °C, 20 bar; H_2/CO molar ratio 2.1.

Catalyst	Space velocity[a]	Conv (%)	mmol CO/g h	S (CO_2)[b]	S (CH_4)[c]	S (C_2–C_4)[d]	S (C_{5+})[e]	TOF (s^{-1})
S-TiO_2 cal300	10,018.6	2.1	3.0	2.61	21.17	12.20	64.02	0.006
S-TiO_2-0.1%PtME1 cal300	10,588.2	11.7	17.8	0.18	12.56	13.80	73.46	0.023
S-TiO_2-0.1%PtME2 cal300	10,027.9	9.5	13.2	0.40	15.07	15.30	69.23	0.021
S-TiO_2-0.25%PtME1 cal300	8797.6	21.1	25.4	0.18	14.95	17.51	67.36	0.030
S-TiO_2-0.25%PtME2 cal300	10,644.6	8.1	12.9	0.56	11.42	10.80	77.22	0.009
S-TiO_2-0.25%PtME1 cal500	6940.4	17.0	16.3	0.23	13.43	13.94	72.40	0.034
S-TiO_2-0.25%PtME2 cal500	7020.2	8.3	8.7	0.37	11.92	10.09	77.62	0.012

[a] Space velocity (N mL of syngas/h gcat).
[b] Selectivity to CO_2.
[c] Selectivity to CH_4.
[d] Selectivity to compounds with 2–4 carbons.
[e] Selectivity to compounds with 5 or more carbons.

of the ME method. However, for solids containing 0.25% Pt activity of ME1 solids is ca. 3 times that of ME2 systems. Moreover, increase in Pt content from 0.1 to 0.25% resulted in an increase in activity for ME1 whereas it was detrimental for ME2.

3.2. Characterization of the systems

Fig. 4A and B represents the X-ray diffractograms of S-TiO_2 and B-TiO_2 systems, respectively. The support (TiO_2) calcined at 800 °C consisted in rutile and anatase in a 74%/26% ratio with particle sizes of 51.1 and 30.2 nm, respectively (as determined from Scherrer formula using 110 and 101 reflections for rutile and anatase, respectively). As can be seen, signals for anatase overlap with those corresponding to cobalt. It was also the case of ZnO (not shown) which consisted in wurtzite particles with average particle sizes of 45 nm as estimated from 101 reflection at ca. 36.5°. Nevertheless, an attempt at estimating Co_3O_4 particle size by XRD analysis, applying Scherrer equation on the 3 1 1 diffraction peak at 2θ of 36.9° [27] was made trying to subtract the contribution of anatase or wurtzite to such a peak. Estimated values for Co_3O_4 are also given in Table 1. Though much less reliable than those obtained from TEM (see below) obtained results evidence quite a similar Co_3O_4 particle size for all the solids calcined at the same temperature and the increase in particle size on increasing calcination temperature from 300 °C to 500 °C, which could account for the decrease in activity expressed as mmol CO/g h (see Table 1).

It is possible to estimate the metallic particle size of Co^0 from the values measured for Co_3O_4 using the formula [28]:

$$d(Co^0) = 0.75 * d(Co_3O_4)$$

With this calculation the estimated metallic (Co^0) particles size for systems calcined at 300 °C are in the range 8.2–11.1 nm.

TEM micrographs of Pt-modified catalysts after reduction at 400 °C during 16 h are represented in Fig. 5. A first conclusion from that study is that overlapping of Co_3O_4 and TiO_2 signals led to a significant overestimation of cobalt particle sizes. In fact, for S-series systems calcined at 300 °C, average particle sizes are in the 3.8–4.7 nm range. Calcination at 500 °C resulted in an increase in particle size (e.g. from 4.1 to 5.5 nm for S-TiO_2-0.25%Pt ME1). The similar cobalt particle sizes obtained for the different systems confirms the suitability of microemulsion technique to obtain a good control of particle size and will allow us a better comparison of catalytic performance.

BET areas measured for all catalysts are in the 20–25 m^2/g range similar to that of the support (TiO_2) after calcination (22 m^2/g). Table 3 includes elemental analysis of systems by ICP-MS, EDAX and XPS (using the Mg anode). Co composition as measured by EDAX is slightly higher than that obtained by ICP-MS, always below the nominal content (12 wt %). It is noteworthy that XPS with the Mg anode are subjected to error due to the interference of O_{KLL} Auger in Co2p signal. That is probably the reason why Co content as determined by XPS is so high. In fact, using the Al anode, all systems exhibit Co contents in the 10–12% range. In contrast, XPS data collected in Table 3 were registered with a more sensitive equipment than that possessing the Al anode which allowed us to detect Pt despite its low content.

Even though the Pt incorporation method differed in ME1 and ME2 (simultaneous or subsequent to Co) Pt content as measured by EDAX was quite similar for both methods and close to the nominal content, thus confirming the success of the incorporation method.

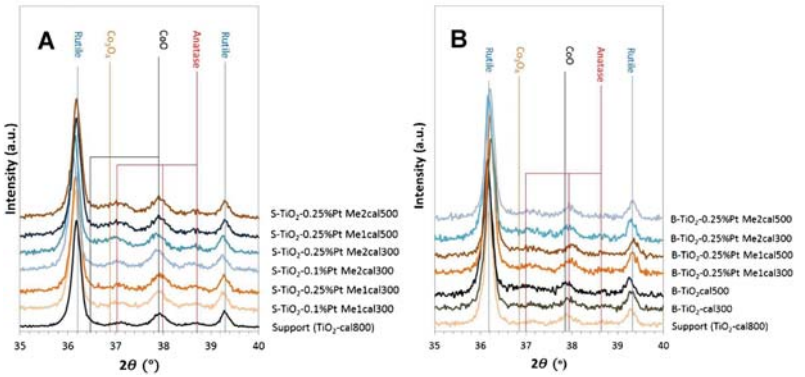

Fig. 4. X-ray diffractograms of the different systems corresponding to S-TiO_2 (A) and B-TiO_2 (B) series. For the sake of comparison, that of the support has also been included.

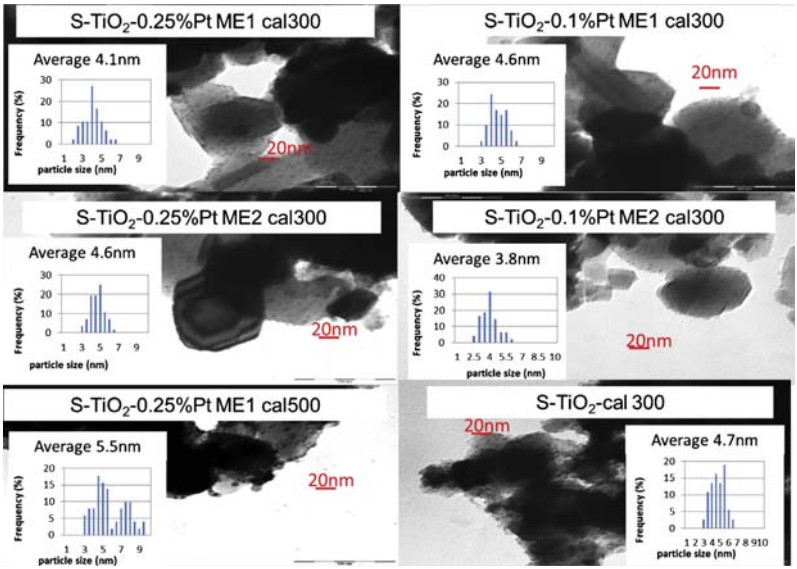

Fig. 5. TEM micrographs of the different S-TiO_2 systems after reduction at 400 °C during 16 h.

However, Pt/Ti ratio as measured by XPS was especially low for the catalyst S-TiO_2 0.25%Pt ME2 as compared to S-TiO_2 0.25%Pt ME1. This could suggest a lower dispersion of platinum in the former solid which in turn could be ascribed to the synthetic method. In fact, assuming similar micelle sizes in both synthetic methods, there will be probably more micelles containing only platinum in ME2 systems thus leading to bigger platinum particles as compared to ME1 solids. This will be more marked for the systems with the highest Pt content (0.25% wt) whereas for the solids with 0.1% wt Pt, this could be somehow compensated by the favoring of Pt^0 nucleation over growth since Pt^{4+} is added to a medium with an excess of reduction agent ($NaBH_4$).

Finally, according to EDAX and XPS results, the amount of chloride is negligible. This confirms the successful removal of chlorine (which is known to be a catalyst poison) coming from platinum and cobalt precursors during the synthetic procedure (through washing and/or release as HCl) [29]. Boron was not detected by EDAX. This species can also act as poison or promoter depending on its concentration [26]. The higher the boron content of Pt-containing systems as determined from XPS (Table 3) the higher the CO

Table 3
Elemental analysis of some of the systems synthesized in the present study.

Catalyst	Weight composition (%)									
	ICP-MS			EDAX				XPS[a]		
	Co	Pt	B	Co	Pt	B	C	Co	Pt	B
S-TiO_2 cal300	8.82	0	0.31	9.32	0	–	45.04	10.03	0	1.34
S-TiO_2-0.1%PtME1 cal300	8.66	0.14	1.05	9.31	0.14	–	19.71	18.50	0.48	3.20
S-TiO_2-0.25%PtME1 cal300	8.54	0.17	1.37	10.2	0.35	–	18.69	19.63	0.92	3.96
S-TiO_2-0.1%PtME2 cal300	9.39	0.05	0.84	10.4	0.13	–	23.55	20.52	0.51	3.00
S-TiO_2-0.25%PtME2 cal300	8.40	0.21	0.88	10.8	0.29	–	16.93	18.89	0.37	3.00

Catalyst	XPS data based on atomic composition[a]			
	Fresh		Reduced 400	
	Pt/Ti	Co/Ti	Co/Ti	Co^0/Co (ox)[b]
S-TiO_2 cal300	0	0.87	0.52	0.12
S-TiO_2-0.1%PtME1 cal300	0.0055	0.76	0.76	0.29
S-TiO_2-0.25%PtME1 cal300	0.0138	0.99	0.59	0.34
S-TiO_2-0.1%PtME2 cal300	0.0075	0.98	0.64	0.18
S-TiO_2-0.25%PtME2 cal300	0.0039	0.63	0.26	0.34
S-TiO_2-0.25%PtME1 cal500	0.0036	0.33	Not det	Not det
S-TiO_2-0.25%PtME2 cal500	0.0021	0.32	Not det	Not det

[a] XPS signals used were C1s, O1s, Co2p, Pt4f, Ti2p and B1s. These XPS data (in particular Co content and Co/Ti ratio) can be subjected to error since they were determined with the Mg anode and thus Co2p photoelectron spectrum presents a contribution of the O_{KLL} Auger. In fact, Co content obtained using Al anode was in the 10–12% range for all systems.

[b] $Co^0/(Co^{2+} + Co^{3+})$ ratio.

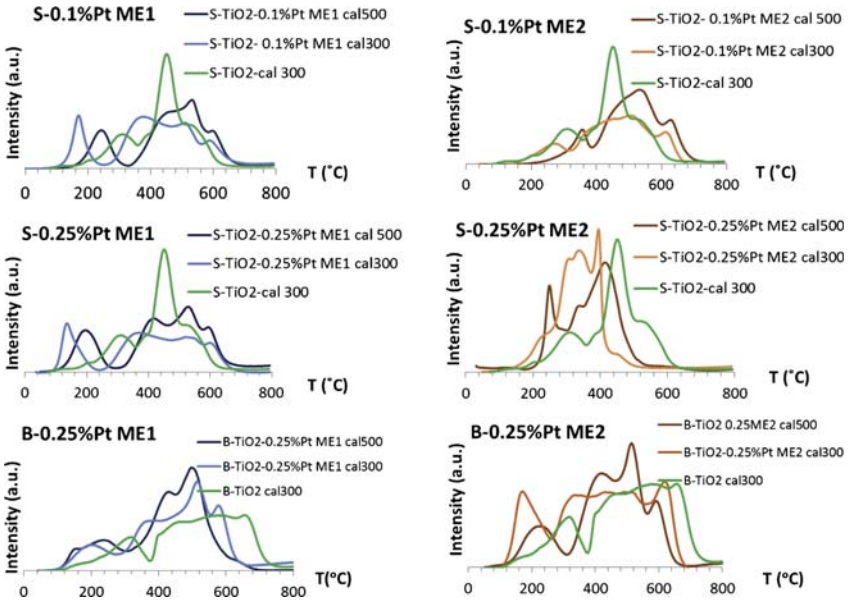

Fig. 6. TPR profiles of S-TiO_2 and B-TiO_2 systems.

conversion (see Table 1 or 2) which could suggest a possible promotion effect of such species. Tan et al. [26] found that the presence of Co_2B species reduced the stability of carbon formed during FT process which prevented to a certain extent deactivation of the catalyst.

In order to study the reducibility of the catalysts, Hydrogen Temperature-Programmed-Reduction (TPR) studies were conducted (Fig. 6). For comparative purposes, all TPR profiles were normalized per gram of catalyst. In all cases the green line represents the Co catalysts without platinum used as the reference (S-TiO_2 or B-TiO_2).

For S-TiO_2 systems two main peaks centered at 289 and 444 °C can be observed, which could correspond to the two-step reduction $Co_3O_4 \rightarrow CoO$ and $CoO \rightarrow Co^0$ [27,30].

The small shoulder at ca. 520 °C could be due to Co–TiO_x interactions which shift the profile to higher temperatures [31,32]. As far as ME1 series is concerned, the incorporation of Pt results in the shift of the first reduction peak to lower temperatures particularly for calcination temperature of 300 °C (see the peak at ca. 160 °C) which is consistent with the expected promotion of Co reduction on incorporation of platinum [12]. In contrast, the relative intensity of the peak appearing at ca. 444 °C in S-TiO_2 seems to decrease in

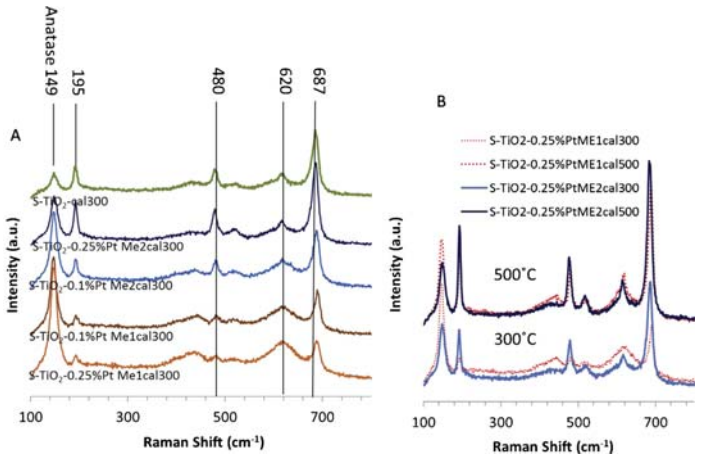

Fig. 7. Raman spectra of the different S-TiO_2 systems. (A) Solids calcined at 300 °C. (B) Comparison of solids containing 0.25% Pt calcined at 300 and 500 °C.

favor of the shoulder at higher temperatures (now centered at ca. 520 °C) which could be indicative of a stronger Co–support interaction. Regarding ME2 series, the different Pt content led to significant changes in TPR profile. Therefore, the solids containing 0.1% Pt presented a shift to higher reduction temperatures whereas the opposite holds true for systems with 0.25 wt% Pt. This could suggest a higher Co–support interaction in the former case. Interestingly, TPR profiles of S-TiO_2 0.1% PtME1 cal300 and S-TiO_2 0.1% PtME2 cal300 are very similar at temperatures over 200 °C which could account for their similar TOF values (ca. 0.020 s^{-1}, Table 2). In contrast, the absence of the TPR peak at high temperatures in S-TiO_2 0.25% PtME2 could indicate the absence of Co–support interaction which could explain its much lower TOF values as compared to S-TiO_2 0.25% PtME1 (0.009 and 0.030 s^{-1}, respectively, Table 2).

Furthermore, the observed promotion effect of Pt on cobalt reducibility in ME1 series unlike ME2 systems could be explained in terms of the synthetic method. For ME1 cobalt and platinum were simultaneously added and then reduced by sodium borohydride. On the contrary, in ME2 method cobalt was added first, reduced by sodium borohydride and platinum precursor was subsequently added. This means that, in principle, a better cobalt–platinum interaction would be expected from ME1 method which is the one for which TPR profiles evidenced the shift of the first reduction peak to lower temperatures.

Finally, in all cases the increase in calcination temperature resulted in a shift of TPR profiles to higher temperatures which led to the decrease in activity expressed as mmol CO/g h though not in TOF (Table 2) which could be ascribed to the increase in cobalt particle size with calcination temperature (Fig. 5).

Regarding B-TiO_2 systems, TPR profiles evidence the promotion effect of Pt on cobalt reducibility (as evidenced by the shift of the peak at ca. 300 °C to lower temperatures on Pt addition) though unlike S-series, irrespective of the method (ME1 or ME2), no Co–support interaction is observed (i.e. no shift of peak at ca. 700 °C at higher temperatures). This could be one of the reasons for the lower catalytic performance of B-series as compared to S-solids. Nevertheless, this requires further studies. In any case, given the better catalytic performance of S-series and that alcohol ethoxylates (as it is the case of Synperonic) has been described as environmentally friendlier substitutes for nonylphenol ethoxylates

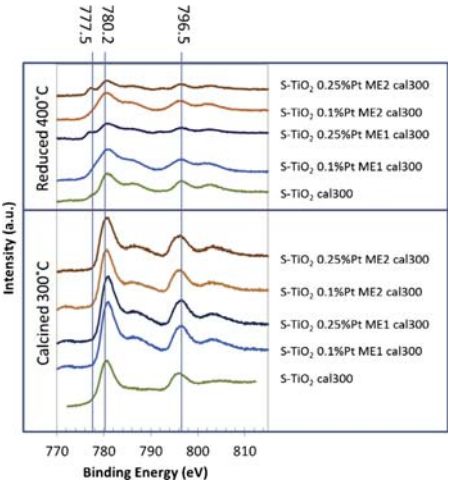

Fig. 8. Co 2p XPS spectra of the different S-TiO_2 solids registered with the Mg anode.

(e.g. berol) [33] attention was focused on the characterization of S-series systems.

All in all, TPR profiles just give us some evidences on the structural differences of the solids which could account for the observed catalytic performance. However, some complementary information from other techniques is needed. In this sense, another important point to consider is the crystallographic form of cobalt in the different solids. To cast further light on that, Raman and XPS spectroscopies were used.

Unlike XRD where Co_3O_4 and TiO_2 signals overlap, Raman spectra of both systems differ. Co_3O_4 Raman spectra exhibits typical bands at ca. 193, 478, 520, 618 and 686 cm^{-1} which can be ascribed to T2g, Eg, F2g, F2g and A1g vibrational modes, respectively [32,34]. CoO also presents these bands though their intensity is comparatively lower [12]. Raman spectra of samples calcined at 300 °C

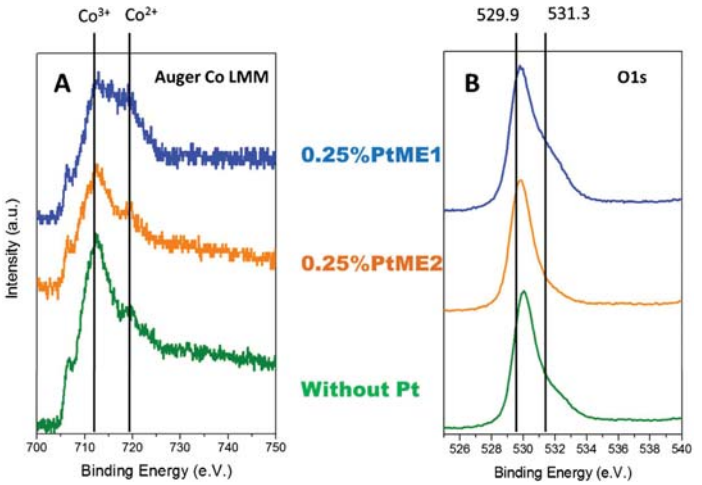

Fig. 9. XPS results with the Al anode of solids reduced at 400 °C. Co_{LMM} Auger (A) and O1s (B) signals.

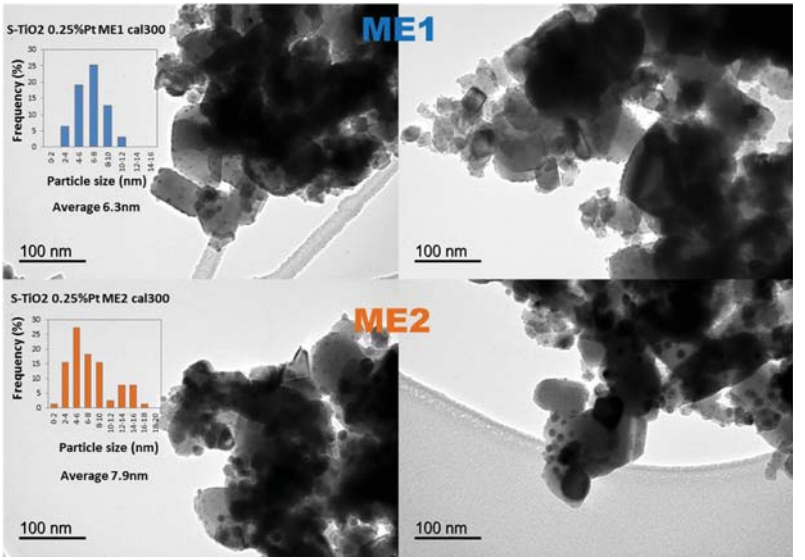

Fig. 10. TEM micrographs of some spent systems. Particle sizes were calculated assuming all particles corresponded to Co_3O_4.

(Fig. 7) exhibit most of these bands. However, in general, (the exception being the band at ca. 620 cm^{-1}) their intensity is lower for ME1 than for ME2 which assuming similar crystallinity (and taking into account that cobalt content and particle size is similar for all samples) could suggest a higher CoO content in ME1 series. Moreover, A1g band at 687 cm^{-1} for S-TiO_2 cal300 and S-TiO_2-0.25%Pt-ME2cal 300 is shifted around 3–4 cm^{-1} to higher frequencies for the other systems which were more active in FTS (Table 2). Some authors explain the shift of Raman bands as a result of interactions of cobalt oxides with the support [32]. This stronger Co–support interaction for ME1 could also be the reason for the higher intensity of the band at ca. 620 cm^{-1}. Finally, as expected, increase in calcination temperature from 300 to 500 °C (Fig. 7B) resulted in an increase in the intensity of Raman Bands probably as a result of a higher crystallinity and particle sizes (as evidenced by TEM).

In order to confirm the presence of different cobalt species distribution in ME1 and ME2 solids (higher proportion of CoO in the former), XPS was utilized. Co^0 exhibits a Co2p3/2 signal at ca. 778 eV. As for Co_3O_4 and CoO they exhibit Co2p3/2 peaks at ca. 779.6 and 780.0 eV, respectively, what makes the differentiation of both species difficult [35].

XPS profiles obtained for our solids in the Co2p region are represented in Fig. 8. As can be seen reduction at 400 °C for 16 h results in the appearance of the Co^0 peak centered at 777.5 eV. Moreover, results reveal the promotion effect of platinum on cobalt reduction (see the increase in the relative intensity of the signal attributed to Co^0 for Pt-containing solids as compared to S-TiO_2-cal300 and the Co^0/Co(ox) ratio in Table 3). However, no clear correlation between such a ratio and catalytic activity is observed. This could suggest that not only the presence of Co^0 but also the distribution of Co^{2+} and Co^{3+} should be considered. It is important to note that Co2p photoelectron spectrum measured with Mg anode presents a contribution of the O_{KLL} Auger [36].

Therefore, experiments were repeated for S-TiO_2, S-TiO_2-0.25% PtME1 and S-TiO_2-0.25% PtME2 using the Al anode. Moreover, Auger signal was registered since it is more sensitive to changes in the chemical state of cobalt than the Co2p signal.

Fig. 9 represents the Auger signal for the solids containing 0.25% Pt. For the sake of comparison the signal of S-TiO_2 system has also been included. Two peaks corresponding to Co_{LMM} Auger lines are observed in these curves at 712.3 and 719.1 eV (Fig. 9A). From those values the modified Auger parameter (α') can be calculated using the following equation:

$$\alpha' = 1486.6 + KE(Co_{LMM}) - KE(Co\ 2p3/2)$$

where KE (Co_{LMM}) is the kinetic energy of the Co_{LMM} Auger electron, KE (Co 2p3/2) is the kinetic energy of Co 2p3/2 photoelectron and 1486.6 is the energy of the Al K_α X-ray excitation in eV. Therefore, values of 1554.5 and 1547.7 eV are obtained which can be attributed to Co_3O_4 and CoO, respectively [36]. Results shown in Fig. 9A confirm that the system synthesized through ME1 method contain a higher proportion of Co^{2+} species than those obtained through ME2. This is consistent with Raman results: all solids contain CoO and Co_3O_4 but CoO phase is more important in ME1 than in ME2. Moreover, 0.25%PtME1 system exhibits a more intense O1s signal at ca. 531.3 eV (Fig. 9B) which could be ascribed to the generation of the above-mentioned metal–support interactions [37]. This Co–support interaction, more important in ME1 systems as compared to ME2 solids could avoid cobalt sintering as the reaction proceeds and thus account for the observed higher activity of ME1 as compared to ME2 and deactivation of the latter solids with time-on-stream (Fig. 3A). In fact, TEM micrographs of spent catalysts (Fig. 10) confirm that ME2 solids are more prone to sintering as the reaction proceeds. Assuming that particles in those figures were Co_3O_4 mainly, it would result in average cobalt particle sizes of 4.7 and 5.9 nm for S-TiO_2-0.25%PtME1 cal 300 and S-TiO_2-0.25%PtME2 cal 300, respectively. The possible influence of some other factors in activity and deactivation, in particular

different nature of carbonaceous deposits in ME1 and ME2 solids, is currently under investigation.

4. Conclusion

Several Pt-modified cobalt catalysts containing 0–0.25 wt% platinum and 12 wt% cobalt were synthesized through microemulsion technique (ME) using TiO_2 as the support. Moreover, Berol 02 and Synperonic 13/6.5 were used as surfactants. Two incorporation methods involving simultaneous (ME1) or consecutive (ME2) reduction of cobalt and platinum with sodium borohydride were essayed. A first screening of catalysts for Fischer–Tropsch synthesis led us to select S-TiO_2 series (TiO_2 as the support and Synperonic 13/6.5 as the surfactant) for subsequent characterization studies. In all cases ME technique led to quite comparable cobalt particle sizes (averaging in the range 3.8–4.7 nm for catalysts calcined at 300 °C as determined by TEM). Moreover, ME1 solids led to higher conversions than their ME2 counterparts. The higher Pt–Co and Co–support interaction in the former case (as evidenced by TPR profile) could account for that. Raman spectra evidenced the presence of Co_3O_4 and CoO in all solids though CoO proportion is higher in ME1 as compared to ME2. There results were confirmed by XPS which together with the increase in the O1s XPS signal at ca. 531.2 eV with the reduction treatment, more significant for ME1 as compared to ME2 solids, is supportive of the existence of a greater Co–support interaction in the former systems. All in all, results showed that both the presence of reduced cobalt species (Co^0) and Co–TiO_2 interactions were responsible for the different behavior of the systems.

Acknowledgements

The authors are thankful to Spanish Junta de Andalucia and FEDER funds (P08-FQM-3931 and P09-FQM-4781 projects) for financial support. SCAI at the University of Cordoba is also acknowledged for ICP-MS measurements and the use of TEM and XPS. SGI at the University of Sevilla is also acknowledged for XPS analyses with Al anode. Finally, the authors are grateful to COST Action CM0903 for financial support and short-term scientific mission (STSM) of V. Montes.

References

[1] E. van Steen, M. Claeys, Chem. Eng. Technol. 31 (2008) 655–666.
[2] C. Perego, R. Bortolo, R. Zennaro, Catal. Today 142 (2009) 9–16.
[3] E. Iglesia, S.C. Reyes, R.J. Madon, S.L. Soled, Adv. Catal. 39 (1993) 221–235.
[4] M. Lualdi, G. Di Carlo, S. Lögdberg, S. Järås, M. Boutonnet, V. La Parola, L.F. Liotta, G.M. Ingob, A.M. Venezia, Appl. Catal. A 443/444 (2012) 76–86.
[5] A.M. Venezia, V. La Parola, L.F. Liotta, G. Pantaleo, M. Lualdi, M. Boutonnet, S. Järås, Catal. Today 197 (2012) 18–23.
[6] R.C. Reuel, C.H. Bartholomew, J. Catal. 85 (1984) 78–88.
[7] A. Barbier, A. Tuel, I. Arcon, A. Kodre, G.A. Martin, J. Catal. 200 (2001) 106–116.
[8] G.L. Bezemer, J.H. Bitter, H.P.C.E. Kuipers, H. Oosterbeek, J.E. Holewijn, X. Xu, F. Kapteijn, A.J. Van Dillen, K.P. De Jong, J. Am. Chem. Soc. 128 (2006) 3956–3964.
[9] Ø. Borg, P.D.C. Dietzel, A.I. Spjelkavik, E.Z. Tveten, J.C. Walmsley, S. Diplas, S. Eri, A. Holmen, E. Rytter, J. Catal. 259 (2008) 161–164.
[10] E. Iglesia, S.L. Soled, R.A. Fiato, J. Catal. 137 (1992) 212–224.
[11] Z.-J. Wang, S. Skiles, F. Yang, Z. Yan, D.W. Goodman, Catal. Today 181 (2012) 75–81.
[12] Y. Khodakov, W. Chu, P. Fongarland, Chem. Rev. 107 (2007) 1692–1744.
[13] S. Järås, S. Lögdberg, M. Boutonnet, European Patent Application Number EP07106863.9 (2007).
[14] S. Lögdberg, M. Boutonnet, J.C. Walmsley, S. Järås, A. Holmen, E.A. Blekkan, Appl. Catal. A 393 (2011) 109–121.
[15] H. Wanga, Y. Yang, J. Xu, H. Wang, M. Ding, Y. Li, J. Mol. Catal. A 326 (2010) 29–40.
[16] F. Morales, E. Smit, F. Groot, T. Visser, B.M. Weckhuysen, J. Catal. 246 (2007) 91–99.
[17] A.R. de la Osa, A. De Lucas, A. Romero, J.L. Valverde, P. Sánchez, Fuel 90 (2011) 1935–1945.
[18] A. Kogelbauer, J.G. Goodwin Jr., R. Oukaci, J. Catal. 160 (1996) 125–133.
[19] K. Okabe, X. Li, M. Wei, H. Arakawa, Catal. Today 89 (2004) 431–438.
[20] M. Reinikainen, M.K. Niemelä, N. Kakuta, S. Suhonen, Appl. Catal. A 174 (1998) 61–75.
[21] D. Xu, W. Li, H. Duan, Q. Ge, H. Xu, Catal. Lett. 102 (2005) 229–235.
[22] K.M. Cook, S. Poudyal, J.T. Miller, C.H. Bartholomew, W.C. Hecker, Appl. Catal. A 449 (2012) 69–80.
[23] F. Diehl, A.Y. Khodakov, Oil Gas Sci. Technol. 64 (2009) 11–24.
[24] Z. Zsoldos, F. Garin, L. Hilaire, L. Guczi, J. Mol. Catal. A 111 (1996) 113–122.
[25] J. Li, N.J. Coville, Appl. Catal. A 181 (1999) 201–208.
[26] K.F. Tan, J. Chang, A. Borgna, M. Saeys, J. Catal. 280 (2011) 50–59.
[27] G. Prieto, A. Martínez, P. Concepción, R. Moreno-Tost, J. Catal. 266 (2009) 129–144.
[28] D. Schanke, S. Vada, E.A. Blekkan, A.M. Hilmen, A. Hoff, A. Holmen, J. Catal. 156 (1995) 85–95.
[29] M.S. Spencer, M.V. Twigg, Ann. Rev. Mater. Res. 35 (2005) 427–464.
[30] A.R. de la Osa, A. De Lucas, A. Romero, J.L. Valverde, P. Sánchez, Catal. Today 176 (2011) 298–302.
[31] R. Riva, H. Miessner, R. Vitali, G. Del Piero, Appl. Catal. A 196 (2000) 111–123.
[32] J. Łojewska, A. Kołodziej, T. Łojewski, R. Kapica, J. Tyczkowski, Appl. Catal. A 366 (2009) 206–211.
[33] US EPA. Nonylphenol (NP) and Nonylphenol Ethoxylates (NPEs) Action Plan. Available from: http://www.epa.gov/oppt/existingchemicals/pubs/actionplans/np-npe.html
[34] D. Gallant, M. Pézolet, S. Simard, J. Phys. Chem. B 110 (2006) 6871–6880.
[35] M.C. Biesinger, B.P. Payne, A.P. Grosvenor, L.W.M. Lau, A.R. Gerson, R.St.C. Smart, Appl. Surf. Sci. 257 (2011) 2717–2730.
[36] R. Moreno-Tost, J. Santamaría-González, P. Maireles-Torres, E. Rodríguez-Castellón, A. Jiménez-López, Appl. Catal. B 38 (2002) 51–60.
[37] E. van Steen, M. Claeys, D. Nabaho, A.P. Petersen, R. Stracey, V Change, J.W. Niemantsverdriet, Proceedings to 15th ICC, Munich, 2012, Available from: http://events.dechema.de/events/en/Events/Materials+for+Energy+.+EnMat+II/Congress+Planer/Datei_Handler-tagung-564-file-7246-p-127866.html